Surface acoustic wave enhanced electroanalytical sensors

Emrah Kaplan

Submitted in the fulfilment of the requirements for the
Degree of Doctor of Philosophy

School of Engineering
College of Science and Engineering
University of Glasgow

Abstract

In the last decade, miniaturised "lab-on-a-chip" (LOC) devices have attracted significant interest in academia and industry. LOC sensors for electrochemical analysis now commonly reach picomolar in sensitivities, using only microliter-sized samples. One of the major drawbacks of this platform is the diffusion layer that appears as a limiting factor for the sensitivity level. In this thesis, a new technique was developed to enhance the sensitivity of electroanalytical sensors by increasing the mass transfer in the medium. The final device design was to be used for early detection of cancer diseases which causes bleeding in the digestive system. The diagnostic device was proposed to give reliable and repeatable results by additional modifications on its design.

The sensitivity enhanced-sensor model was achieved by combining the surface acoustic wave (SAW) technology with the electroanalytical sensing platform. The technique was practically tested on a diagnostic device model and a biosensing platform.

A novel, substrate (TMB) based label-free Hb sensing method is developed and tested. Moreover, the technique was further developed by changing the sensing process. Instead of forming the sensitive layer on the electrodes it was localised on polystyrene wells by a rapid one-step process.

Results showed that the use of acoustic streaming, generated by SAW, increases the current flow and improves the sensitivity of amperometric sensors by a factor of 6 while only requiring microliter scale sample volumes. The heating and streaming induced by the SAW removes the small random contributions made by the natural convection and temperature variation which complicate the measurements. Therefore, the method offers stabilised conditions for more reliable and repeatable measurements.

The label-free detection technique proved to be giving relevant data, according to the hemoglobin concentration. It has fewer steps than ELISA and has only one antibody. Therefore, it is quick and the cross-reactivity of the second antibody is eliminated from the system. The additional modifications made on the technique decreased the time to prepare the sensing platform because the passivation steps (i.e., pegylation), prior to structuring a sensitive layer were ignored. This avoidance also increased the reliability and repeatability of the measurements.

Dedications

To my family:

For their continued support and prayers throughout the duration of my Ph.D. course in the UK.

Conferences / Seminars/ Publications

1. **E. Kaplan,** A. Şahin, J. Reboud, J. M. Cooper "Hemoglobin Detection Via Electrochemical Sensing", Bio & Nano Technology Congress, İstanbul, Türkiye, 1-3 October 2013, poster presentation.

2. **E. Kaplan,** J. Reboud, A. Glidle and J. M. Cooper "Ultrasensitive Hydrodynamic Electrochemistry Using Sound Wave Driven Microstreaming" 17th International Conference on Miniaturized Systems for Chemistry and Life Sciences, Freiburg, Germany, 27-31 October 2013, poster presentation.

3. **E. Kaplan,** J. Reboud, A. Şahin, N. Geoghegan, A. Glidle, J. M. Cooper "Turning An Electrochemical Sensor In To An Ultrasensitive Diagnostic With Acoustics" Sensor in Medicine, London, UK, 25-26 March 2014, poster presentation.

4. **E. Kaplan,** J. Reboud, A. Glidle and J. M. Cooper "Promising Effects of Sound Waves for Electrochemistry", Scottish Ultrasound Group Meeting, University of the West of Scotland, Glasgow, UK , 4 July 2013, oral presentation.

5. **E. Kaplan,** J. Reboud, R. Wilson, J. M. Cooper "Metallization Ratio Effect on Surface Acoustic Wave Actuators in Lab-on-a-Chip Platforms" International Conference On Technology And Sciences (ICAT'15), Antalya, Türkiye, Accepted & Will be presented on 4-7 August 2015, oral presentation.

6. **E. Kaplan,** J. Reboud, M. Tassieri, J. M. Cooper "Surface Acoustic Wave Enhanced Electroanalysis" Lab on a chip, to be submitted.

Table of Contents

List of Figures

Acknowledgement

First of all I would like to acknowledge Prof. Jon Cooper for giving me the opportunity to carry out this research within his group. His support for my progress and patience are greatly appreciated.

Thanks to Dr. Julien Reboud, Dr. Robert Wilson and Manlio Tassieri who were always ready to help. Thanks to Dr. Andrew Glidle for his valuable guidance.

Special thanks to my dear friend Thom. Thanks to Stephan Henry for sharing his experience in electrochemistry. Thanks to Dr. Rama Yusvana for his support and guidance in microfabrication techniques and biochemical test processes. Thanks to the team of the James Watt Nanofabrication Centre, to the people of the electronics and mechanical workshops and to Mr. Tom O'Hara for his continued technical support and lively humour.

I warmly thank all of the following colleagues and friends: Eloise Larson, Mohd Hafiz Ismail, Malgorzata Baranowska, Benjamin Tiller, Niall Geoghegan, Muhammad Arslan Khalid, Christian Witte, Shahid Mohammad Naseer, Bala Boyi Bukata, Ellie Pulleine, David Paterson, Xiaofe Yuan and Hemanth Pasumarthi.

My special gratitude extends to my sponsor, the University of Gümüşhane (Turkey), for providing me with this valuable opportunity by funding my Ph.D. research.

Finally, thanks to my wife, my parents and my sisters for their infinite support.

Author's Declaration

The work presented in this thesis was conducted by the author and has not previously been submitted for a degree or diploma from this university or any other institution.

Emrah Kaplan

Abbreviations

Ab	Antibody
AFM	Atomic force microscopy
anti-Hb	anti-haemoglobin
APTES	3-aminopropyltriethoxysilane
BAW	Bulk acoustic wave
CAD	Computer aided designs
CE	Counter electrode
CMOS	Complementary metal oxide semiconductor
CV	Cyclic voltammetry
Da	Damköhler number
DEP	Dielectrophoresis
EDC	1-ethyl-3-(3-dimethylaminopropyl)carbodiimide
ELISA	Enzyme-linked immunosorbent assay
EWOD	Electrowetting on dielectric
FCS	Fluorescent correlation spectroscopy
FIA	Flaw injection analysis
FIDT	Focused (targetted) IDT
GI	Gastrointestinal
HRP	Horseradish peroxidase

IDT	Interdigitated transducers
IR	Infrared
K-L	Koutecky Levich
LDV	Laser Doppler Vibrometry
LOC	Lab-on-a-chip
LOR	Lift off resist
M/ S	Mark to space ratio
MEMS	Micro-electro-mechanical-systems
MES	2-(N-morpholino)ethanesulfonic acid
PBS	Phosphate buffered saline
PDMS	polydimethylsiloxane
PCR	polymerase chain reaction
PFDT	1H,1H,2H,2H-perfluorodecanethiol
POC	Point of care
PPy	polypyrrole
RBC	Red blood cell
RDE	Rotating disc electrode
RE	Reference electrode
Re	Reynolds number
SAM	Self assembled layer

SAW   Surface acoustic wave

SFIDT   Slanted finger interdigitated transducer

SPR   Surface plasmon resonance

SPUDT   Single phase unidirectional transducers

SW   Surface wave

TMB   3,3',5,5'-Tetramethylbenzidine

UV   Ultraviolet

WE   Working electrode

11-MUA   11-mercaptoundecanoic acid

1. Introduction

1.1.   Cancer Diseases

Cancer is a very unfortunate disease; at least 12.6 million people are diagnosed with cancer every year and more than 7.5 million people lose their life because of it [1]. For a more efficient and simpler treatment, the early diagnosis has a crucial role. Otherwise, the problematic location can convert into a worse case, or even the diseases can spread to the other parts of body [2].
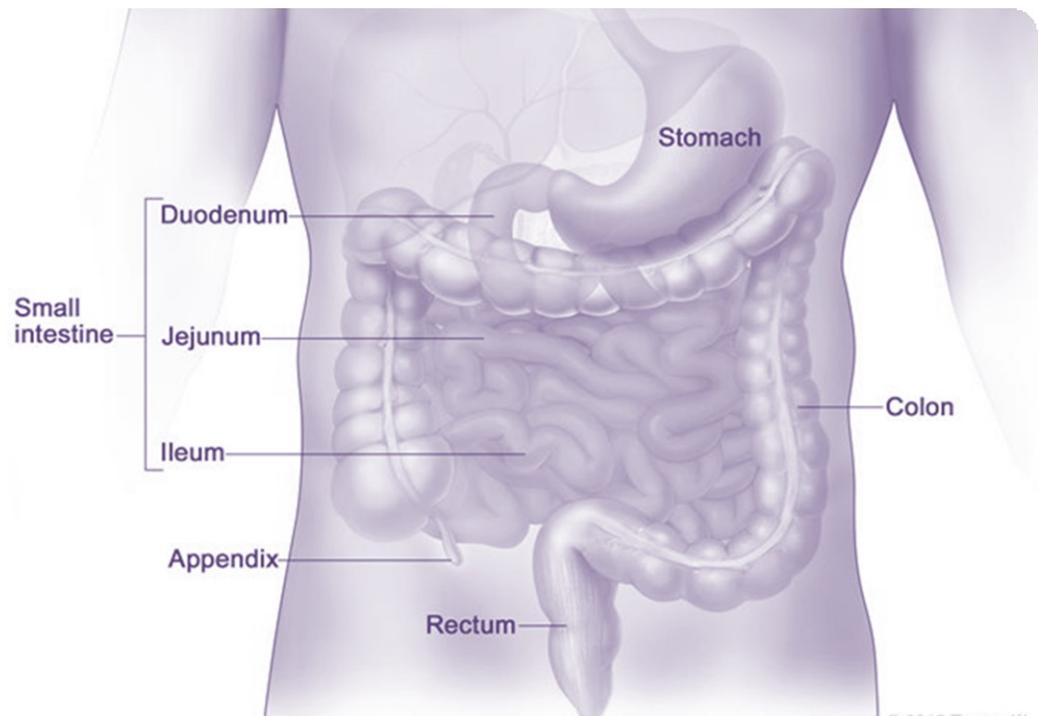
Figure 1. 1: Parts of the body where gastrointestinal cancer tumours can form [3].

Different types of cancers show different symptoms. Occult bleeding is one of the symptoms of the cancers in gastrointestinal (GI) system. Patients may not notice a small amount of bleedings in the stool or urine. However, a test device can detect it at very early stages. Finding cancer in the body earlier makes a significant difference [4]. The removal of precancerous growths and to start the treatment at early stages can be done by periodic body screenings [5]. Therefore, the necessity of diagnostic devices which has the ability for early diagnosis of cancer and other types of illnesses is enormous.

1.2.   Lab-on-a-chip for Point-of-Care Diagnostics

Biosensors comprise biological components, which can be an antibody, an enzyme or a membrane, to have a sensitivity for a particular analyte [6][7]. In 1962, the first biosensor, an

enzyme-based sensor, was developed by Clark and Lyons [8][9]. Updike and Hicks designed a modified version of the sensitive system in 1967 [10]. It was able to measure the background current by a secondary electrode (enzyme free) and giving differential results [9].

Generally, diagnosis of a disease is not based on a single sensing process alone. It often requires various complicated preparation steps performed in laboratory environments with specific instruments. Since moving bench sized instruments is not a possible option, in most cases samples are needed to be transferred into the labs. The sample transfer and delays due to limited numbers of equipment in laboratories appear as all disadvantages for the classic laboratory centralised diagnostics.
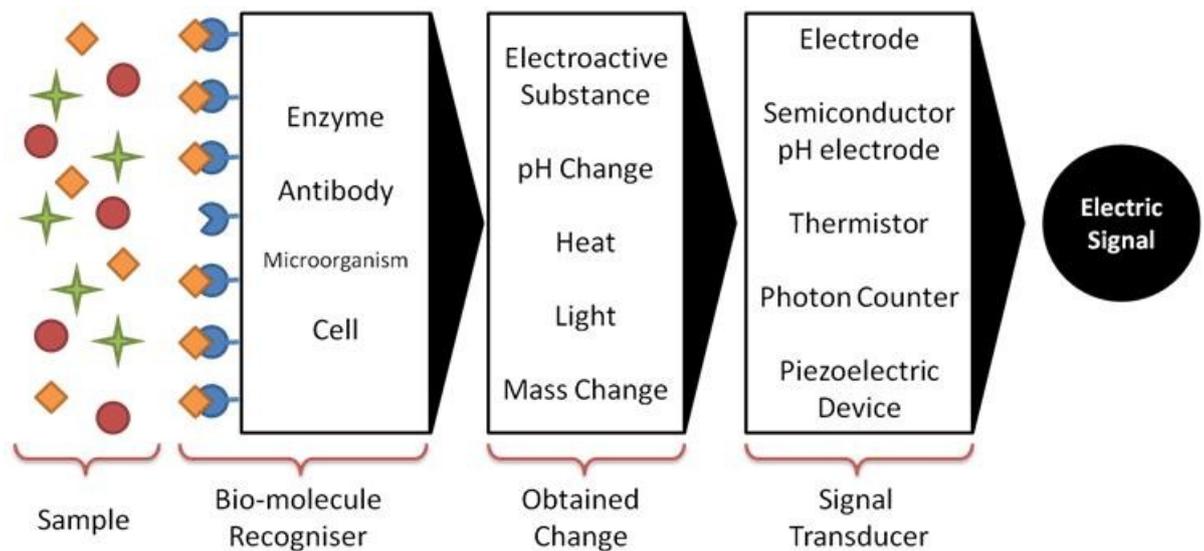
Figure 1. 2   Components of a basic biosensor that includes a bio-receptor, a transducer and a processor. Bio-receptor can be a biological system such as cells, tissues, whole organisms or biological species such as protein, enzyme and antibody. The physical change obtained by the bio-receptor is measured as an electric signal.

Miniaturisation and integration of complicated laboratory functions in small chips (lab-on-a-chip) eliminate the requirement of central laboratories. This also enables the point-of-care (POC) diagnostics which give substantial advantages for early and cheap diagnostics. Design and fabrication process of lab-on-a-chip (LOC) device is a challenging and expensive process. However, a well-designed LOC can cost less than a regular lab test process by mass production. POC diagnostic leads to conduct the tests at any location without transferring the samples to a laboratory. Therefore, the measurements can give more reliable results since it is done with fresh samples. Another advantage of the POC is the simplicity to use. Thus, the concept reduces the number of required operators for the analytical process. In some cases, people may run the tests at home as well.

1.3. Electro-analytical spectroscopy

Electro-analysis is a standard technique that is concerned with the electron transfer to/ from chemicals [11]. Measured electrical values (current and potential) can give information about physicochemical parameters such as reaction rate and concentration. This technique has various advantages over other analytical measurement techniques. It can give each oxidation step during the entire reaction instead of a single analytical result of a final product.

There are various analytical methods requiring optical transparency to operate such as colorimetric analysis [12] and fluorescent imaging [13]. However, electroanalytical sensors can work in turbid environments and can give sensitive results. It is easy to fit into LOC applications since the equipment can be miniaturized via micro or nanofabrication techniques [14].   Moreover, it can present excellent sensitivity with small sample volumes [15].

1.3.1. Measurement Methods

The current flow during the electrochemical reaction is obtained from the solution electrode interface [16]. The electron transfer, during the reduction or oxidation of the electroactive analyte, may be detected by the equipment used for electrochemical measurements. This happens while the non-equilibrium system moves towards the equilibrium case. Electroanalytical methods are mainly split into two classes: amperometry and voltammetry. Voltammetry is an electrochemical process to obtain an analytical result according to the rate of chemical reaction and to have a current graph vs. applied potential. The current flow is obtained by the polarisation of a working electrode which is promoted by the applied potential. Amperometry method is performed at a fixed potential to obtain a current flow proportional to the concentration.

Cyclic voltammetry (CV) is a very versatile electrochemical technique allows examination of redox couples, provides quick information for the transport properties, electron transfer kinetics and rates of systems [17][18]. The CV method is also used for electro-polymerisation to obtain sensitive sensors by the entrapment of bio-sensitive molecules [19]. During the CV process a triangle waveform, within certain limits, is applied to the sample. Measured current contains various data about the sample such as quantity of a particular analyte, impedance [20] or the thickness of a polymer layer [21].

Specifically, electrochemical sensors are mostly based on amperometric measurements in which the current flow caused by an imposed voltage is monitored. The fixed potential is

applied via an electrodes system. The observed current is plotted as a function of time [22]. Chronoamperometry, which is a voltammetry at a fixed potential, is the current measurement as a function time [23]. The electrons flow between the electrodes and the electroactive molecules as a function of the molecule concentration.

As an important instrument of electrochemistry experiments, the potentiostat has two primary roles. Firstly, it accurately controls the potential difference between working electrode (WE) and counter electrode (CE) [22]. Secondly, it measures the current flow between WE and CE and ensures that no current passes through the RE.
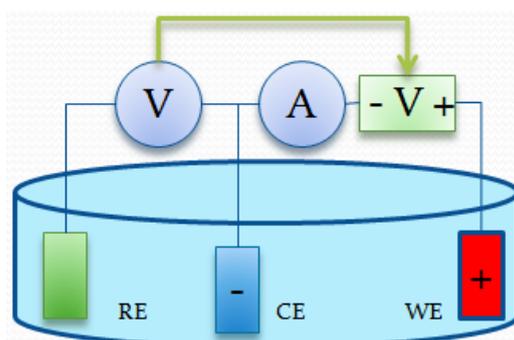
Figure 1. 3 A basic depiction of a potentiostat and an electrochemical cell with three electrodes. The system controls the potential difference between working electrode (WE) and counter electrode (CE). Secondly, it measures the current flow between WE and CE and ensures that no current passes through the RE.

As it is shown in Figure 1. 3 the potentiostat contains a voltage source which is manipulated by the voltage follower presented as "V" in the figure. The result obtained from the sample according to the input voltage is measured by an ampere meter (A) in a format that is relevant to the current flowing through the sample.

1.3.2.   Hydrodynamic effect

The mass transfer, which is the movement of material from one location to another in the liquid, has a significant effect on the dynamics of the electrochemical reaction. There are three types of mass transfer [24]: migration, diffusion and convection. The slowest step in electrochemistry defines the rate of the reaction. Therefore, the speed of the reaction can be controlled by the rate of fresh material brought to the electrode surface (e.g. convection) by mass transport or by the kinetics of electron transfer [17].

Application of external convection can significantly increase the mass transferring rates. This results in higher current flows and rapid establishment of the steady state of the system. Therefore, both the sensitivity and the sensing time of the sensors are improved [22]. There

are different hydrodynamic techniques such as, rotating disc electrode (RDE) [25][26], channel electrode [27], sonochemistry [28][29] and electrode heating [30]. Combining more than one hydrodynamic techniques can also create additional enhancements [31].

1.4.   Surface acoustic wave

Microfluidic systems enable highly specific biology, chemistry and medicine analysis by referring to a set of technologies those are capable of manipulating the small amount of liquids in miniaturized designs [32][33][34]. Microfluidic devices require tiny space, consume a tiny amount of sample and hence produce less waste. Moreover, the reaction conditions can be controlled precisely, and the experimental results can be obtained in seconds instead of hours or days. However, this micro designs causes manipulation difficulties such as capillary effect which forces the sample to be dragged along the channel. The regime of microfluidic systems is entirely different from those moving through large channels because of very effective interactions between the fluids and surrounding surfaces [35]. This different behavior mechanism is due to the increased effect of wettability, surface tension, adhesion, viscosity and other parameters of samples and surfaces. For example, a hydrophobic surface portion can block the liquid motion inside a microfluidic channel.

Various types of micro-devices were developed to overcome difficulties of fluid manipulation within microfluidic systems. Such as micro-pumps, micro-mixers, micro-heaters, etc. Some of the most promising micro-pump applications proposed with electro & magneto-hydrodynamic techniques. Micro-mixer solutions are categorized as active and passive mixers. Active mixers, require external energy to operate such as dielectrophoresis, magnetohydrodynamics [36], pressure, temperature, and acoustic techniques [37]. SAW included microfluidic approach appears as a very promising solution, in between other applications used for the construction of different microfluidic devices, due to its simplicity, the ease of construction and planar integration [32].

SAW was first studied by Lord Rayleigh in 1885 [38][39], and it is named as Rayleigh waves. SAW is a type of mechanical wave propagated along the surface of a solid material [40]. They are produced by localised physical effects and also by piezoelectric transduction at various scales. SAW transducers are widely used in modern signal processing as filters due to their high sensitivity, fast response, stability and small size [40], and according to estimations several millions of SAW devices are produced yearly [39].

In the last two decades, SAW devices, are started to be used outside of communications and signal processing: as temperature [41], stress [42], chemical sensors [43] and biosensor [44],

micro-heater [45]. Travelling SAW can couple its momentum and energy into a liquid, on its path, and induce streaming. The scientific researches proved that the energy anticipated by the SAW is large enough to induce acoustic fluid streaming to obtain further results [46]. Therefore, they were used for microfluidic actuation, such as pumping [47], micro-mixing [12], droplet manipulation [48], centrifugation [49] and atomization [50].

1.4.1.   Piezoelectricity

The materials which can convert electrical energy to mechanical energy and vice versa are named as piezoelectric. Piezoelectricity was first theorised by Charles Coloumb in 1817 when he suggested that some materials may generate electrical charge under physical pressure [51]. The first actual discovery of piezoelectricity was made by French scientists Curie brothers in 1880 [52]. Micro-electro-mechanical-systems (MEMS) including acoustic wave applications are often used piezoelectric materials [41].
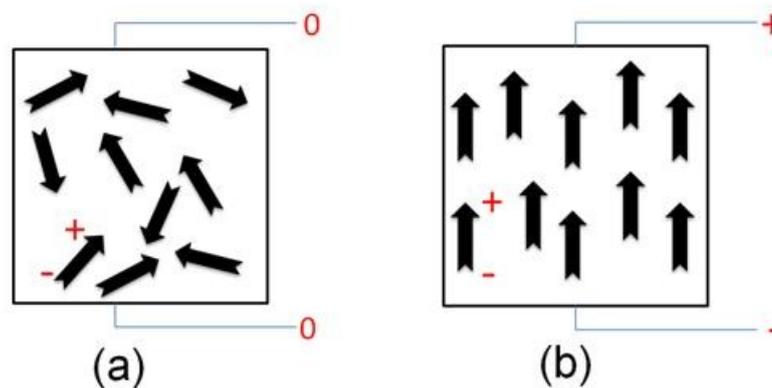
Figure 1. 4 Orientation of dipoles before (a) and after (b) the application of a DC electric field. The potential application is reoriented the dipoles. The reorientation also makes a shape change on the piezoelectric material.

A polarisation effect on the surface of a piezoelectric material is obtained (Figure 1. 4), by the separation of positive and negative charges, when a mechanical stress is imposed [53]. Thus, an electrical field due to the voltage difference can be obtained. The piezoelectricity is a reciprocal phenomenon since it is possible to obtain an inverse piezoelectric effect. Applying a voltage on the material can create physical deformation on the surface (Figure 1. 5). An acoustic perturbation is obtained when an appropriate voltage is applied via the metal transducers fabricated on the piezoelectric substrate surface. Continuous application of sinusoidal electric signal creates synchronised mechanical displacements on the surface which depends on the amount area affected by the polarisation. Additionally, the distance between the expanded and contracted surface is directly proportional to the peak to peak voltage value of the applied electrical signal.
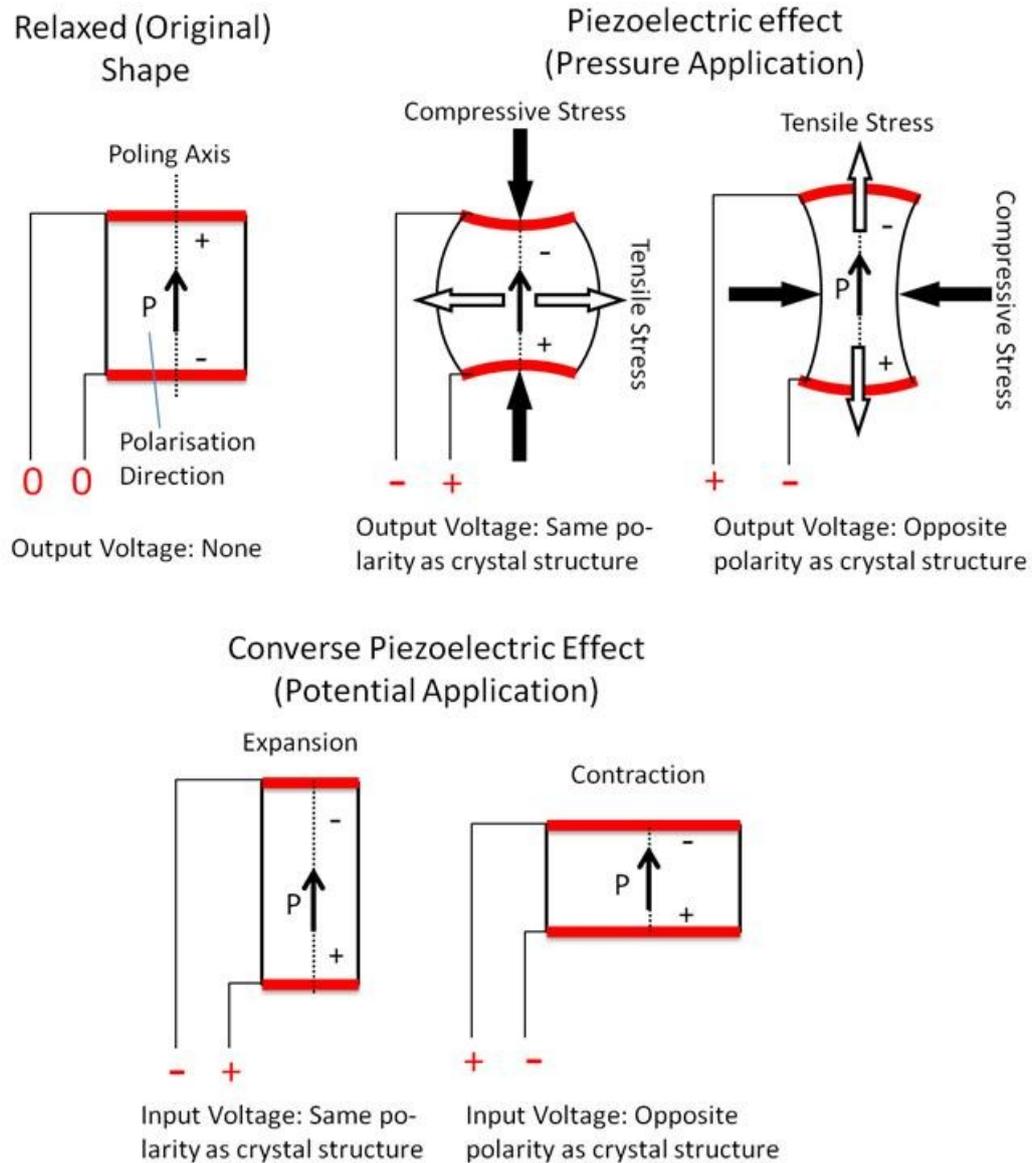
Figure 1. 5 Application of a compressive or tensile stress changes the relaxed shape of a piezoelectric material and generates an electric field. Conversely, a dimensional change is obtained when an electric field is applied to the piezoelectric material (converse piezoelectric effect)

1.4.2.   SAW transducers

Surface Acoustic Waves (SAW) can be generated on piezoelectric substrate (such as $LiNbO_3$) by comb shaped interlocked metallic patterns [54]. Application of electrical field across a piezoelectric material results an elastic deformation because of the converse piezoelectric effect (Figure 1. 5) [49]. As presented in **Error! Reference source not found.**, the resonance frequency of a SAW device is based on two parameters; the finger spacing (d) and the acoustic velocity of the substrate (Cs) [55].
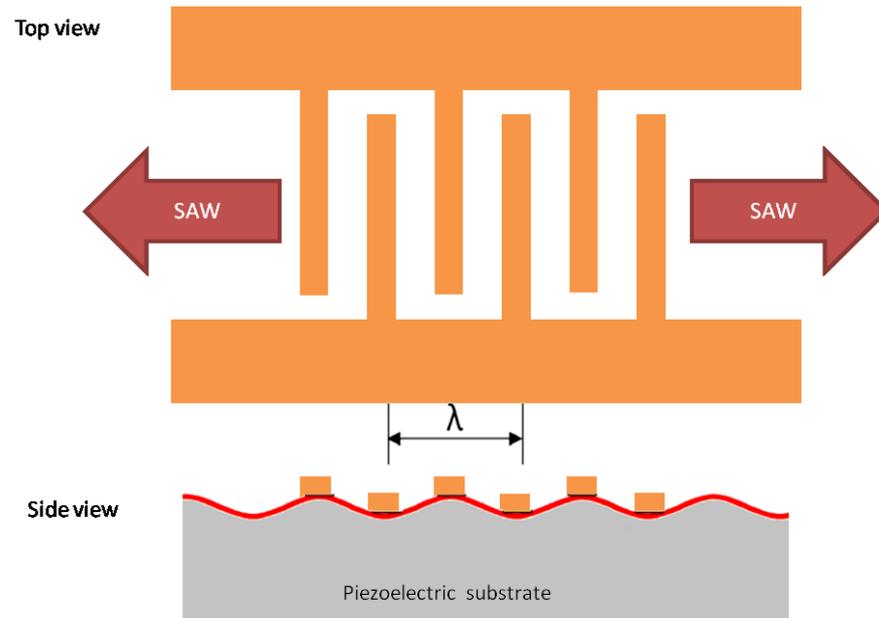
Figure 1. 6   Schematic of a SAW transducer fabricated on a piezoelectric substrate. The device resonates at a specific frequency and generates SAW (Rayleigh wave) in both directions. The finger spacing defines the resonance frequency.

$$f = \frac{Cs}{\lambda} = \frac{Cs}{2d}$$

Equation 1

1.4.3.   Wave modes in piezoelectric materials

Acoustic waves in piezoelectric materials are divided into two main groups; the bulk acoustic wave (BAW), which travels through the substrate, and the surface acoustic wave (SAW), which propagates on the surface of piezoelectric material [56]. Rayleigh wave, which is a type of SAW, is comprised of longitudinal (compressional) waves and shear waves in z and y directions as presented in Figure 1. 7. Moreover, electrostatic wave travels along with the propagating mechanical wave [57][58].   In this research the use of "SAW" specifically indicates Rayleigh waves as similar to most of the SAW based microfluidic research reports [59]. Another commonly used acoustic device concept is flexural plate wave resonators which generate Lamb waves (Figure 1. 8) [33]. This wave mode can be used for sensing or fluid pumping applications [60].
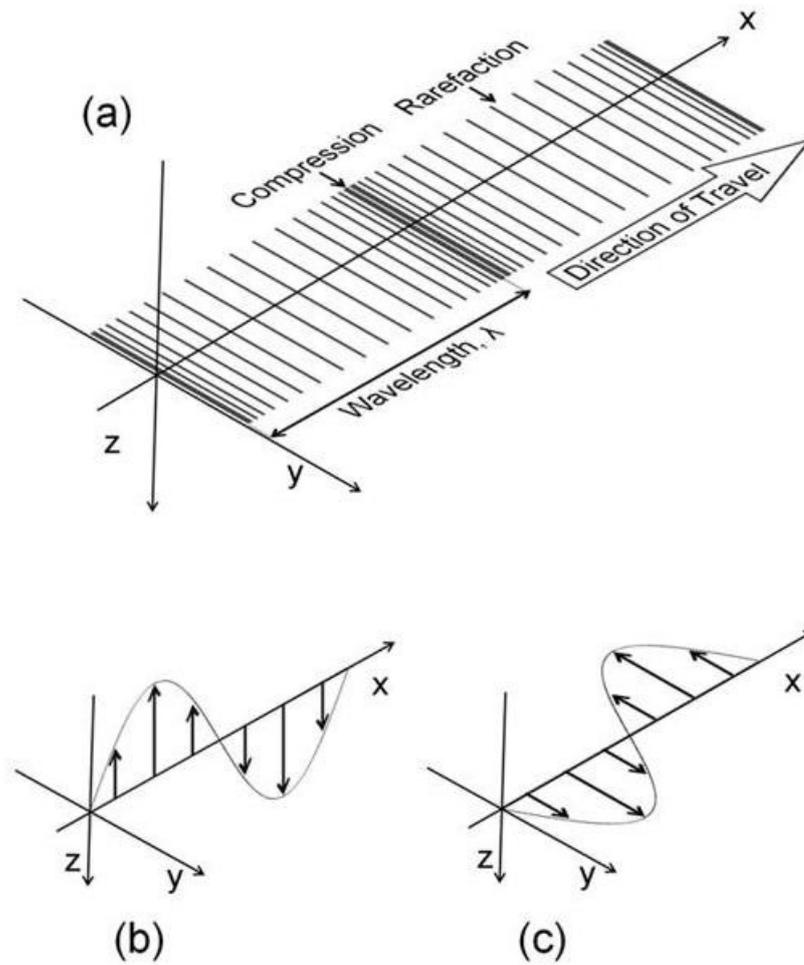
Figure 1. 7 Representation of a SAW combining longitudinal (a), z-polarised shear (b) and y-polarised shear wave (c). Travelling direction of all acoustic waves is in the x direction. The x-y plane represents the surface of the piezoelectric substrate where the SAW transducer is fabricated. z-direction represents the motion that is vertical to the surface.
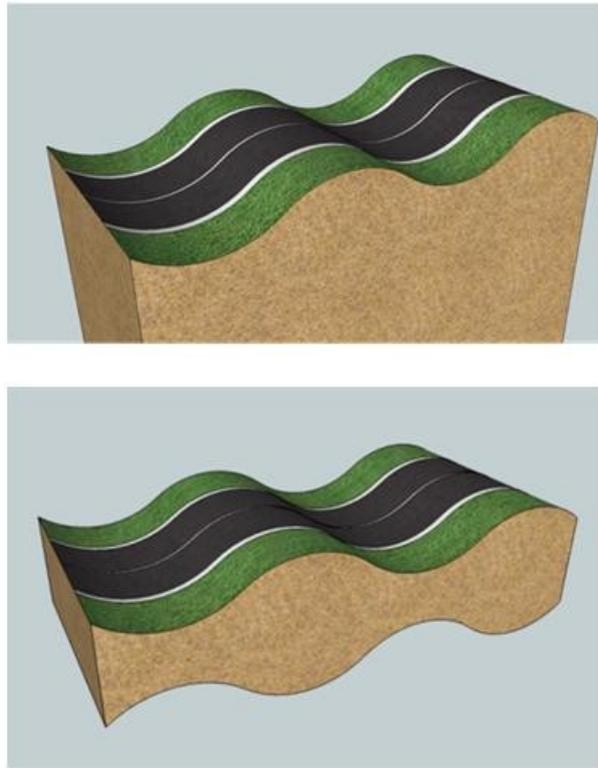
Figure 1. 8 Depiction of two wave modes; Rayleigh (SAW) wave (Top) and Lamb wave (Bottom). Lab waves are also referred as plate waves [61] since they can be generated on plates with free boundaries.

1.4.4.   SAW in droplet-based application

The liquid converts the mechanical energy into leaky waves on the surface and, pressure waves and temperature in the liquid [62][63]. As presented in Figure 1. 9 (a), the mixing obtained in a droplet, due to acoustic pressure gradients, is the first activity to observe during SAW propagation. The flow patterns in the droplet appear in different shapes according to the point of the SAW induction into the droplet. When the SAW radiated from the right side of the droplet, circulation direction occurs in an anti-clockwise direction (Figure 1. 9 a-I). However, when the SAW beam hits from the middle of the droplet, it creates two separate horizontal vortexes from the top view as parallel to wave direction (Figure 1. 9 a-II). While the left portion has flow pattern on anti-clockwise the right part of the droplet has a clockwise circulation in it [64].
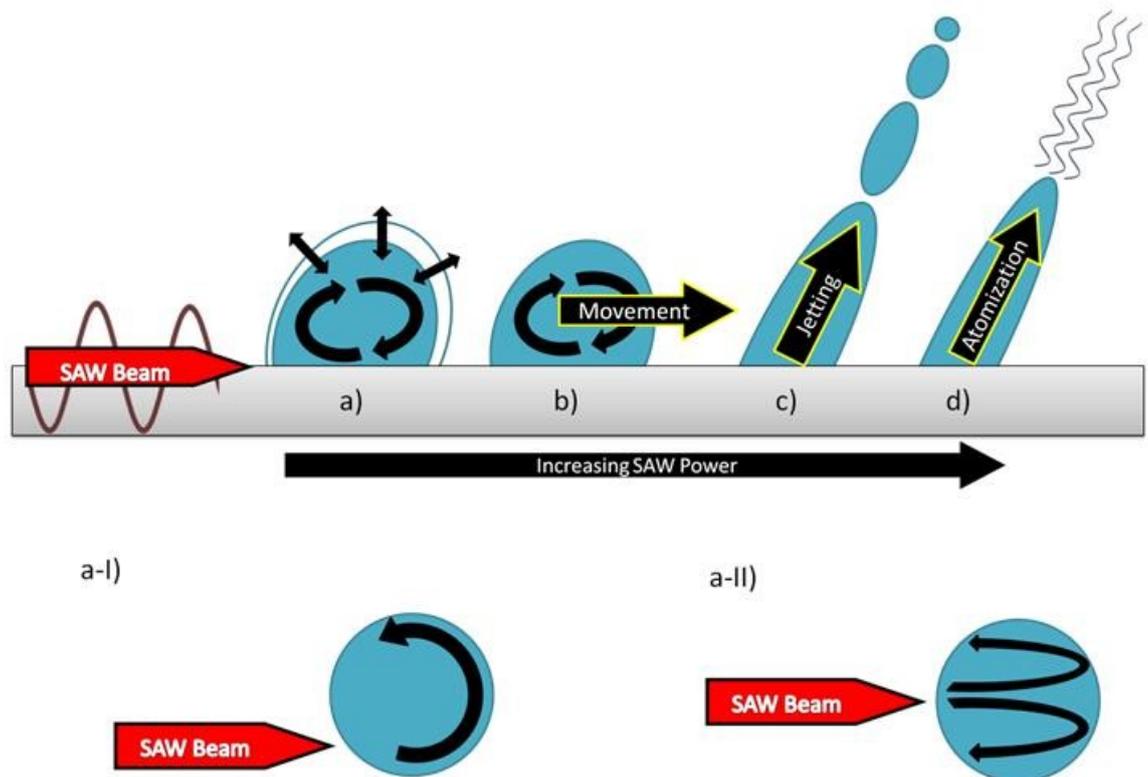
Figure 1. 9 Different behaviours can be obtained from a SAW platform by increasing the applied SAW power. A SAW induced droplet/ liquid sample can be mixed, pushed, jetted or atomized. These options enable the production of various LOC devices based on SAW technology.

When the RF power reaches critical values the droplet, positioned in front of the SAW path, starts to move. Strong acoustic streaming creates an inertial force and drives the droplet, however, the mixing effect inside the droplet continues during the motion. This is used for sample collecting/ dispensing and pumping applications [46]. After increasing SAW power to a secondary critical level, the liquid is jetted into the air [46][65]. Finally, if the power is further increased, the droplet atomise due to the strong capillary waves appearing at the air-liquid interface [60]. SAW actuated atomization was used in inhalers for rapid generation of protein aerosols [60]. The critical values depend on the IDT design (such as finger shapes, number of fingers), fabrication quality, surface hydrophobicity under the mass of the sample and properties of the sample (viscosity, volume, density).

Fouling and clogging, in large or micro-scale applications, is a common issue in chemical and biological processes. SAW driven applications help to minimize those problems. Rapid surface displacements on the surface, due to the travelling SAW, apply a mechanical force onto the coating materials and remove them. This helps to obtain repeatable results from analytical systems. Acoustic treatment also increases the lifetime of the sensing devices by cleaning the measurement chambers and critical sensing surfaces.

1.4.5.   SAW induced mixing

Mixing of two or more substances is an important step of various chemical or biochemical processes, such as protein folding [36] and enzyme reactions [14]. However, it is a delicate and challenging task in micro scale volumes [46][58][66] since the Reynolds number is relatively small (<1) in microfluidic systems [67]. This is caused by the small surface to volume ratio and the viscosity dominated inertia [32]. Thus, the hydrodynamic behaviour of micro-volume liquids makes mixing difficult and slow. Extending the length of mixing microchannel is one of the proposed schemes to promote mixing in passive devices [66]. However Chan and Yang claims that an effective mixing cannot be obtained in channels with the two-dimensional flow, it requires repeating stretching and folding of fluid layers by a chaotic advection mechanism [36]. Electrowetting on dielectric (EWOD) [14], dielectrophoresis (DEP) [68] and acoustics [69] are some of the common micro mixing schemes. Electrowetting technique generates flow advection, by merging and splitting droplets, to enhance mixing of droplets or other microfluidic systems [36].

SAW induced streaming application is a promising alternative method for rapid mixing in microfluidic platforms [70]. The internal flow obtained due to the acoustic effect creates a stirring inside the liquid. While the stirring efficiency is directly related to the size of the droplet, the stirring speed is controlled by the RF power applied on the IDTs [46]. A better mixing can be obtained by keeping the SAW wavelength smaller than the droplet diameter and increasing the RF power [33]. Figure 1. 10 presents a few depictions about the SAW interaction with a droplet pipetted on the surface of a substrate and a superstrate.
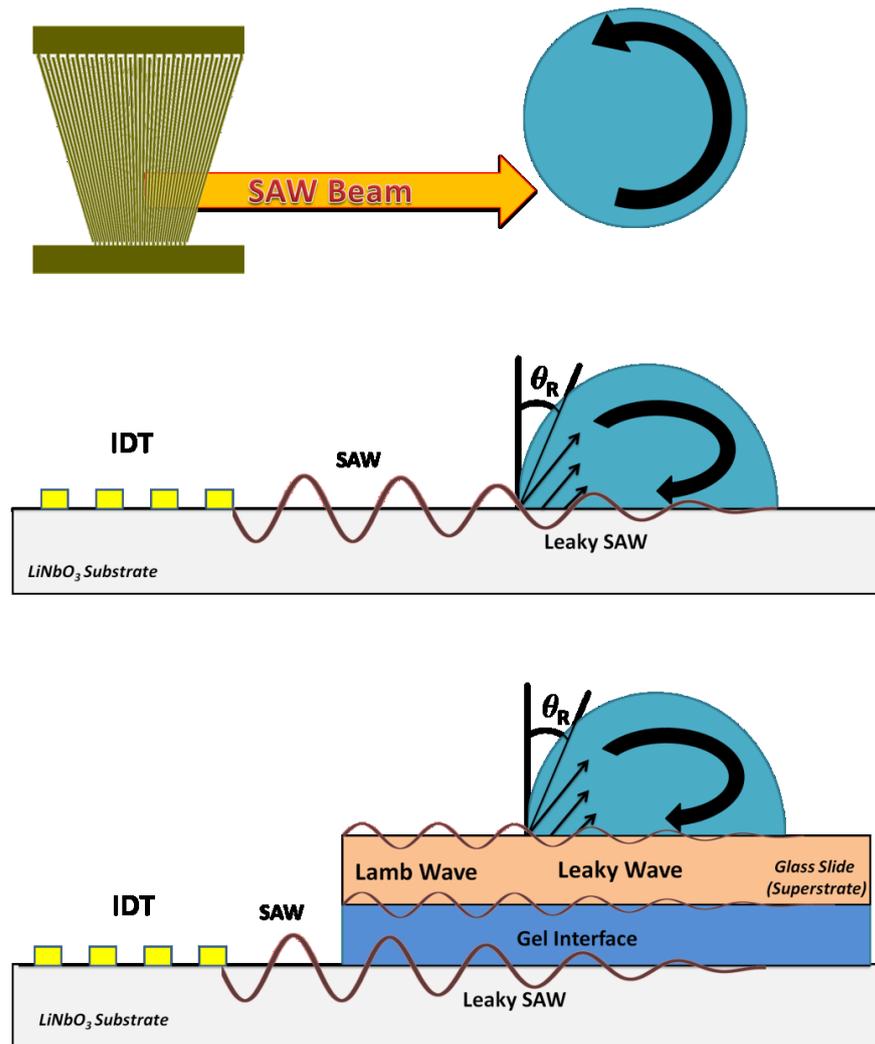
Figure 1. 10 Scheme of acoustic wave propagation from a slanted IDT into a droplet. SAW beam resulting rotational flow (top and side views) is depicted. Acoustic radiation is presented in two different cases. First, when the droplet is on the same plane with SAW device. Second, when the droplet is pinned on a glass slide, which is coupled to the SAW platform with a gel interface. The waveform in the second case is converted from Rayleigh wave to Lamb wave. Note: The drawings are not drawn to the scale.

1.5.   Motivation and objectives

GI system cancers kill more than half a million people every year. Cancer cells can be carried to different parts of the body through blood vessels. At the distant stage, cancer has spread around the human body, organs and tissues. However, early detection, before that stage, can save many lives by enabling timely and high-quality treatments.

GI system cancer diseases may cause occult bleeding such as cancer in the oesophagus, stomach and duodenum. However, it is mostly not possible to notice a small bleeding in the stool before a critical stage. Therefore, development of highly sensitive diagnostic platforms is a need for increasing the survival rate. Moreover, the miniaturisation of the sensing devices is one of the most important targets of the researchers. Smaller and easy to operate devices,

which can be used by people at home, can lead to higher cancer screening rates. Size decrement can enable mass fabrication of the devices and decrease the production costs. Thus, the prevalence rate of cancer screening among low-income and hard-to-reach communities can be increased.

There are existing methods for monitoring blood in the stool by the concept of using the anti-haemoglobin (anti-Hb) antibodies in a sandwich enzyme-linked immunosorbent assay (ELISA). Those techniques can be readily implemented on an electrochemical platform. The electrochemical sensors have proven their ability to work in different environments with high sensitivity levels. Moreover, their sensitivity can be further enhanced by removing the limitations created by the diffusion rates of the electrochemical systems. Sonochemistry and rotating disc electrode (RDE) methods are commonly employed for such purposes by the researchers.

The goal of the Ph.D. was to develop a highly sensitive electroanalytical diagnostic method. Such system would work on haemoglobin sensor application for early diagnosis of cancers with bleeding symptoms. The digital monitoring technique was targeted to be simple to use, reliable and fast. The LOC design would provide simplicity by reducing the amount of bench sized instruments required for tests. The SAW technology, which is commonly used for microfluidic applications, was adapted in the electroanalytical sensing platform to enhance both sensitivity and the speed of the test process. Additionally SAW can increase the reliability of the immunoassay measurements by removing the wrongly occurred bio-molecule bindings.

First measurement series were performed on a model solution system. A three electrode sensing platform was modified by the addition of SAW platform. This gives a similar mixing characteristic to an ultrasound coupled RDE method. The device concept developed through experimental investigations on the SAW device, chamber fabrication and the SAW coupling methods. Secondary tests series were performed by an ELISA using the anti-haemoglobin (anti-Hb) antibodies. The mechanical waves created significant improvements in the sensitivity of the electroanalytical method. As a final stage, the aim of the thesis was extended to mediator based label-free Hb detection method. Experiments performed in stagnant solution cases presented promising quantifiable results.

2. Materials and methods
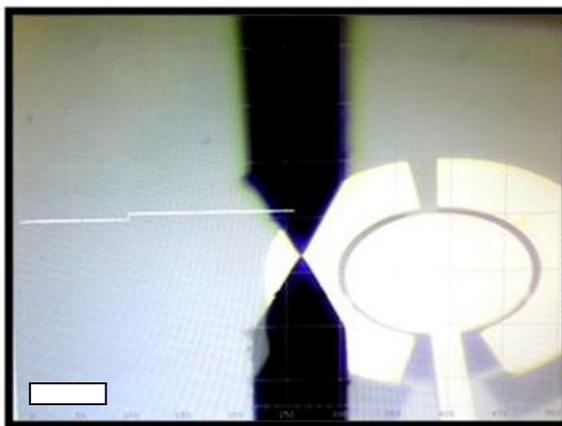
Figure 2. 1 Surface scanning of a microfabricated three electrode system using a Veeco Dektak 6M height profilometer. This device was used to examine the parameters, such as height and surface roughness, of fabricated structures. The structure could be a patterned photoresist or a metal electrode. Therefore, the examination can be done at any stage during the fabrication process. (Scale bar 3 mm)

This chapter includes all the experimental microfabrication (SAW devices, sensing electrodes and hydrophobic patterns), their characterisation methods and electroanalytical test techniques used in the research.

2.1.   Microfabrication

Figure 2. 2 Two glass substrates, fixed on the chuck, after the metallisation (20 nm Ti and 100nm Au) process. At the following stage, the samples were immersed in hot acetone for the lift-off process.

This part includes the photolithography and metal lift-off based protocols developed for the experimental investigations. The fabrication procedures are explained in detail. The depiction

(Figure 2. 3) presents the photolithography process used to obtain empty patterns surrounded with removable photoresist and the lift of process after the metallisation. Three main methods were investigated to decide which to use for the fabrication process through the research.
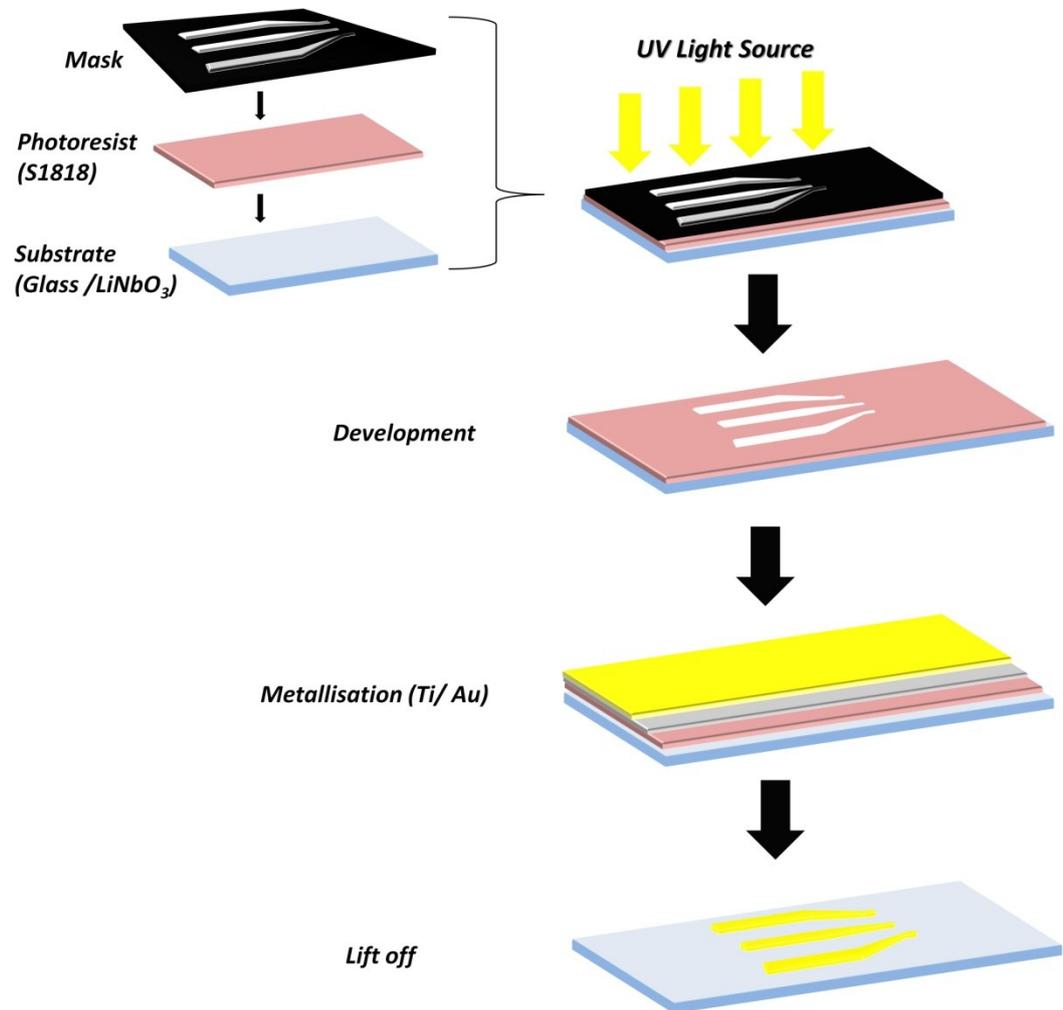
Figure 2. 3 Depiction of a microfabrication process. It includes the patterning of a photoresist (S1818) layer by the development stage after the UV exposure, metallisation process and the lift-off step.

2.1.1.   Mask

The mask is a crucial part of the photolithography process. Two types of masks were used in this research: acetate and glass plate masks. The patterns were designed by L-EDIT (Tanner EDA), and the mask was obtained from JD-photo (http://www.jdphoto.co.uk/).

2.1.2.   SAW actuator

The SAW device is composed of interdigitated electrodes located on a piezoelectric material. The IDTs were microfabricated via photolithography and metal patterning techniques. However, three different resist coating techniques were tested to obtain the best

photolithography recipe. The methods were applied to three different samples at the same time. The surface of the S1818 layer on the first sample was hardened by a predevelopment process to obtain undercuts. The second sample was directly coated with an S1818 layer without any previous or post process. The surface of the third sample was spin-coated with a lift-off resist (LOR) before the S1818 spin-coating.

The photolithography process started with cleaning the piezoelectric substrates (128° Y-cut X-propagating 3 inch $LiNbO_3$) in acetone bath (5-minute sonication). All three samples were rinsed with flowing water for 2 minutes and blow-dried with N_2. Then they were treated in O_2 Plasma for 3 min at 100 W. Only the third wafer was spin-coated with 0.5 μm thick LOR (30 s at 4000 rpm) and baked on a hot plate at 115 °C for 3 minutes. Following that, all the samples were spin-coated with ~1.9 μm thick S1818 photoresist (30 s at 4000 rpm) and baked on a hot plate at 95 °C for 3 minutes. The two-dimensional profile of a developed S1818 pattern is presented in Figure 2. 4. Only the first sample was soaked in a 1:1 (v:v) dilution of Microposit developer and water for 2 minutes and rinsed under flowing water for 30 seconds. The pattern on the mask was transferred into the photoresist layer by ultraviolet light (UV) exposure for 5 s (MA-6, SUSS Micro Tec AG) and development using a 1:1 (v:v) dilution of Microposit developer and water (first sample: 4 minutes, second sample 1.5 minutes and third sample: 1 minute). Photoresist particle residues after lift-off were removed by rinsing the samples under flowing water for 5 minutes. After blow-drying all the samples were treated in O_2 Plasma again for 2 min at 60 W. A 20 nm titanium adhesion layer and a 100 nm of gold layer were evaporated on their surfaces prior to the lift-off in acetone (at 45 °C) for 2 hours. The third sample was additionally soaked in 1165 stripper solution (at 50 °C for 15 minutes) to remove the LOR layer (Figure 2. 10). Finally, all unwanted parts of the metal layer were removed by lifting off the photoresist layer underneath, and the IDT fingers were obtained.
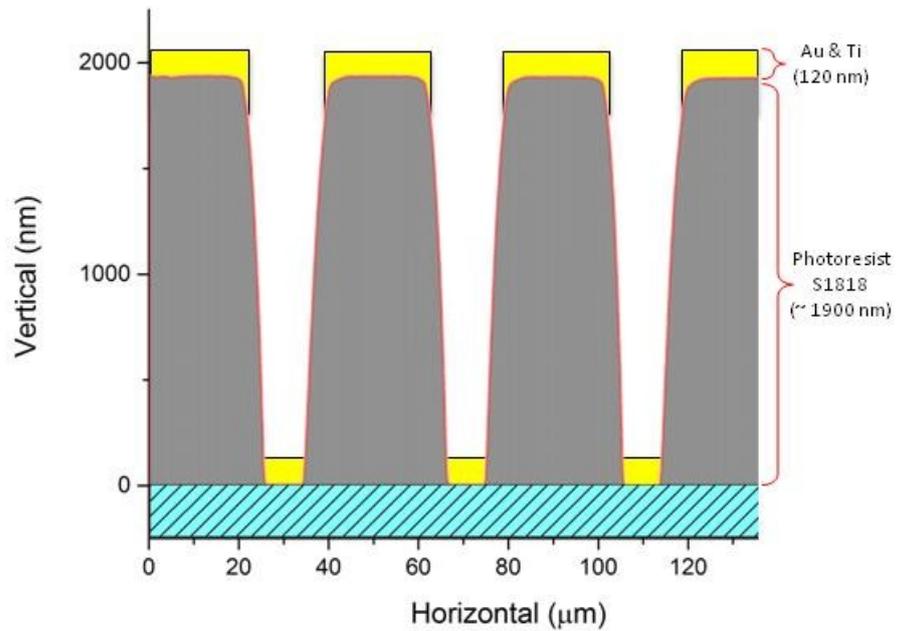
Figure 2. 4 Surface profile of an S1818-photoresist pattern (grey area), on a LiNbO₃ substrate, after the development stage is presented. The measurement determined using a Veeco Dektak 6M height profilometer. A 20 nm titanium adhesion layer and a 100 nm of gold layer (yellow area) were evaporated on this pattern. The metal layer is presented above the grey colored image as a scetch. Ater the final process, lift-off in acetone (at 45 °C) for 2 hours, the photoresist layer was removed and the metal structures localised directly on the substrate surface were obtained.
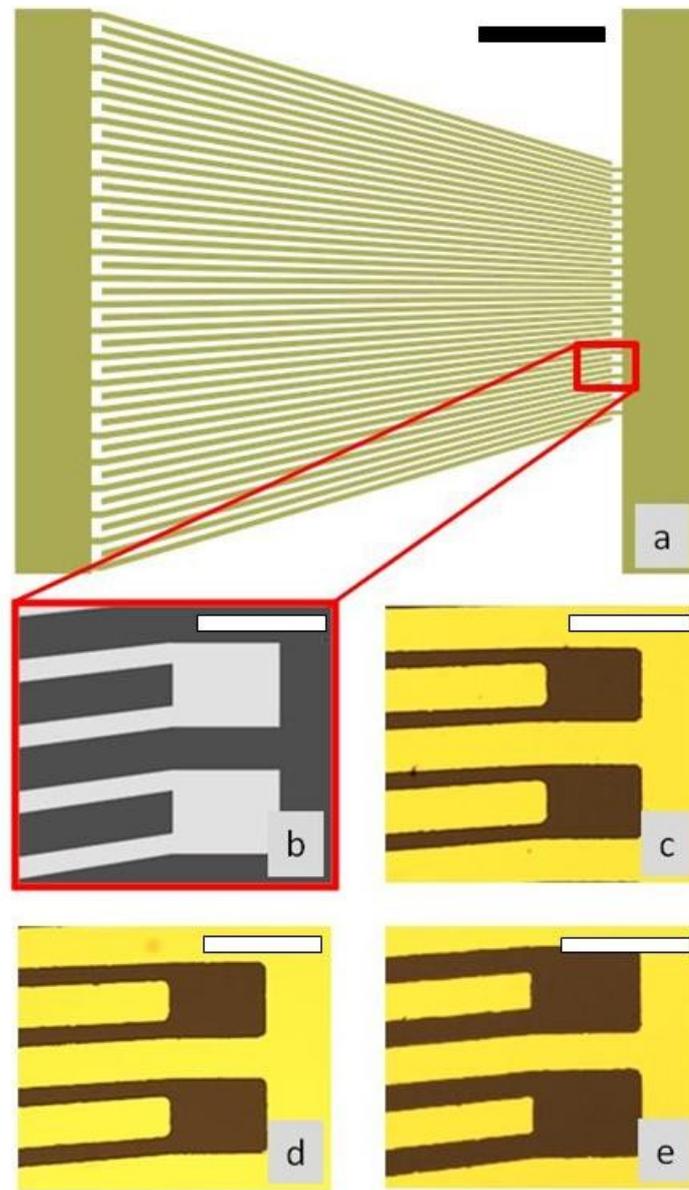
Figure 2. 5 Electrode fabrication results obtained via first (c), second (d) and third (e) fabrication methods. Microscope images are the fabricated fingers. Results show that the LOR (third) method gives sharper corners than the other two techniques. Therefore, the result is more identical to the pattern on the mask (b). The white scale bars represent 240 μm and the black scale bar represents 2.5 mm distances on relevant images.
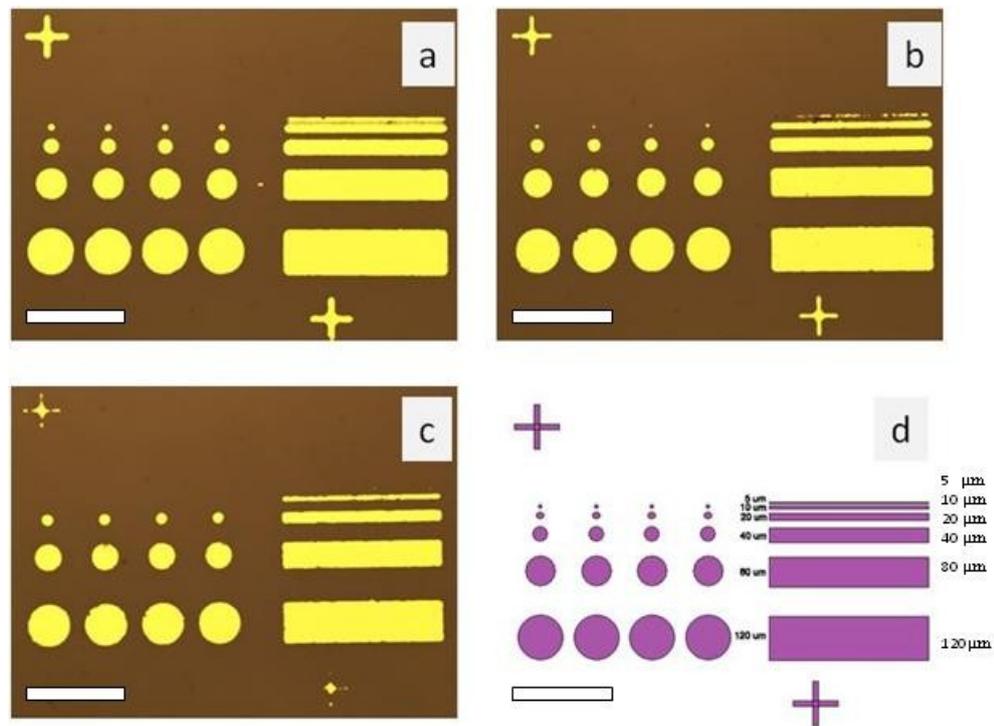
Figure 2. 6 Comparison of three different fabrication techniques (first: a, second: b, third: c) via light microscope images. The circular and straight structures on the mask pattern (d) has varying sizes (5, 10, 20, 40, 80 and 120 µm). The experimental fabrication process of the alignment mark shows that the first (predevelopment included) technique can give metal patterns with a higher resolution (10- 20 µm).

Additional marks added at the corners of the design pattern used for aligning the masks. They also helped to fabricate secondary designs at precise locations on the previously fabricated structures.

Results obtained from three different fabrication recipes are presented in Figure 2. 5 and Figure 2. 6. Outcomes show that the third protocol gives sharper corners and more identical shapes with the actual mask pattern. However, the minimum size of the fabricated structure was not lower than the edges of metal features are not as straight as the first method.

Figure 2. 8 presents the minimum structure sizes which could be obtained with three different methods. The first method gave the smallest features, 10 wide fingers and circles with 10 µm radiuses. The results obtained from the second technique were not as good as the first method (20 wide metal fingers). The third technique gave the largest structures. The low-resolution issue was due to the relatively large undercut obtained with LOR (see Figure 2. 8). The problem can be solved by using a thinner LOR, such as LOR1A. Another disadvantage of the LOR included protocol is the additional steps which take extra time to fabricate.

The fabrication tests on the glass gave the same results with the LOR based technique. Overall, the first method, including a pre-development process, was chosen as the protocol to be used for the micro-fabrication process through the research.

2.1.3.   Sensing electrodes

Different types of electrodes were designed and fabricated for electroanalytical tests. Previously explained three different microfabrication protocols gave similar results for the fabrication of circular shaped electrodes (Figure 2. 7). Fabrication on different substrates (Glass and LiNbO$_3$) gave similar results.
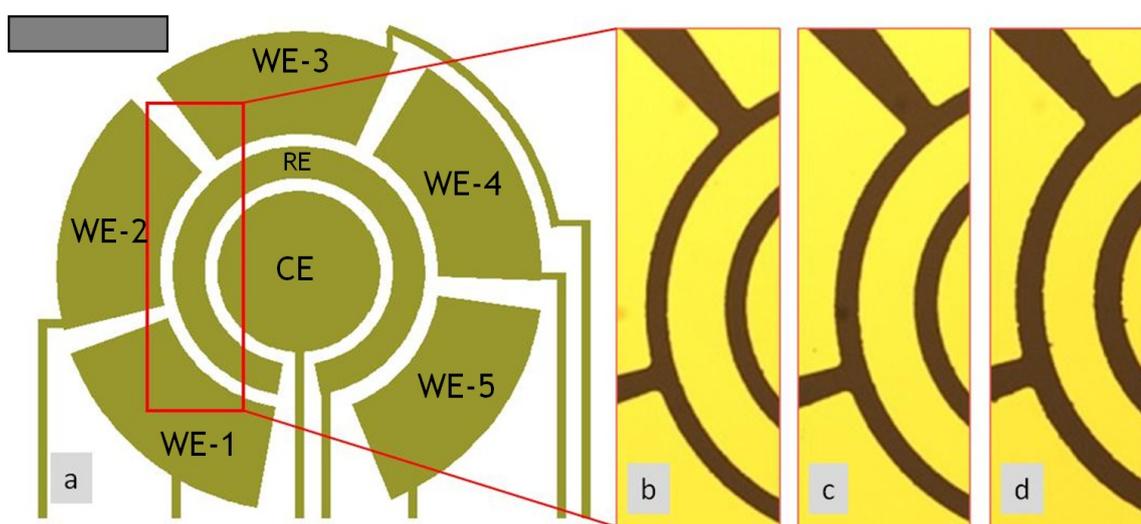
Figure 2. 7 Sensing electrode (a) fabrication results with first (b), second (c) and third (d) techniques. This electrode has a reference electrode (RE), the counter electrode (CE) and five different working electrodes (WE-1,2,3,4,5) to perform five different measurements in the same solution. Images were obtained via a light microscope. (Scale bar 0.5 mm)
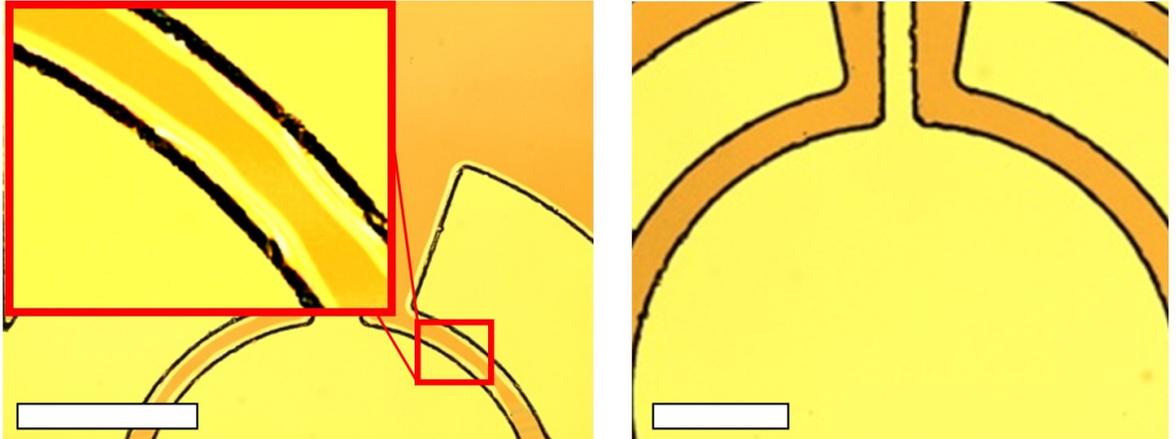
Figure 2. 8 The photoresist (S1818) patterns (dark coloured areas) obtained after the development stage. The undercut shown in the image (Left) appears due to the LOR layer under the photoresist. When LOR is not used, no undercut appears as shown (Right). (Scale bars 125 µm)
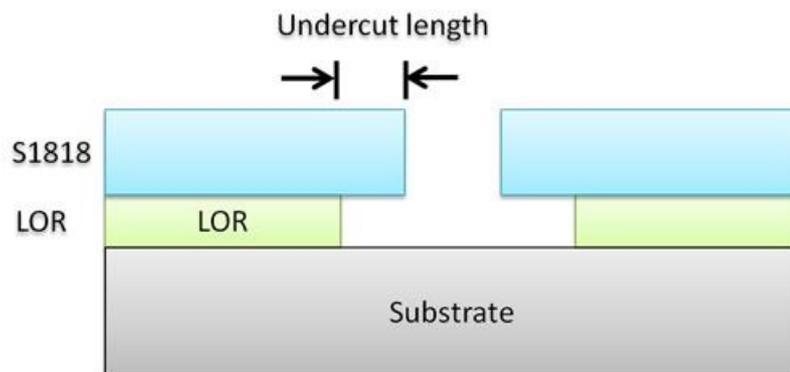
Figure 2. 9 A depiction of the undercut profile of S1818/ LOR layer. The length of the overhanging LOR layer is defined as the undercut length. The depiction presents the case shown in the previous image.
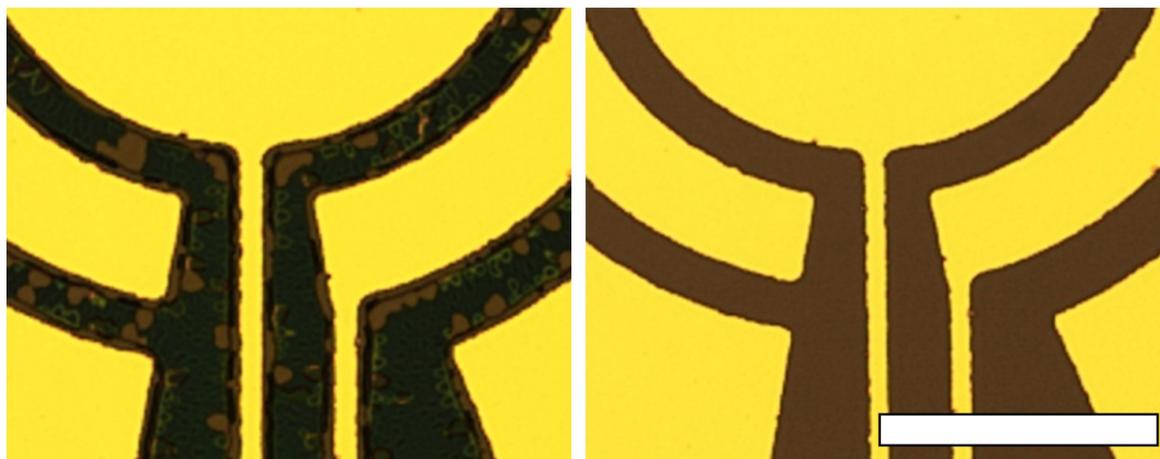
Figure 2. 10 Lift-off images of the substrate patterned via the third (LOR) method. Lift-off with acetone can remove only the S1818 layer with the gold layer on it. However, the Stripper-1165 removes the remaining LOR layer (at the bottom), and the actual metal (gold) pattern is obtained. (Scale bar 0.25 mm)

LOR included method did not give straight and smooth edges. The reason can be the large undercut lengths (Figure 2. 8 and Figure 2. 9). Therefore, the technique requires further investigations to obtain shorter undercuts. Lollypop shaped electrodes (Figure 2. 11) and various three electrode designs (Figure 2. 12) were fabricated for experimental investigations via the first method. The electrodes were used for electroanalytical (cyclic voltammetry / amperometry) tests of the ferrocyanide-ferricyanide redox couple. Also, thickness characterization tests of polymer (polypyrrole) chains immobilized on electrode surfaces were performed with the use of lollypop electrodes.
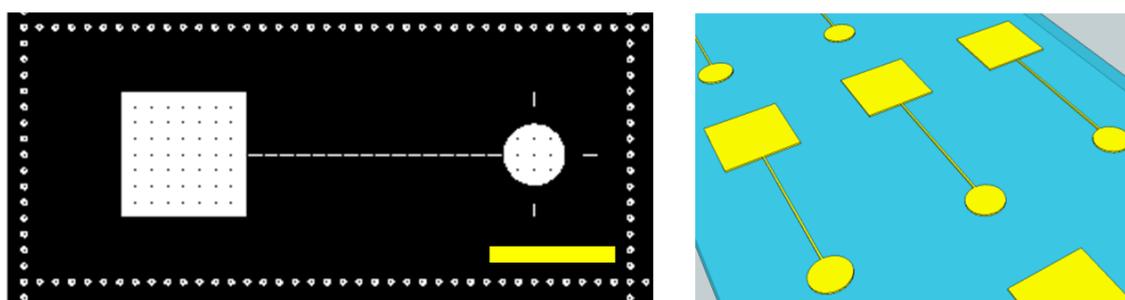
Figure 2. 11 Lollypop electrode mask (Left). The radius of the circle was defined as 1 mm. Schematic of the fabricated electrodes, on a glass slide (Right). The lollypop electrodes fabricated by this design were used for cyclic voltammetry tests of the ferrocyanide-ferricyanide redox couple. Also, the electrodes were used for thickness characterisation of polypyrrole polymer chains immobilized on electrode surfaces. (Yellow scale bar 2 mm)
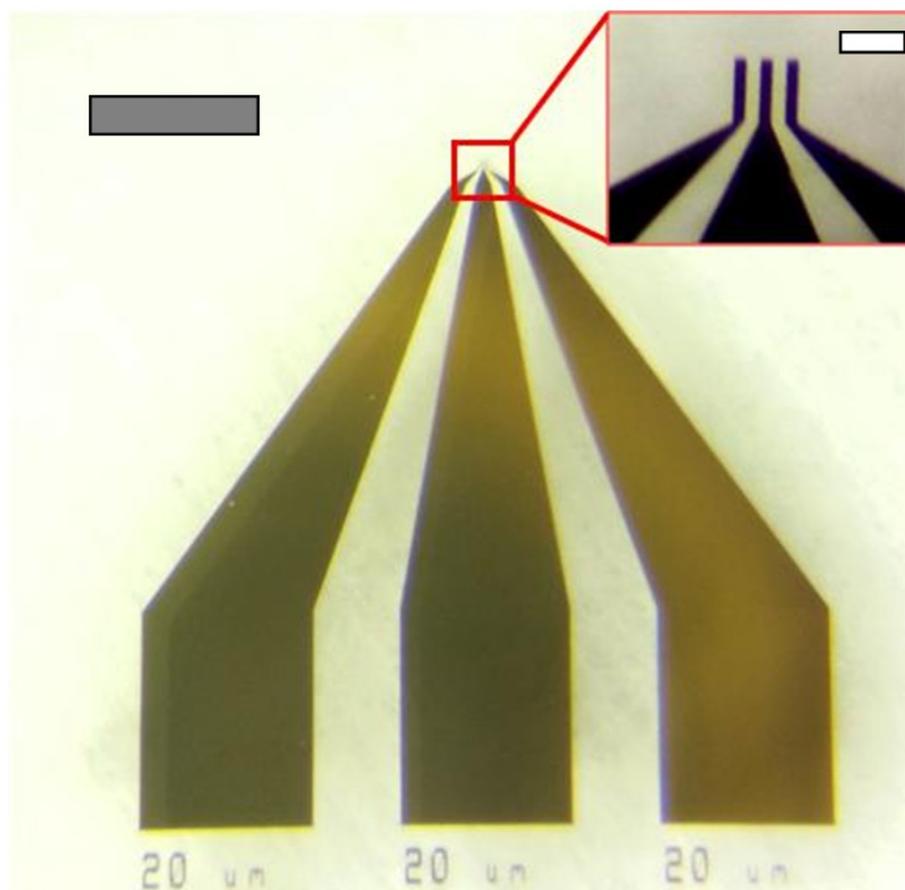
Figure 2. 12 Three-electrode design used for cyclic voltammetry experiments. Both the electrode width and the distance between electrodes were defined as 20 µm. The length of the straight parts of the electrodes was 100 µm. The images were obtained with a Nikon light microscope. (Grey scale bar 1.5 mm, white scale bar 100 µm)

Connection pad resistivity
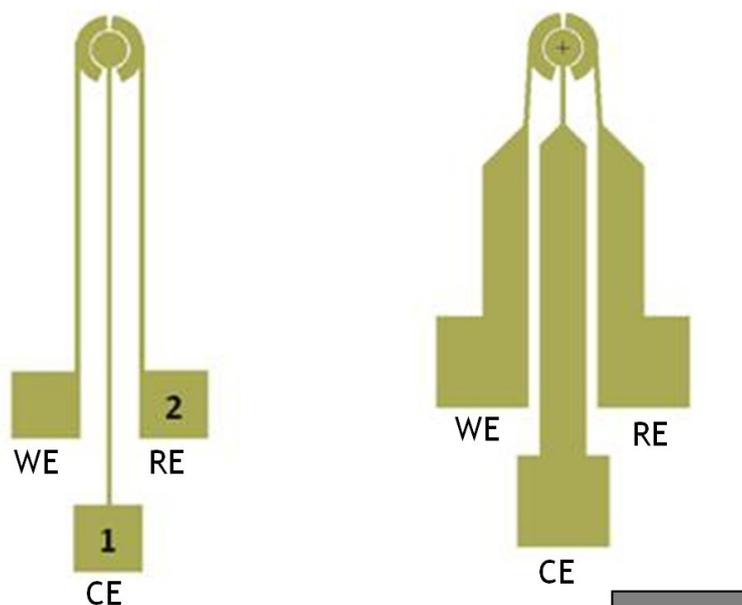
Figure 2. 13 electrodes fabricated by sputtering 10nm Ti and 100nm Au. The three electrode system with thin (100 μm) connection pads was (Left) replaced with a new design (Right) due to the resistivity problem. The resistivity values between the electrodes and the connection pads (1 and 2) were, 52.2 and 32.5 ohm. (Scale bar 3 mm)

The fabricated electrodes did not work consistently during the electroanalytical tests. Investigations showed that the current flowing through the pads were very tiny due to the highly resistive connection pads. Therefore, the applied voltage was not being efficiently transferred into the electrochemical cell. In order to solve the problem, the width of the connection lines was increased up to 1000 μm from 100 μm. This modification decreased the resistivity down to 5 and 7.7 ohm, and the electrochemical analyser started to give quantitative results from the sample solutions.

2.1.4.   Sample holding features

The wetting effect and the electric charge on the gold surface drag the fluid along the electrode connection pads. Moreover, the SAW radiation creates more water spread due to the powerful pressure waves [71]. Different methods (droplet traps and chambers) were applied to keep the shape of the samples during the electroanalytical measurements. Fixing the area of the electrode, covered with the electroanalytical sample, is relatively important to obtain quantifiable data.

Hydrophobic patterns

Hydrophobic patterns are commonly used in various types of applications for different purposes such as droplet pinning [72][73] and droplet handling [74]. Two different hydrophobic materials were tested in this work: Teflon (Du Pont, 6% (w/w) solids contents, Teflon AF 601S2 - Du Pont) and trichlorosilane (trichloro(1H,1H,2H,2H-perfluorooctyl)silane - Aldrich).

Teflon patterning

Teflon coating creates highly hydrophobic surfaces due to its low surface energy [75]. The method is applied in bio patterning applications (i.e. neural cell) [75][76], droplet manipulation in microfluidic chips [49], digital microfluidic devices [77] and a SAW induced microfluidic motor for fluid trapping under the disc rotor [78].

Teflon patterning process (Figure 2. 14) was started by wafer (1mm thick glass slide and $LiNbO_3$) cleaning, in acetone bath (5-minute sonication). The substrates were rinsed in flowing water for 2 minutes, blow-dried with N_2 and treated in O_2 Plasma (3 min at 100 W). They were spin-coated with ~1.9 μm thick S1818 photoresist (30 s at 4000 rpm) and baked on a hot plate at 95 °C for 3 minutes. The pattern (circle with 1.5mm radius) on the mask was transferred into the photoresist layer by ultraviolet light (UV) exposure for 5 s (MA-6, SUSS Micro Tec AG) and development, using a 1:1 (v:v) dilution of Microposit developer and water (1.5 minutes) and rinsed under flowing water for 5 minutes to clean the lifted photoresist particles. After blow-drying, all the samples were treated in O_2 Plasma again for 2 min at 60 W. The first Teflon layer was created by spin-coating 0.2 % (w:w) Teflon AF solution at 3000 rpm (reaching to 3000 rpm in 25 seconds) for 1 minute. The second hydrophobic layer was obtained by spin coating 1.2 % (w:w) Teflon AF solution with the same parameters. Teflon AF solutions were obtained by dilution with a perfluorinated solvent (CAS 86508-42-1, Larodan Fine Chemicals AB). In order to convert the Teflon layer into a permanent form, the samples were baked at 150°C for 8 minutes. However, the hard baking step caused two problems. Firstly, the $LiNbO_3$ substrate broke into pieces after removing it from hot-plate to a watch glass, because the piezoelectric material is not durable against temperature changes. The second problem was the photoresist, underneath the Teflon, which also became a permanent (pink coloured) structure. Sonication of the glass slide in acetone could not remove the photoresist, and caused micro scale cracks on the Teflon surface. After 5 minutes sonication, the entire Teflon layer on the surface lifted off from the surface of the glass substrate. This case shows that the Teflon coated substrates should not be sonicated.

UV Light Source

a)

b)

c) Acetone

d)

| Substrate (Glass) | AU (100nm) | S1818 (1900nm) | Teflon 800nm | mask |
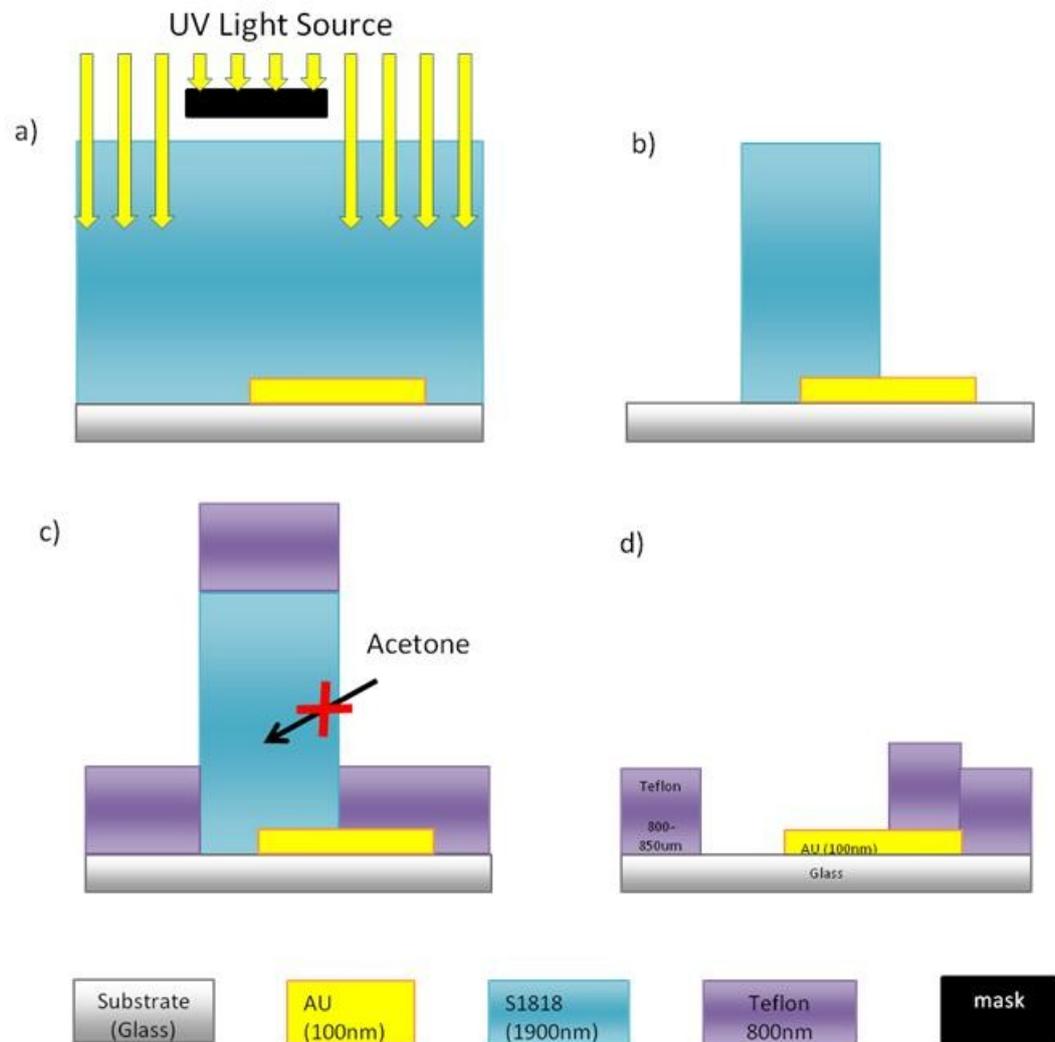
Figure 2. 14 Schematic presentation of Teflon AF patterning. The photoresist (S1818) layer was patterned via photolithography technique. First Teflon AF layer was created by spin-coating the 0.2 % (w:w) Teflon AF solution at 3000 rpm (reaches 3000 rpm in 25 seconds) for 1 minute. The second layer was obtained by spin coating 1.2 % (w:w) Teflon AF solution with the same parameters. However, the proposed final Teflon AF pattern could not be achieved (d) because the acetone did not lift-off the hard baked S1818 layer (c).

An LOR coating stage was added to the protocol to solve the lift-off problem (Figure 2. 15). The substrate (glass) was spin coated with 200 nm thick LOR1A (1 minute at 2000 rpm) and baked at 150 °C for 20 minutes before the S1818 spin-coating. After following the same stages with the previous recipe, the lift-off process was performed with Shipley Remover 1165 on Teflon AF coated surface. However, the unwanted parts did not come off because the Teflon layer was thicker than the LOR layer and did not allow the remover solution to reach the LOR. This problem was solved by increasing the speed of the Teflon spin coating process from 2000 to 4000 rpm that decreased the Teflon thickness down to 150 nm. Finally, the hydrophilic trap was obtained after removing the photoresist layer from the substrate surface. After the unwanted Teflon AF sections had been lifted off, the substrate was washed in a bath of isopropanol then water, and was blow-dried.
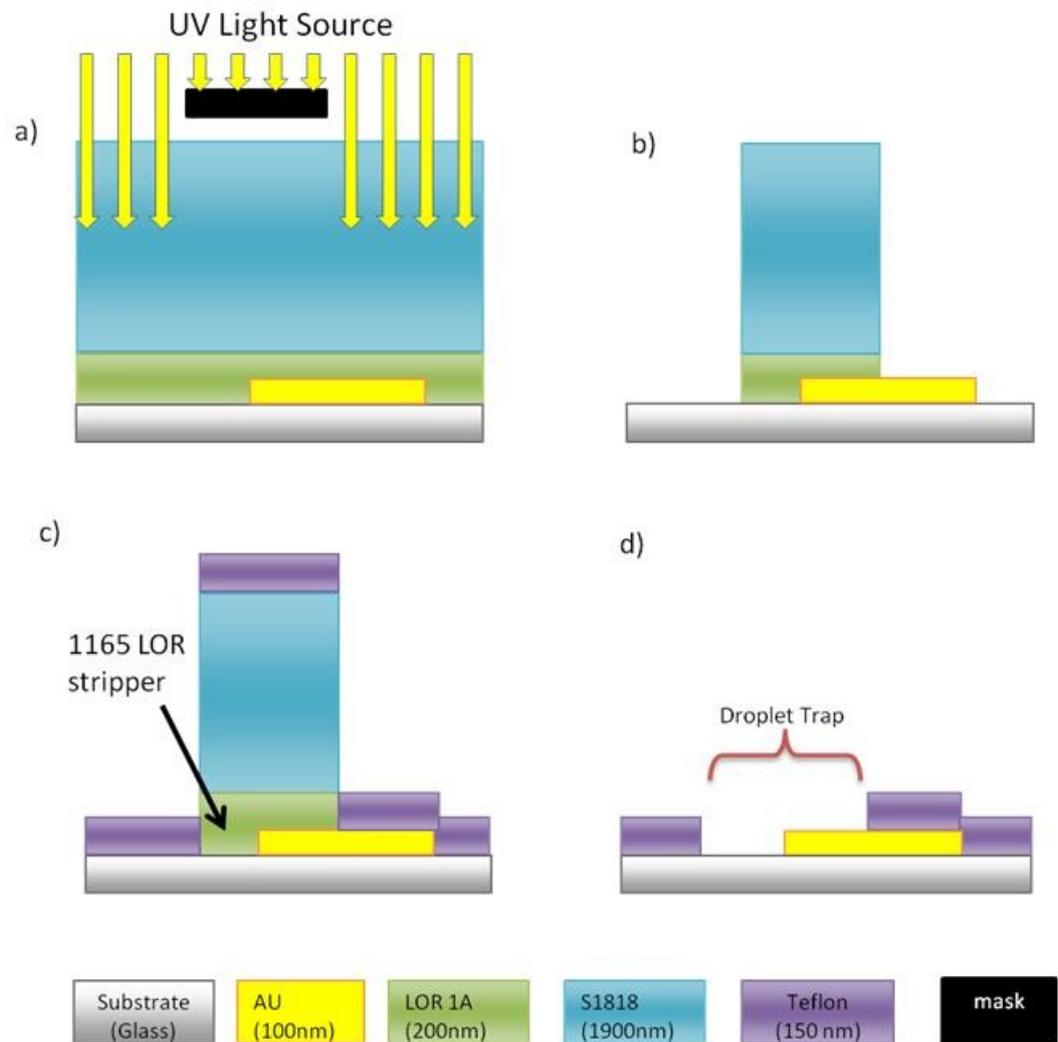
Figure 2. 15 Depiction of LOR included Teflon AF patterning process. LOR coating prior to the S1818 coating process enabled the removal of unwanted Teflon parts. Finally, the Teflon surrounded hydrophilic sample traps were obtained (d).

The Teflon based droplet traps were used in SAW induced voltammetry tests. Teflon is an active hydrophobic material. However, it has a limited adhesion on substrates since the attachment is not based on a chemical bond [79]. The hydrophobic layer was not stayed on the surface after the first SAW induced electroanalytical test. Therefore, this method does not suit for the SAW induced electroanalytical measurements.

Hydrophobic silane patterning

Same steps in the device fabrication process were followed until the development stage of the S1818 layer. The samples kept in a solution consisting trichloro(1H,1H,2H,2H-peruorooctyl)silane (Aldrich) and heptane (30µl:50 ml) for 10 min then removed into a beaker filled with acetone (50 $^{\circ}$C for 3 minutes). Rinsed samples (under flowing water for 3 minutes) were ready to be used. The droplet traps fabricated on glass, LiNbO$_3$, silicone substrates by silanised patterns could still stay on the surface even after 30 experiments

performed in the chamber. However, the electrodes were not coated with a hydrophobic layer because, the trichlorosilane does not bind on the gold surfaces (Figure 2. 16). Therefore, the sample spread along the gold areas during the electroanalytical measurements due to the charge difference between the sample and the electrode. Moreover, SAW increases the spreading effect. This problem was minimised by using circular shaped electrodes which had thin connection lines (100 µm wide) to the cable connection pads (Figure 2. 16).
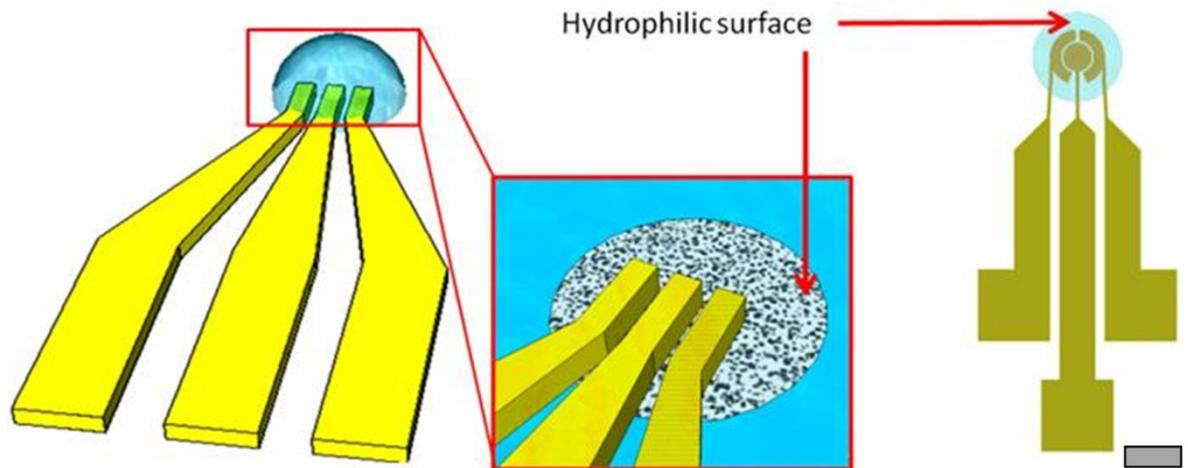
Figure 2. 16 Schematic of the three electrode designs with hydrophilic traps. The traps were made by surrounding a specific area with hydrophobic silane layer. Left: straight electrodes, Right: circular electrodes. (Scale bar 1.5 mm)

The method was revised (Figure 2. 17), by adding a gold modification stage, to make its surface hydrophobic. The substrate (glass) was spin coated with 200 nm thick LOR1A (1 minute at 2000 rpm) and baked at 150 °C for 20 minutes. A thin (5000 nm) SU8 (SU8-3005) layer was spin coated and patterned, via photolithography, to secure the hydrophilic trap area. The glass surface was functionalised with the hydrophobic silane as explained previously. Secondly the gold surfaces were functionalised with 10 mM hydrophobic thiol;1H,1H,2H,2H-perfluorodecanethiol (PFDT) in ethanol for 8 hours. Finally, the sacrificial resist layer was lifted off by keeping the substrate in 1165 LOR stripper at 50 °C for 10 hours.
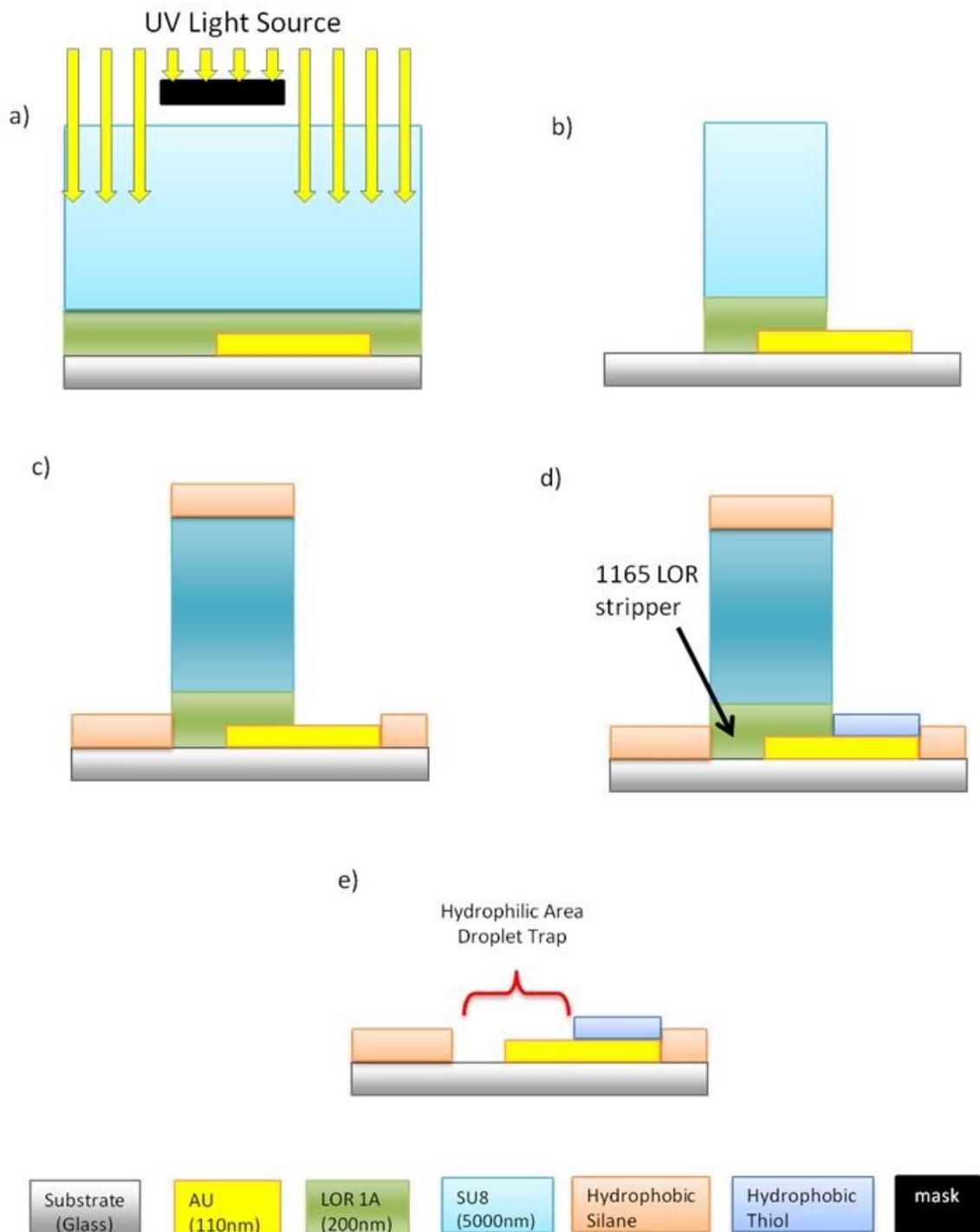
Figure 2. 17 Depiction of the hydrophilic trap fabrication. The substrate was LORA thin SU8 layer is used for hydrophobic layer patterning. The substrate (glass) was spin coated with 200 nm thick LOR1A (1 minute at 2000 rpm). A thin (5000 nm) SU8 (SU8-3005) layer was spin coated and patterned, via photolithography, to secure the hydrophilic trap area. The glass surface was functionalised with the hydrophobic silane. Secondly the gold surfaces were functionalised with a hydrophobic thiol;1H,1H,2H,2H-perfluorodecanethiol (PFDT) in ethanol for 8 hours. Finally, the sacrificial resist layer was lifted off by immersing into LOR stripper solution.
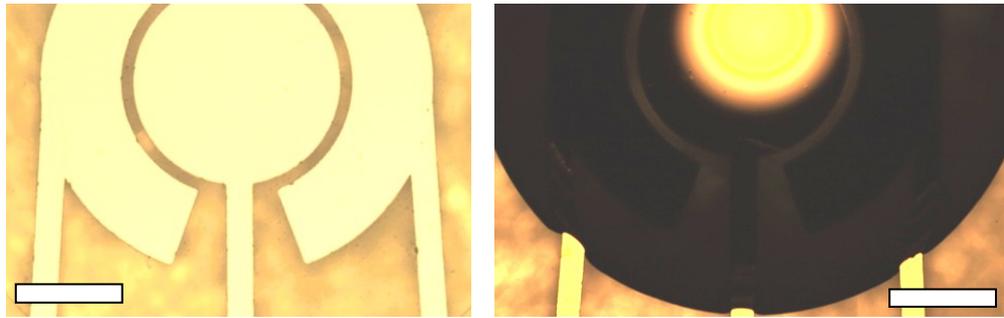
Figure 2. 18 A three electrode system with and without a water droplet (three µl), pinned on it. The droplet is surrounded with a hydrophobic silane pattern on glass surfaces and a hydrophobic thiol on the gold surface. The hydrophobic patterns keep the shape of the droplet constant. However, this method is not very practical since it requires two separate coating steps for each material surface. (Scale bars 0.3 mm)

This modified method is capable of structuring hydrophobic layer both on glass and gold surface (Figure 2. 18). However, the fabrication process is complicated and requiring long time periods. Another disadvantage is the LOR baking stage at 150 °C since it breaks the piezoelectric substrate.

SU8 chamber

One of the techniques for a sample trap fabrication was using a thin layer of SU8 (SU8-3005) negative photoresist as a sample chamber. SU8 was used instead of the hydrophobic saline. The droplet spreading problem was solved with the use of SU8 since it was also able to bond to gold surfaces.
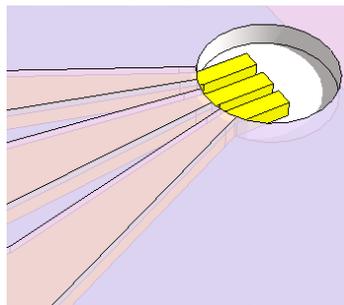
Figure 2. 19 Schematic of a droplet trap (surrounding the electrodes) made with as SU8 negative photoresist pattern. The height of the pattern was 5 µm.

A glass substrate (with a three-electrode system on it) was cleaned in acetone sonication for 5 minutes. Plasma treated samples were 5000 µm SU8 spin-coated at 4000 rpm for 30 seconds and soft baked at 95 °C for 5minutes. The circular pattern was transferred on the resist via UV exposure (30 seconds). Samples were prebaked at 65 °C for 1 minute, and post baked at 95 °C for 3 minutes then they were developed in Microposit EC Developer for 1

minute and rinsed with IPA for 10 seconds. The SU8 structures were ready for experiments after hard baking at 180 °C for 20 minutes.
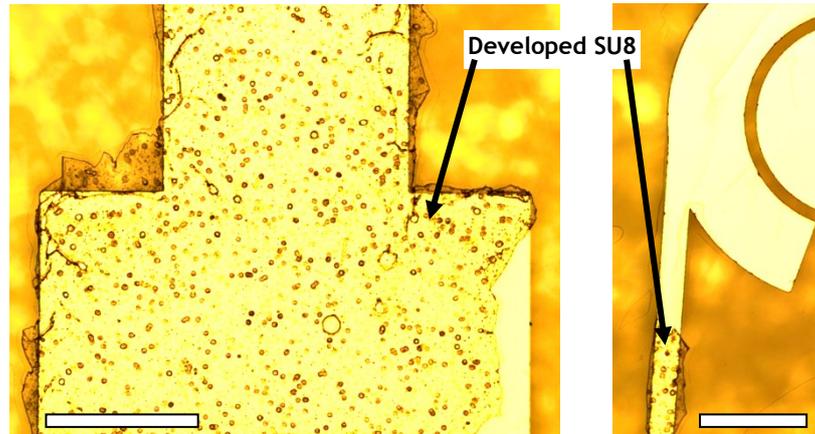
Figure 2. 20 SU8 bonding on a gold surface. Images are taken after the development stage. Due to the insufficient exposure time (5 s) the SU8 did not bond on the glass surface. (Scale bars 0.5 mm)

Figure 2. 20 shows that only the non-transparent parts remained after a short (5 seconds) UV exposure. This shows that the SU8 adhesion on gold was even better than glass. A well defined circular SU8 pattern (Figure 2. 22) was obtained after 5 seconds exposure time was increased to 30 seconds.
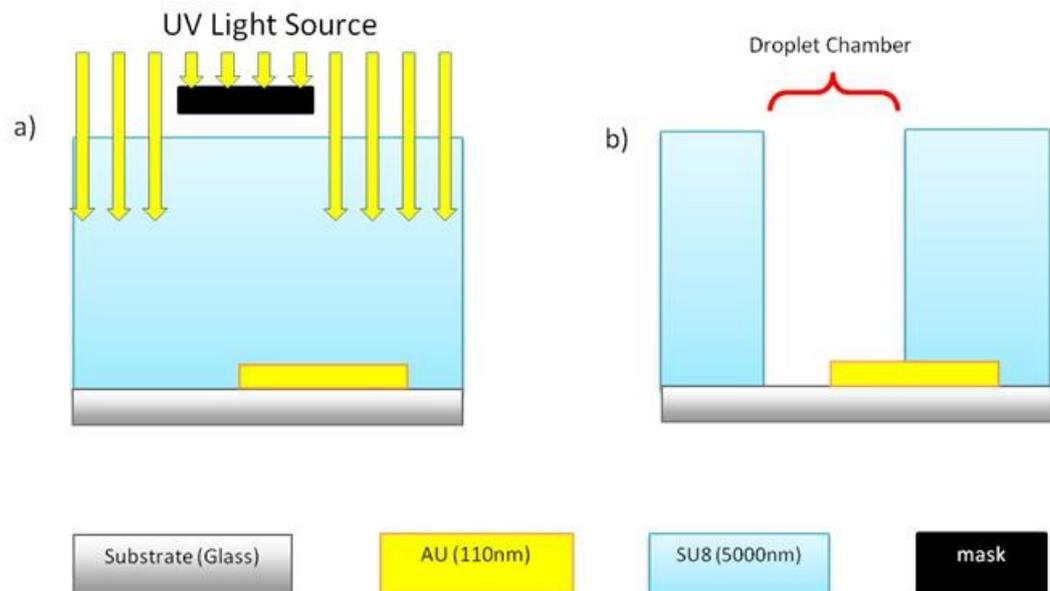
Figure 2. 21   Depiction of the trap fabrication with a hard baked SU8 pattern. The circular pattern was transferred on the resist via UV exposure (30 seconds). The sample was developed in Microposit EC Developer for 1 minute and rinsed with IPA for 10 seconds.
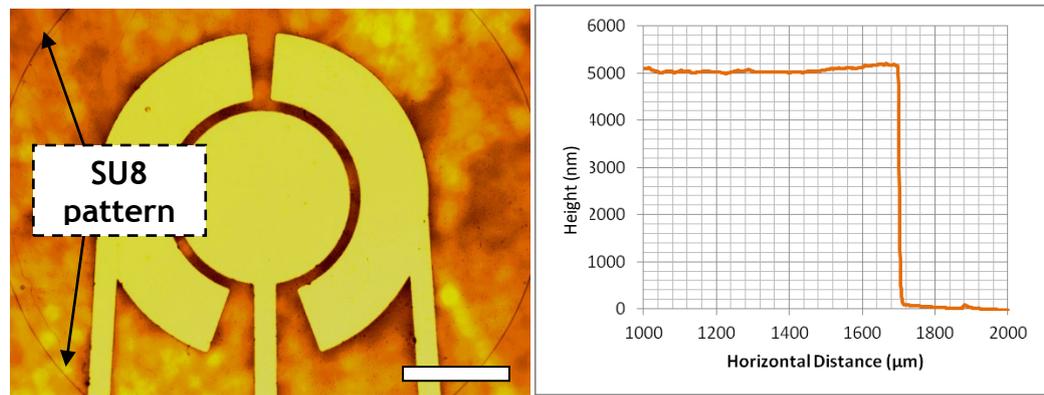
Figure 2. 22 The SU8 pattern around the three electrode sensing system (Left) after the fabrication. Surface profile (Left) determined using a Dektak profilometer shows the height of the chamber (5 µm). (Scale bar 0.5 mm)

Hard-baked SU8 remains on the surface permanently and repels the water. Therefore, the droplet stays in the surrounded circular area. The disadvantage of this method is the hard baking stage (180 °C). The technique cannot be used on a SAW platform since the high temperature can easily break the LiNbO$_3$ substrate.

PDMS Chamber

Polydimethylsiloxane (PDMS) is commonly used for channel fabrication in microfluidic applications [47]. This chapter explains the fabrication and bonding stages of a PDSM chamber on sensing platforms.
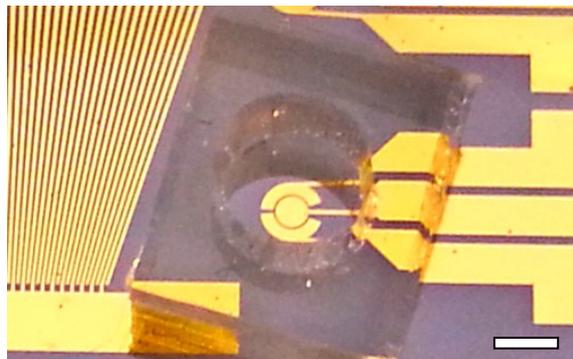
Figure 2. 23 Image of a PDMS chamber bonded on a piezoelectric substrate. The chamber is used to hold the sample on the sensing electrodes during the SAW induced fluid streaming. (Scale bar 1.5 mm)

The PDMS reaction chamber was prepared by mixing elastomer (Sylgard 184) with a curing agent (Sylgard 184), at a 1 to 10 weight ratio and then poured onto a solid hydrophobic surface. Following the degassing under vacuum, the PDMS was cured at 65 °C for 2 hours and peeled from the surface. A hole with 1.75 mm radius was drilled through the PDMS cube (W: 6mm, L: 6mm, H: 4mm) to form a sample chamber. Both the PDMS cube and LiNbO$_3$ substrate

was treated with O_2 plasma technique [47][80] (Gala Instruments Plasmaprep 5) for 1 minute (at 80W) to facilitate bonding to each other.

Using a PDMS structure as a sample chamber has various advantages. The process does not lead to any problem with the existing devices (SAW IDTs and sensing electrodes) on the wafer since the chamber is fabricated separately. Binding on a $LiNbO_3$ substrate surface does not require treatments at high temperatures and does not risk the fragile wafer. Moreover, the chamber can be covered from the top. Thus, the closed chamber stops the evaporation caused by the SAW streaming.

2.2.   Characterisation

2.2.1.   Hydrophobicity analysis
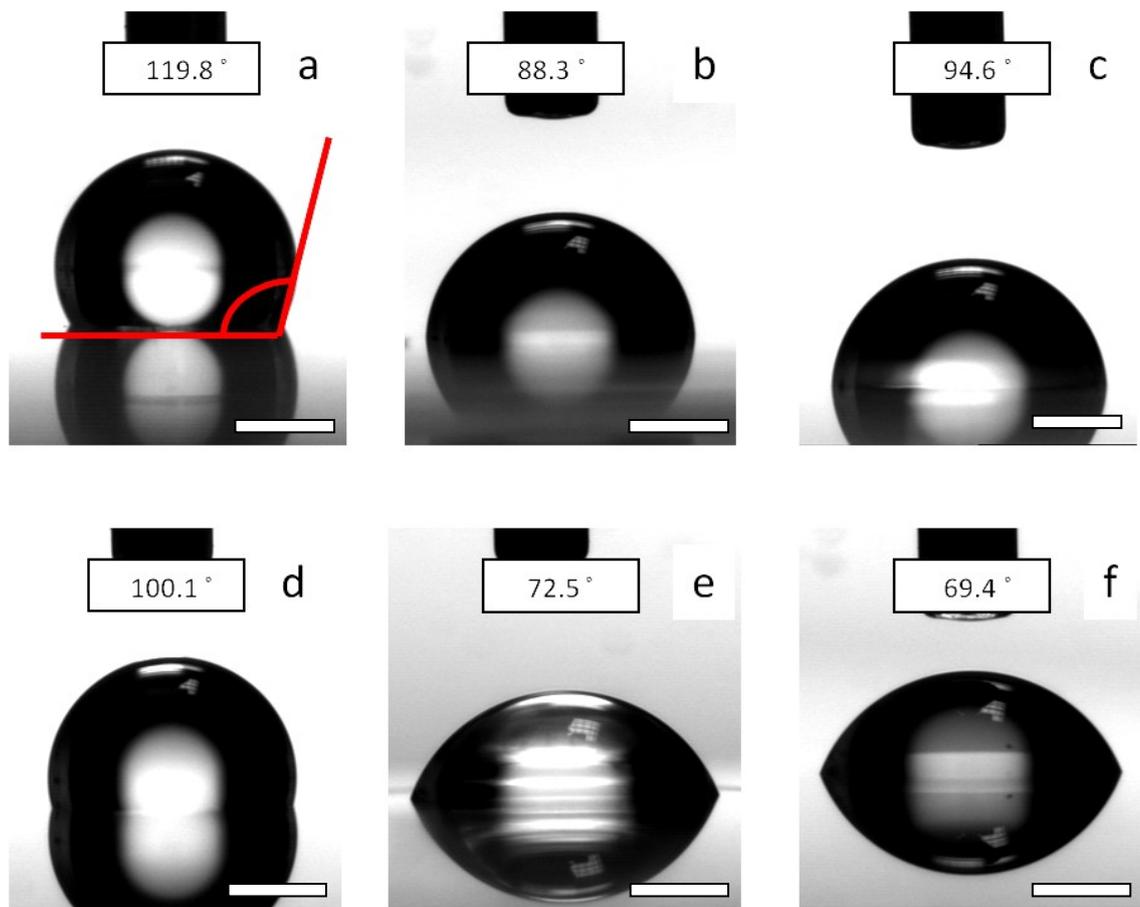
Figure 2. 24   Contact angle measurements on 3 µl Water droplet pinned on a Teflon AF coated glass surface (a), a 5000 nm thick SU8 coated glass surface (b), a hydrophobic silane coated glass surface (c), a hydrophobic silane coated LiNbO$_3$ surface (d), an SU8 surrounded hydrophilic trap on glass (72.5 ˚) (e) a silane covered trap on LiNbO3 (f). (Scale bar 0.8 mm)

The water repelling properties of the materials used for the trap fabrication are examined. Contact angle measurements given in Figure 2. 24 shows that the best hydrophobicity was obtained on Teflon. SU8 can be used for trap fabrication due to its water repelling properties.

Results also show that hydrophobic silane coating on LiNbO$_3$ gives higher contact angle than a glass surface. Increasing the sample volumes leads to smaller contact angles (Figure 2. 25) due to increased mass on the surface.
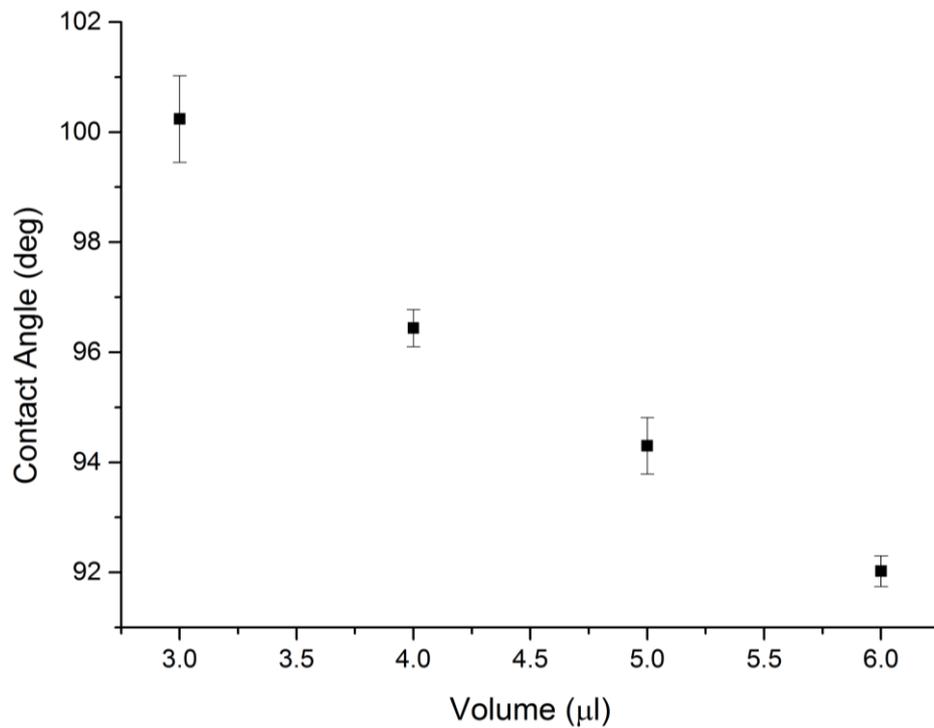
Figure 2. 25 Contact angles measured on different droplet sizes pipetted on a hydrophobic silane coated glass surface. Increasing droplet volumes caused a decrease on the contact angle between the droplet and the droplet. (The error bars obtained from 4 measurements)

2.2.2.   SAW actuator

A way to examine the SAW devices is obtaining the scattering characteristics (S-parameters). The parameters are influenced by the frequency of the applied signal and the impedance of the load. The measurements, performed by a network analyzer, give information about the reflected (S_{11}) and transmitted (S_{21}) power characteristics of the load.

SAW devices, fabricated via three different techniques (see in microfabrication section), are tested by an Agilent Technologies (E5071C ENA Series) network analyzer. S_{11} scattering results (Figure 2. 26) shows that the SAW device fabricated via the first fabrication method, which has an additional predevelopment step before the UV exposure, gives a higher electrical to mechanical energy conversion ratio than the other devices. This was a result of the fabrication of wider electrode fingers. The LOR based technique gives the lowest values since the sizes were smaller than others. This difference does not necessarily mean significant performance enhancements between the actuators.
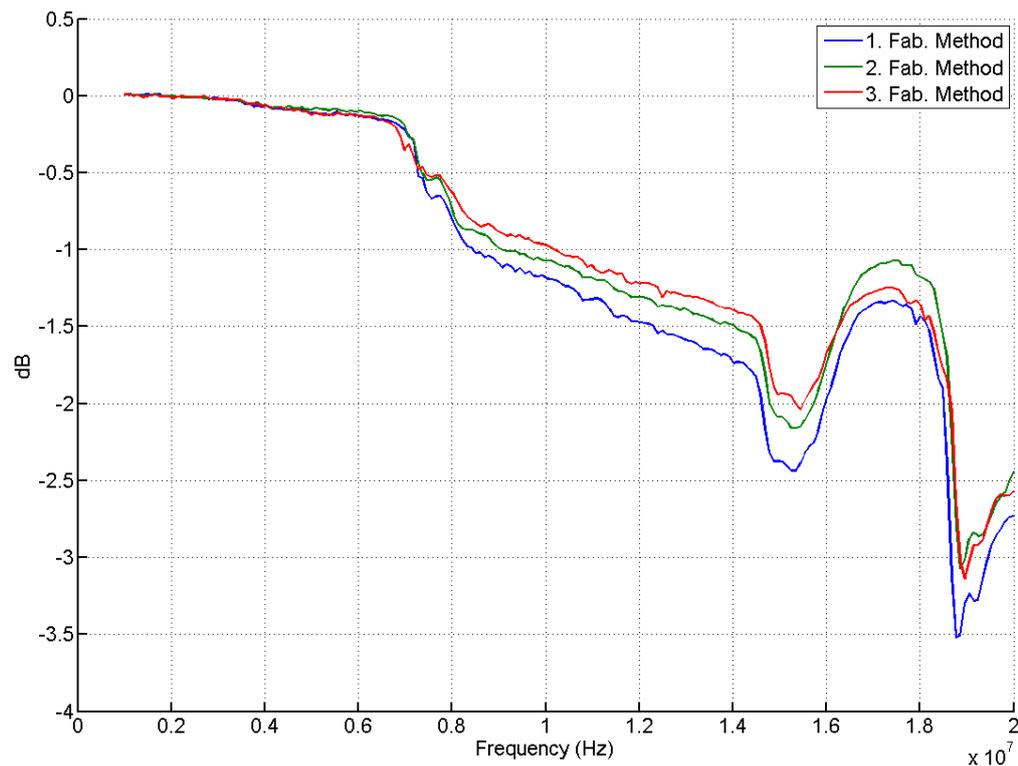
Figure 2. 26 S_{11} **scattering analyses of the SAW devices fabricated via three different methods (see in microfabrication section). The most efficient transducer is fabricated by the 1st technique. However, the less effective device is the one fabricated by the 3rd technique (LOR based) because LOR method gives smaller electrode widths.**

SAW devices designed in this research were also tested by a Doppler vibrometry device (Polytec UHF-120 Vibrometer). SAW propagation measured in front of the resonator device gives a 3D graph of the generated wave pattern. This data can be used to obtain the speed of the sound wave on a particular material. Also, it can provide the amplitude of surface displacement due to the travelling mechanical waves. High-resolution surface displacement measurements require several hours of measurement time depending on the area of scan and the wavelength of the SAW. However, there is a faster way to recognise the travelling SAW beam. SAWs create a temperature effect proportional to the frequency and the voltage (peak to peak) of applied RF signal. There are two primary heat sources in SAW systems interfaced with liquids, namely the absorption of the heat created by the motion of crystal atoms [33] in the substrate (or superstrate), and the interaction between the SAW and the liquid as longitudinal waves propagating in the liquid are dampened through the viscosity of the fluid [46]. Higher viscosity leads to more energy dissipation due to the increased viscous friction [81]. A viscous water-based gel was used in the systems in order to obtain a larger temperature scale. This enabled to measure the SAW related heat variation with a relatively high definition, as a proxy for the acoustic power obtained. The exact location of the SAW beam generated by a slanted design can be measured rapidly with this method. Moreover, it helps to make fine adjustments in the SAW frequency to obtain optimum electrical energy to mechanical energy conversion rate from the transducers. However, direct observation of

individual waves via the vibrometry device gives further details about the characteristics of the design.
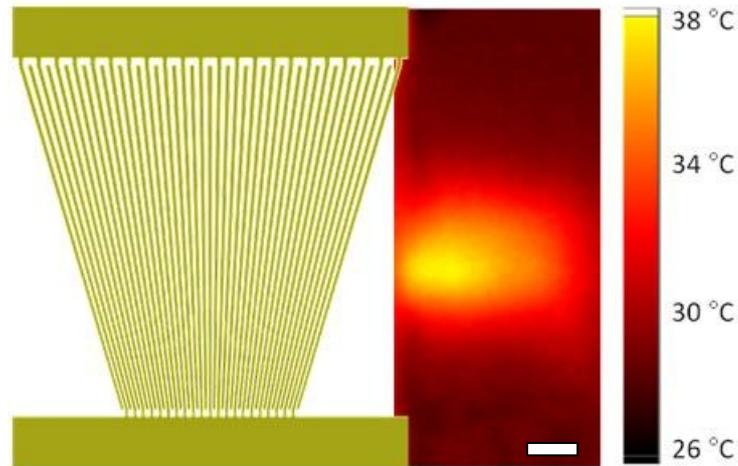
Figure 2. 27   SAW beam observation technique via thermal observation. The measurement was conducted with an IR Camera (Fluke Ti25) on a glass cover slide. It was coupled with a water based gel in front of the 43 fingers slanted transducer. The frequency of the applied SAW signal was 11 MHz (0.5 W). (Scale bar 1.5 mm)

2.2.3.   SAW induced streaming

SAW induced fluid streaming characterisations was conducted with two different systems. They were a fluorescent correlation spectroscopy (FCS) system and a micro-particle image velocimetry (μ-PIV) setup. The volume of the micro-scale sample was relatively large in comparison to the FCS detection volume (approximately 1 fl). Therefore, μ-PIV was used as the primary speed monitoring system in this study.

The high frame rate (3000 frames per second at 1024 by 1024 pixels resolution- Photron APX RS) μ -PIV system (TSI) consists a high repetition rate laser (10mJ at 1 kHz) for illumination of the red dyed fluorescent particles. The high-resolution stereo μ-PIV System was used to observe the flow pattern inside droplets and samples in chambers to measure the velocity of the flow [82]. Red dyed fluorescent particles (3 μm, Fluoro-Max Aqueous Fluorescent particles, No: R0300), at a concentration of 4×10^6 particles/ml, are used as flow tracers. The particles behave similarly to the flow of the fluid. Therefore, the particle visualization can give relevant data about the flow patterns and characteristics. It should be noted that the velocities measured by the μ-PIV system gives only 2D (horizontal) information.

The transducers were re-fabricated on a transparent LiNbO$_3$ substrate [49] since the microscope of the PIV system was inverted. Therefore, the optical sample monitoring could be performed through the substrate.
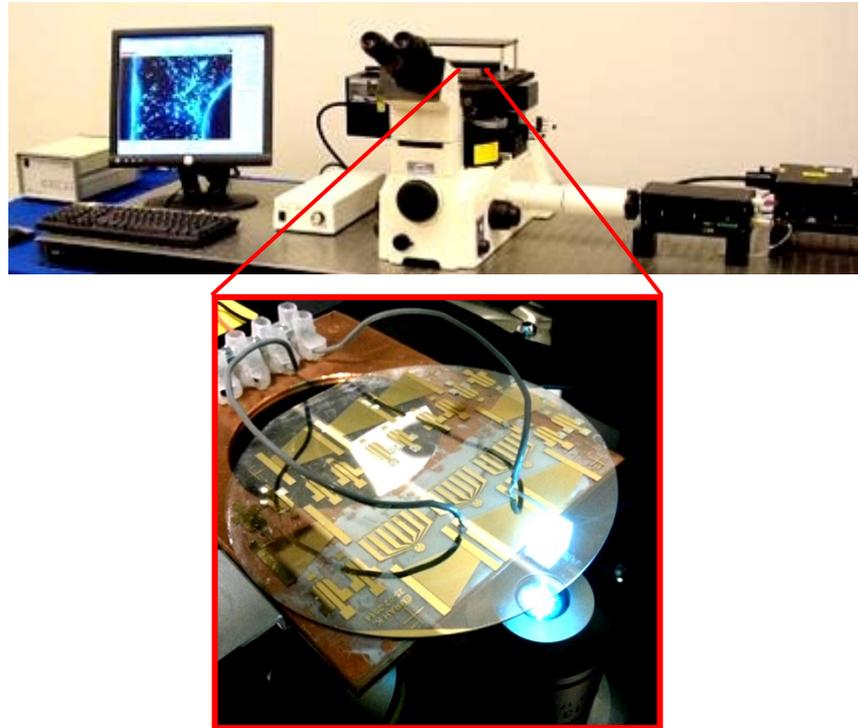
Figure 2. 28 Image of the μ -PIV system (Top) and the experimental setup of the SAW platform. The 43 finger SAW device was microfabricated on a transparent piezoelectric substrate (LiNbO$_3$)

2.2.4.   Surface examination

Surface scanning is an effective way for the investigation of surface treatments. In this research, the surface examinations were firstly made via microscopes. Two-dimensional surface profile measurements and three-dimensional topographical measurements were also performed when more detailed data was needed.

Surface measurements during microfabrication procedure were determined using a height profilometer (Veeco Dektak 6M). The examinations on electro-polymerised surfaces were conducted by an atomic force microscopy (AFM) system (NanoWizard II AFM - JPK Instruments AG, Germany). AFM provides three-dimensional detailed (nm scale) data about the surface topography.

2.3.   Electroanalytical analysis

Electroanalytical measurements (cyclic voltammetry and amperometry) were performed on model solutions including potassium ferrocyanide (K$_4$[Fe(CN)$_6$], Sigma-Aldrich) at varying

concentrations (5 mM, 10 mM, 20 mM and 40 mM). The samples also included 100 mM KCl as a supporting electrolyte for the system.
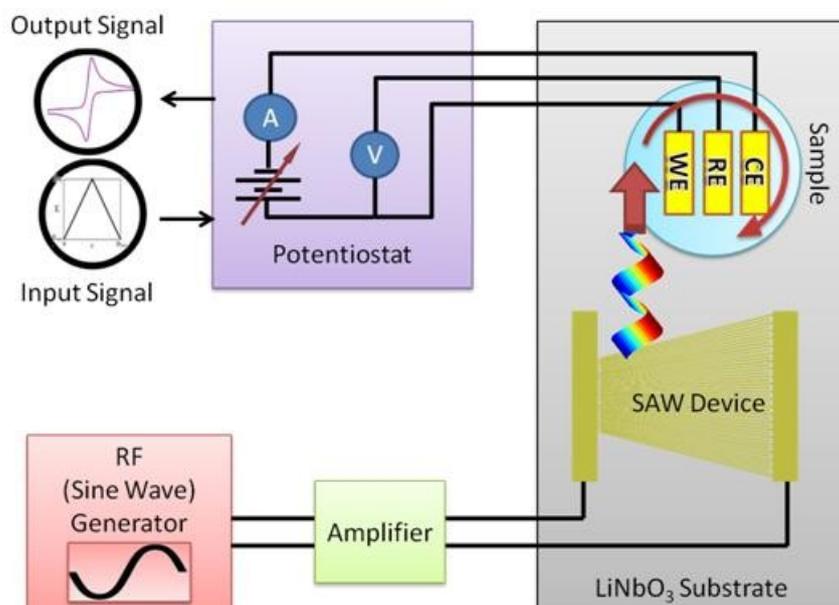
Figure 2. 29 Schematic of the SAW enhanced hydrodynamic electroanalytical system. The complete system setup composes a potentiostat (CHI760C), a three-electrode sensing system (with a 3µl sample pipetted onto it), a slanted SAW IDT (10nm Ti, 100nm Gold), an amplifier (Mini-Circuits ZHL-5W-1, 5-500 MHz with a 3 A, 24 V DC power supply) and a function generator (Agilent Technologies MXG Signal Generator N5181A).Travelling acoustic wave is radiated into the sample and created extra fluid motion. Electroanalytical measurements were performed on the sample in the absence and the presence of hydrodynamic effect.

Cyclic voltammetry and amperometry tests were performed for quantitative measurements and also for electro- polymerisation tests on gold surfaces with a CHI 760C Series Electrochemical Workstation. The quantitative tests were also performed in hydrodynamic conditions. This effect was provided by the SAW induced fluid streaming. The schematic representation of the hydrodynamic system setup is given in Figure 2. 29. Hydrodynamic electrochemistry systems include an external convection effect in addition to the diffusion of the system. This external convection increases the mass transfer in the medium and improves the reaction rate [17]. The SAW-enhanced hydrodynamic voltammetry microchip comprises a three electrode sensing part and a SAW transducer. Hydrodynamic chemistry tests were performed with microliter scale droplet solutions. The same system setup (Figure 2. 29) was also used for quantitative electroanalytical bioassays.

3. Surface acoustic wave actuator designs and fluid streaming

3.1.   Introduction

SAW devices are commonly used as passive filters in electronic equipment [83]. However, in recent years SAW technology has attracted a significant interest as physical actuator devices. There have been various publications concerning micro fluid manipulation [37], heating [45] and mass transport enhancement in electroanalysis [84]. Varying requirements of different applications led to the creation of various interdigitated transducer (IDT) designs, such as slanted [45], focused [85] and single phase unidirectional transducers (SPUDT) [12].
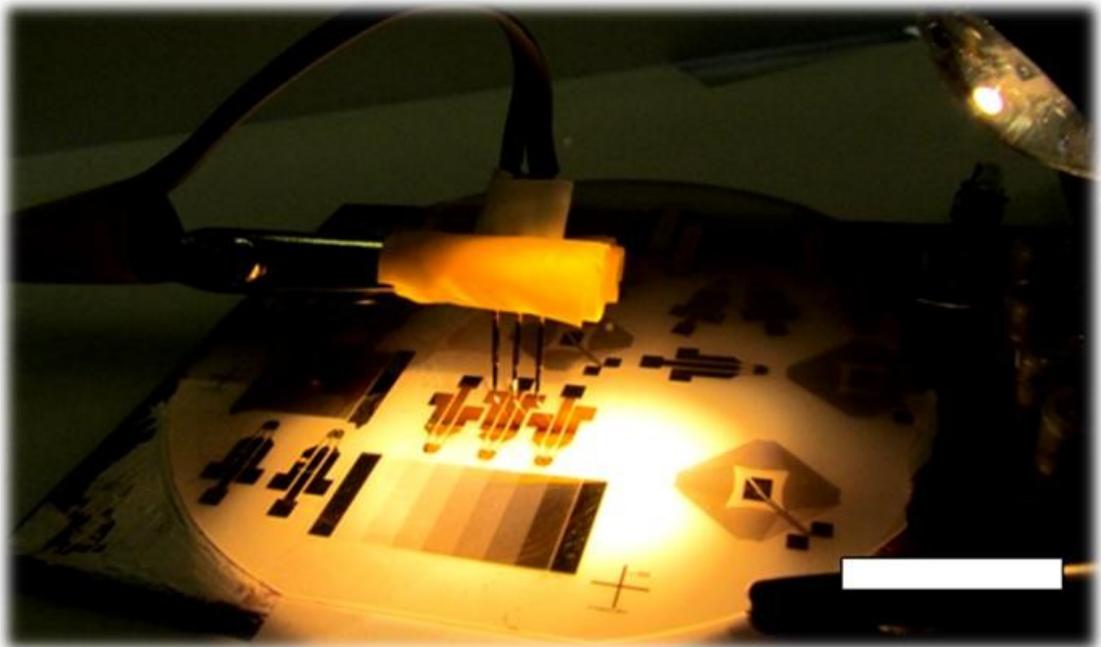
Figure 3. 1 The image of a LiNbO$_3$ substrate pasted on a heat-sink with a heat-compound material. The substrate has electroanalytical sensors, and various types of SAW transducers microfabricated on it using photolithography. Three electrode sensors were used for the investigation of SAW induced hydrodynamic electroanalytical analysis (see chapter "SAW induced electroanalysis" for details). (Scale bar 2.3 cm)

This work is focused on the enhancement of the efficiency of SAW actuated mixing platforms and their characterisation. Various SAW IDT designs and system setups were experimentally investigated via different techniques such as surface displacement and thermal measurements. The actuator design combinations were also used for SAW induced (hydrodynamic) electroanalytical measurements in the following work (see details in the next chapter "SAW induced electroanalysis").

3.2.   SAW device designs and characterizations

3.2.1.   Straight design

Straight SAW IDT (Figure 3. 2) is one of the most common types of designs used in microfluidic applications. All the parameters of the model are kept same all over the device. Those parameters are the pitch distance, finger width and mark to space ratio that is kept as equal.
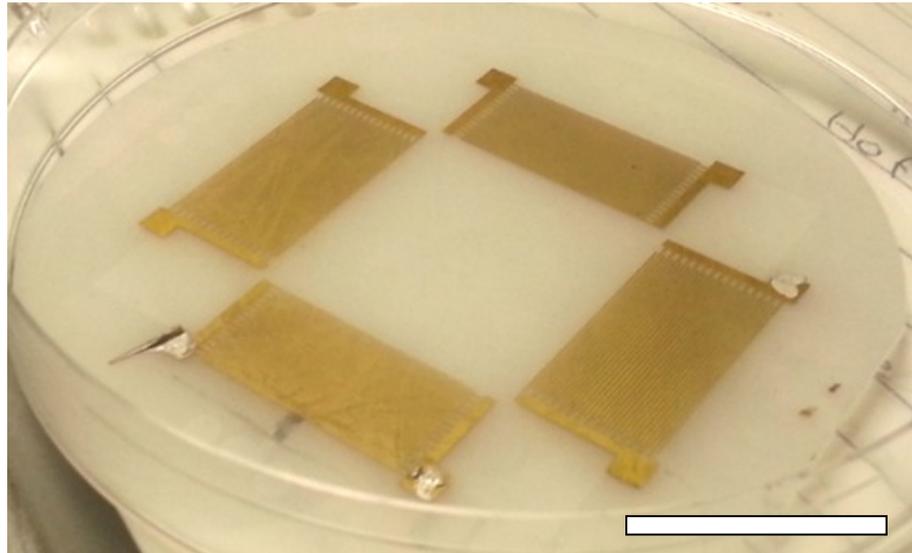
Figure 3. 2 Image of straight SAW IDTs fabricated on a LiNbO$_3$ (128° Y-cut X-propagating LiNbO$_3$, c = 3996 ms^{-1}) substrate. The devices were designed to work at 5 MHz (λ= 800 μm). The LiNbO$_3$ substrate was coupled on a heat sink with a thermal compound in order to avoid breaking due to overheating. (Scale bar 30 mm)
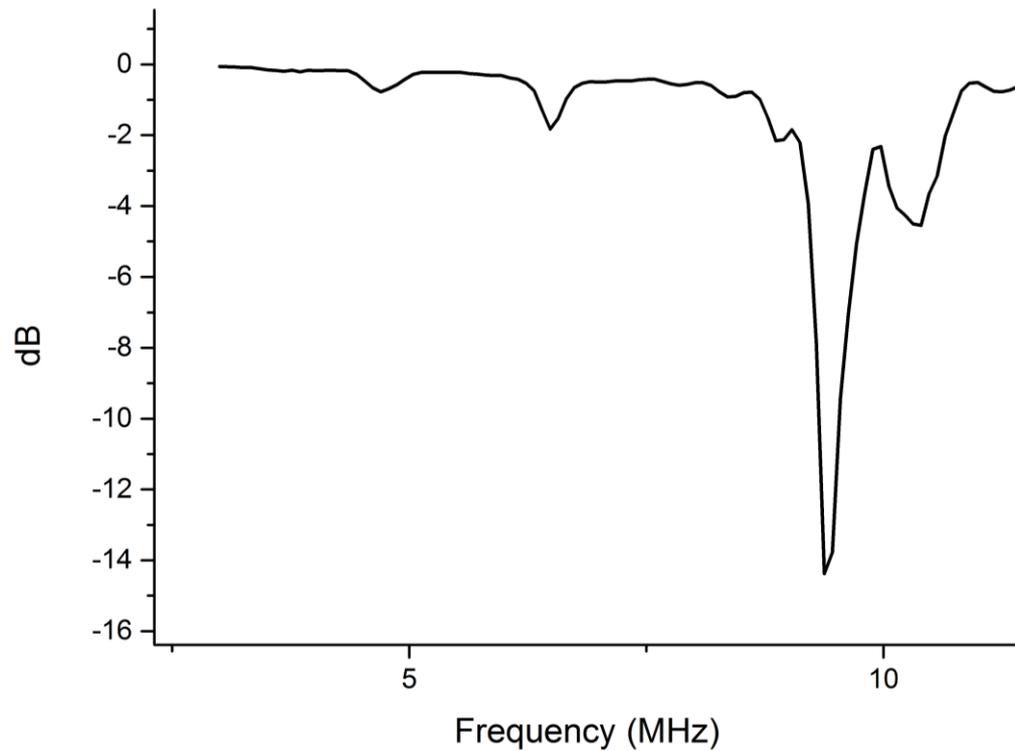
Figure 3. 3 Resonance performance of the SAW transducer. The graphic shows the magnitude of the S11-parameter obtained with an Agilent Technologies E5071C ENA series network analyzer. The S11-parameter gives information of the refection coefficient. The resonance occurs at 4.7 MHz on the device. The transducer can also resonate at a few harmonic frequencies such as 6.5 MHz and 9.38 MHz.

The SAW devices were fabricated onto a 127.68^0 Y-X cut $LiNbO_3$ substrate, as previously described [45]. Briefly, using standard UV photolithography, IDTs were obtained by the lift-off of 10 nm of titanium adhesion layer and 100nm of gold. The SAW devices were firstly tested with S_{11} reflection tests with an Agilent Technologies E5071C ENA series network analyzer. The analyser sends signals between a range of frequencies and compares it with the reflected signal. The comparison starts to present difference when a signal at the resonance frequency is sent to the SAW transducer. The electrical energy gets converted to mechanical energy, therefore, the reflected signal decays. This gives the down peaks as shown in the Figure 3. 3.

The purposed resonance frequency of the straight design was 5 MHz. However, the scattering (S_{11}) analyses (Figure 3. 3) showed that the resonance occurred at 4.7 MHz in that particular device. The reason for the frequency shift was the transition errors first from the digital design on a PC to a mask and from the acetate mask to the actual metal pattern on the substrate. Moreover, Figure 3. 3 showed that the transducer was also capable of resonating at a few other frequencies such as 6.5 MHz and 9.38 MHz.

A three-electrode system, fabricated on a 1 mm thick glass slide, was coupled on the systems for electroanalytical test purposes. 3 μl water based gel (KY Jelly; Johnson and Johnson)

bonded the two platforms to each other. The temperature generated on the sample droplet which was pinned on the superstrate was investigated. Thermal measurements were made at a harmonic resonation frequency (9.38 MHz) at varying SAW powers from 0 to 4 W by an IR camera (Fluke Ti25). Figure 3. 5 presents the temperature increment from 27.72˚C to 39 ˚C.

Figure 3. 4 IR image of the ultrasensitive electrochemical sensor chip (9.38 MHz, 0.05W). Thermal measurements were performed by an IR camera (Fluke Ti25). The left side of the image shows the SAW platform. The right side is the electrochemical sensing part which is attached on the SAW platform with a thin gel layer. Cable connections were made via silver paste bonding. There is a droplet on the tips of the electrodes.
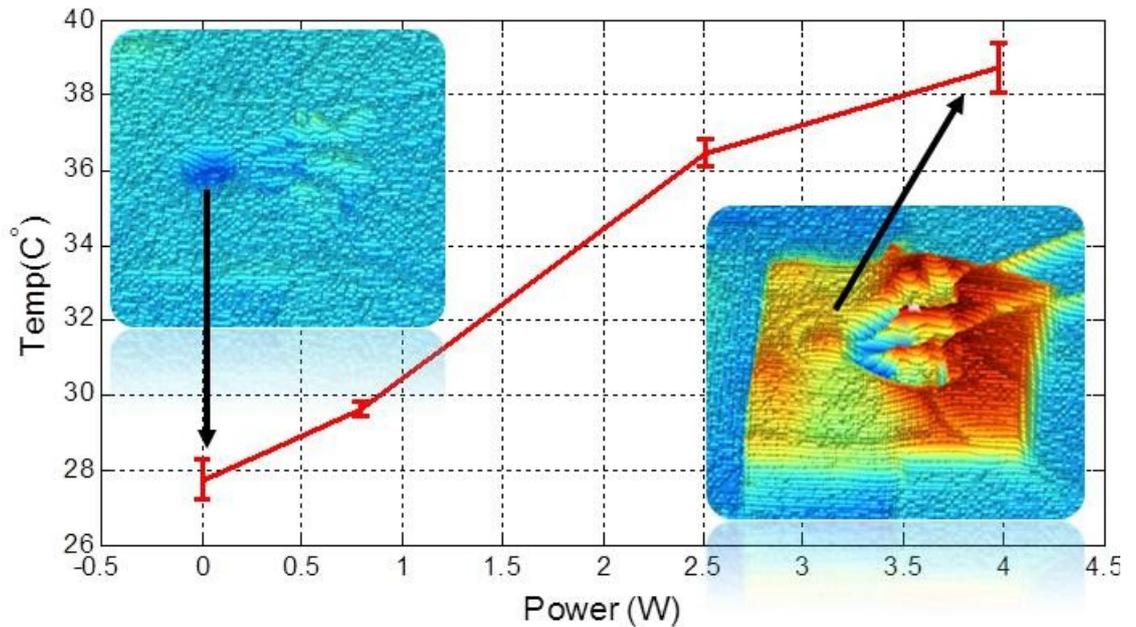
Figure 3. 5 Temperature change inside the droplet during the SAW streaming at 9.38 MHz. Powers applied to the SAW IDT were 0, 0.8, 2.5 and 4 W. The measurements were performed on the device explained in the previous figure.

3.2.2.   Slanted finger design

Slanted (or tapered) finger IDTs (SFIDT) are commonly used in various microfluidic applications due to their powerful wave position manoeuvring capabilities. Changing the frequency enables to shift the position of the SAW beam horizontally (Figure 3. 9). These types of devices are used for droplet manipulation [40], mixing [84], manoeuvrable propulsion (swimming) on water [86] and cell patterning [87] applications.

The SAW induced fluid streaming experiments, included in this work, were carried out using two different SFIDTs. Scattering (S_{11}) analysis of the first, 29 finger (black line), and second, 43 finger (Red solid line), SFIDTs are presented in Figure 3. 6.
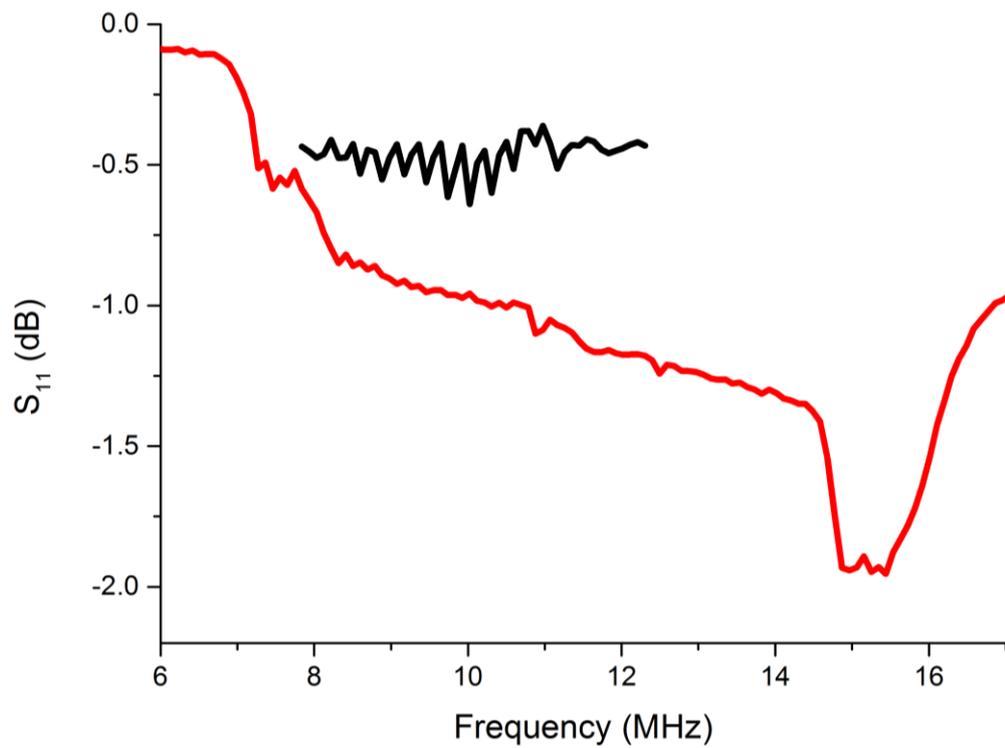
Figure 3. 6 Scattering (S_{11}) analysis of the first, 29 finger (black line), and second, 43 finger (Red solid line), SFIDTs. The frequency working range of the fists SFIDT was between 8 - 12 MHz and the working frequency range of the second device was between 7.6-16.6 MHz.
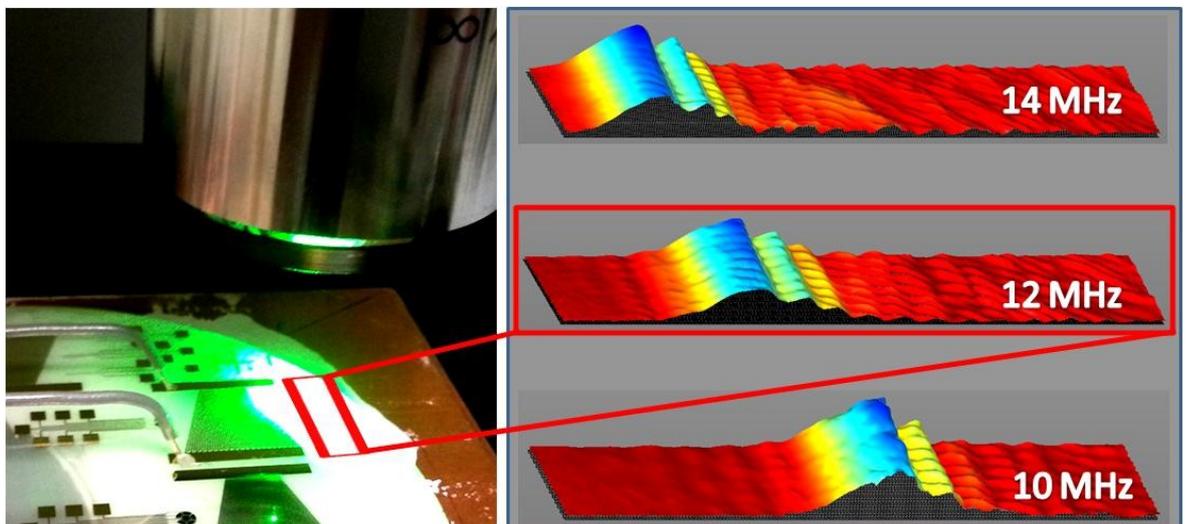
Figure 3. 7 Left: The setup for surface displacement measurements on the SAW platform (43 finger SFIDT). The vibrometry tests were conducted by a Laser Doppler vibrometry (Polytec UHF 120 Vibrometer) device. Right: Total displacements obtained in front of the resonator at three different resonation frequencies (10 MHz, 12 MHz and 14 MHz).
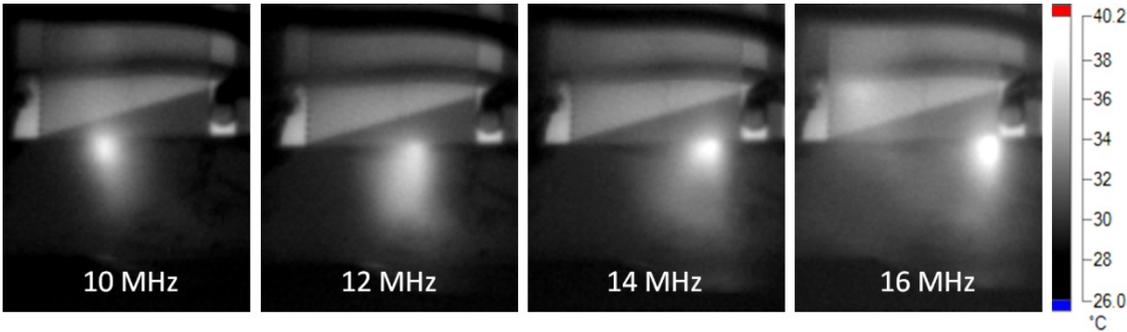
Figure 3. 8 SAW induced temperature variation on the glass cover slide, coupled with gel in front of the 43 finger SFIDT, was measured with an IR Camera (Fluke Ti25). The resonator device was able to shift the location of the SAW beam, along its 1cm length of aperture distance. The manipulation was being made by varying the applied SAW frequency between 7.6MHz and 16.6MHz. The period (λ) of the design varied from 520 μm (on the left-hand side of the device) to 240 μm (on the right-hand side of the drop). This method was commonly used, for the characterisation of SAW devices, during the entire research.

Figure 3. 9 presents the working characteristics of the SFITD (43 fingers) device. The results show how the varying SAW frequencies change the position of the SAW beam. The calculated locations of the SAW paths are found in agreement with the surface displacement and thermal measurements as shown in the graph in Figure 3. 9.
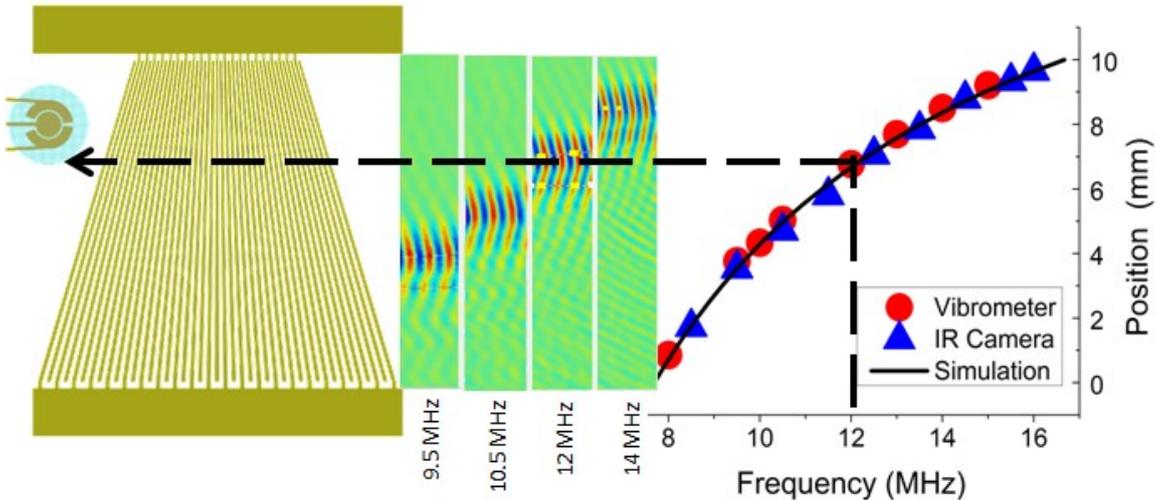
Figure 3. 9 Working characteristics of the 43 finger SFIDT. Left to right: Electroanalytical sensor (three electrode system), the SFIDT SAW device, surface displacement pattern due to the SAW propagation and the graph of the working frequency range of the SAW transducer. The graph contains a simulation and two experimental test results of the SAW device. Two experimental data were obtained via Laser Doppler vibrometry and IR Camera (Fluke Ti25) measurements.

3.2.3.   Step IDT design

A complex actuator, Step-IDT device (Figure 3. 11), was designed for more efficient mixing applications. The device included three different finger series that were able to resonate at three different frequencies: 7.9 MHz, 9.6 MHz, and 11.5 MHz. The design works in a similar fashion with the SFIDT. However, the resonating parts of the fingers can be specified much more accurately. Therefore, the widths of the SAW beams can be defined precisely just by arranging the lengths of straight patterns.
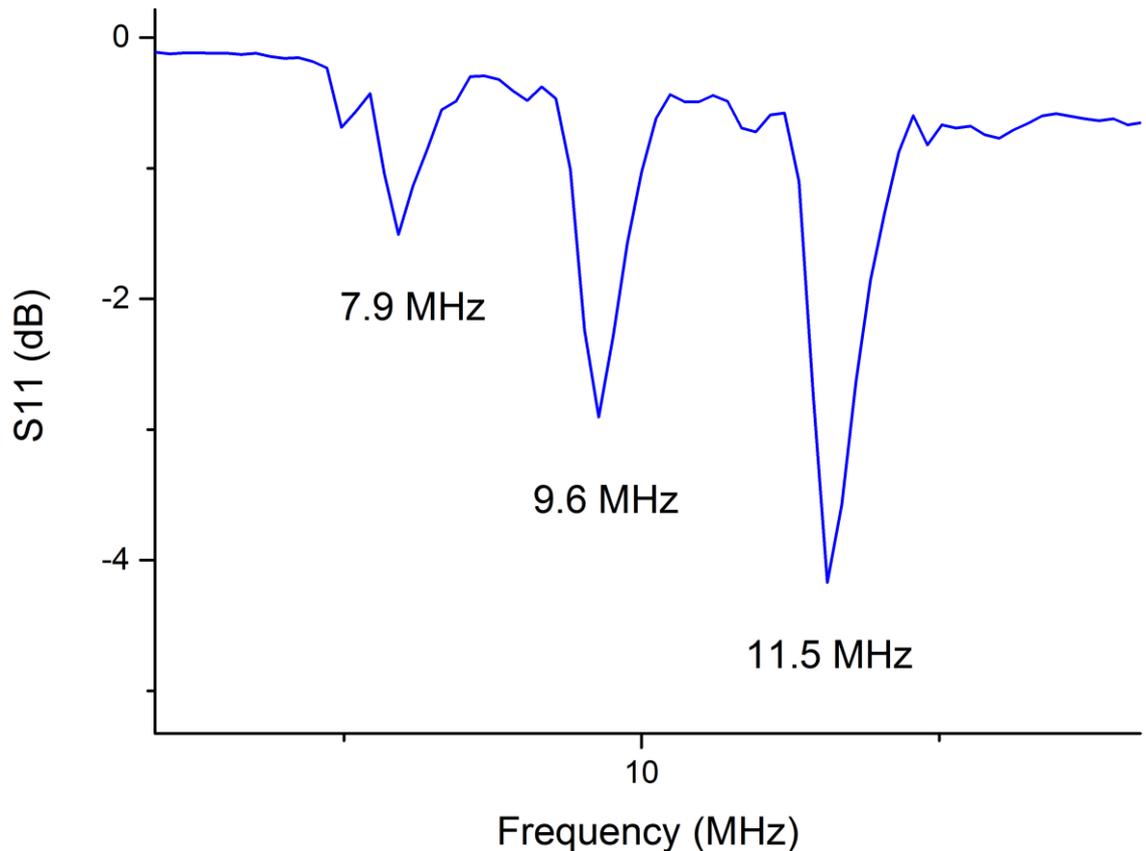
Figure 3. 10   Scattering (S_{11}) results obtained from Step IDT by a network analyser device (Agilent Technologies, E5071C 9kHz-3Ghz ENA Series). Each of three finger series resonated at a different frequency.

The resonating parts of the SFIDT devices are limited and depends on the period (λ) variation and the length of the slanted fingers. This method can enhance the efficiency of SAW generation by actuating larger portions of piezoelectric crystal located under the straight fingers. More acoustic energy enables to obtain a more powerful mixing or cell patterning method than the SFITD method. Moreover, the working frequencies can be specified more precisely as shown in scattering (S_{11}) analysis presented in Figure 3. 10.
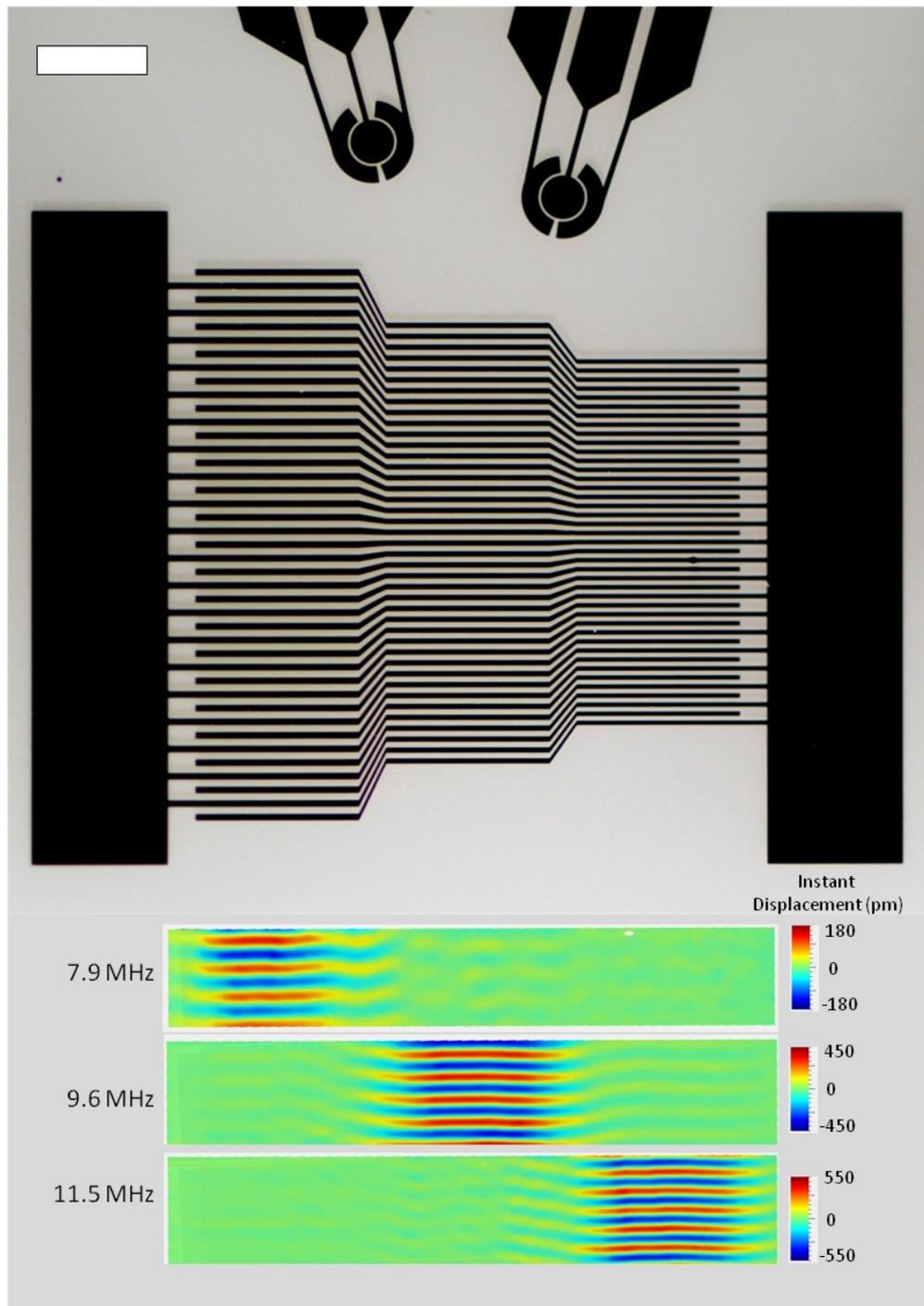
Figure 3. 11 Propagating mechanical wave patterns obtained from three different finger series of the Step-IDT device. Each SAW beam obtained at different frequencies (7.9 MHz, 9.6 MHZ, 11.5 MHz). This design enables to control the rotation direction in the sample precisely when the sample is pinned on the circular sensors. (Scale bar 2 mm)

3.2.4.   Focused multiple IDT design

Maximum physical energy transition into the sample is one of the most prior targets in microfluidic applications. On SAW platforms, using a targeted IDT (FIDT) design [88] or a phononic lattice structure [60] are the ways of obtaining an adequate acoustic energy transmission. Targeted devices consist of circular/ curved finger design to concentrate the acoustic energy on a particular focus point. They have proven their efficiency [59] in various applications such as jetting [89] and particle separation [90].

This part explains a multi-actuator design which was designed to perform multiple mixing on four separate sensing systems. Each circular finger set was designed to work at a different frequency. The transducers were focused on sensing electrodes which were located at various positions. Thus, the design gives the freedom to choose any of the transducers at any time. It is also possible to activate more than one finger set at a time. For this, the applied signal must be the sum of signals, defined by four resonance frequencies. The frequencies of the transducers were 10 MHz ($\lambda_1 = 400$ μm) for FIDT-1, 11 MHz ($\lambda_2 = 364$ μm) for FIDT-2, 12 MHz ($\lambda_3 = 333$ μm) for FIDT-3 and 13 MHz ($\lambda_4 = 308$ μm) for FIDT-4.

The IDTs were first investigated by thermal monitoring. Some of the acoustic energy is dissipated as heat when travelling from one medium to another such as solid to liquid. This heat, generated in the fluid, is proportional to the viscosity of the liquid. A water-based gel, a viscous liquid, was used in the thermal investigation test. It was manually spread between a thin glass slide and the substrate. Thermal images helped to define the absolute resonance frequency of the FIDTs.

Finally the instant surface displacement due to the travelling mechanical waves, were investigated. The result showed that the actual resonance frequencies of FIDTs were lower than the calculated values. This was caused due to printing accuracy error, a disadvantage of acetate mask, and the errors due to the photolithography process. However, each FIDT of the complex design managed to produce mechanical wave propagation towards the sensing electrodes.
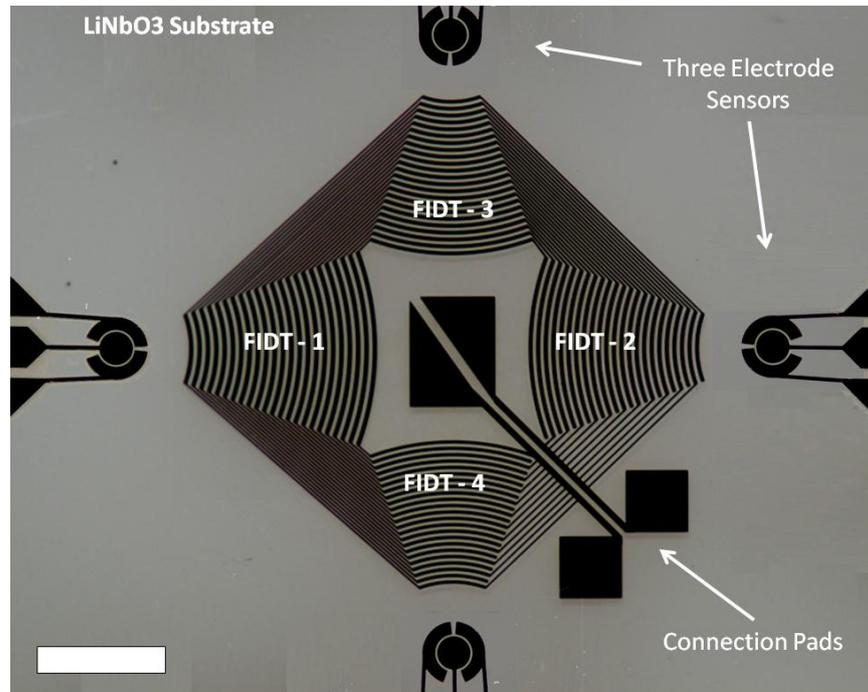
Figure 3. 12 Image of the multiple FIDT design. The design was comprised of four FIDT transducer device with different pitch distances (λ_1 = 400 μm, λ_2 = 364 μm, λ_3 = 333 μm, λ_4 = 308 μm). Each FIDT series was positioned towards a different direction (+ 45 °) with a three electrode sensing at the front. (Scale bar 3mm)
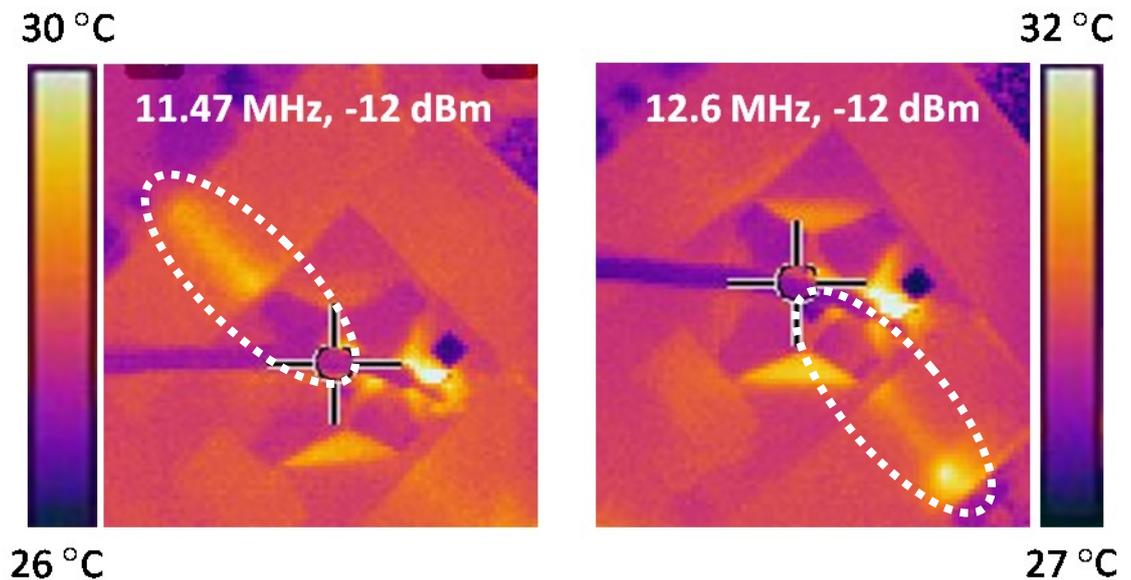
Figure 3. 13 Thermal tests performed for the definition of exact working frequencies of FIDT transducers. The working frequencies of FIDT-3 and FIDT-4 were measured as 11.47 MHz and 12. 6 MHz. The performances of SAW devices were investigated via thermal imaging using an IR camera (Fluke-Ti25).
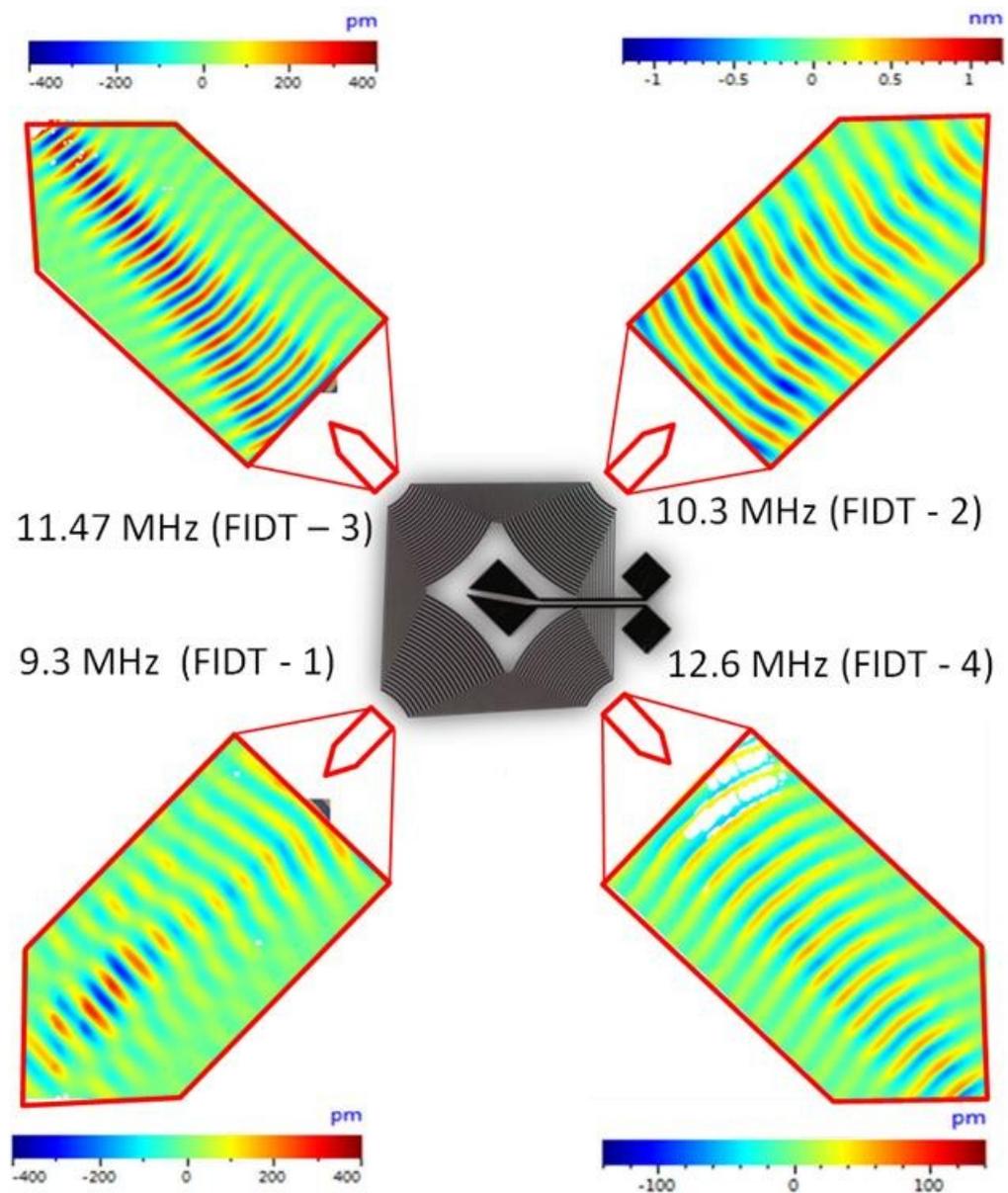
Figure 3. 14 Instant surface displacements created by travelling mechanical waves. Measurements were performed with a Polytec UHF 120 vibrometer. The power of the applied signal was 0.032 W. (Measurement areas are not to scale)

3.2.5.   Wide finger design

A dedicated SAW IDT model was used for testing the effect of M/S (finger width / space) ratio [91] on the efficiency of electrical energy to mechanical energy conversion. The 65 finger straight IDT design, presented in Figure 3. 15, was comprised of 7 different finger series with different M/S ratios. The width of the electrode sets varied linearly from 20 μm to 140 μm while maintaining the pitch distance (2d).

The transducer was fabricated as described previously [40] by lift-off using standard photolithographic techniques. The S1818 resist was used for defining the device pattern on a 128° Y-cut X-propagating 3 inch LiNbO$_3$ (c=3996 ms^{-1}) substrate. Metal layers of 10 nm titanium and 100 nm gold were deposited by e-beam evaporation and lifted off in acetone. The LiNbO$_3$ substrate was pasted on a heat sink with a thermal compound.
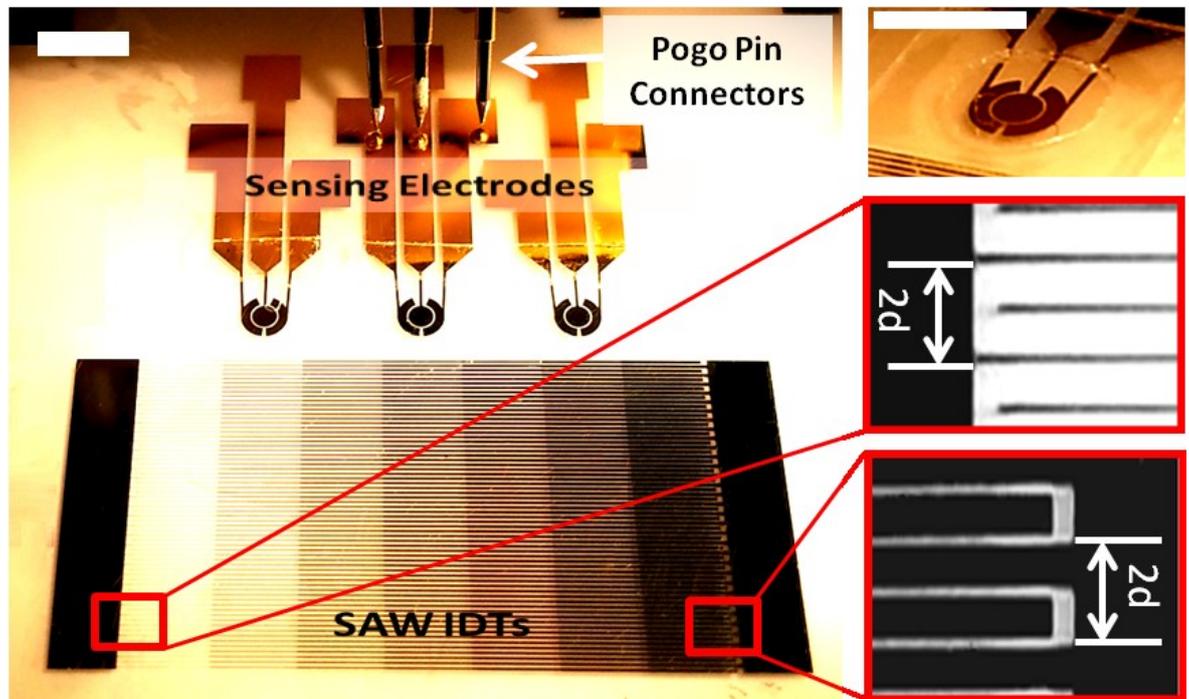
Figure 3. 15 The SAW device and three electrode sensing systems were fabricated on a LiNbO$_3$ (128° Y-cut X-propagating LiNbO$_3$, c = 3996 ms^{-1}) substrate (Left). PVC chambers (1.25 mm radius, 200 µm thick) were attached on sensing electrodes (Top right) (Scale bars, 2.5 mm). All the transducer series had the same pitch (2d), 160 µm (Middle, bottom right).

The resonance frequency of the device was characterised using a network analyser (Agilent Technologies, E5071C 9kHz-3Ghz ENA Series). The resonant frequency of the transducer was measured to be 12.24 MHz via S$_{11}$ scattering analyses as shown in Figure 3. 16. Moreover, the reactance measured at the resonance frequency was very close to zero. This improved the power transfer from the RF signal source to the resonators.

Surface displacement measurement of SAW propagation was performed in front of the SAW device, directly on the substrate surface, by a Polytec UHF-120 Vibrometer.

An infrared camera (Fluke Ti25) was used for monitoring the temperature variation created due to the absorption of mechanical waves by a water-based gel layer. The temperature observations were made on a thin (0.2 mm thick, 2 mm wide and 17.5 mm long) glass superstrate which was coupled in front of the resonator. Coupling was made with manual

application of 2 μl water based gel (KY Jelly; Johnson and Johnson) between the thin glass and LiNbO$_3$ substrates.
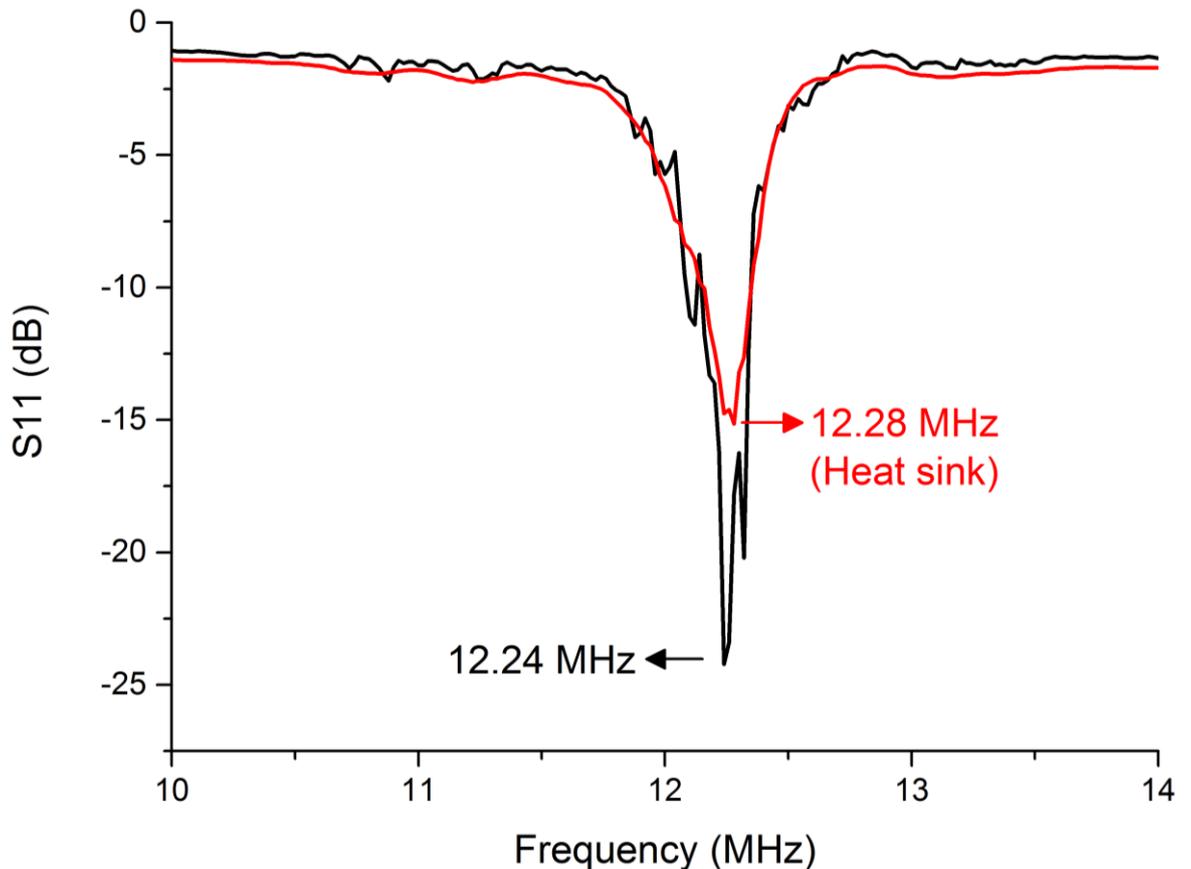
Figure 3. 16 Scattering (S$_{11}$) analyses of the SAW transducer, with and without coupling on a heat-sink. The LiNbO$_3$ substrate was coupled on a heat sink with a thermal compound in order to avoid breaking due to overheating. Coupling on a heat sink decreased the energy conversion from 24 dB to 15 dB ratio. This happened because of the mechanical absorption characteristics of the thermal compound.

Electroanalytical measurements were performed with the three-electrode sensors localised in front of the SAW device (Figure 3. 15), as described previously [84]. All the electrodes (working, reference and counter electrodes) were fabricated at the same time, through the same process and on the same substrate as the SAW transducer. A redox sample was used as a model (5 mM ferrocyanide and 100 mM KCl). 4 μl sample droplets were dispensed into a circular chamber made out of PVC (Figure 3. 15 - top right). Cyclic voltammetry (CV) measurements were performed with a potentiostat (CHI 760C- CHI Instruments): voltage range between -0.3V and 0.5 V (vs. gold reference electrode), scan rate 0.1 V/s.

Surface displacement measurements

The averaged total surface displacement measurements are presented in Figure 3. 17, showing that the average surface displacement, created by the 7th finger series (M/S=7), was 52.5 % higher comparing to equal finger - space design (M/S = 1).

The instant wave pattern of the travelling SAWs (containing phase information), are presented in Figure 3. 18. This result showed that the wide finger structures can produce SAWs within the same phase and wavelength with the classical design (M/S=1).
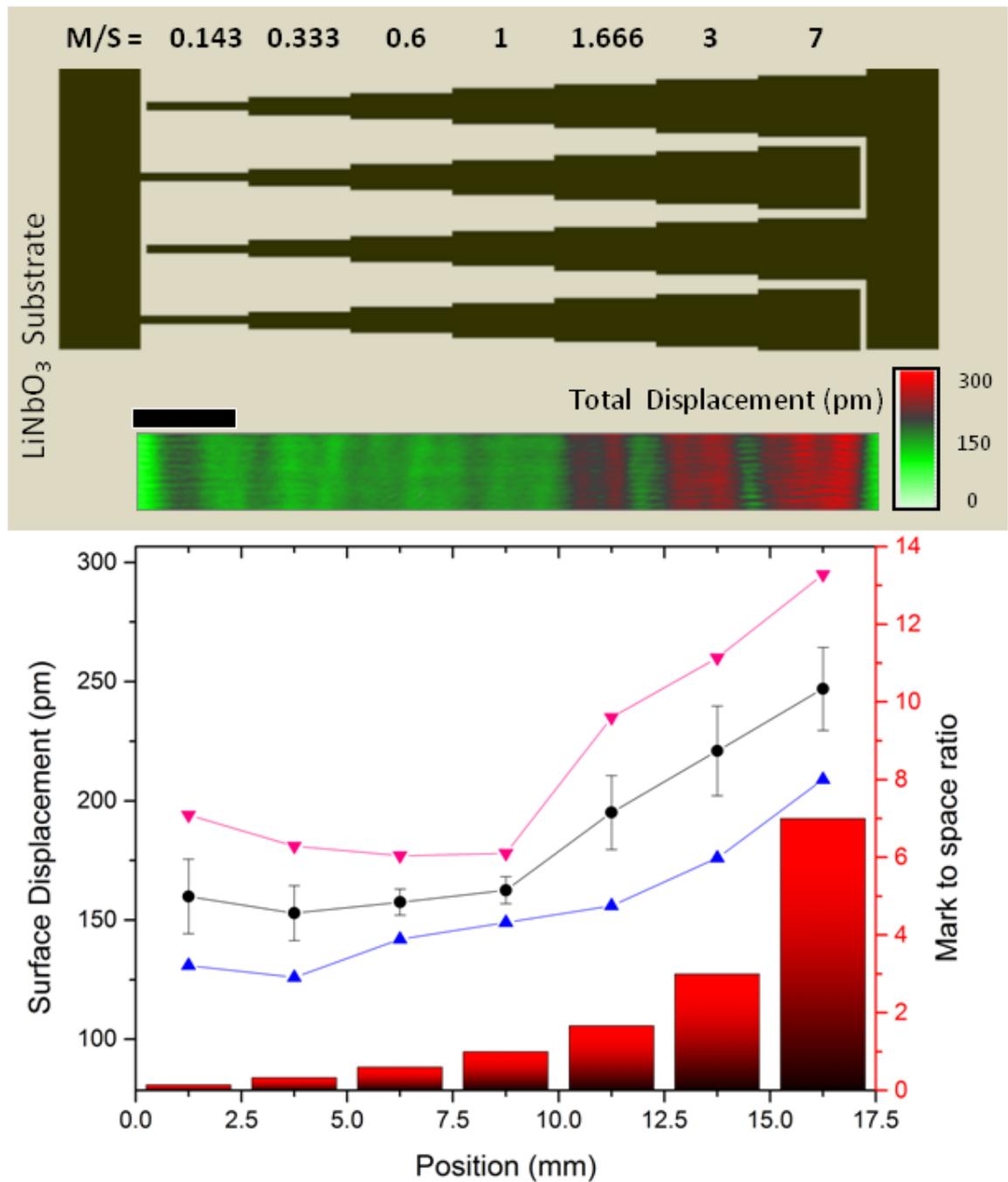
Figure 3. 17 Schematic of the SAW device design (top), comprised of different interdigitated electrode series, and the corresponding vibrometry measurements (middle) (Horizontal scale bar, 2.5 mm). The surface displacement measurement was made in front of the device. The dimensions of the rectangular area were 1.9 mm and 17.5 mm. (Bottom) Average (circle), minimum (up triangle) and maximum (down triangle) total displacement values. M/S ratios (bar graph) of the finger series were varying from 1:7 (0.143) to 7:1. The SAW frequency was fixed at 12.24 MHz with 0.032 W applied power. Wide finger series with the ratio of 7:1 (M/S) presented 85 pm higher surface displacement in comparison to the classical finger design (M/S =1).
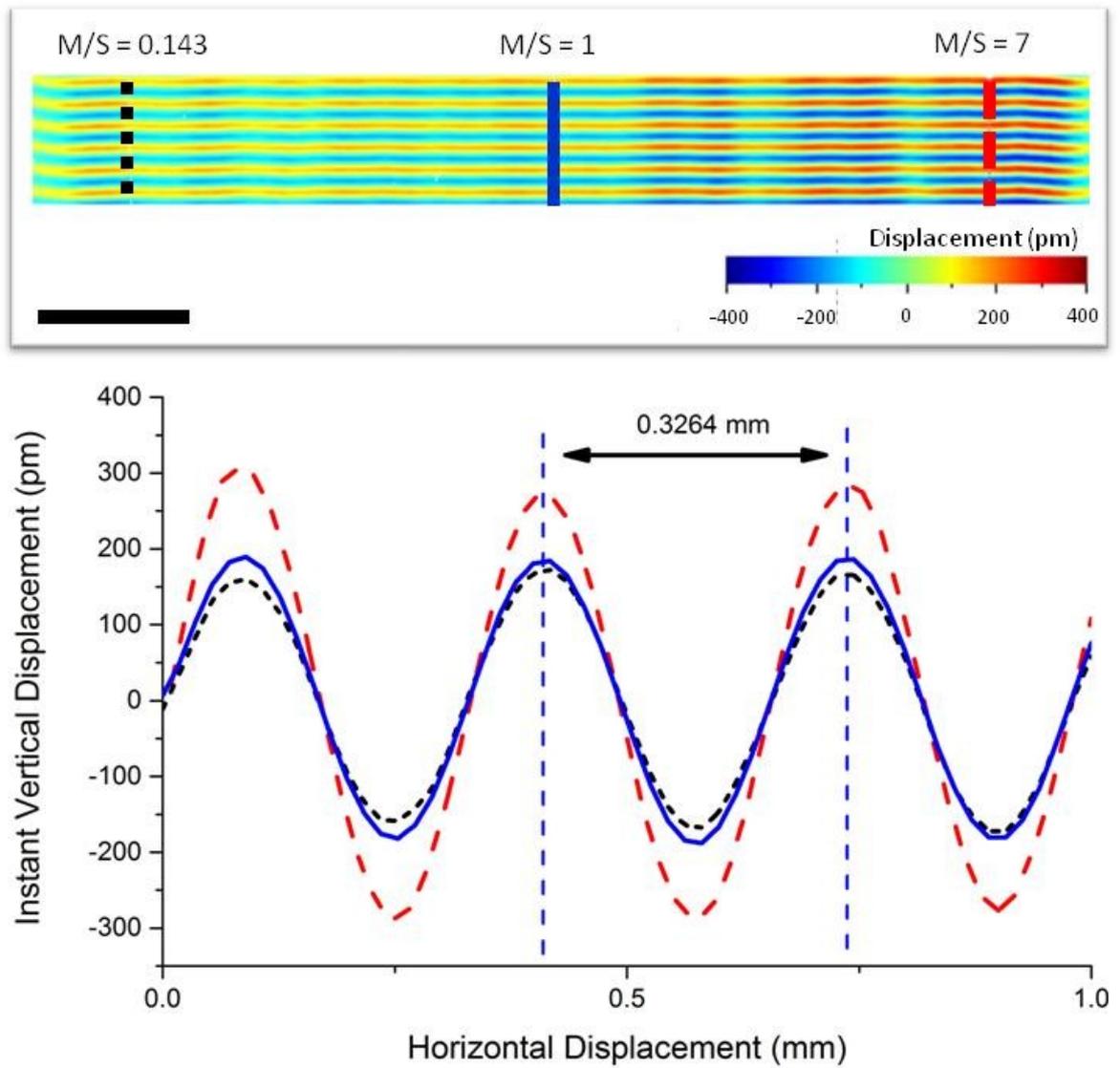
Figure 3. 18 Top: Instant vertical surface displacements immediately in front of the SAW device (Horizontal scale bar, 2.5 mm). The dimensions of the scanned area were 1.9 mm and 17.5 mm. Bottom: Cross section profiles of mechanical waves produced by 1st finger set (dashed black line), 4th finger set (dotted blue line) and 7th finger set (dashed red line), corresponding to the location marked on the top image.

SAW induced heating
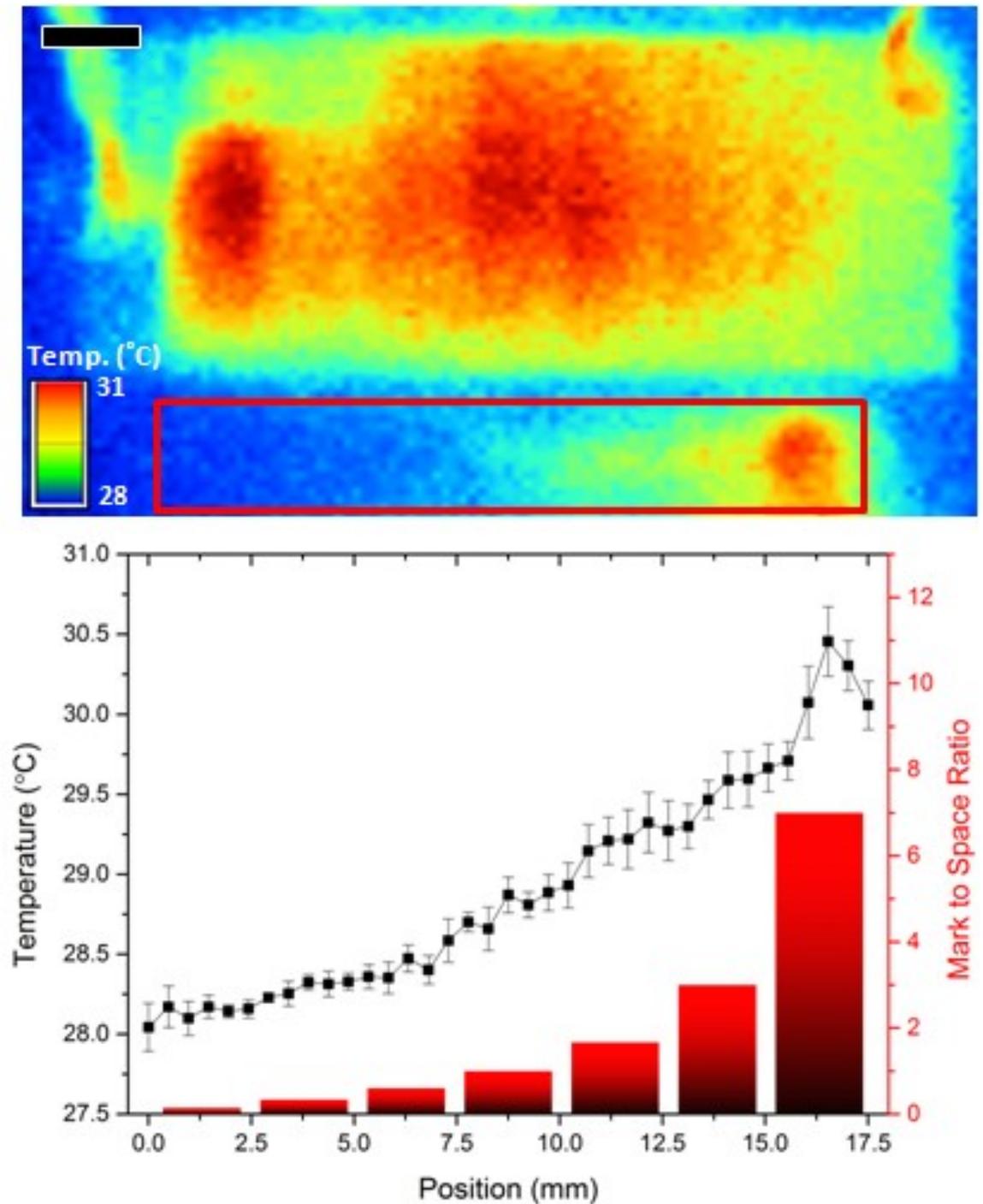
Figure 3. 19 Thermal images obtained from the SAW system and its graphical analysis. A thin cover glass (0.2 mm thick, 2 mm wide and 17.5 mm long) was coupled in front of the SAW IDT with a gel layer (KY Jelly; Johnson and Johnson). IR camera measurements were performed at 12.24 MHz with a power of 0.79 W.

SAWs create a heat as proportional to the frequency and the voltage (peak to peak) of applied RF signal (see details in Characterisation section in Material and Method chapter). This enables to measure the SAW related heat variation with a relatively high definition, as a proxy for the acoustic power obtained. A viscous water-based gel was used in the system in order to get a larger temperature scale (28 ˚C to 31 ˚C).

Thermal measurements (Figure 3. 19) showed that the average temperature in front of the widest (M/S ratio= 7) electrode structure was increased to 30 +/- 0.5 ˚C while the temperature in front of the equal finger-space design (M/S ratio=1) was 29˚C. The rise of the M/S ratio from 1 to 7 enabled a 20 % enhancement in temperature, compared to the starting temperature (24 ˚C) of the observation region.

Monitoring SAW streaming via electroanalysis

To illustrate the potential impact of applying this technique in a biosensing application, we performed cyclic voltammetry (CV) experiments, using three different M/S sets (1/3, 1, and 3). The frequency of the applied RF signal, on the SAW device, was 12.24 MHz and its power was fixed to 0.79 W. The fluid motion induced by SAW enabled to increase the diffusion limited current from 8.3 μA to 34 μA for M/S =3, an 85 % increase in signal (Figure 3. 20). Higher current flows created by wider electrodes were due to the faster streaming rates within the fluid sample. In biosensing, this increase directly correlates with sensitivity gains, which has immediate benefits in diagnostic applications for detecting infections earlier for example.
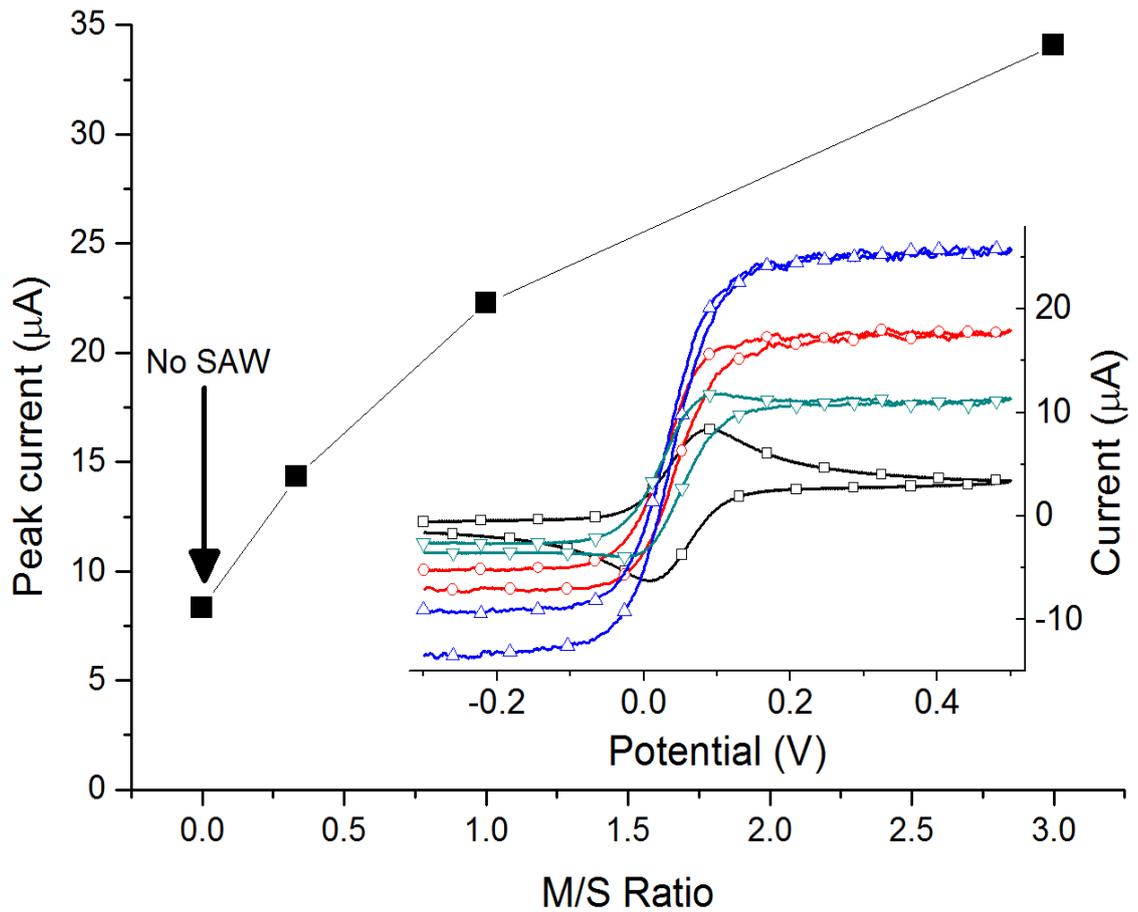
Figure 3. 20   Diffusive peak current plot (filled square) as a function of electrode dimensions (metallisation ratio). The inset shows the CV results performed at 0.1V/s scan rate between -0.3 and 0.5 V. The first voltammetric test was performed in the absence of SAW streaming (empty square). Following tests were made in front of three different, SAW propagating, finger sets; 2nd set with 0.333 M/S ratio (down triangle), 4th set with an equal M/S ratio (circle) and 6th set with 3 M/S ratio (up triangle). The applied SAW signal was at 12.24 MHz and its power was fixed to 0.79W. The concentration of the ferrocyanide solutions was 5 mM (in 100 mM KCl). The area of the straight electrodes used in the system was 0.19 mm^2. Enhanced mass transport rates helped to improve the amount of material which was being included in the electrochemical reaction during the application of triangle CV voltage. The fluid motion induced by SAW enabled to increase the diffusion limited current from 8.3 µA to 34 µA for M/S =3, an 85 % increase in signal.

This part explained a method to enhance the efficiency of SAW transducers in biosensing applications. Electrical energy to mechanical energy conversion ratio was improved without using any external impedance matching circuit or increasing the applied voltage (peak to peak). The results show that increasing the M/S ratio led to improvements in SAW generation. The enhancement stems from the wider area coverage of the electrodes, which interacts with a larger area of the piezoelectric substrate, causing displacement of a larger volume of the piezoelectric crystal. The photolithography based fabrication process may require a precisely specified mask for very closely (less than 10 µm) positioned electrode structures.

3.3.   SAW induced fluid streaming
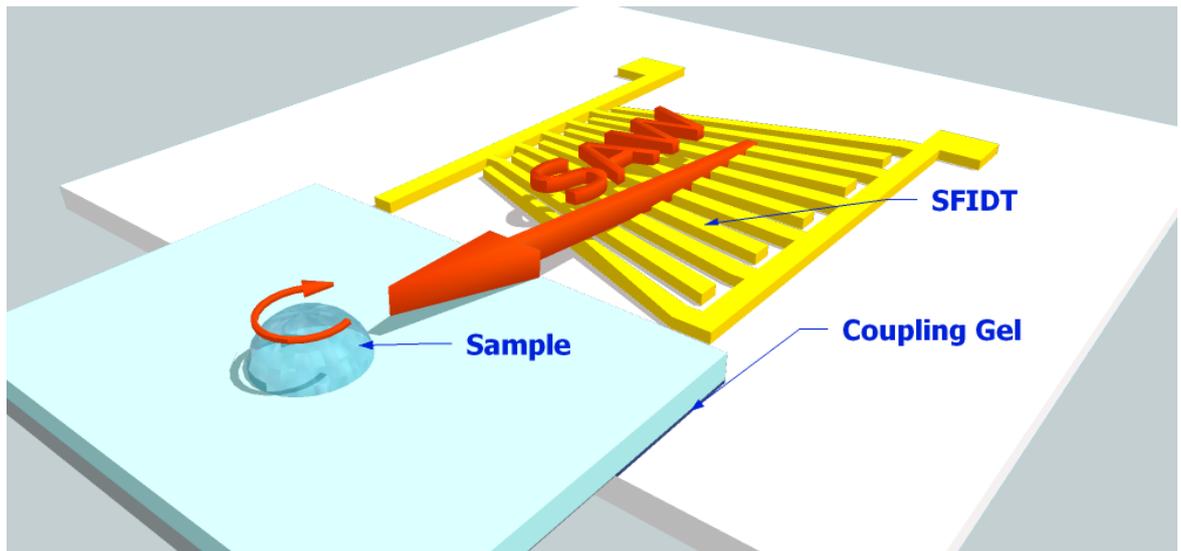
Figure 3. 21   Depiction of the superstrate based system setup. SAW induced streaming applications were conducted on a glass slide (1 mm) coupled on SAW platform. The slanted resonator was capable of working from 8 to 12 MHz. The fluid rotation speed in the droplet is controlled by the applied SAW power.
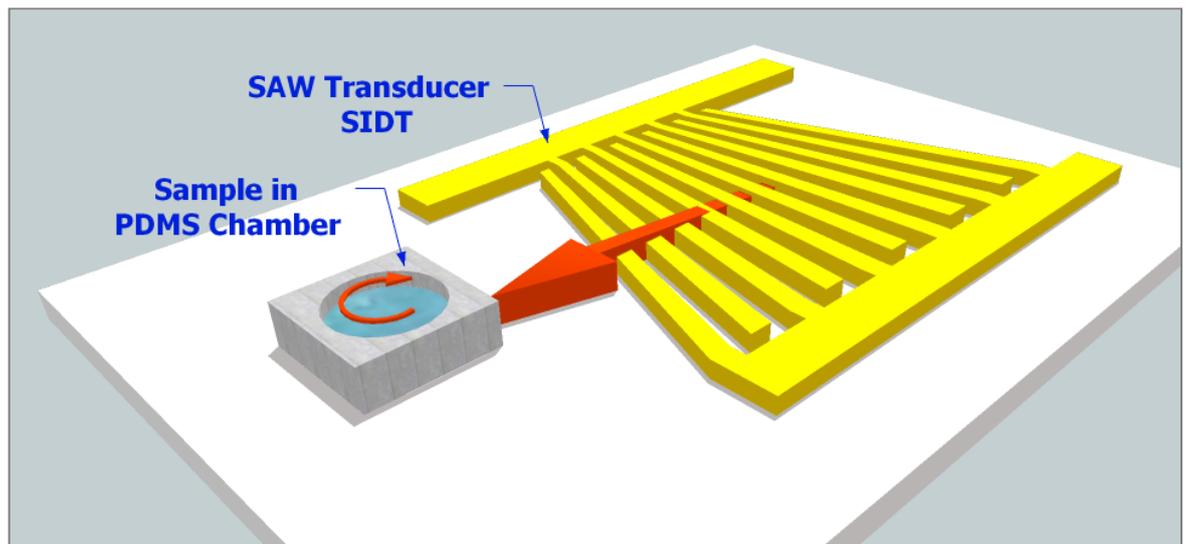
Figure 3. 22   Depiction of fluid streaming in a PDMS chamber via SAW excitation. The working frequency range of the SAW generator was from 7.6 to 16.6 MHz. The mixing chamber is located on the same substrate surface with the SAW transducer to decrease the power loses.

Fluid streaming experiments were conducted with two different setups. Firstly, 3 µl droplets were analysed on a superstrate based system (Figure 3. 21). A trap (radius: 1.5 mm) fabricated on the glass slide controlled the circular shape of the droplets. The trap was fabricated by the hydrophilic/hydrophobic interface pinning method [73]. The second setup was free from any superstrate and included a PDMS (radius: 1.75 mm) chamber for sample handling. The working frequency range of the SFIDT was between 7.6 MHz and 16.6 MHz.

3.3.1. Fluorescence correlation spectroscopy measurements
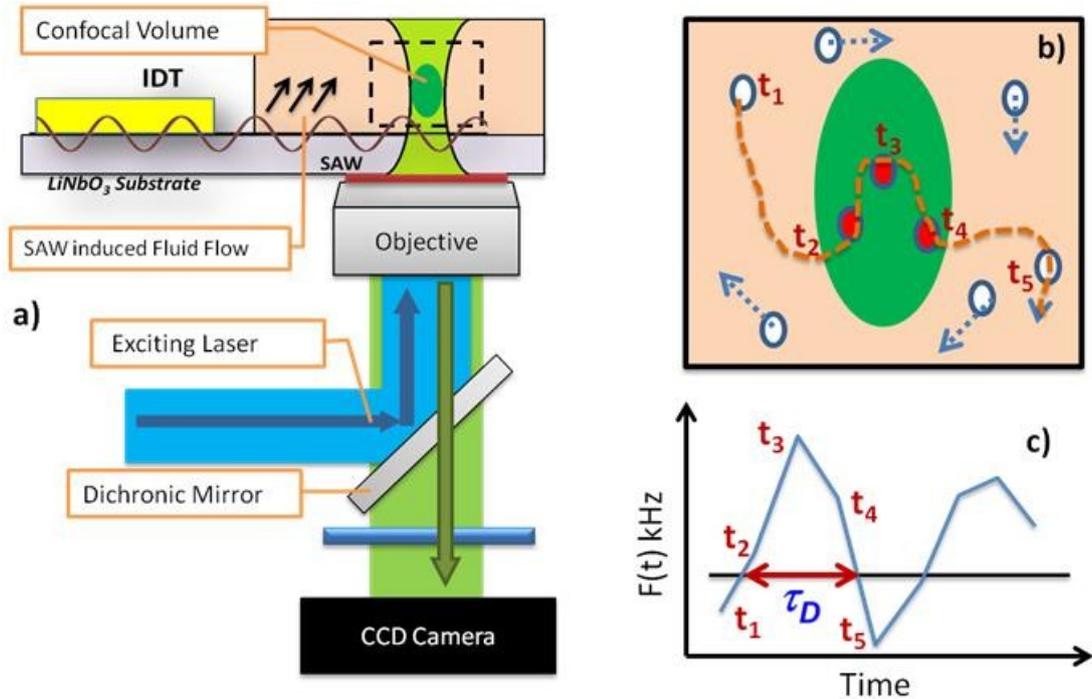
Figure 3. 23 a) Schematic diagram of FCS measurements on a SAW based microfluidic platform. The dynamically active sample was illuminated by the focused laser beam through a 40x, 1.2 numerical aperture (NA) water immersion objective lens, and then the resultant fluorescent photons were detected by a hybrid photomultiplier tube (PMT) with single photon precision. b) The confocal volume where intensity fluctuations are measured with 100 nm fluorescent microspheres driven by fluid flow. c) Graph of detected fluorescence fluctuations within the confocal volume. The duration of the fluctuations provides information on the average time a particle resides in the confocal volume. With knowledge of the volume dimensions, information on the speed of the fluid flow can be determined. Moreover, the function provides information about the concentration of the material in the sample.

As mentioned above, SAW induction into a fluid sample leads to streaming at different speeds, depending on various parameters such as SAW power and measurement location in the sample. In this section, fluorescence correlation spectroscopy (FCS) [92] was used to measure streaming velocities on the superstrate based acoustic mixing platform (Figure 3. 21). A 170 µm thick coverslip was used due to the short working distance of the high NA lens. The coverslip was attached on the SAW platform via a gel interface. SAW was applied to a 3ul droplet at varying powers ranging from 0.05 to 0.2 W. The auto-correlation function, G (τ), (Equation 2) was fit to the curves shown in Figure 3. 24 (left) providing the flow time, τ_{flow}. From this the flow velocity could be determined from the relationship shown in Equation 2. In Equation 3, ω_0 is the lateral radius of the confocal volume determined with a nM solution of a small diffusing fluorescence molecule in water, as outlined in [93], and V is the measured velocity. The velocities obtained from the fitted auto-correlation function (Figure 3. 24- left) gave the results shown in Figure 3. 25 (right).

$$G(\tau) = \frac{1}{\langle N \rangle} e^{\left(\frac{-\tau}{\tau_{flow}}\right)^2}$$

Equation 2

$$\tau_{flow} = \frac{\omega_0}{V}$$

Equation 3

A secondary FCS measurement series performed at different heights inside a 3µl droplet. The SAW power (0.125 W) and the frequency (11.7 MHz) was fixed. Velocity values obtained from FCS measurements performed at four different heights in the droplet are presented in Figure 3. 25.
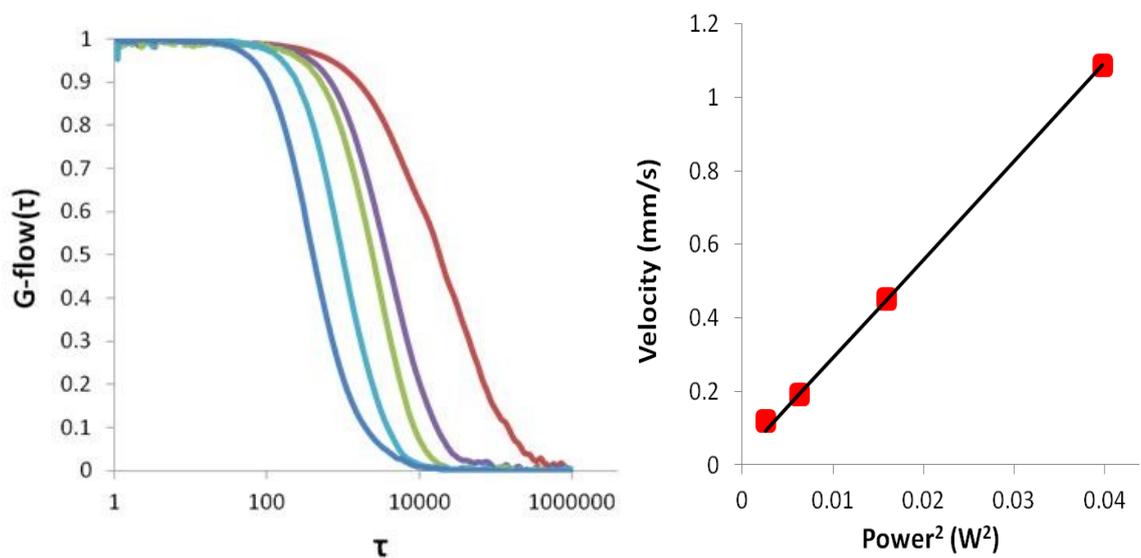
Figure 3. 24   FCS results obtained at the height of 110 µm in a 3ul droplet located on a coverslip substrate. The produced sound waves were travelling through the surface of the piezoelectric material and coupling to the glass slide through a gel interface. The frequency applied to the SFIDT was 11.7 MHz and the input power was varied; 0 W (red), 0.05W (purple), 0.08W (green), 0.13 W (turquoise) and 0.2W (blue). Left: Measured auto-correlation functions for 100 nm fluorescent microspheres driven by fluid flow. Right: The flow velocities (square) calculated from the τ-flow values obtained from the fitted auto-correlation function. A curve (solid line), varying according to the power (V = (26.745 ∗ P² + 0.025) ∗ 10⁻³) , is fitted on the experimental data.
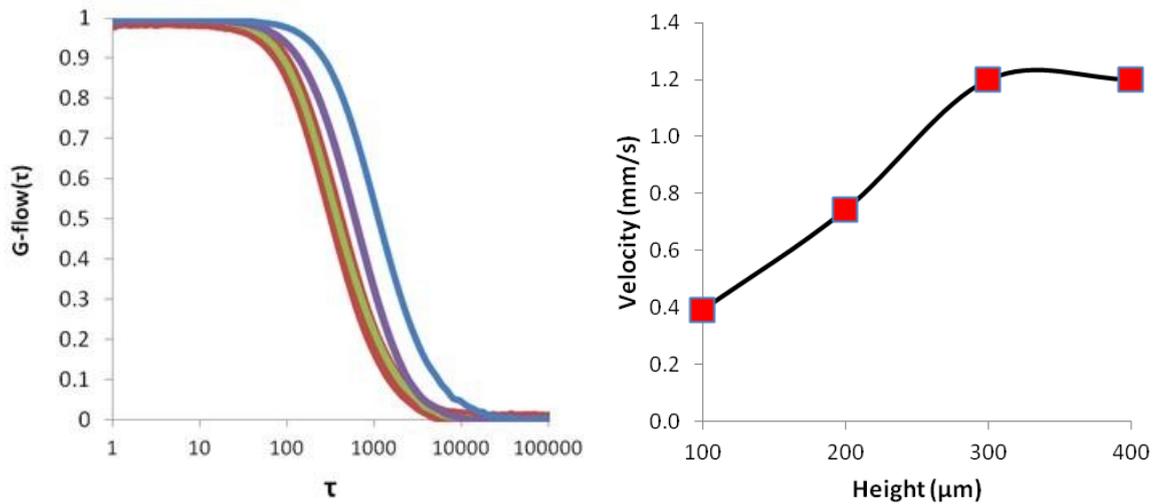
Figure 3. 25   FCS results obtained in a 3ul droplet, at different heights; 100 μm (blue), 200 μm (purple), 300 μm (green) and 400 μm (red). Left: Measured auto-correlation functions for 100 nm fluorescent microspheres driven by fluid flow. Right: The flow velocities (square) calculated from the τ-flow values obtained from the fitted auto-correlation function. The frequency of the signal applied on SAW IDT was 11.7 MHz, and the input power was 0.13 W.

It has been demonstrated that FCS can be used to measure SAW induced streaming velocities. However, the volume of the micro-scale sample was relatively large in comparison to the FCS detection volume (approximately 1 fl). Meanwhile the streaming pattern and the speed are not always even in the volume of the droplet. Therefore the FCS technique requires multiple measurements, at different locations of the sample. Also, FCS provides no information on directionality with respect to the SAW induced fluid streaming. This long experimental process must be repeated after each SAW streaming test. Moreover, it can also be difficult to obtain quantitative data on high power (over 0.5 W) SAW streaming due to evaporation led by the acoustic heating. Consequently, FCS measurements in SAW actuated droplet cannot provide relevant results. Increasing the humidity of the surrounding environment may be used to decrease evaporation.

3.3.2.   Particle image velocimetry (PIV) measurements

SAW induced streaming was characterised by the micro particle image velocimetry (μ-PIV) method [94]. The μ-PIV device consisted of a Nikon eclipse TE2000 microscope, a high frame rate camera (3000 frames per second at 1024 by 1024 pixels resolution- Photron APX RS), a laser source (10 mJ at 1 kHz) for illumination of the red dyed fluorescent particles and a laser pulse synchronizer. The SFIDT transducer was re-fabricated on a transparent LiNbO$_3$ substrate because the microscope of the μ-PIV system was inverted; therefore, it was required to observe the droplet from the bottom of the substrate. It should be noted that the velocities measured by the μ-PIV system gives only 2D (horizontal) information.

Measurements were performed in 3 µl water droplet samples which contained fluorescent particles (Fluoro-Max Dyed Red Aqueous Fluorescent particles, R0300 – Thermo Scientific) at a concentration of 4.10^6 particles/ml.
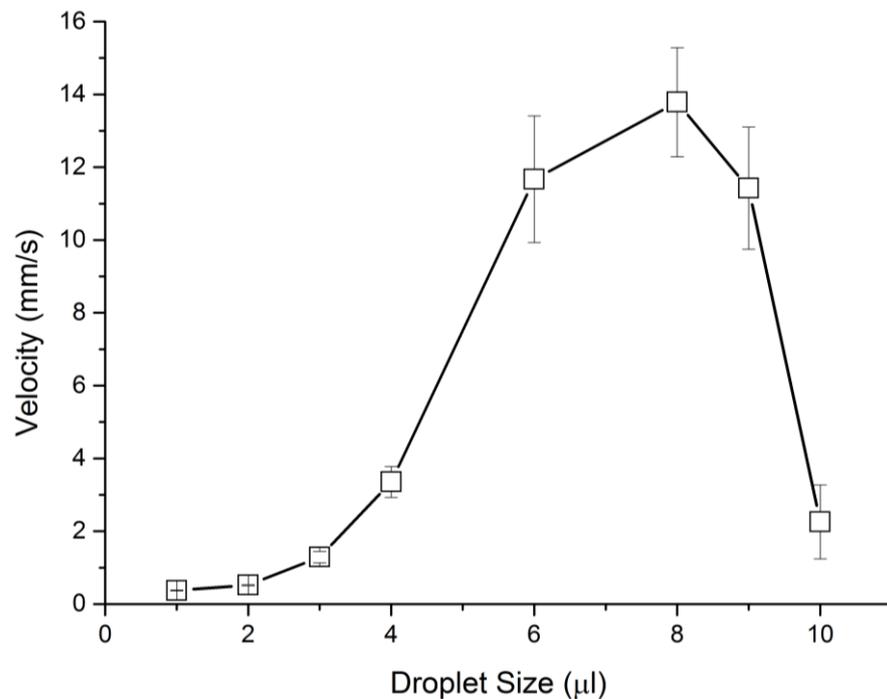
Figure 3. 26 SAW induced streaming measurements on droplets in different volumes (from 1 to 10 µl). The velocity reached to the maximum level, 13.8 (+/- 3.7) mm/s, when the droplet size was around 8 µl. The SAW streaming performed with a fixed frequency (9.2 MHz) and power (0.16 W). The centre of the droplets were localised 5 mm away from the SAW transducer. Error bars presents the standard deviation obtained from the average speeds measured in three tests.

SAW induced mixing process presents different situations, according to the size of the droplet. The velocity change due to the volume variation of the droplet is explained in this part. Results, given in Figure 3. 26, reveal that the velocity of the streaming reached the maximum, 13.8 (+/- 3.7) mm/s when the droplet size was around 8 µl. Various physical parameters can affect the streaming velocity or the efficiency. The combination of SAW radiation angle, acoustic beam excitation point, attenuation length, and the height of the droplet are highly influential parameters on the velocity obtained in the droplet. Inertial forces of the system resists towards the flow direction, therefore, cause speed decreases. For example, the flow velocity decreases as the height of the sample decreases, due to the increased shear forces [95]. In the opposite case, when the droplet volume is larger, the viscous forces decrease however various types of motions happen on the droplet such as jumping [96], vibration (squeeze release action) [97] and capillary waves [46] on the droplet surface. This energy absorbing actions cause acoustic energy loss. Therefore, an optimum sample volume can be defined for any particular setup, to obtain an efficient acoustic streaming.
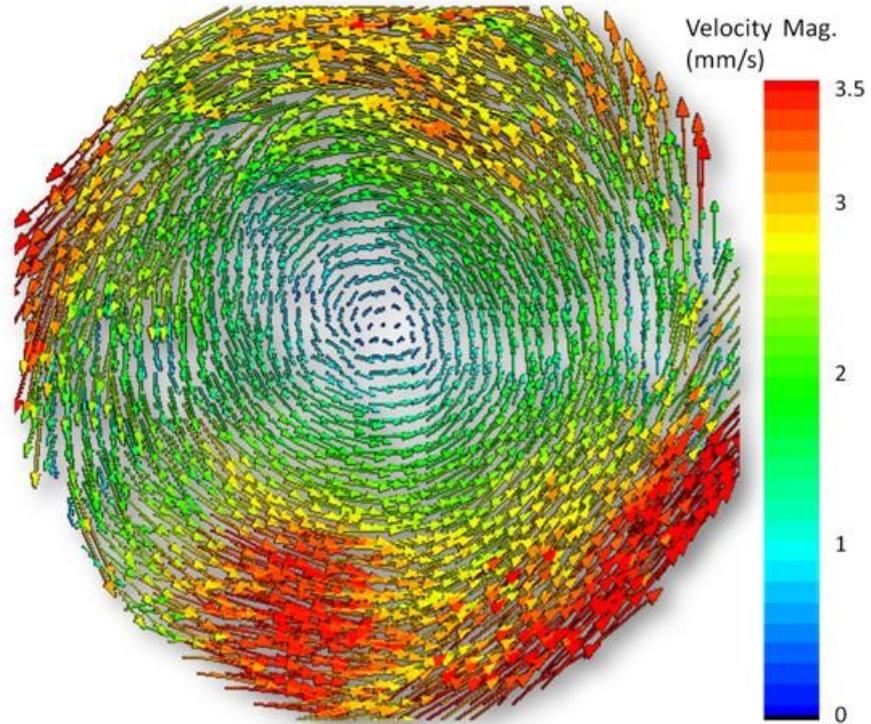
Figure 3. 27 The graphic shows the SAW (9.2 MHz, 0.16 W) induced flow pattern inside a 3 μl droplet. μ-PIV measurements give the 2D velocity profile at 200 μm high from the substrate surface. Asymmetric excitation of the droplet created an angular momentum. The streaming was reached up to 3.5 mm/s thanks to the vortex created by SAW streaming radiated from the 29 finger SFIDT.
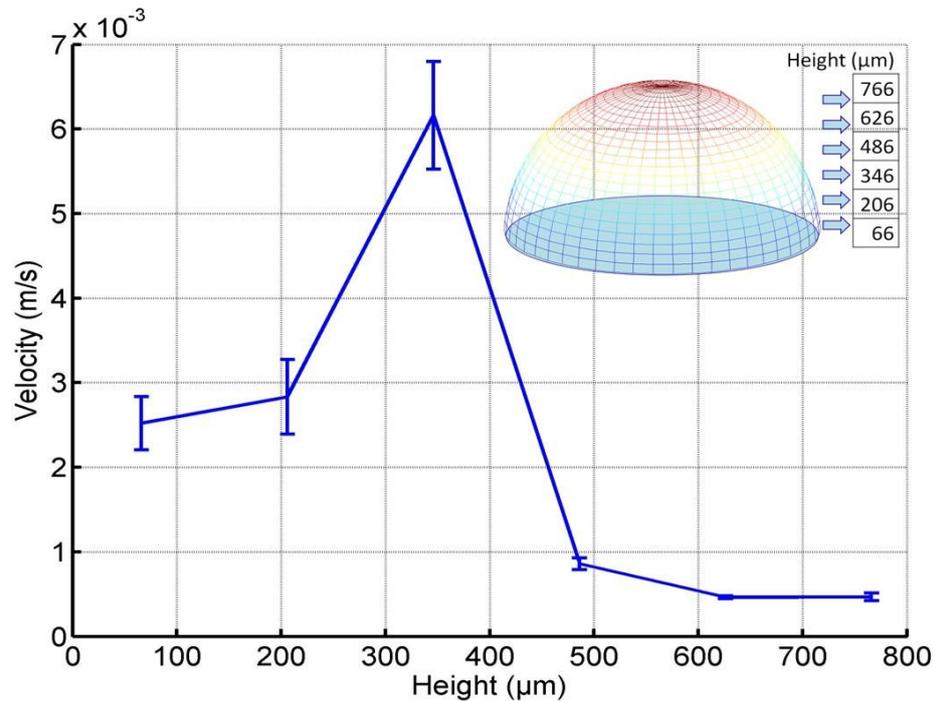
Figure 3. 28 Speed measurements obtained at various heights (66, 206, 346, 486, 626, 766 μm) inside a 3 μl droplet. The vortex was obtained thanks to the SAW (0.16 W and 9.2 MHz) beam radiating from the side of the droplet. The error bars represent the standard deviation obtained from three independent experiments at each height level.

Figure 2. 17 exhibits the observed velocities, via the μ-PIV device, at different heights. Maximum speed, 6.11 mm/s (± 0.64 mm/s), was obtained at the middle height (∼350 μm). The plot in Figure 2. 17 was the product of averages velocities obtained from the flow patterns. Figure 3. 27 gives an example of a flow pattern obtained at 200 μm height.

The μ-PIV technique managed to reveal quantitative data at various experiments since it was able to capture the velocity data by a single step in a short time (∼4 seconds). This capability was an advantage over the FCS technique. However, the vibration of the droplet was creating an additional motion, in the line between the centre and the outer chamber, in addition to the rotational motion. The extra movement was making the flow difficult to quantify. This effect also created noise problems in electroanalytical experiments (for further details see the electroanalytical measurements performed in the superstrate based system in the following chapter).

Rotational flow velocity in a PDMS chamber

A substrate based system (Figure 3. 22) was designed, and tested (via μ-PIV method), in order to achieve the issues faced during the optical monitoring and electroanalytical measurements (see details in "SAW induced electroanalysis" chapter). The addition of a closed PDMS chamber into the actuation platform enabled the avoidance of the vibration and the evaporation of the sample. The capillary waves on the surface and the general vibration of the sample (droplet) were minimised by the surrounding PDMS structure.

The μ-PIV measurements were performed on 20μl samples at five different SAW powers; 0.5, 0.79, 1, 1.26, 1.59 W. The fluid sample included fluorescent beads (Fluoro-Max Dyed Red Aqueous Fluorescent particles, R0300 − Thermo Scientific) at a concentration of 4.10^6 particles/ml.

Figure 3. 29 illustrates the azimuthal velocity data obtained inside the PDMS chamber. Ring-shaped regions at different distances/radiuses from the centre of the vortex were analysed individually for each SAW power level. The velocity was at the highest levels in the middle ring areas. Moreover, the velocity decayed towards the closer regions to the chamber walls. This was caused by the friction effect of the wall surface. The shear forces resisted towards the fluid motion. Additionally the SAW beam was less efficient at the sides of the chamber due to the cubic shape of the PDMS layer. The PDMS/ Substrate interface was larger, therefore, absorbing more acoustic energy, at the sides of the chamber.
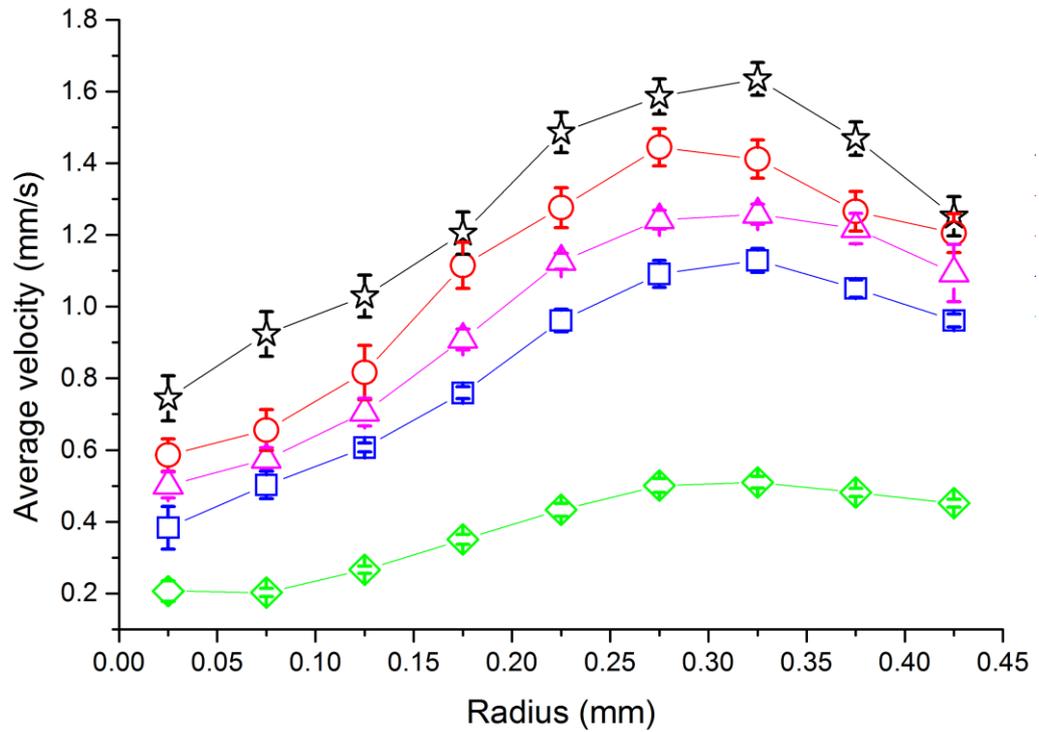
Figure 3. 29   Velocity graph obtained by the velocity patterns received from μ-PIV measurements. SAW induction into the sensing chamber was performed at various powers; 0.5W (diamond), 0.79W (square), 1W (triangle), 1.26W (circle) and 1,59W (star). The graphic presents the observed horizontal velocities at different radius inside the cylindrical PDMS chamber.
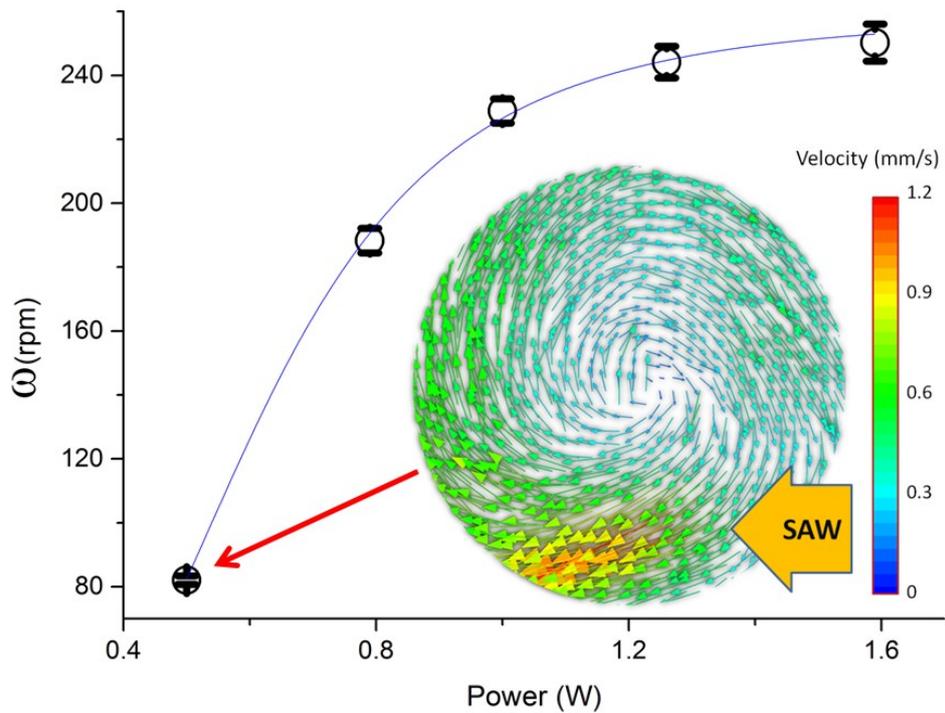
Figure 3. 30   Rotational flow velocity graph: measured inside the PDMS chamber at five different SAW power using a μ-PIV system. The data are fitted well with a Hill function model (Vmax = 258.37396, k = 0.60792 n = 3.91659). The inset shows an example streaming pattern observed at 0.5 W SAW power. The height of the measurement plane was 366μm from the surface. The physical depth of the focus of the μPIV system was 16.27μm.

Rotational velocity (ω) of the fluid streaming inside a PDMS chamber is presented in Figure 3. 30. The flow velocity in the chamber was precisely controlled by the applied SAW power. This relationship was obtained from the μ-PIV velocity data to be used for Koutecky-Levich plots in the next chapter ("SAW induced electroanalysis" section). An example of azimuthal fluid velocity patterns, obtained at 12 MHz and 0.5 W of SAW power, is presented in Figure 3. 30.

Switching to a substrate based system from the superstrate based system compensated the power loss led by the PDMS chamber because the acoustic coupling through the gel layer was decreasing the mechanical energy. Running the mixing tests in a covered PDMS chamber blocked the evaporation and vibration problems. These achievements enabled to capture repeatable μ-PIV data. Moreover, the noise effect in electroanalytical measurements was decreased thanks to the contribution made by PDMS chamber.

3.4.   Conclusion

This chapter focused on the enhancement of SAW streaming efficiency and its monitoring. Various types of SAW transducer and mixing platforms were tested. Characterisations of the systems were performed by scattering (S_{11}) analysis, thermal observations, surface displacement measurements and streaming velocity measurements.

Experimental investigations were started with a basic straight IDT design which presented powerful characteristics due to the collectively resonating large electrode structures. At the following stage, it was replaced with an SFIDT transducer to obtain a controllable angular momentum in the fluid samples. This new case enabled the system to give similar characteristic with the rotating disc electrode application which is a standard technique in the hydrodynamic electrochemistry analysis (see "SAW induced electroanalysis" chapter for details). The design was further developed by extra modifications such as making the system one piece rigid design by removing the superstrate and using a PDMS chamber instead of a hydrophilic trap. The direct handling of the sample on the surface of substrate increased the efficiency due to the avoidance of the loss created by the gel interface. Meanwhile, the system started to present more stabilised characteristics.

Despite the advantages, the SFIDT designs have a draw back. The width of the SAW beam is constrained due to the characteristics of the slanted fingers. At a particular frequency, only a tiny portion of the metal pattern can create travelling waves. However, the step IDT combined the advantages of the straight and the slanted designs. Increasing the amount of straight finger series, with various resonance frequencies, can easily increase the precision of

beam shift. Additionally, the width of the SAW beam can be controlled, according to the requirements of a particular microfluidic platform, by ranging the finger lengths.

Moreover, the wide finger tests results showed that the increased M/S ratio enhances the performance of the transducers without requiring any other equipment such as an impedance matching circuit. The method can be used to obtain a more efficient mixer, pump or heater applications in Lab-on-a-Chip devices. It can also improve the cell patterning applications performed with SAW resonators. Importantly, the design modification based performance enhancement does not cause any cost increment.

4. Saw induced electroanalysis

4.1.   Introduction
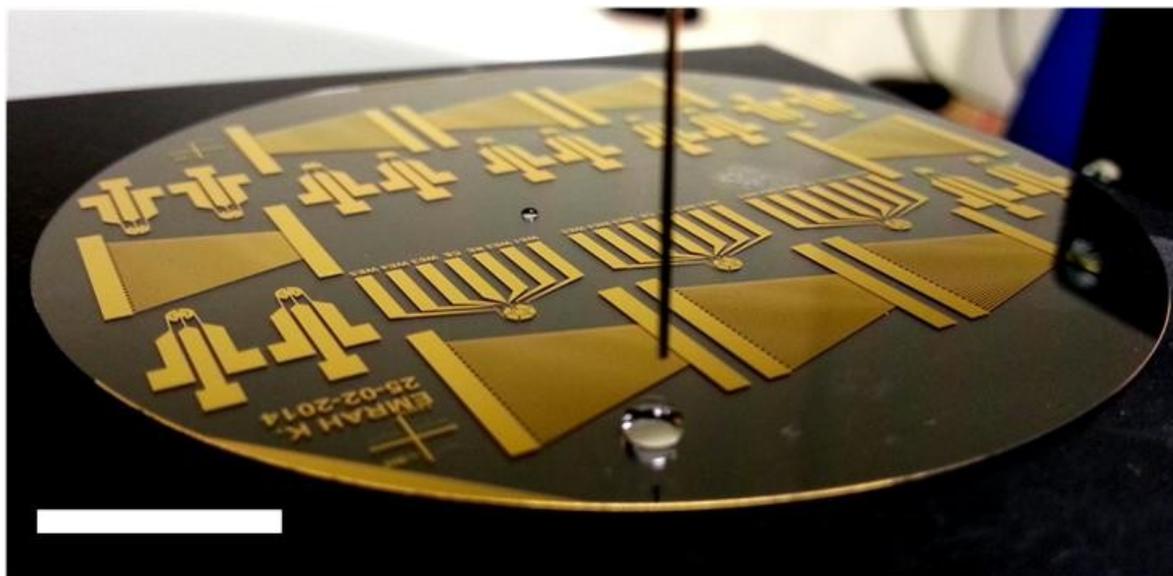
Figure 4. 1   Image of several "SAW enhanced electroanalysis platforms" fabricated on the same substrate (128° Y-cut X-propagating 3 inch transparent LiNbO$_3$, c=3996 ms^{-1}). Metal structures were obtained by lifting the UV patterned S1818 layer (scale bar, 10mm).

Within lab-on-a-chip (LOC) systems, electrochemical sensors have been shown to reach pico-molar sensitivities[98][99], using only microliter-sized samples, enabling them to have a significant impact in clinical practice (e.g. heavy metal [100], and melamine sensors [99]) . The ability of electrochemical sensors to operate in turbid environments has enabled them to perform in applications outside the reach of optical techniques. This characteristic has demonstrated potential in healthcare applications, such as point-of-care diagnostics (e.g. glucose sensing [101]).

Although miniaturisation has enabled the use of small (pin-prick sized) volumes of samples, thus providing the potential for low costs (e.g. reduced reagents and device fabrication cost) and non-invasive sampling, it puts pressure on the performances achievable. In the case of electrochemical sensors, the diffusion layer, localised on electrode surfaces, limits the amount of electron flow. Hydrodynamic techniques create an external convection effect to increase significantly the mass transferring rates to reduce the size of the diffusion layer. This results in higher currents and the rapid establishment of the steady state of the system. Therefore, both the sensitivity and the sensing time of the sensors are improved [22], as is the case in techniques such as rotating disc electrode (RDE) [102][103][25][26], channel electrode [27], sonochemistry [28][29] and dropping mercury electrode [104]. Further enhancements were also obtained by the application of the different hydrodynamic technique

combinations on electroanalysis platforms [31], up to 1.5 times in signal. However, most of these techniques have had limited applications in LOC systems, mostly due their complexity, which also requires bulky equipment and large volumes of sample (e.g. high-speed RDE [105]).

Recently, surface acoustic waves (SAW), nanometres mechanical deformations travelling at the surface of devices at ultrasonic frequencies, have shown potential in enabling advanced liquid sample manipulation, thus enhancing conventional sensing systems [42][96] [121][85][48][107]. Rayleigh waves, a particular type of SAW, are most commonly excited by interdigitated transducers (IDTs) localised on a piezoelectric material [45][108]. SAWs become leaky when they reach a liquid sample. This produces longitudinal pressure waves and creates streaming [47][109]. The effective radiation's depth depends on the fluid viscosity and the acoustic energy.

The application of SAW enables the non-contact actuation of fluids, as the waves refract into the liquid as longitudinal waves, imparting energy to the fluid. This results in devices that are simple, reliable and easy to fabricate and operate [33], especially when compared to systems where convection is enabled via moving parts[105][31]. For example, when used in combination with a Surface Plasmon Resonance (SPR) sensor, SAW allowed efficient mixing that resulted in faster and more sensitive assays [110][111]. Additionally nanometre SAW actuation of the surface along with acoustic streaming recirculation showed the ability to reduce non-specific binding in biosensing applications[112].

Here we show that the use of acoustic streaming, generated by SAW, enables to enhance the sensitivity of an amperometric sensor by a factor of 6, while only requiring microliter sample volumes on a low-cost system (Figure 4. 1).

4.1.1.   Theory

Application of the electrical potential creates a concentration difference between the electrode surface and the bulk solution. This drives fresh material from the bulk solution towards the electrode surface via diffusion. However, the rate of the mass motion becomes the limiting factor of the system. In addition to the diffusion, the mass transfer in a fluid system is driven by two other effects; electro- migration and convection [113]. The diffusion becomes more efficient in such systems with low Reynolds and high Damkohler numbers [114]. The application of SAW streaming on solid-liquid interfaces can cope with mass transfer issues of the systems. The streaming, created via mechanical waves, increases the motion of fresh analyte towards the area of interest. Therefore, the reaction rate can be

increased by the application of SAW effect. Figure 4. 2 depicts the mechanism of model system's, potassium ferrocyanide ($K_4[Fe(CN)_6] \cdot 3H_2O$), reaction.
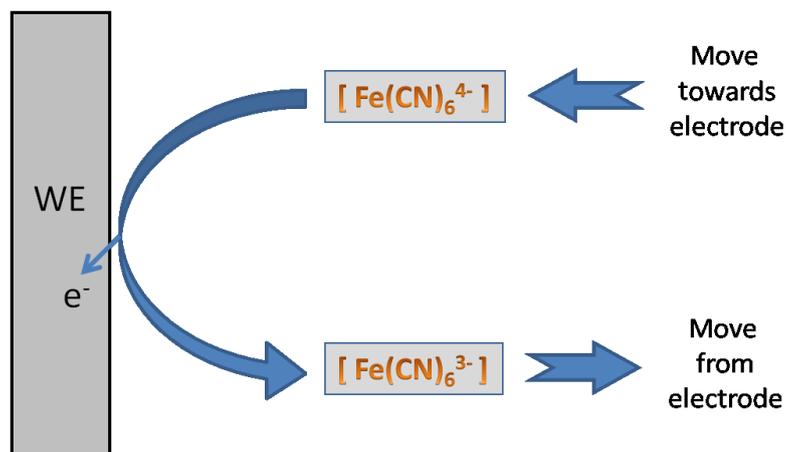
Figure 4. 2 Transport of ferrocyanide toward the electrode surface and the oxidation of ferrocyanide to ferricyanide ($Fe(CN)_6^{3-}$) following the transport of ferricyanide away from the surface.
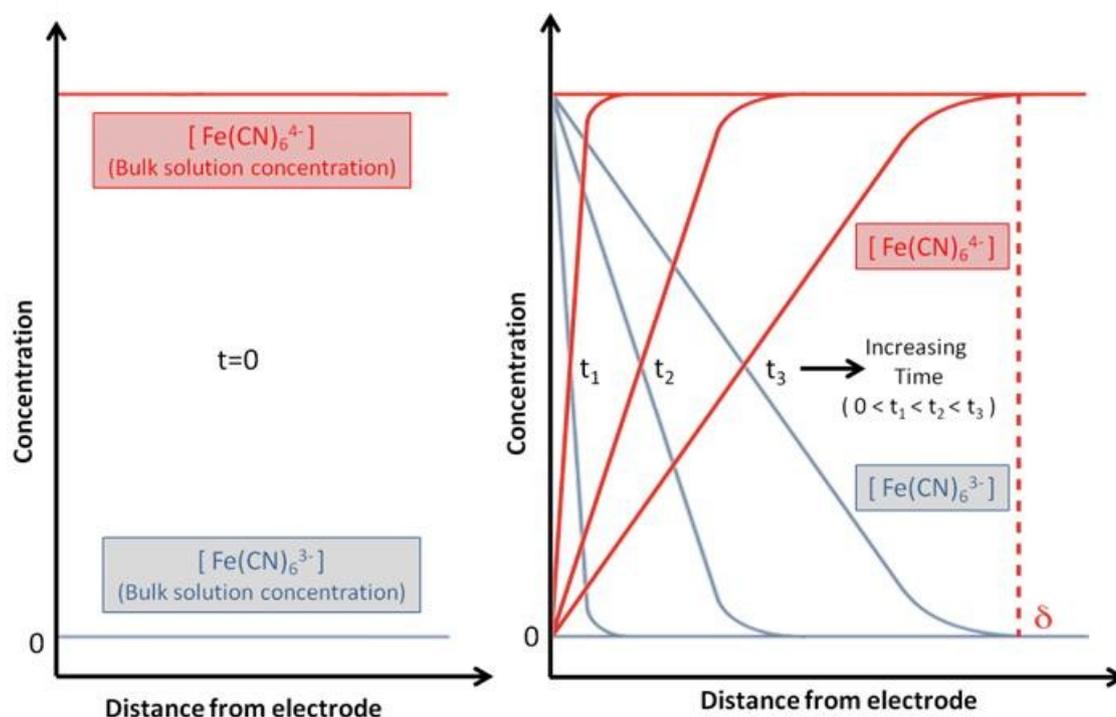
Figure 4. 3   Concentration gradients of ferrocyanide (Red) and ferricyanide (blue) on the electrode surface. The first graph depicts the stabilised concentrations, at the distances from the electrode surface, before the application of potential (t=0). After applying the potential, the concentration of ferrocyanide drops to zero at the electrode surface, and it starts to diffuse toward the electrode. The longer the potential is applied, the thicker the diffusion layer through which the diffusion process continues. The extent of the diffusions layer, at the time "t_3" is presented with the dashed red line.

4.1.2.   Damköhler Number

Damköhler Number (Da) is the ratio between the chemical reaction rate and the mass transport rate (Deen, 1998). If the number decreases, that means the chemical reaction characteristics becomes the dominant parameter and controls the reaction [114]. In this work, SAW streaming was applied to a chemical cell to decrease the Damköhler number by increasing the mass transport rate.

$$\text{Da} = \frac{\text{Chemical Reaction Rate Constant}}{\text{Mass Transport Rate Constant}}$$

$$= \frac{\text{Mass Transport Characteristics Time}}{\text{Chemical Reaction Characteristics Time}} \quad = \quad \frac{T_M}{T_C}$$

Equation 4

4.1.3.   Streaming at low Reynolds numbers

Microfluidic systems are governed by more active inertial forces than what we are used to. Surface effects such as wettability, surface tension, adhesion, and others become more predominant. This occurs due to the relatively small ratio between the volume of the liquid and the area of the solid surface. The physical explanation of this behaviour is explained by Reynolds number (Equation 5). It is a parameter presenting the ratio between inertial forces and viscose forces [32]. Microfluidic systems operate under a strong influence of surface effects. This increases the viscose forces and presents low Reynolds numbers. Moreover, the microfluidic systems are very limited by the diffusion due to the laminar flow regime. Lack of turbulence flow puts enormous adverse effects on the chemical reaction rates.

$$\text{Re} = \frac{\rho v \text{L}}{\mu} = \frac{\text{Inertial Forces}}{\text{Viscous Forces}}$$

Equation 5

Reynolds formula is explained via the Equation 5 where ρ is the density, v is the velocity of the flow, L is the length, μ is the dynamic viscosity of the fluid.

4.1.4.   Hydrodynamic Electroanalysis

Compared to quiescent (i.e. in absence of fluid flow) electrochemistry, hydrodynamic electrochemistry has the advantage of significantly enhancing the rates of mass transfer towards the electrodes; with a resulting higher current flow that increases the accuracy of the measurements. Moreover, the fluid motion decreases the time duration required for the

establishment of the steady state of the mass transport system. These enhancements increase both the speed of measurement [22] and the sensor sensitivity. There are two ways of creating convection in electrochemical cells. First, to move the electrode and second, to move the liquid. Both motions enhance the rate of mass transfer and change the behaviour of the system. There are different techniques for the hydrodynamic analysis of electrochemical cells, such as rotating disc electrode (RDE) [102][103][25][26], channel electrode [27], sonochemistry [28] [29] and dropping mercury electrode [104].

The leading scientist and the establisher of hydrodynamic electrochemistry are Levich, Veniamin (Benjamin) Grigorievich. He is the developer of the well known Levich equation, describing the diffusion (transport limited) current at the surface of a rotating disk electrode [115].

Further enhancements can be obtained by the application of the different hydrodynamic technique combinations on electroanalysis platforms. Lorimer et al. has reported a maximum average increase of some 1.5-fold by the application of ultrasound to the rotating disc electrode in an aqueous solution of potassium ferrocyanide and potassium chloride as the electrolyte [31]. Also, researchers at the University of Sherbrooke incorporated SPR sensor with a SAW platform. Their findings proved that the concept works faster and more gave sensitive assays in SPR based biosensors [70]. Hydrodynamic electroanalysis can also be used for other measurement purposes such as the velocity of the microfluidic stream. In the University of Berkeley Tsao et al. benefited from electrochemical detection technique (diffusion limited cell current) for the quantification of fluid mixing in their Flexural-plate-wave devices, caused by both standing and travelling flexural waves, in 1991 [116]. The electrochemical cell was comprised of two electrodes, a working electrode (WE) and a counter electrode (CE), a DC voltage source, and an ampere meter. One of the most noticeable results of the research was; the current enhancement obtained by standing wave was bigger than the travelling waves because of the greater mixing effect induced by many localised narrow flow cycles. They got 80 % current enhancement by the application of standing waves on the system (and 30% with travelling wave). Monash University researchers combined SAW platform with a drop scale chemical reactor. Consequently, the application of travelling mechanical waves was significantly increased the speed of the chemical synthesis [117].

This paper will be explaining the results obtained by the combination of two platforms; SAW based resonator system and an electrochemical sensing system. A similar fluid motion with the well known RDE technique was obtained inside the chamber, thanks to the specially designed device combination.

Flow Injection Analysis

This method is based on the motion of the fluid on the surface of the sensing area. The liquid sample is forced to flow through the channel. The sensing area is embedded in the walls of the channel. Numerous electrochemical applications can benefit from the incorporation of an FIA system[118]. Flow-induced amperometry is an electroanalytical technique benefited from an FIA attachment [119].

Rotating Disc Electrode
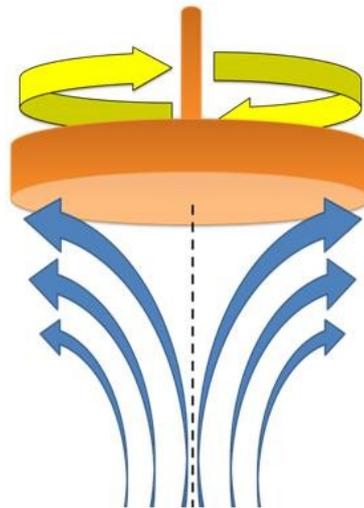
Figure 4. 4 Schematic of a rotating disc electrode (RDE) mechanism (Arrows indicate the direction of fluid). The flow created by the rotation drags fresh material towards the surface of the electrode to react.
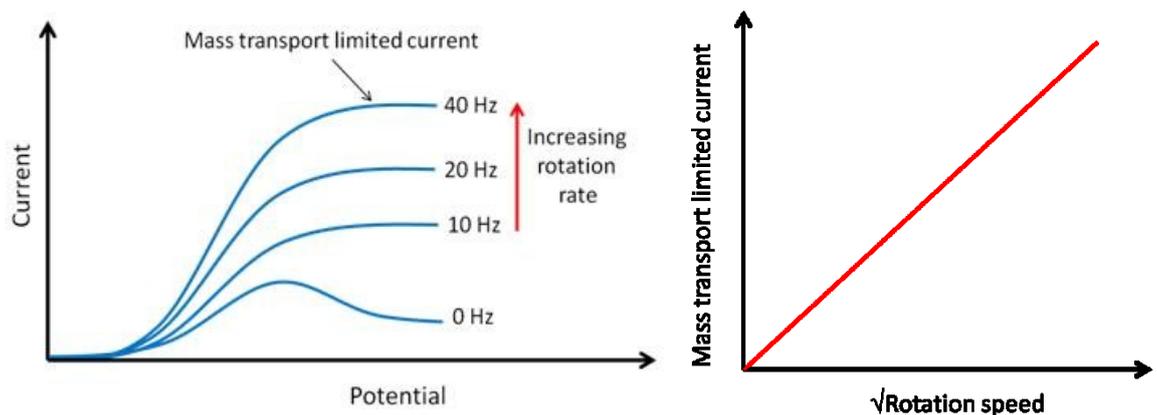
Figure 4. 5 Increasing rotation rates enhance the reaction rate and, therefore, the diffusion limited (Levich) current, presented by sigmoidal waves (Left). The Levich current values are measured and plotted against the square root of the angular velocity. This produces the Levich plot. The chemical reaction rate constant defines the upper limit of the current flow. The lower limit of the current flow is defined by the diffusion rate at the stagnant case.

Rotating disc electrode (RDE) is a standard method used for electroanalytical applications [120]. Increased rotation rate helps to improve the current flowing through the interface

between the electrode and the liquid. The circular motion of the electrode increases the mass transfer rate in the surrounding environment of the electrode [120]. Therefore the angular speed (ω) can tune the thickness of the diffusion layer.

$$\omega = 2 \pi f$$

<div align="right">**Equation 6**</div>

where f is the revolution per second (RPM). This formula is used for the conversion of rotational speed to the angular velocity (ω).

Relationship between the diffusion layer and the rotation rate is described by this equation;

$$\delta = 1.61 \, D^{1/3} \, V^{1/6} \, \omega^{-1/2} \, [m]$$

<div align="right">**Equation 7**</div>

where D is the diffusion coefficient of the material used and V is the kinematic viscosity of the electrolyte. The kinematic viscosity is the ratio of viscosity to the density of the fluid. It is measured in stokes ($cm^2 \, sec^{-1}$).

The Levich Equation is written as;

$$I_L = 0.62 \, z \, F \, A \, D^{2/3} V^{-1/6} \, w^{1/2} c_0$$

<div align="right">**Equation 8**</div>

where F is the Faraday constant, A is the electrode area and C_0 is the analyte concentration. According to the Levich equation, I_L changes as proportional to the square root of the angular velocity. Increasing rotational velocity creates more current flow through the electrode [11]. This makes the system more sensitive and rapid, comparing to a stationary system.

Koutecky Levich

The reciprocal current in a real electrochemical system is based on the mass transfer and the charge transfer rates. This can be presented as shown below.

$$\frac{1}{I} = \frac{R_k}{V} + \frac{R_d}{V} = \frac{1}{I_k} + \frac{1}{I_d}$$

Equation 9

In the equation, R_k represents the charge transfer resistance since the current must flow accross the electrolyte-electrode interface. The R_d represents the mass transfer resistance since the current must flow through the diffusion layer. The Koutecky-Levich equation is based on the combination of Equation 8 and Equation 9. Unlike the Levich equation, this equation can be used when the kinetics contribute to the current flow.

$$\frac{1}{I} = \frac{1}{I_k} + \frac{1}{0.62\, z\, F\, A\, D^{2/3}\, V^{-1/6}\, w^{1/2} C_0}$$

Equation 10

I_k represents the kinetic rate limited current;

$$I_k = FAkC$$

Equation 11

where the kinetic rate constant is presented by k, which is dependent on the applied potential through the electrodes and the concentration (C) of the analyte. If the angular speed goes to infinity, the diffusion becomes very fast. Therefore, the diffusion layer disappears, and the diffusion limited current becomes zero. The system starts to be controlled purely by the reaction rate [115][11]. This method enables to obtain the current in the absence of diffusion control. When the system is controlled by the electron transfer rate constant, the current flow would be I_k (Equation 11).

Heated electrodes

Chemical reactions are highly influenced by the temperature changes. It is a scientific fact that the average kinetic energy of the molecules increases by the increased temperature. According to the equation of Arrhenius [115], the molecules start to move faster. Therefore the amount of molecules, with minimum energy to react, increase [121]. This enhances the sensitivity of the detection systems by increasing the frequency of the molecule collisions [11] and creates a similar effect with mechanical stirring [30].
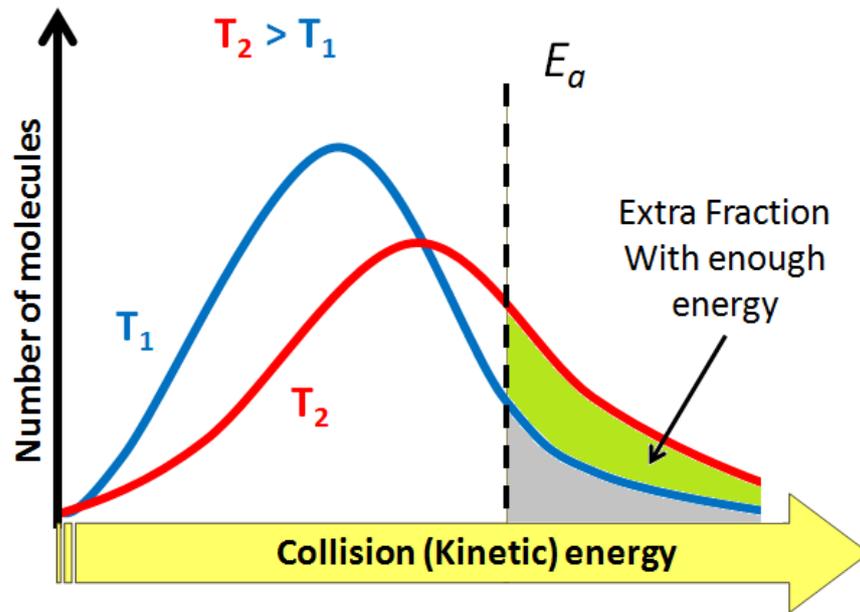
Figure 4. 6 The energy distribution of molecules, depending on the temperature variation. Increasing the temperature, from T1 to T2, prepares more molecules with enough energy to react. This extra fraction of molecules is represented by the green shaded area in the graph. Therefore, more molecules can overcome the activation energy (Ea). This increases the reaction rate.

4.2. Device Concepts

The SAW-enhanced hydrodynamic voltammetry microchip comprises of a sensing platform and a SAW platform. Fabrication of both devices was made by metal deposition (10nm Ti Adhesion layer / 100nm Au) and lifting off the photoresist (S1818). While the sensing electrodes were fabricated on glass slides (1 mm thick), SAW devices were fabricated on the piezoelectric substrates ($LiNbO_3$).

4.2.1. Superstrate based concept

The superstrate based design was obtained by coupling the two separate systems. A water-based gel interface (approximately 50-µm thick) was used for the attachment of sensing platform on to the primary substrate (SAW platform) [45]. Three µl water-based gel layer (KY Jelly; Johnson and Johnson) was spread manually between the $LiNbO_3$ layers.

Superstrate aspect is promising for the future disposable sensor designs. This has the potential to save the cost by enabling to reuse the SAW device with new sensors. Coupling of travelling mechanical waves through the gel interface is explained in the previous chapter.
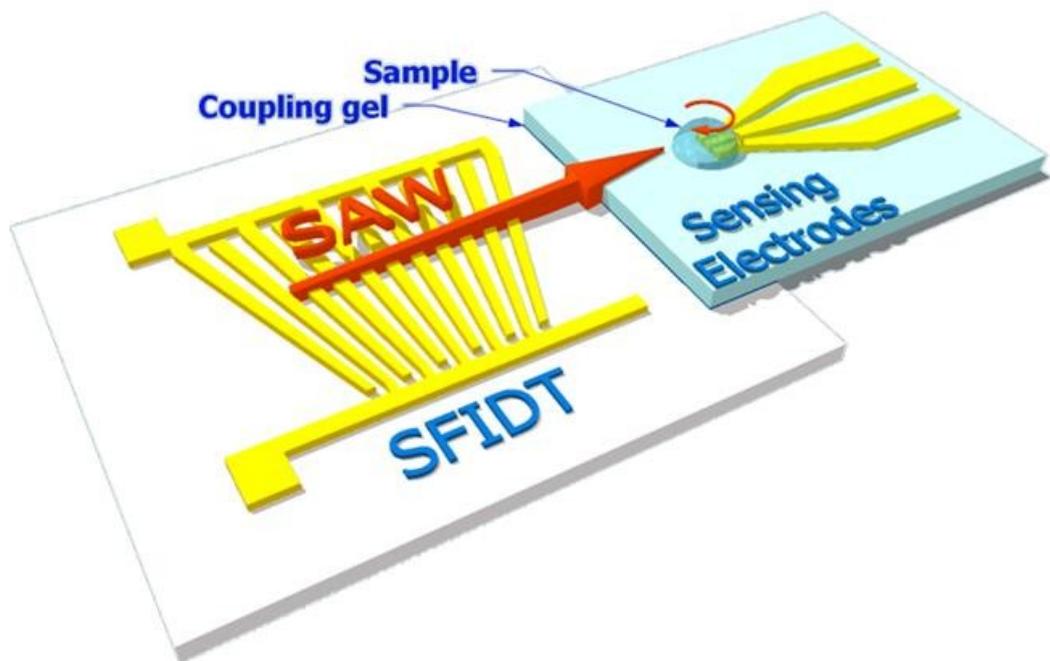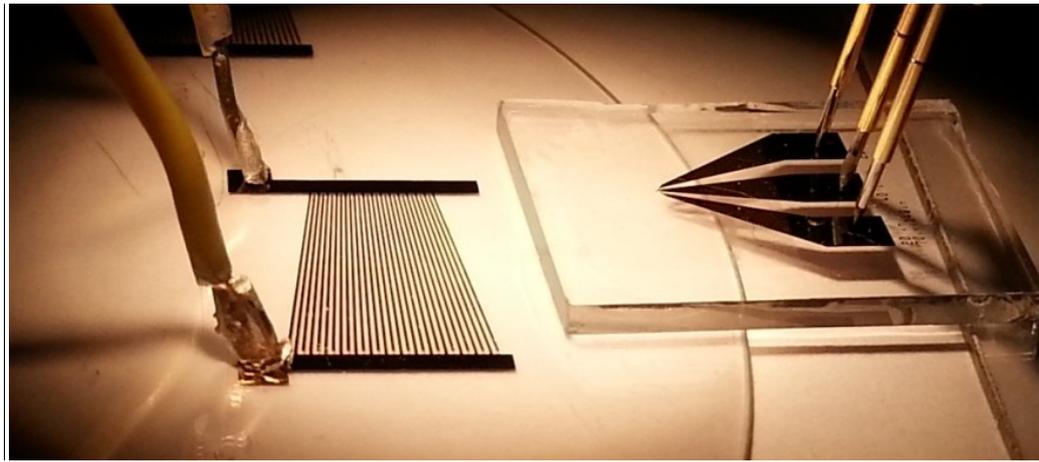
Figure 4. 7 Image and schematic of the superstrate based electrochemical sensor chip. The system is designed to perform analyses in sample droplets. The microchip comprises of a sensing platform and a SAW platform. The superstrate design is obtained by coupling two separate systems. A water-based gel interface (approximately 50-µm thick) was used for the attachment of sensing platform on to the primary substrate (SAW platform) [45]. Three µl of water-based gel layer (KY Jelly; Johnson and John- son) was spread manually between two layers.

SAW, propagated from the SIDT, causes a mixing effect inside the droplet. When SAW interacts with a side of the droplet, it creates a rotational momentum. This leads a fluid motion similar to an RDE system. Details of the SAW induced mixing are explained in the previous chapter.

4.2.2. Substrate based concept

Single substrate based design was obtained by the fabrication of both systems, the sensing electrodes and the SAW platform, on the same substrate (128˚ Y-cut X-propagating LiNbO$_3$)

at the same time. The same fabrication process was followed with the superstrate based system.
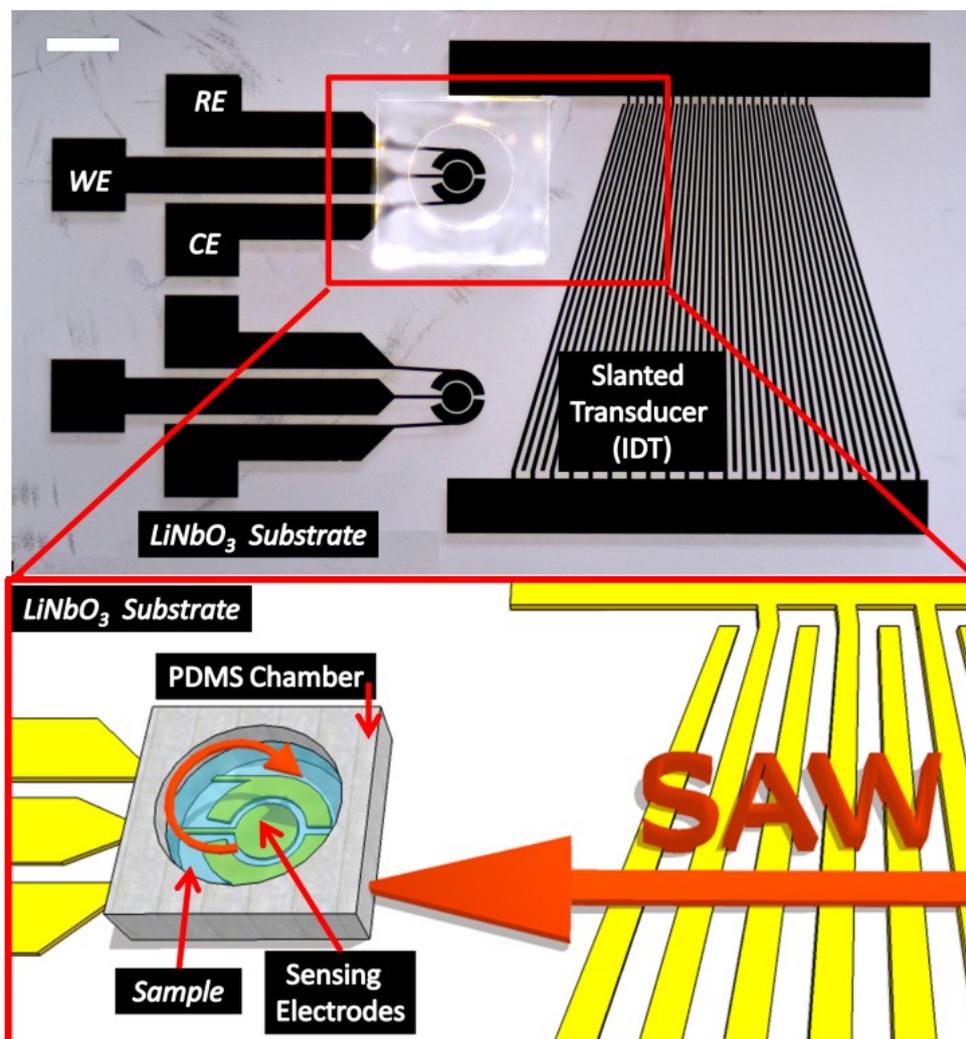
Figure 4. 8 Top: Image (scale bar, 2mm) of the substrate based design (SAW enhanced electroanalysis platform). Both the sensing system and the SAW device were fabricated on the same LiNbO$_3$ wafer. Circular sensor model consisted of a reference electrode (RE), working electrode (WE), and counter electrode (CE). A PDMS cube (W: 4.5 mm, L: 4.5 mm, H: 3.5 mm), with hole in it (1.7 mm radius), was coupled to the sensor (first from the top) as the sample chamber. Bottom: Schematic representation of a close-up on the SAW radiation into the PDMS chamber. SAW was performed at 12 MHz frequency. Propagated waves were radiating from the left side of the chamber. Longitudinal pressure waves inside the liquid were creating the streaming effect [47][109]. (The depiction is not to scale.)

4.3.   Results and evaluation

RDE formulas presented previously can be used to explain our SAW induced hydrodynamic electro- analysis since our design has similar flow characteristics inside the sample. Those statements were proved with the experimental CV results (voltammograms). Increased RF power was causing faster fluid streaming and so higher current flows. This hydrodynamic method is also able to perform fast stationary mode voltammetry measurements on the

micro scale samples due to the rapid establishment of the stationary case during the voltage sweep (Figure 4. 9).

Electrolyte solutions of 5, 10, 20 and 40 mM Potassium ferrocyanide ($K_4[Fe(CN)_6] \bullet 3H_2O$) with 100 mM KCl, purchased from Sigma-Aldrich, in RO water were the model samples used in this work. Experiments were performed with a 5µl sessile droplet in droplet traps and 20 µl samples in PDMS chamber.

Cyclic voltammetry (CV) and chronoamperometry were utilised as two detection techniques. CV studies were carried out by applying a voltage scan at a fixed scan rate (0.1 V/s), to the working electrode (vs. Au- pseudo reference electrode). Chronoamperometry measurements, where the current is recorded as a function of time, were done at a fixed potential (0.2 V) for 20 seconds.

Firstly, stationary mode (while the SAW device was off) CV and chronoamperometry measurements were performed for various concentrations of ferrocyanide. Secondly, SAW was generated, and the induced hydrodynamic measurements were carried out. The power of the RF signal applied on IDTs was varied from 0 to 4 W, and the frequency was 12MHz. Figure 4. 9, Figure 4. 10 and Figure 4. 11 present the comparative data obtained at both stationary and SAW induced hydrodynamic mode. Each test was performed three times.

Mainly two different system setups were used; a superstrate and a substrate based platforms. Samples were held in droplet traps on the first one and in closed PDMS chambers on the second setup, which was the final design. The top of the chamber was always covered with a piece of the glass slide, (1 mm thick, 10 mm width, and 10 mm length). Closing the chamber helped to limit evaporation. This was keeping the concentration constant in the liquid. The surface of the glass cover was coated with a PVC tape to implement a rougher surface, comparing to the surface of the glass. This made the cover less adhesive to the PDMS. Thus, the removal of the cover became simple when the sample in the chamber was needed to be replaced.

4.3.1. Measurements on the superstrate platform

SAW induced voltammetry within hydrophilic traps

A sample of potassium ferrocyanide (20mM) with potassium chloride (100 mM) was pinned on the glass surface using a hydrophilic droplet trap (1.75 mm radius). The trap was fabricated by photolithography as explained in the methods chapter (Chapter 2). The sample

droplets were trapped thanks to the surrounding hydrophobic layer of trichloro(1H,1H,2H,2H-perfluorooctyl)silane (FOTS, Aldrich).
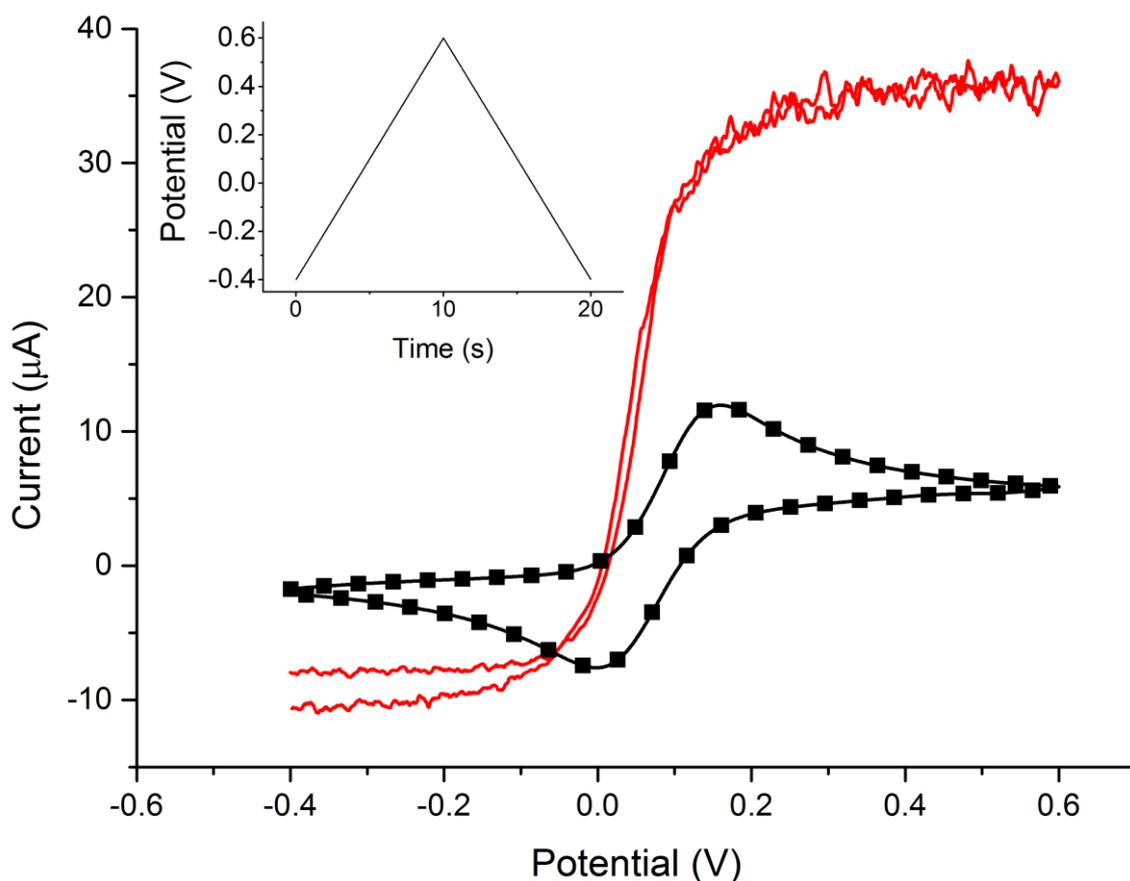
Figure 4. 9 Comparison of CV (at 0.1 V/s scan rate between -0.4 and 0.6 V) results without (square) and with SAW (solid line) streaming. The concentration of the ferrocyanide solutions was 20 mM (in 100 mM KCl). The area of the straight electrodes used in the system was 0.19 mm^2. The streaming for the hydrodynamic mode was obtained by the propagating mechanical waves obtained at the frequency of 11.73 MHz with 4 W of power. Enhanced mass transport rates helped to improve the amount of material which was being included in the electrochemical reaction during the application of triangle CV voltage. Thus, the diffusive peak current was increased from 12.1 μA to 43.2 μA.

Figure 4. 9 shows that the SAW streaming (11.73 MHz with 3.98 W) enhanced the diffusive peak current from 12.1 μA to 43.2 μA. The reaction rate was enhanced thanks to the increased mass transport.

The result (Figure 4. 9) was affected by the noise due to the vibrations, induced by the acoustic streaming. It was creating a pressure variation on the diffusion layer on the electrode due to the general motion (squeezing and releasing) of the droplet. Moreover, the area of the electrode in contact with the sample was varying over time due to the same effect. However, the most significant reason for the problem was attributed to the lack of ability of the silane to bind on gold surfaces. Therefore, the gold surface was not coated with the self-assembled hydrophobic layer. This was allowing an additional current variation due to the changing contact area between the sample and electrodes.

Figure 4. 10 presents the steady-state current values of voltammograms obtained in stationary and hydrodynamic modes. Applied SAW power was varied from 0 W to 4 W. Changing from a complete stationary mode to hydrodynamic mode with maximum SAW power, increased the steady-state output current (averaged) from 8.6 (+/- 0.87) μA to 45.64 (+/- 4.54) μA (Figure 4. 10).
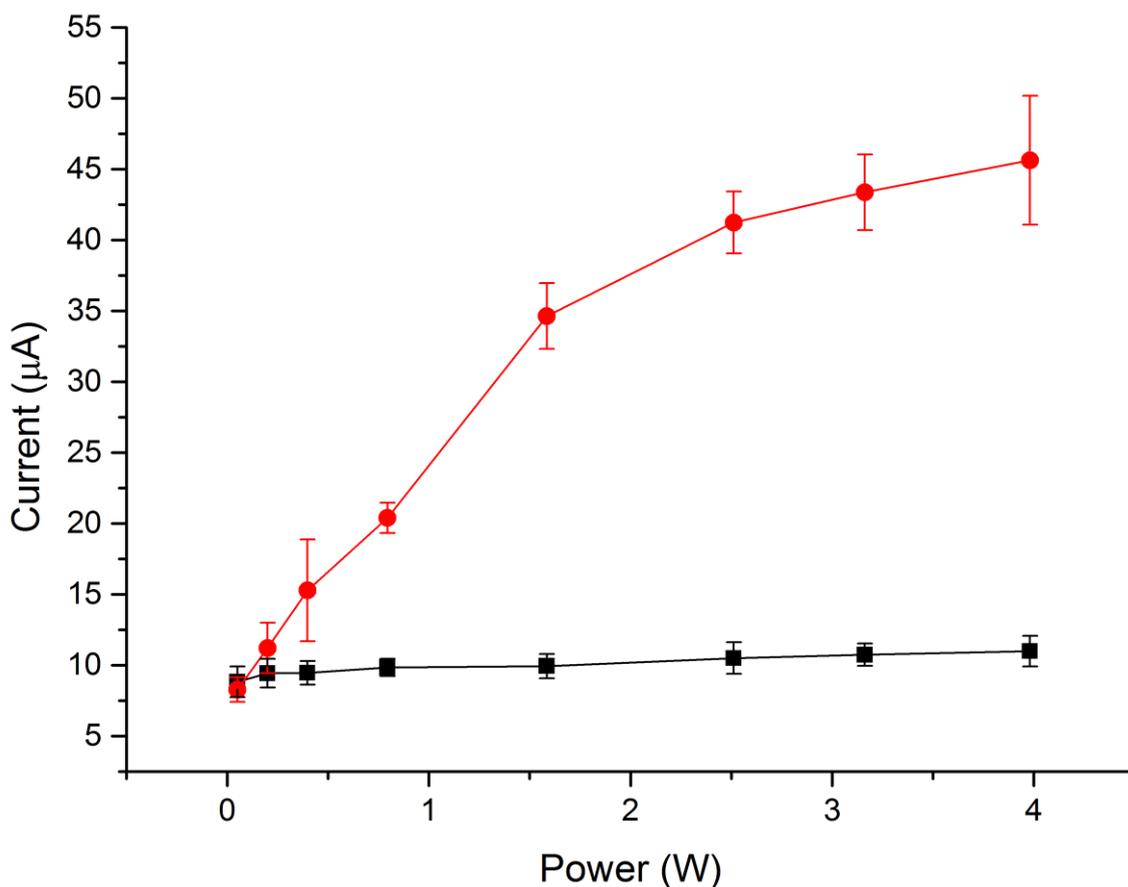
Figure 4. 10 Comparison of steady state currents obtained from voltammetry results in the absence (black square) and presence (red circle) of SAW (11.73 MHz) streaming. The superstrate based platform with a hydrophilic droplet trap was used in the test. The sample solution contained 20 mM ferrocyanide and 100 mM KCl. RF power of the SAW signal was increased from 0 W to 3.98 W.

SAW induced voltammetry within SU8 traps

This section explains the application of the same technique on different ferrocyanide concentrations (5 mM, 10 mM, 20 mM and 40 mM) in aqueous KCl (100 mM) solutions. Importantly, the droplet trap used previously was changed in here to a chamber with SU8 walls. 5 μm thick SU8 layer, surrounding the droplet, was used instead of trichlorosilane. This solved the problem of sample spreading on the electrodes.

SAW was produced at 11.73 MHz frequency. CV measurements were performed at different RF powers ranging from 0 to 4 W same as the previous experiments.
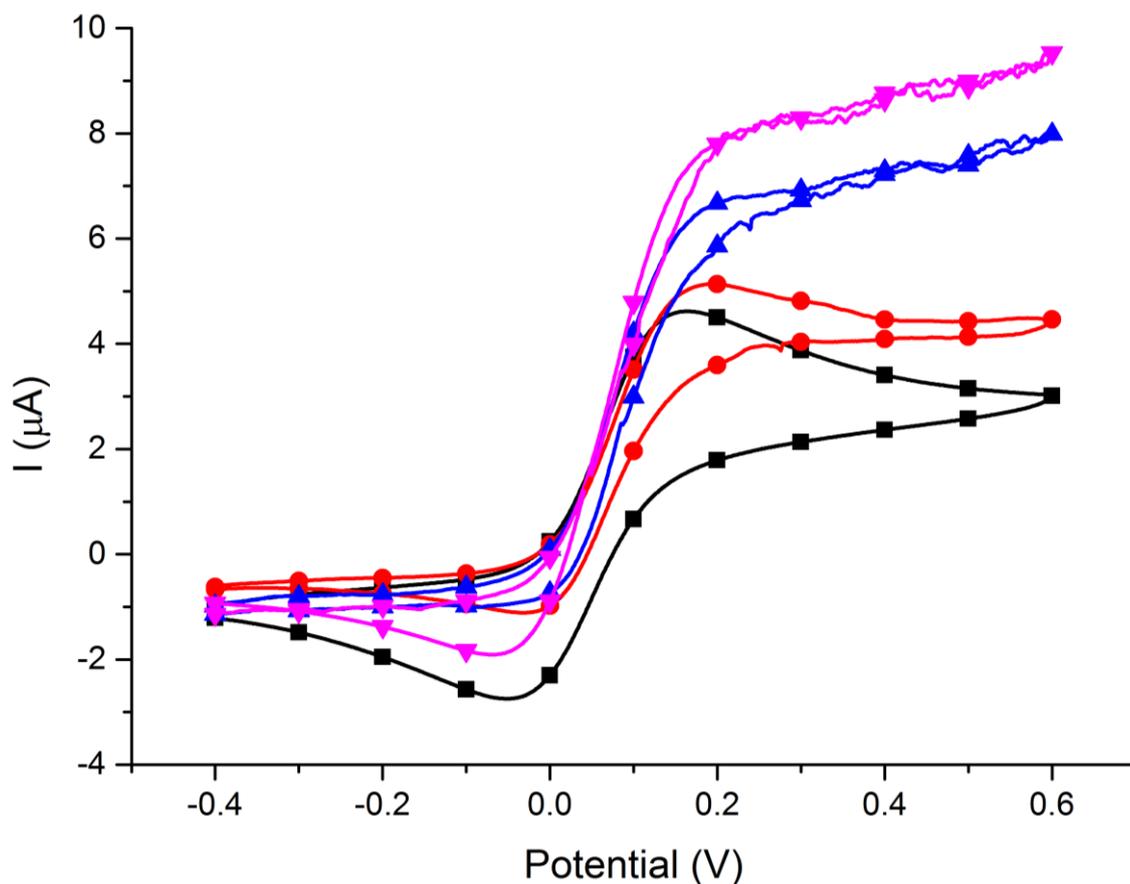
Figure 4. 11 CV measurements performed in SU8 electroanalytical chambers with and without SAW enhancement. Voltammograms obtained from 10 mM ferrocyanide sample (in 100 mM KCl containing water). The voltage applied (scan rate: 0.1 V/s) during the CV tests was between -0.4 V and 0.6 V vs. a pseudo gold reference electrode. Applied power levels of the SAW (11.73 MHz) propagation were; 0 W (black square), 0.8 W (red circle), 2.51 W (blue up triangle) and 4 W (pink down triangle). The area of the straight electrodes used in the system was 0.13 mm^2.
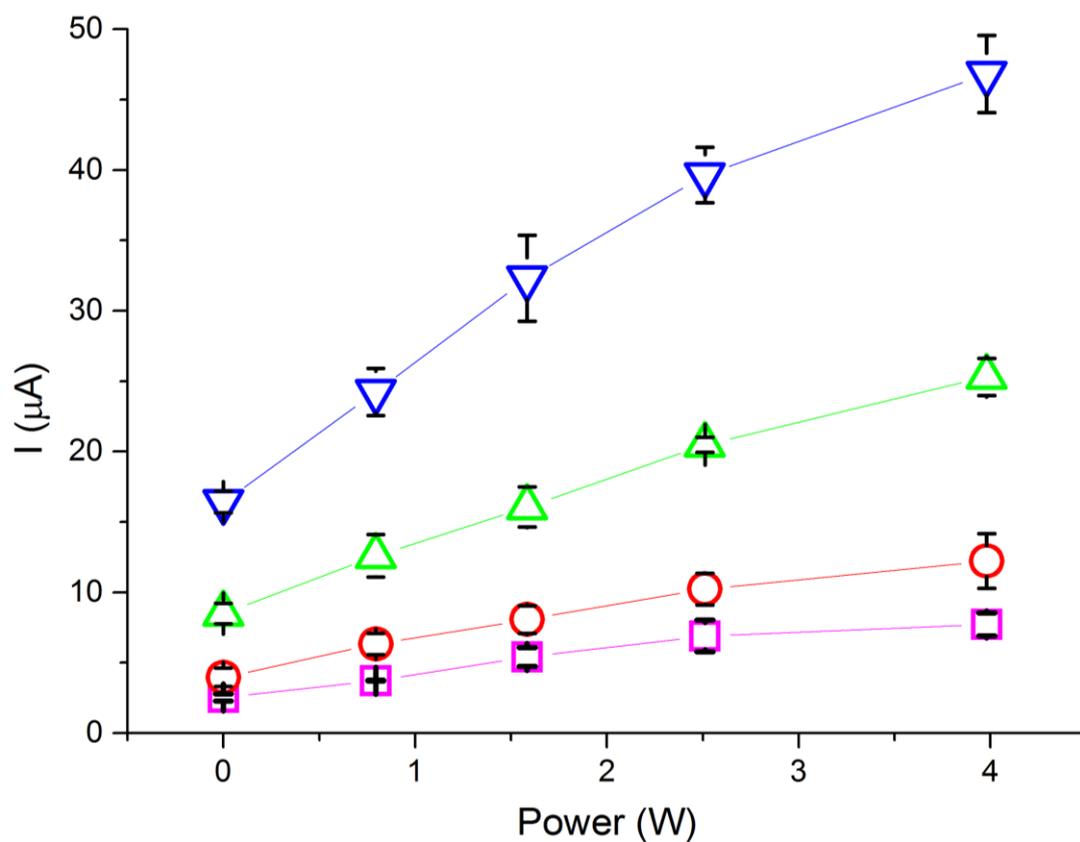
Figure 4. 12   Diffusive peak current values obtained from ferrocyanide solution at different concentrations; 5 mM (square), 10 mM (circle), 20 mM (up triangle) and 40 mM (down triangle), in KCl (100mM). CV measurements are performed in SU8 electroanalytical chambers (see in previous figure). The voltage applied (scan rate: 0.1 V/s) during the CV tests was between -0.4 V and 0.6 V vs. a pseudo gold reference electrode. The power of the applied sine wave was increased from 0 to 4 W while the frequency was kept at 11.73 MHz.
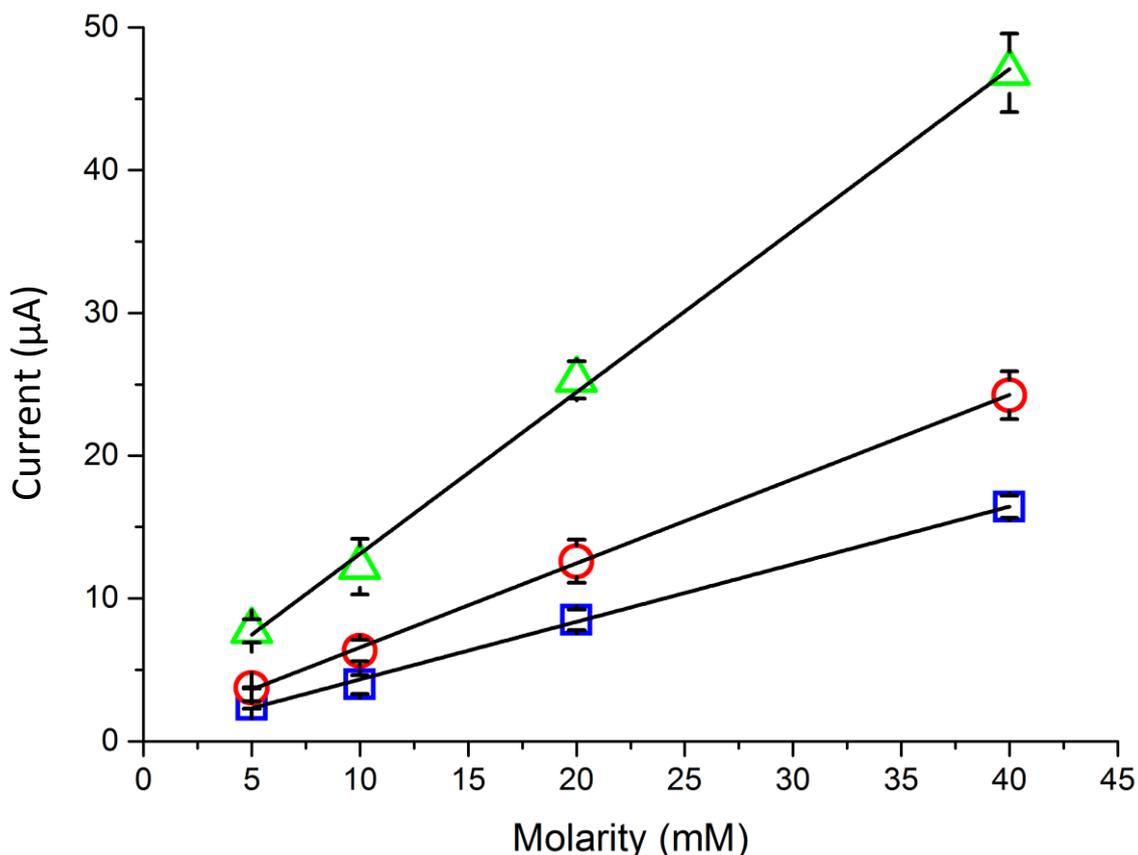
Figure 4. 13 Diffusive peak current variation according to the applied three different SAW power; 0 W (blue square), 0.8 W (red circle), 4 W (green triangle). CV measurements performed in SU8 electroanalytical chambers (see previous figure) potassium ferrocyanide solutions. The concentration of the potassium ferrocyanide solutions were; 5, 10, 20, and 40mM. The voltage applied (scan rate: 0.1 V/s) during the CV tests was between -0.4 V and 0.6 V vs. a pseudo gold reference electrode. The power of the applied sine wave was increased from 0 to 4 W while the frequency was kept at 11.73 MHz.

As it is presented in Figure 4. 12 and Figure 4. 13, SAW induced mass transport increased the output current significantly over a range of different concentrations. For example, the current obtained from 40 mM sample was increased from 16.42 µA to 47.04 µA. This corresponds to a ~3 times enhancement of the current value.

Previous CV measurements, performed in the hydrophilic trap (trichloro-silane), were noisier (Figure 4. 9). Changing the droplet handling method to an SU8 chamber led to a noise decrement in CV measurements (Figure 4. 11). However, the current enhancement ratio decreased to 300 % (from 380 %) as a drawback of this solution. The thickness (~5 µm) and the characteristics of the photoresist layer resulted in the decrement in current enhancement. The layer was absorbing a portion of acoustic energy and converting it to heat. Thus, only the remaining part of the mechanical energy was reaching the liquid medium, and the streaming efficiency was decreased.

4.3.2.   Measurements on the substrate platform

The device, which is mentioned above (substrate based concept), used in this part has no coupled superstrate platform. Both the ultrasound mixer (SAW platform) and the sensing platform were fabricated on the same LiNbO$_3$ substrate. The electrode system was comprised of three circular gold electrodes with the surface area of 0.663 mm^2. The design did not include any gel interface. This kept it free from the inconsistencies caused by the drying gel interface.

Most importantly, a PDMS chamber was added to the system in order to obtain more noise decrease by constraining the sample, thanks to the increased interface area between the fluid and the rigid walls. The PDMS structure coupled on the surface is capable of absorbing acoustic energy as SU8 layer did previously. However, the superstrate free, one-piece design was efficient enough to compensate the power loss caused by the PDMS walls.

SAW frequency optimisation

The design was able to work at various SAW frequencies between 7.6 MHz and 16.6 MHz. However, a series of experiments were performed to define an efficient frequency. The frequency determined can induce an efficient forced convection on the sensor to obtain high current enhancements.

The effective frequency of the device is highly related to the position of the sensing electrode. The frequency variation on the slanted IDT design changes the resonating parts of the finger series and thereby shifts the position of the SAW beam. A detailed evaluation of the slanted transducer is given in the previous chapter (slanted design). The alignment of the beam with the fluid chamber is achieved by changing the frequency of the RF signal. Thus, the enhancement of mass motion can be maximised by characterising the frequency. The achievement of the streaming maximisation can be monitored via electroanalytical tests or optical observation methods.
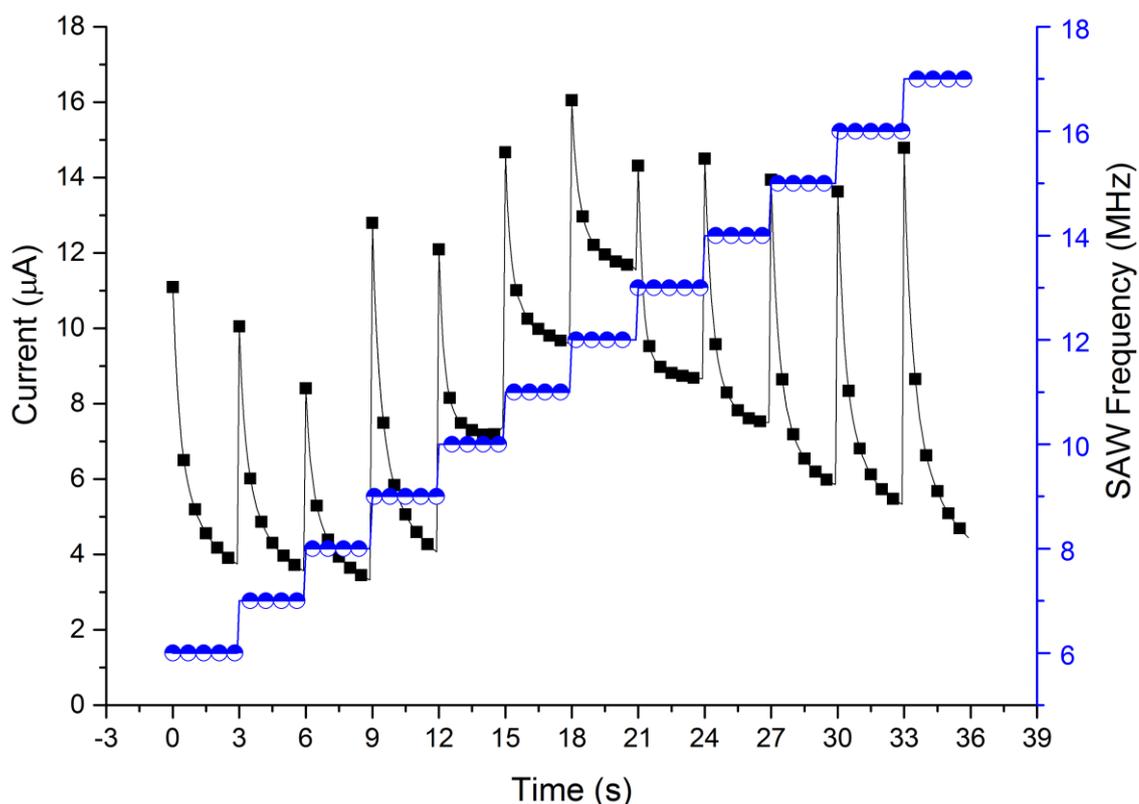
Figure 4. 14 Amperometric tests for the frequency optimisation of the substrate based SAW platform (see in Figure 4. 8). Various SAW frequencies (half filled circle) were applied on 5 mM potassium ferrocyanide aqueous KCl (100 mM) solution (square). The frequency scanning process of a slanted SAW transducer can be seen in Figure 3. 9. A different SAW frequency, between 6 and 17 MHz, was applied on the slanted SAW transducer for each tests period. The potential (0.2 V) was applied to the three electrode sensing system for 3 seconds for each experiment. Highest current enhancement is obtained at 12 MHz.

Results, presented in Figure 4. 14, demonstrate that 12 MHz was one of the most efficient frequencies to obtain an optimum current enhancement rate because the acoustic streaming rate was the best in between the other tested frequencies. This was a result of the combination of two main parameters. The first parameter is the amount of acoustic energy produced by the fingers. It is directly related to the conversion rate from electricity to mechanical energy. The quality of finger pattern and the electrical impedance matching, between the SAW device and the RF signal generator, both have a significant impact on the transformation rate. The second parameter is the transmission of acoustic energy into the sensing chamber through the PDMS walls. The alignment of SAW beam towards the sample location and the radiation rate into the sensing chamber are the important controlling factors of the transmission rate.

Moreover, the SAW beam at 12 MHz was inducing from the side of the droplet/chamber and creating a vortex inside the liquid sample.

SAW induced voltammetry

The vortex formation inside the sensing chamber creates a similar mass transport scheme as that of the RDE technique. Therefore, the RDE formulas explained previously can be used to describe the hydrodynamic electroanalysis of the design. According to the Equation 7 the diffusion layer on the rotating disc electrodes decreases due to the increasing rotating (vortex) effect in the sample. The Levich equation (Equation 8) states that the increment of diffusion limited current is linked to the increased rotation rate. These statements were in agreement with the experimental CV results (voltammograms) in Figure 4. 15. Increased RF power caused faster fluid streaming and so higher current levels.
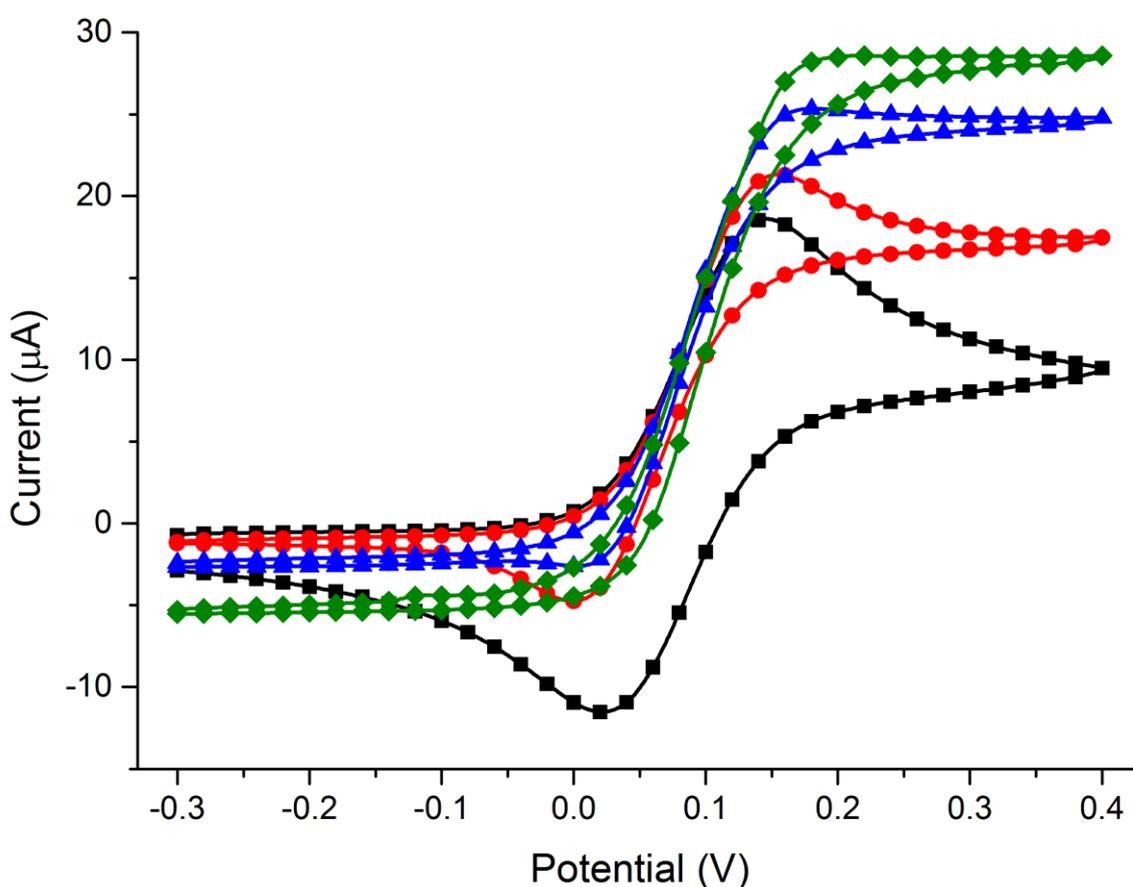
Figure 4. 15 Voltammetric graphs of 10 mM ferrocyanide in 100 mM KCl in the absence and the presence of SAW streaming. Applied SAW powers were 0 W (square), 0.25 W (circle), 0.8 W (triangle), 1.6 W (diamond). The Hydrodynamic effect induced by the 1.6 W SAW power increased the limited current from 17.91 μA to 32.31 μA. All the measurements were conducted between -0.3 V and 0.4 V potential ranges vs. gold reference electrode. The scan rate was 0.1 V/s. Prior to the replacement of the new sample, the electrodes were washed firstly with water and then with the following sample with SAW propagation (1.6 W). Then the actual test sample was being filled into the sensing chamber for measurement.

This hydrodynamic method is also able to perform fast stationary mode voltammetry measurements on the micro scale samples due to the rapid establishment of the stationary case during the voltage sweep.
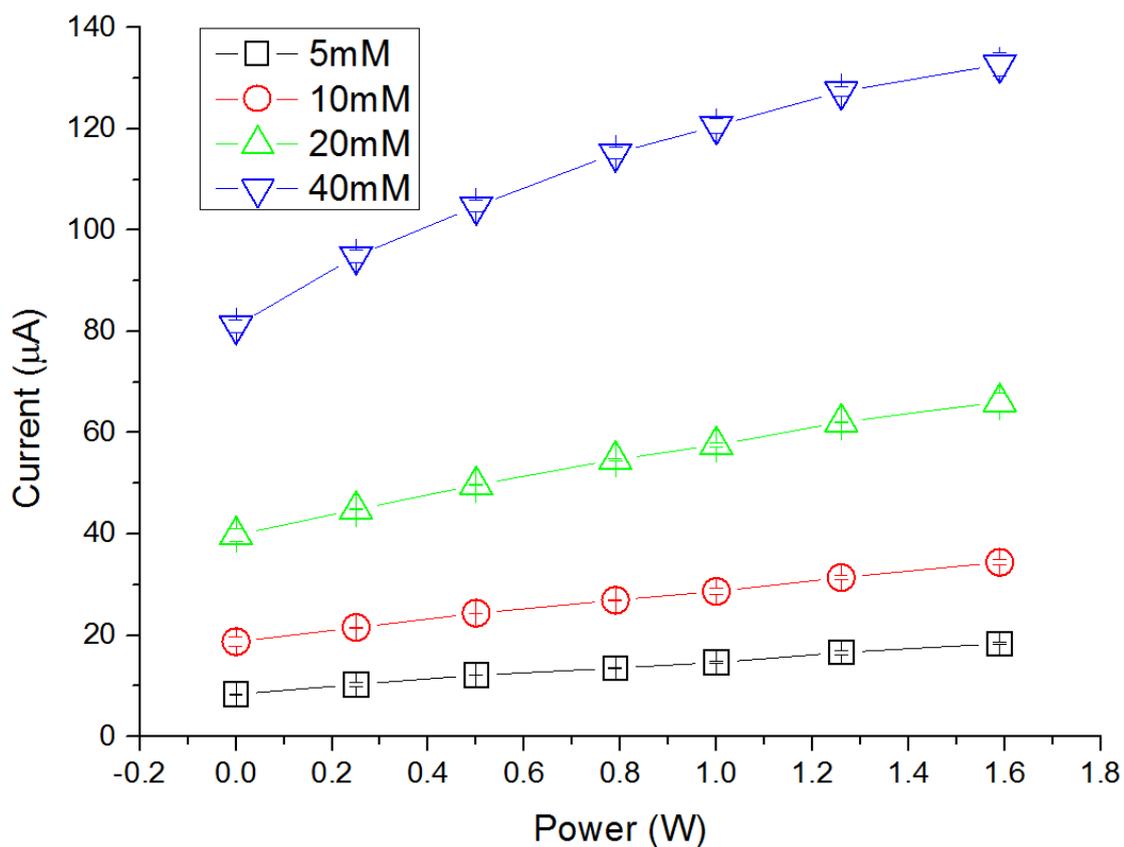
Figure 4. 16   Diffusive peak current values obtained from the CV measurements made with the substrate based device. Measurements were performed on 20 μl samples which included four different potassium ferrocyanide concentrations (5, 10, 20, 40mM) in a 100mM KCl supporting electrolyte buffer. The electrode system was comprised of three circular gold electrodes with the surface area of 0.663mm^2. The experiments were continued at various SAW powers from 0 to 1.6 W.
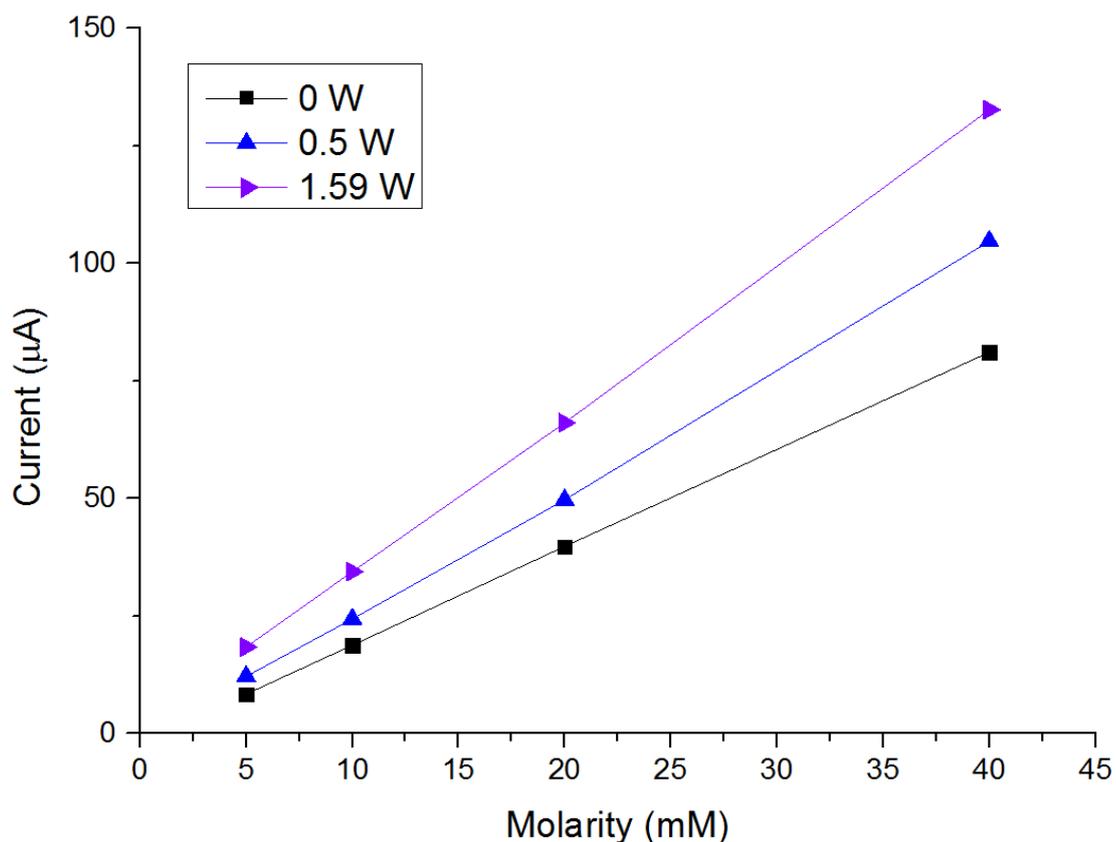
Figure 4. 17 Diffusive peak current variation according to the tested four different ferrocyanide concentrations (5, 10, 20, 40 mM) in a 100mM KCl supporting electrolyte buffer. The graph presents the results obtained without SAW streaming (square) and with SAW streaming at two RF power 0.5 W (Up triangle) and 1.6 W (Right triangle).

CV tests were made with the substrate based device. Measurements were performed on 20 µl samples with four different ferrocyanide concentrations (5, 10, 20, 40mM) in a 100mM KCl supporting electrolyte buffer. The experiments were carried out at various SAW powers (0, 0.25, 0.53, 0.8, 1, 1.26, 1.6 W).

SAW induced diffusive peak current measurements presented significant achievements. The average increment of the electron flow was obtained as 91%. The results are capable of being enhanced to higher levels by making further developments in substrate based design.

SAW induced amperometry

Amperometry, voltammetry at a fixed potential, is the current measurement as dependent on a parameter, such as concentration or time [23]. This section explains the amperometric measurements, performed for the assessment of potassium ferrocyanide samples (5, 10, 20 and 40mM) in 100 mM KCl. Ferrocyanide samples were analysed with chronoamperometry tests in stationary and SAW induced hydrodynamic modes. As presented in Figure 4. 18, the

chronoamperometry result obtained in the PDMS chamber was increased by the SAW induced fluid streaming.
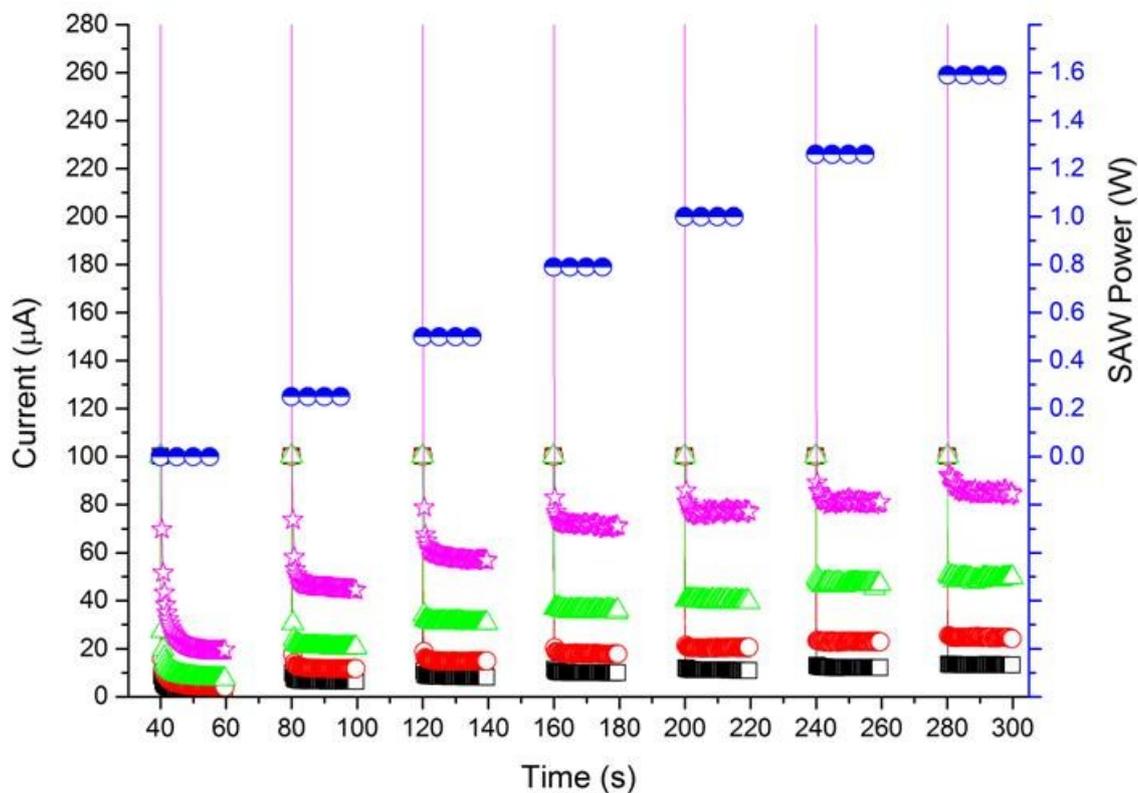
Figure 4. 18 Chronoamperometry tests inside the PDMS chamber. These results present the current enhancements obtained due to the SAW induced streaming in a PDMS sensing chamber. The experiment series were made on a substrate based device platform. Measurements were performed on 20 µl samples at four different potassium ferrocyanide concentrations (5, 10, 20, 40 mM) in a 100mM KCl supporting electrolyte buffer. The electrode system was comprised of three circular gold electrodes with a surface area of 0.663 mm^2. Amperometric measurements were performed at 0.2 V potential for 20 seconds. After the first tests had been carried out while the SAW transducer was off, experiments were continued at various SAW powers (0.25, 0.53, 0.8, 1, 1.26, 1.6 W). Prior to the introduction of a new sample, the electrodes were washed firstly with water and then with the following sample with SAW propagation (1.6 W). Then the actual test sample was filled into the sensing chamber for measurement. Results show that the SAW induced amperometry can be used for enhancing the sensitivity of electroanalytical systems.
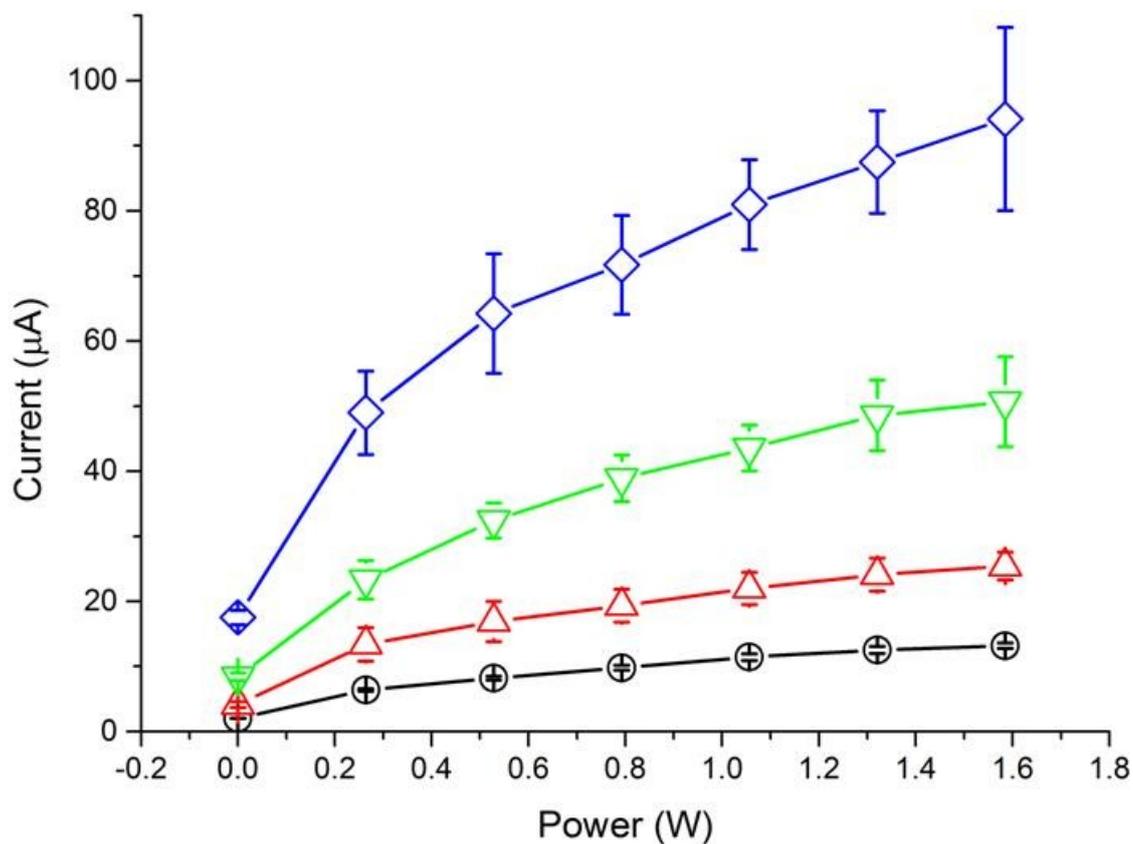
Figure 4. 19 Steady-state currents obtained from chronoamperometry measurements. The graphic presents triple test results achieved by four different ferrocyanide concentrations (5, 10, 20, 40 mM) in a 100mM KCl supporting electrolyte buffer solution at various SAW powers; 0, 0.25, 0.5, 0.8, 1, 1.26, 1.6 W. Increased SAW power resulted in higher current values due to the enhanced ion transfer towards the electrode surface.
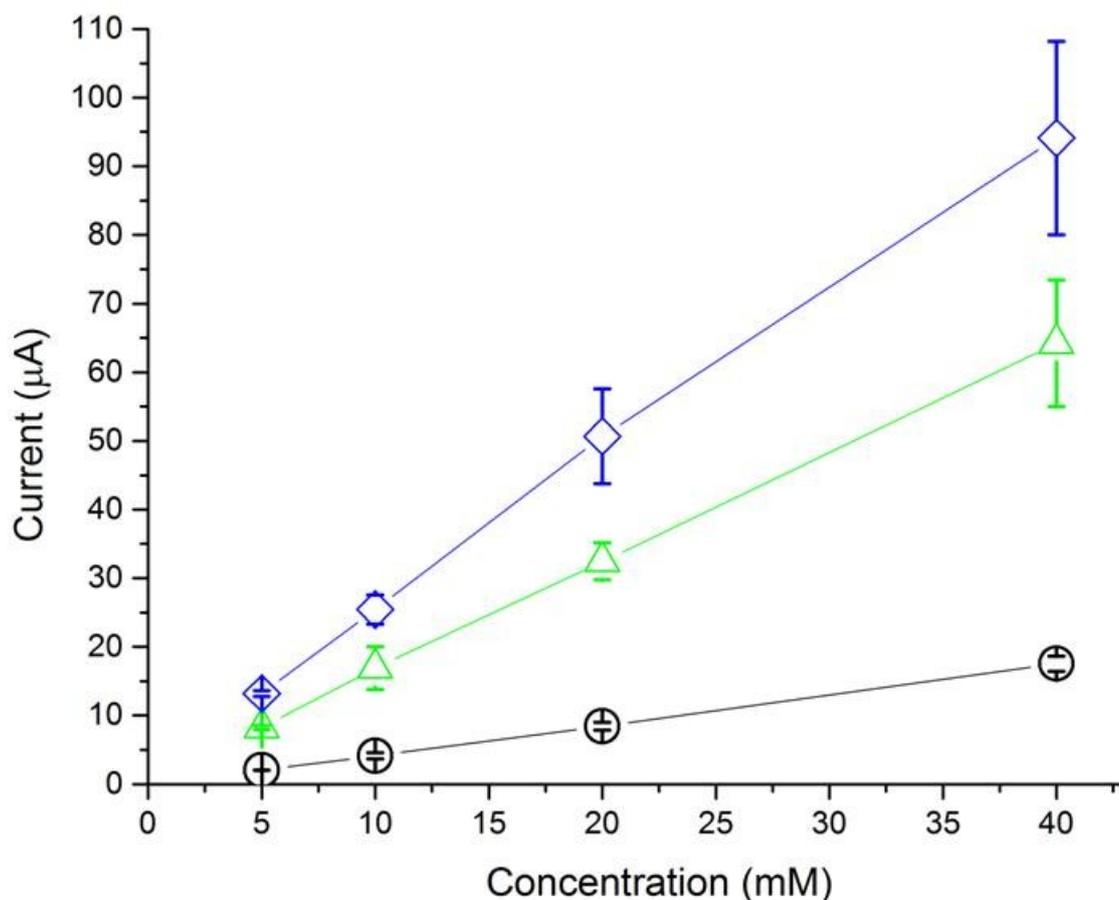
Figure 4. 20 Currents measured at steady state during the amperometric tests. The graph shows how the measured current changed when increasing the ferrocyanide concentration, in the stationary case (Black) and in two separate, 0.53 (Green) and 1.58W (Blue), SAW induced hydrodynamic cases.

Figure 4. 19 illustrates the chronoamperometry tests performed on different ferrocyanide solution at varying RF powers applied to SAW transducer. Increasing SAW power causes larger surface displacements on the vertical (z) axis. Therefore, the fastest fluid streaming is obtained with the maximum SAW power. When the maximum external convection with the highest SAW streaming (1.6 W) was present the current obtained from 5mM ferrocyanide solution was ~6 times greater than the current in the stagnant solution.

Roof effect on SAW streaming
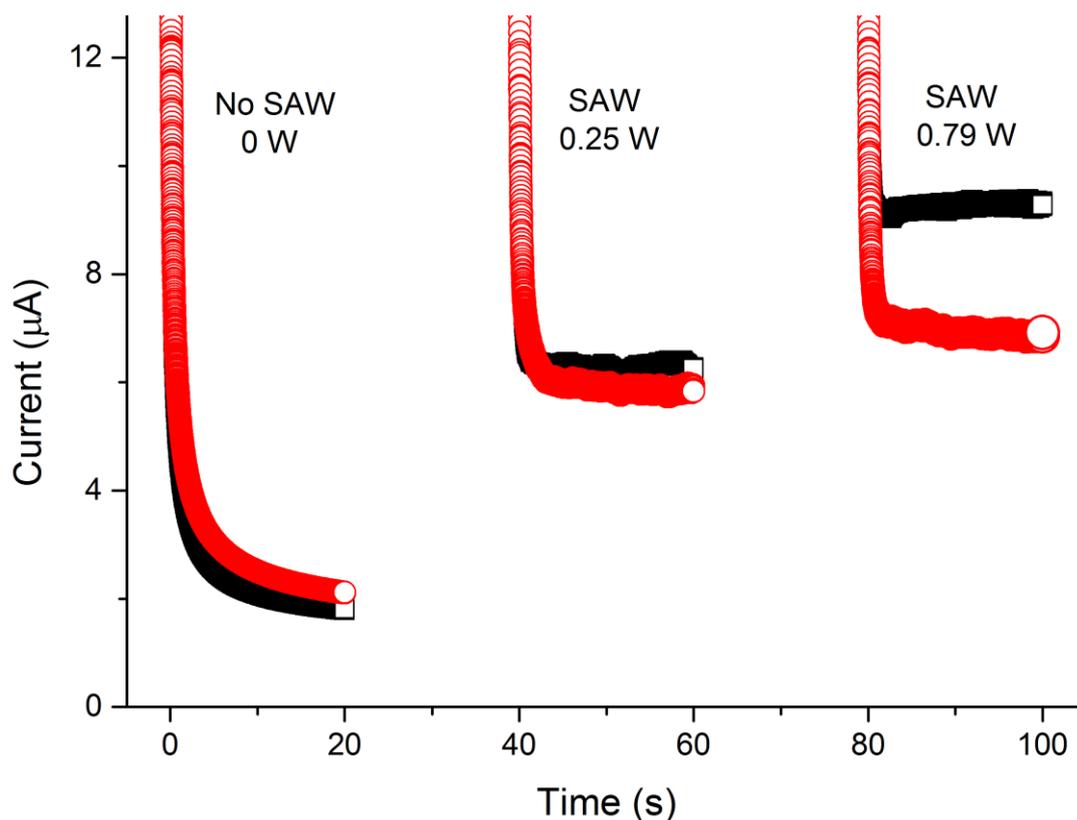
Figure 4. 21 The effect of increased shear stress on hydrodynamic amperometry measurements. This graphics demonstrates the change in SAW induced the hydrodynamic effect, on amperometry measurements when the fluid sample touches to the top of the chamber cover. Two sets of measurements were performed, with a same amount of sample (20 µl), in two different cases. In the first case, the height of the PDMS chamber was 3.5 mm (black square), and it was reduced to 2 mm (red circle) in the following case. Outcomes showed that the hydrodynamic effect in the short chamber was lower comparing to the high chamber which had an air gap between the cover and the sample. SAW transmission from sample to the surrounding rigid surfaces and the shear stress was increased because of the increased liquid-rigid surface interface. The amperometric current was decreased due to the decayed acoustic streaming.

Amperometric measurements performed with the same amount of sample (20 µl) in two different cases. The height of the PDMS chamber was 3.5 mm in the first case, and it was reduced to 2 mm in the following case. Therefore, the sample in the second case was physically in contact with the cover of the chamber while it was not in the first instance. Experimental results (Figure 4. 21) showed that the amperometric current was stabilising at a higher value when the sample was not touching to the cover. Decreased mixing effect caused a current difference between first (9.3 µA at 0.8 W) and second (6.9 µA at 0.8 W) cases. Therefore, the enhancement of the mass transport rate was lower. This showed that a liquid sample can be mixed faster by reducing the area of the interface between the fluid and the rigid surface.

The fluid speed was decreased due to two main effects created by increased liquid-solid interface area. First, the rigid surfaces (PDMS walls and glass cover) severely attenuate the

acoustic energy radiated into the liquid. Therefore, the mixing efficiency was decreased. Second, the total shear stress was increased, again due to the increased interface area. This was creating a higher resistance to the fluid motion. Those were the reasons for less efficient acoustic streaming in the short chamber test.

Koutecky - Levich Plot

Koutecky-Levich (K-L) plot, which is obtained by plotting I^{-1} vs. $\omega^{-1/2}$ [103], includes both the kinetically controlled current and the mass transfer limited current [22]. It also enables to obtain the current in the absence of diffusion control. Since the kinetics of the redox system used in the experiment was faster, the system was mass transfer limited. Therefore the kinetic transfer limited current (I_k) was tiny comparing to diffusion limited current (I_d).
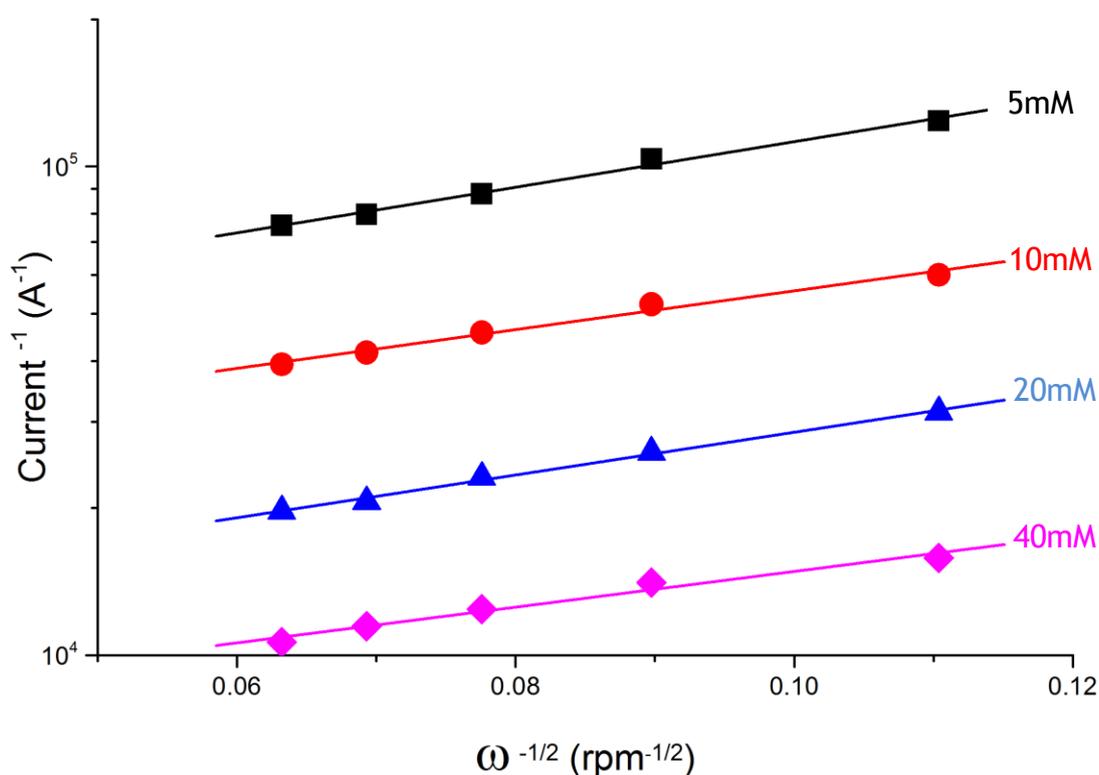
Figure 4. 22   Koutecky–Levich plot for different molarities of ferrocyanide; 5 mM (square), 10 mM (circle), 20 mM (triangle) and 40 mM (diamond). The values are obtained from the amperometry tests performed at 0.2 V potential. Rotation values obtained from the PIV measurements at different SAW power were used for the plotting.

The oxidation of potassium ferrocyanide was recorded at various SAW streaming speeds via amperometric measurements (Figure 4. 18). In this part, the diffusion limited current measurements were further analysed by K-L plots. As shown in Figure 4. 22 the fit lines of the K-L plots for various molarities present the expected parallelism and the linear relationship. This indicates that the SAW streaming technique in electroanalytical systems can be used as the conventional RDE technique.

Fast steady state achievement

The application of travelling mechanical waves on the sensing platform helped to control the diffusion characteristics of the system. For example, shorter times were needed to reach steady state current when the SAW propagation was activated in the system. As it is presented in Figure 4. 23, the timings to reach steady state in non-actuated solutions for different concentrations were between 10 and 14 seconds, however when the hydrodynamic effect was activated, the time durations were decreased to smaller values between 0.2 and 0.5 second. So the average timing was decreased down to 35 times smaller values.
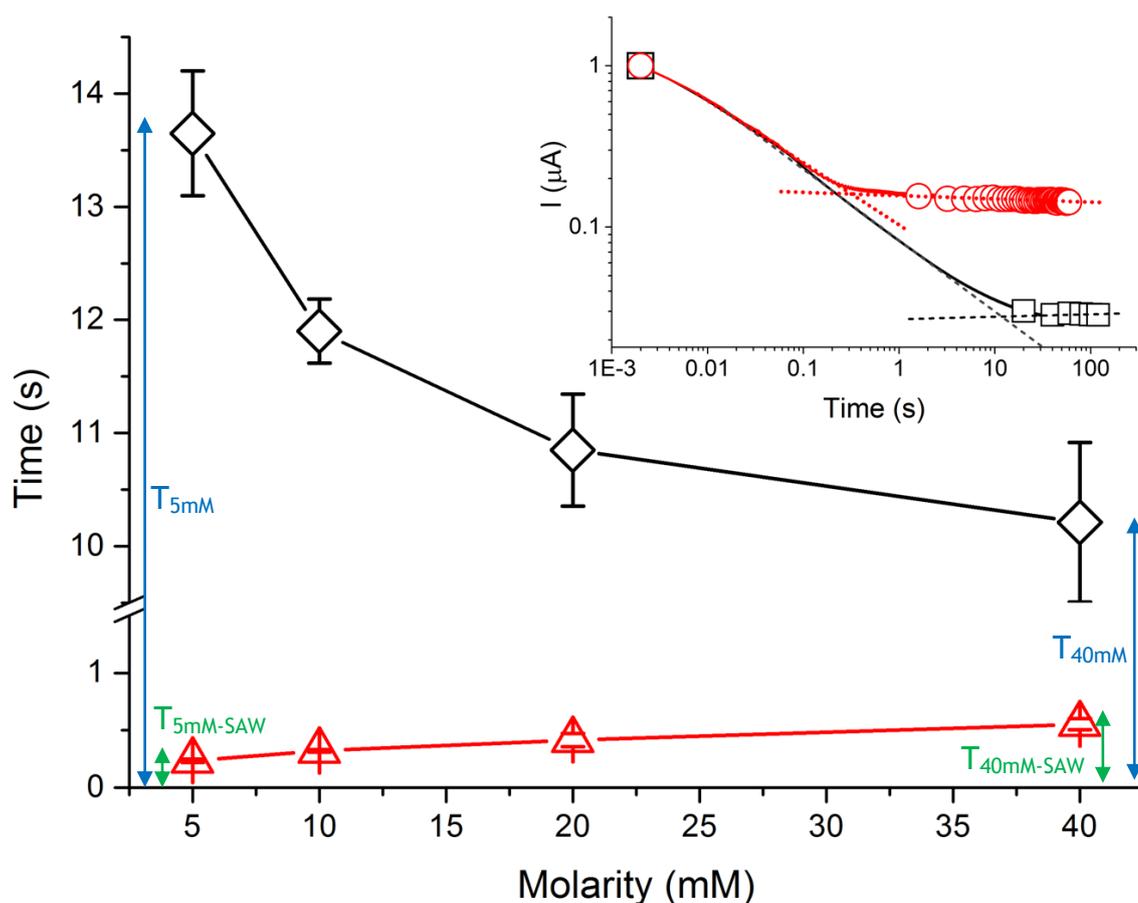
Figure 4. 23 The amperometric steady state achievement time graph at stationary (diamond) and hydrodynamic modes (triangle). Inset: The amperometry graph of 10mM solution presents how the timings were defined in stagnant (square) and hydrodynamic (circle) solutions. Measurements performed on four different ferrocyanide solutions (5, 10, 20, 40 mM in 100mM KCl) for 60 seconds while the external mixing was active and for 130 seconds in the stationary mode. The fluid streaming was activated by the propagation of SAW at 12 MHz frequency and 1.6W of power. Hydrodynamic mode measurements enabled the rapid establishment of the steady state diffusion limited current. Acoustic mixing effect inside the reaction chamber was decreased the time for steady state case from 10-14 to 0.2-0.5 seconds. This offers a faster determination of the substance concentration in the sample.

The induction of SAW streaming into the sensing chamber changed the timing characteristics of amperometry measurements. As it is presented in Figure 4. 23, increasing molarities caused a decrease in the steady state reaching times, in stagnant solution. On the contrary,

the higher molarities ($T_{40mM-SAW}$) taking more time than the low molarities ($T_{5mM-SAW}$) to achieve the steady state in SAW induced hydrodynamic cases. However, there was an opposite behaviour in stagnant case.

4.3.3.   Additional effects of SAW on electroanalysis

Until this section, the complete effect of SAW streaming in the sample during electrochemical measurements was investigated in CV and amperometry measurements. In here the focus is directed on the differentiation of hydrodynamic effect of acoustic wave propagation from the other factors created by SAW. Some of those are also capable of influencing the rate of electrochemical reactions, therefore, the analytical measurements.

The following sections will explain different aspects about SAW on electroanalytical measurements such as noise, sample heating and direct electrical charging created by travelling acoustic waves on a piezoelectric material.

SAW induced noise
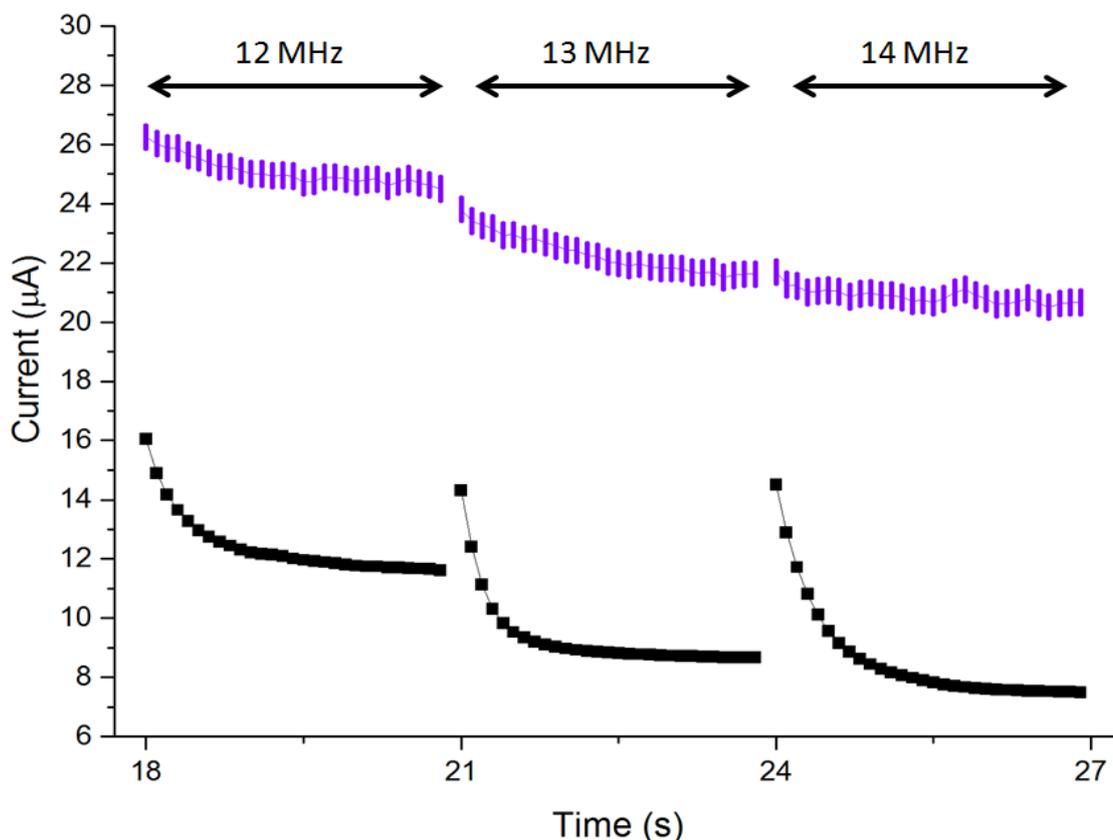
Figure 4. 24 Amperometric graphs, presenting the noise absorption of PDMS walls. SAW streaming was applied, by SIDT transducer, at three different frequencies (12 MHz, 13 MHz and 14 MHz) on 5 mM ferrocyanide (with 100mM KCl) samples. The potential (0.2 V) was applied to the three electrode sensing system for 3 seconds for each experiment. First test series was performed on a 5 μl droplet pinned on the electrode surface (vertical bars). The second experiment carried out on the same system however the sample was 20 μl and most importantly located inside a PDMS chamber (square).

Ultrasound application on electroanalytical systems mostly creates a noise problem [122]. In this section two series of measurements performed, in order to characterise the noise in a SAW induced electroanalytical system. Figure 4. 24 shows three different SAW frequencies (12 MHz, 13MHz and 14 MHz) applied on 5mM potassium ferrocyanide (with 100mM KCl) samples for each test series. The amperometry voltage (0.2 V) was applied for 3 seconds. First test series was performed on a 5 μl droplet pinned on the electrode surface. The second experiment carried out on the same system however the 20 μl sample was located in a PDMS chamber.

Results in Figure 4. 24 show that the PDMS chamber is capable of absorbing the noise, in current measurement, created by SAW because the squeeze/release and vibration type motion do not occur inside the encapsulated chamber. Therefore, the local fluctuations of the current density decrease. However, using a PDMS chamber in the system causes a decrease also in electroanalytical measurements. This may happen due to two main reasons. Firstly,

the PDMS walls absorb a portion of SAW and reduce the amount of longitudinal pressure waves radiated into the chamber. Secondly, the increment of the interface area (between the solid surface and the liquid) means more frictional forces against the fluid motion. Therefore, the enhancement of the mass transfer decreases as a result of slowing streaming velocity.

SAW induced heating

Here we focused on the temperature change inside the droplet, during the SAW induction, and how it affects the diffusion limited current of the system. Travelling acoustic waves create a heat proportional to the frequency and the voltage (peak to peak) of the applied RF signal. It is well known that the temperature on the surface rises as proportional to the wave amplitude [123]. There are two primary heat sources in SAW systems, interfaced with liquids, namely the absorption of the heat created by the motion of crystal atoms [33] in the substrate (or superstrate), and the interaction between the SAW and the liquid as longitudinal waves propagating in the liquid are dampened through the viscosity of the fluid [46]. Higher viscosity leads to more energy dissipation due to the increased viscous friction [81].

Temperature variation in the electrochemical analysis can cause significant changes on the reaction rate. The temperature variation creates a convectional mass motion. This makes a minor contribution to the forced convection caused by the SAW streaming. Additionally the viscosity decreases with increasing temperature as shown in Equation 12 (Arrhenius equation). More importantly, the diffusion coefficient also increases by the heating effect and the decreased viscosity as presented in Equation 13 and Equation 14 (Stokes-Einstein Equation). Increased viscosity creates more current flow in the system (Equation 8). Consequently, the sensitivity of the analytical system improves.

$$\eta = \eta_0 e^{\frac{E_a}{RT}}$$

Equation 12

$$D = \frac{kT}{6\pi\eta r}$$

Equation 13

$$D = \frac{kT}{6\pi r \eta_0 e^{\frac{E_a}{RT}}}$$

Equation 14
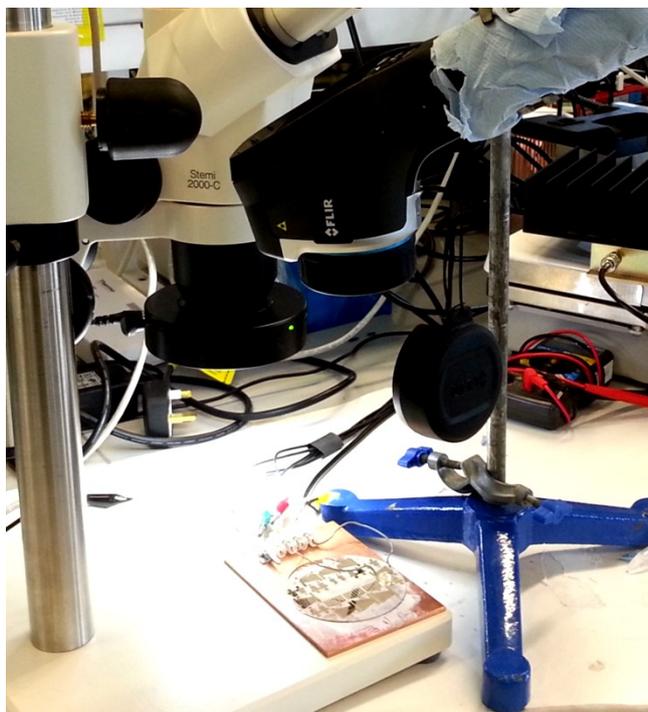
Figure 4. 25 The experimental setup for the measurement of the temperature variation on the SAW induced system. An IR (FLIR E60bx) camera was used to observe the temperature variation inside the droplet and PDMS chamber.
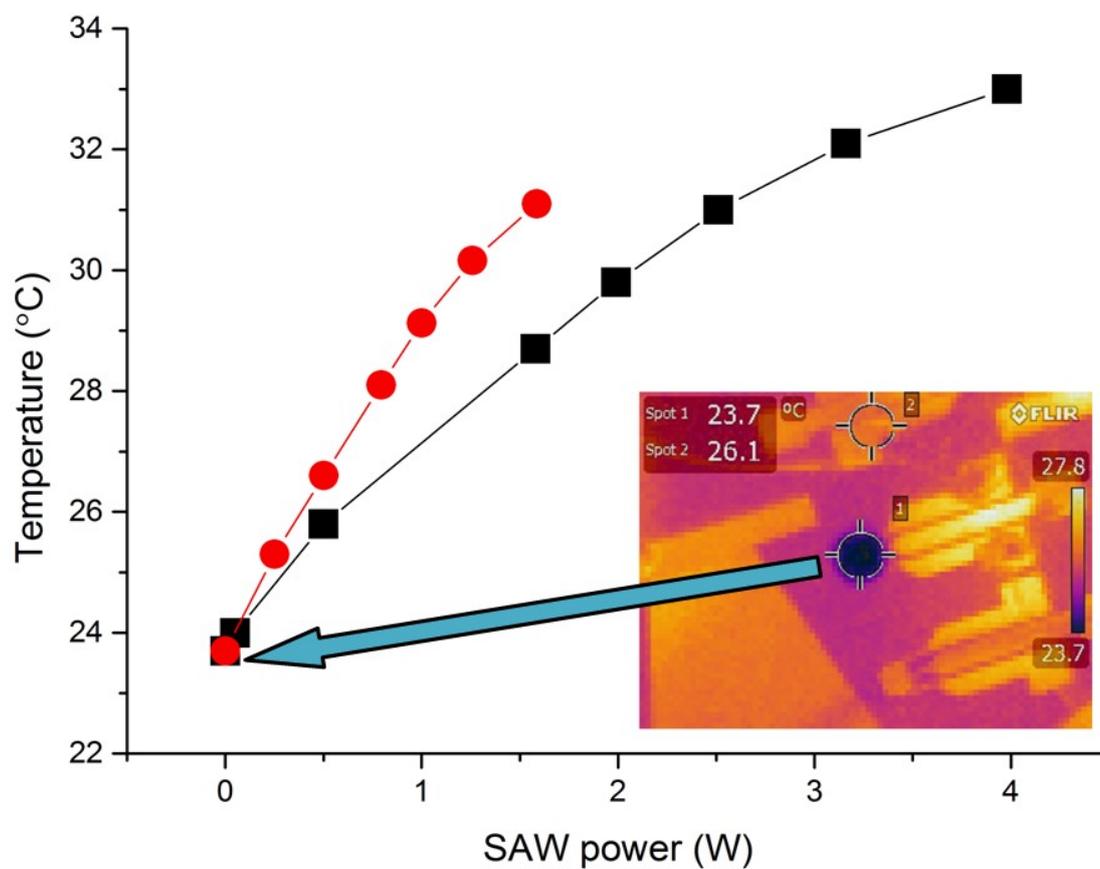
Figure 4. 26 SAW induced heating in the droplet (5 µl sample - black square symbol) and PDMS chamber (20 µl sample - red circle symbol). Measurements performed in the substrate based design. PDMS chamber created more heat generation than the droplet-based system.

The temperature changes, in two different device concepts, were observed via an IR camera (FLIR E60bx). The temperature graphs in Figure 4. 26 presents the temperature variation due to the increased SAW (12 MHz) power. The sample contained 10 mM potassium ferrocyanide and 100 mM KCl. Both devices were comprised of a single part without any additional superstrate attachment. However, the second one had a PDMS chamber bonded to it.

Each experiment performed with fresh samples. Each time the IR camera measurements performed after 10 seconds of SAW streaming. This enabled to obtain a stabilised temperature for each test.

In the first system, SAW power was changed from 0 to 4 W. This increased the temperature of the droplet (5 μl) from 23.7 °C to 39.8 °C. When the SAW power was 1.6 W, the temperature of the droplet was increased to 28.7 °C. However, the temperature of the PDMS system led to 32.4 % higher temperature values by increasing up to 31.1 °C. Results showed that the PDMS chamber in front of the SAW beam causes a faster temperature enhancement comparing to PDMS free design. This case is led by the SAW absorption of the PDMS [50][58]. Additionally, the heat release on the PDMS system does not happen as fast as a single standing droplet.

The next section will present the test results about temperature influence on the reaction rate. The practical work was made to differentiate the SAW induced heating effect from the hydrodynamical effect on the chemical reaction of ferrocyanide.

Heating effect on CV

In this section, the influence of temperature variation during CV measurements is explained through experimental investigation. The tests were performed on 10mM ferrocyanide containing droplet samples. The applied voltage range was between -0.4 V and 0.6 V. The scan rate of the triangle voltage was 0.1 V. Heat induction, provided by a hot plate, presented significant improvements on diffusive peak currents. The variation of temperature values to higher levels was increasing the amount of high energy collision of the molecules. Moreover, the diffusion was increasing due to the increased kinetic energy of the particles. This was dragging more fresh material to the electrode surface. Due to those two primary reasons the rate of the reaction, therefore, the current flow was increasing (Figure 4. 27 and Figure 4. 28).

A problem with the droplet-based system was the evaporation due to the heat generation of the SAW system. This was changing (increasing) the original concentration of the sample and causing extra current flow. Additionally, the measured current values were not consistent.

This fluctuation problem was also the result of the evaporation. However, the new design with a chamber solved this problem in the following experiments.
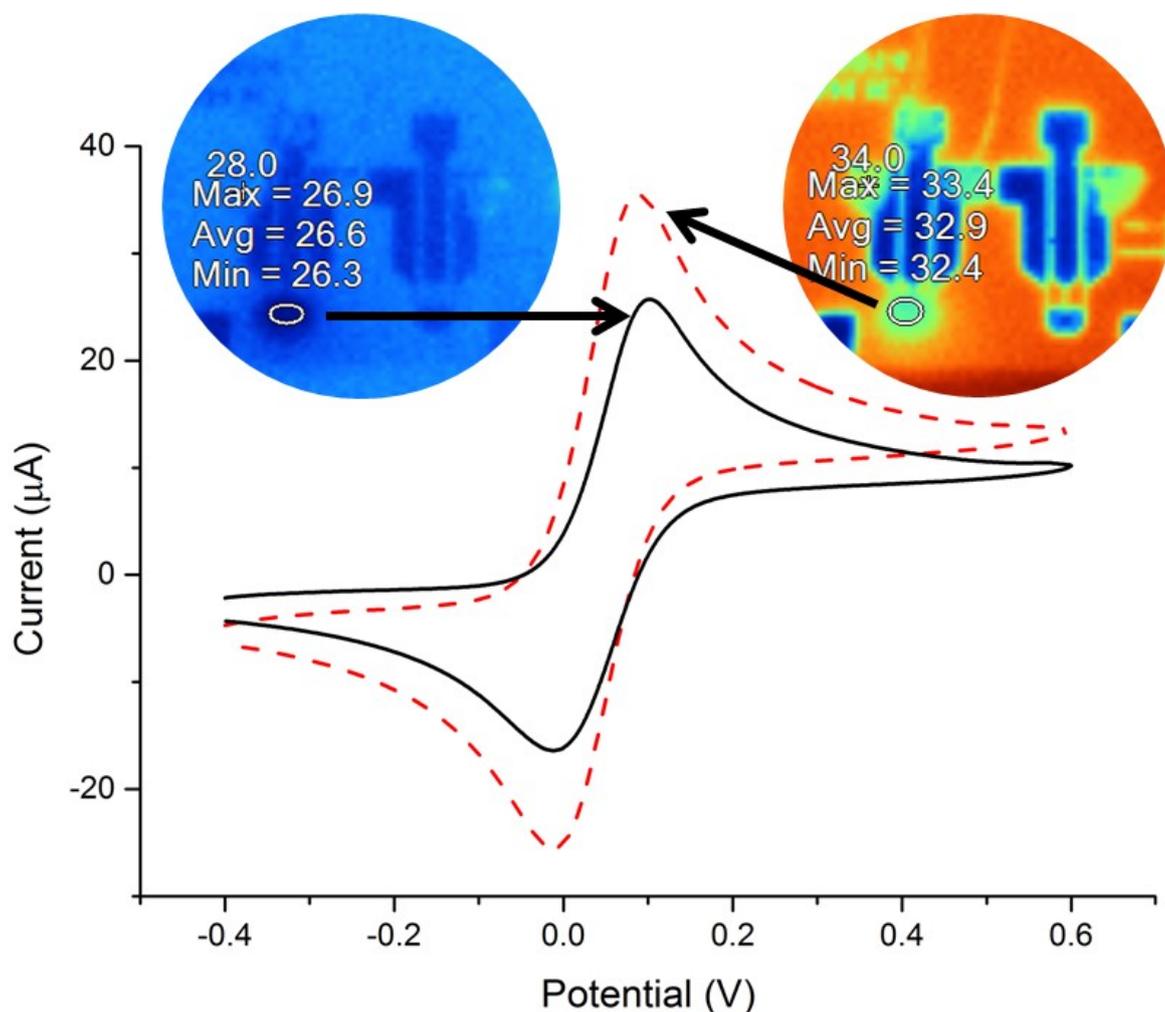
Figure 4. 27 The effect of temperature variation on CV analysis. The voltage applied (scan rate: 0.1 V/s) during the CV tests was between -0.4 V and 0.6 V vs. a pseudo gold reference electrode. The voltammogram obtained at 26.6 °C (solid line) presented a lower current flow comparing to the one performed at 32.9 °C (dashed line). This was received due to the increased amount of energised molecules in the second solution. Therefore, more molecules were able to pass through the reaction process. More reaction created more electron flow. Any other parameters of the CV tests were the same apart from the temperature variation. The 5 μl sample contained 10 mM potassium ferrocyanide and 100 mM KCl. The device was a single piece design without any additional superstrate attachment.
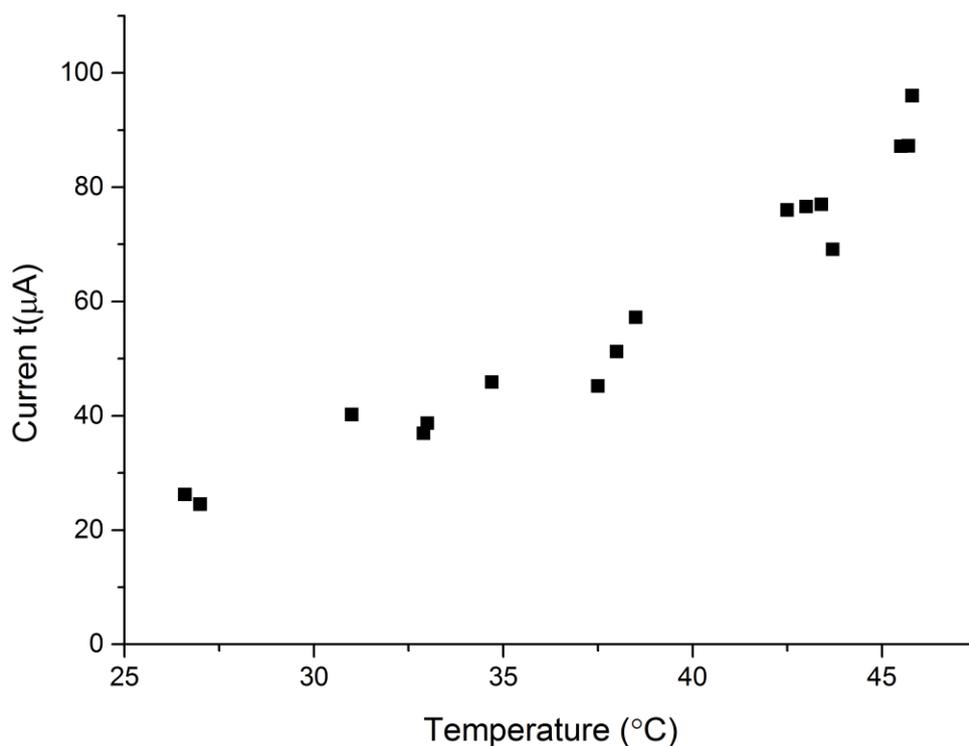
Figure 4. 28 The effect of heat variation on CV measurements. The graphic presents the enhancement of the diffusive peak current due to the increasing temperature. The measurements were performed on the circular electrode system fabricated on glass slides. The voltage range applied (scan rate: 0.1 V/s) during the CV tests was between -0.4 V and 0.6 V vs. a pseudo gold reference electrode. The temperature of the system was controlled via a hot plate. The heating effect presented an enhancement of the diffusive peak current of voltammetry measurements. An IR (FLIR E60bx) camera was used to observe the temperature variation inside the droplet.

Temperature effect of SAW on PDMS containing system

Figure 4. 29   The experimental setup for running amperometric measurements at different temperatures.
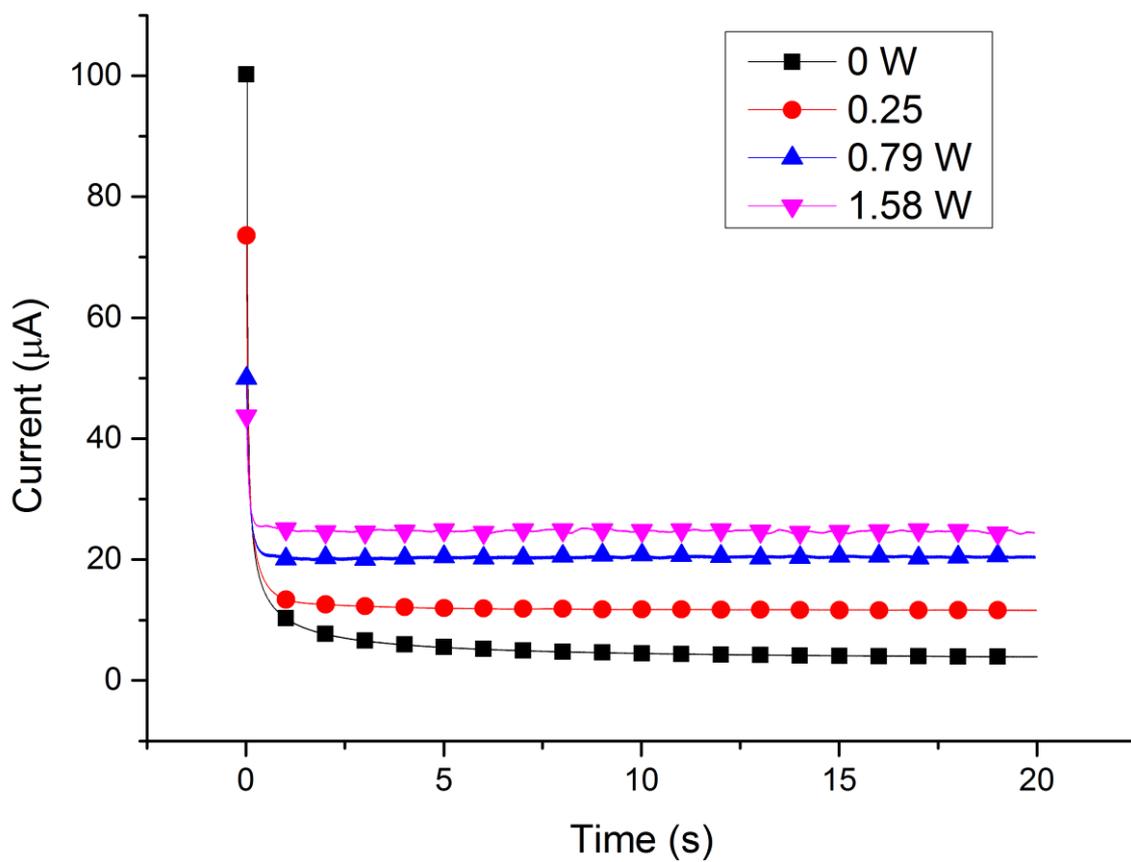
Figure 4. 30 Amperometric curves obtained at different acoustic streaming speeds. Applied SAW powers, in the presented plot, were 0 W (square), 0.25 W (circle), 0.8 W (up triangle) and 1.6 W (down triangle).
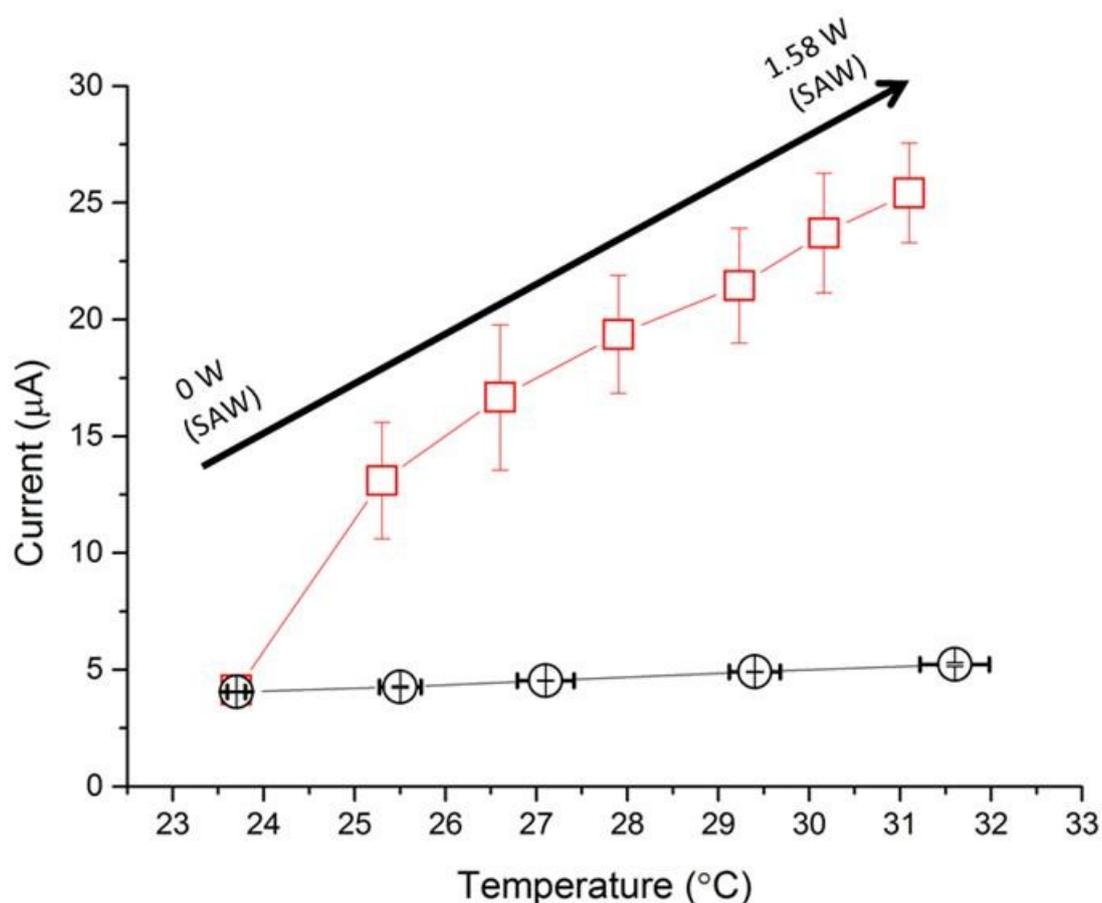
Figure 4. 31   The effect of temperature increment in SAW induced hydrodynamic amperometry. Measurements were performed with the substrate based system on 10 mM ferrocyanide solution. The first graph (circle) was obtained by varying the temperature of the system via a hot plate. The second graph (square) was obtained by running amperometric measurements while the SAW propagation was activated. SAW was produced at 12 MHz with varying power values (0 μA to 1. 6 W). The error bars represent the standard deviation of three experiments. Induction of SAW streaming, at 1.58 W, increases the stationery mode current from 4.14 to 22.42 μA. The enhancement lead by the heating, induced by SAW radiation, comprises 5 % of the total enhancement created by SAW streaming.

This section describes the effect of temperature in SAW induced hydrodynamic amperometry performed with the latest design. Figure 4. 31 shows the amperometric measurements obtained from the 10 mM potassium ferrocyanide solution. The latest design, with a PDMS chamber, was used for the amperometric measurements. The first graph (circle) was obtained by varying the temperature of the system. The temperature changes were controlled via the utilization of a hot plate. The second graph was obtained by running amperometric measurements while the SAW propagation was activated. Increasing power values created higher current values and also higher temperatures in the chamber.

The usage of an enclosed chamber in the electroanalytical system produced a significant improvement in the system. As a drawback, the temperature increment was faster (Figure 4. 26) due to the SAW absorbing PDMS layer. However, it did not cause any problem in the measurement because, the evaporation of the sample was significantly minimised thanks to the cover of the chamber. The enclosed chamber enabled the rapid establishment of a humid

environment inside the small air gap (13.5 mm^3), between the sample and the cover of the chamber. Therefore, the concentration of the sample was kept at the same level.

Most importantly, the data presented in Figure 4. 31 give a clear perspective about the details of the observed current enhancement in SAW induced design. The results show that the induction of SAW into the amperometric chamber created significant current improvements. Applied maximum SAW power (1.58 W) caused more than six times current improvement. The enhancement was due to the streaming effect and the heating effect of the SAW propagation. Both the collusion (kinetic) energy and the diffusion rate enhancements of the molecules were created by the heating effect of the SAW. However the current enhancement, produced by the heating effect of 1.58 W SAW power, only comprised the 4.84 % of the total current enhancement. Moreover, this percentage was lower at SAW application with less power. For example, the ratio was only 1.34% during the SAW induction at 0.25 W. Therefore the substantial amount (more than 95 %) of the obtained current enhancement was due to the hydrodynamic effect created by the SAW streaming.

SAW induced charge interference
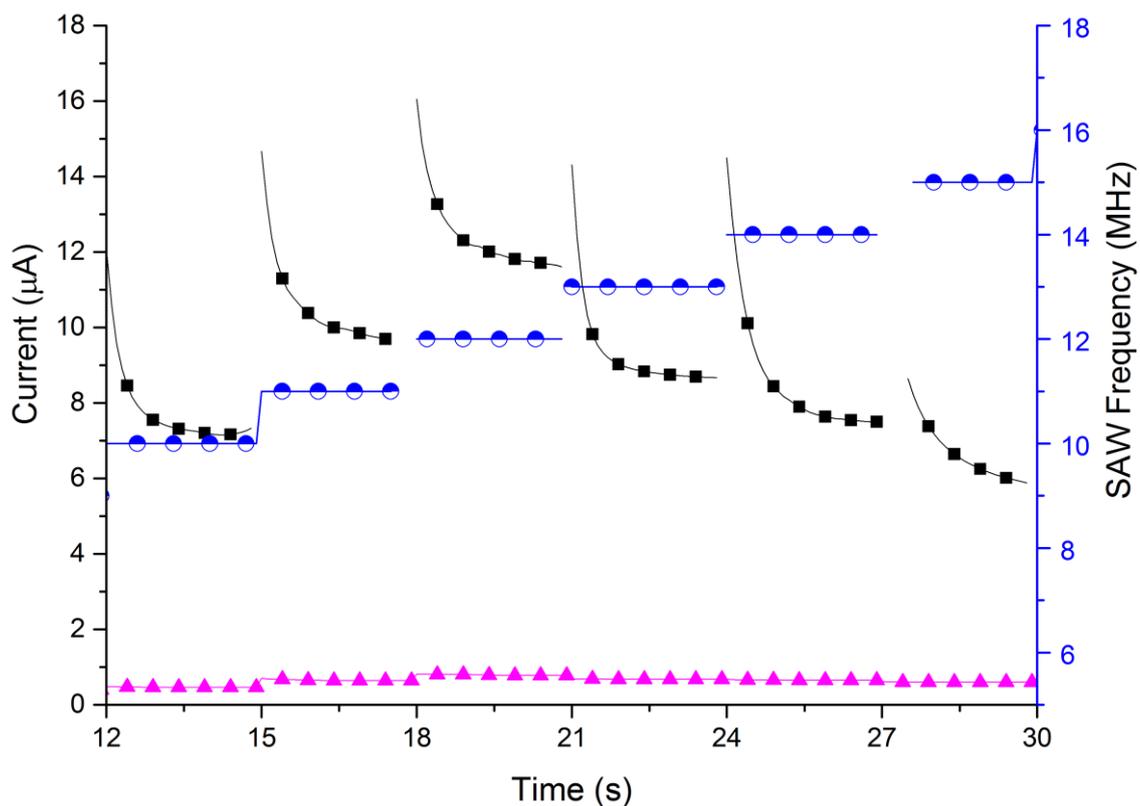
Figure 4. 32   Amperometric test results present the effect of direct SAW interference on the measurements. Various SAW frequencies (half filled circle) ranging from 10 MHz to 15 MHz (1 W) were applied to two different samples; 5 mM Potassium ferrocyanide (with 100 mM KCl) (square) and 100 mM KCl (up triangle). The amperometric voltage (0.2 V) was applied for 3 seconds in each experiment.
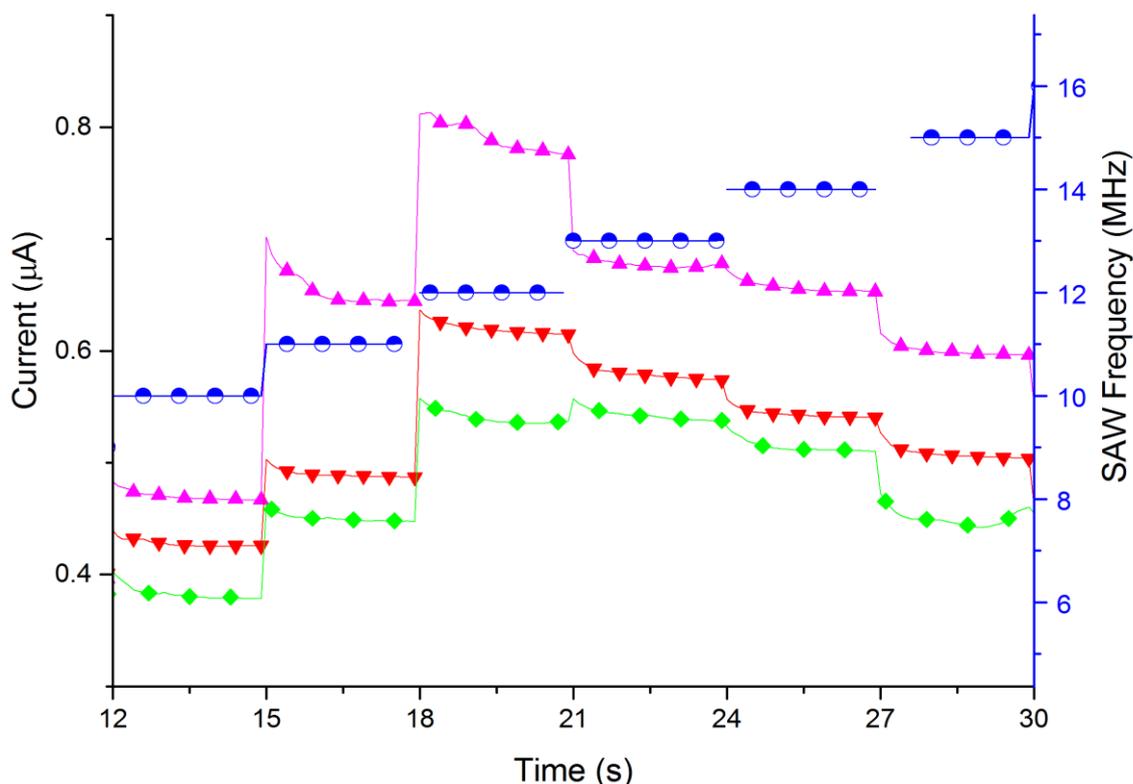
Figure 4. 33 Amperometric test results presenting the effect of direct SAW interference on the measurements. Various SAW frequencies (half filled circle) ranging from 10 MHz to 15 MHz (1 W) were applied to three different samples; 100 mM KCl (up triangle), pure water (down triangle) and dry chamber (diamond). Measurements performed in the dry chamber also presented a current flow because of the charging effect of the mechanical waves on the sensing electrodes.

Piezoelectric materials are capable of converting electrical energy into mechanical energy or vice versa. On a piezoelectric substrate, a propagating elastic wave will be accompanied by an electric field. This has the potential to create interference on electroanalytical measurements, by directly interacting with the three electrode sensing platform. This section focuses on the effect of direct interference of the SAW on the electroanalytical tests.

Amperometric measurements were performed with the PDMS chamber based sensor design. The power of the SAW propagating from the slanted IDT design was 1 W. The first test series was conducted on 5 mM Ferrocyanide (in 100 mM KCl) samples. Secondly, the samples containing only the supporting electrolyte (100 mM KCl) were tested. Comparison of those two results (Figure 4. 32) show that the current enhancement is not only obtained due to the SAW enhanced reaction properties of the ferrocyanide molecules, because the second graph proves that the SAW was still increasing the current flow while there was only KCl solution in the chamber.

Amperometry tests on pure water (Figure 4. 32) presented a further step to explain the direct SAW interference. Removal of the KCl from the sample caused a decrease in the current

due to the decreased ion level in the liquid system. Moreover, the SAW induced streaming was still increasing the amount of electron flow in the system.

The empty PDMS chamber measurements during the SAW propagation at varying frequencies are presented in Figure 4. 33. The current value at 12 MHz was improved by 0.16 μA. This enhancement is comprised less than 2% of the current enhancement in 5 mM potassium ferrocyanide measurements. This result indicates that the SAW induced current enhancement was not purely obtained due to the enhanced electrochemical characteristics of the molecules. Because the three electrode sensing platform was also working like a SAW receiver and converting mechanical energy back into the electrical current form. However, the presence of a liquid sample in the reaction chamber decreases that effect. The liquid converts the mechanical wave energy into leaky waves on the surface, pressure waves and temperature in the fluid. Further details can be found in the introduction chapter. Therefore, the direct interference of the remaining leaky waves on the surface is not expected to create a considerable interference on the measured signal.

SAW induced RF Interference

As an additional test, the system was checked for RF interference, propagated from the SAW device. Amperometric measurements were performed via a separate three-electrode system. The sensing platform was located on the heat sink of the SAW platform. They were aligned same as the PDMS based sensing platform, but the substrates were ~2 mm apart from each other. This was needed to block any SAW coupling between the resonator platform and the sensing platform. Therefore, the signal measured by the sensor would only be created by the electrical field induced by the SAW device. The amperometric test was performed at the entire working frequency of the slanted IDT at the maximum SAW power (1.58 W). However, no signal was observed due to the interference of the RF. This meant the design was not affected by the RF signal interference.

4.4.   Discussion

The experiments mentioned above were performed via two main device designs; superstrate based (half disposable) device (Figure 4. 7) and the substrate based design (Figure 4. 8). The sensor part of the first design was capable of being detached from the SAW platform and disposed. Therefore, the SAW device can be used for new experiments by the attachment of new sensing electrodes. This advantage put the first design, one step forward in terms of the fabrication costs. However, the coupling compound between the sensing and SAW platforms was drying and becoming more viscous over time. This was decreasing the SAW coupling

characteristics of the system. Moreover, the gel was creating more heat, due to the absorption of the SAWs, and the heat accelerated the drying process. Therefore, the attached electrodes are required to be used around three hours time at room temperature. Otherwise the streaming of the sample, located on the superstrate, starts to lose its power, and the enhancement of current flow begins to decay. The coupling of the superstrate on SAW platforms needs further research to present more repeatable and steady characteristics. On the other hand, the substrate based device displayed steady and repeatable streaming characteristics of the sample.

Using a closed PDMS chamber, instead of a droplet trap, for the sample handling eliminated the evaporation problem. Acoustic energy attenuation was a drawback of the PDMS walls. However, the contribution of the chamber on noise decrement was a more vital issue.

The heat generation appeared as another problem of the PDMS based system. The SAW radiation through a PDMS layer creates more temperature increment comparing to the direct radiation into a droplet. The heat increases the energy level of the molecules and creates an extra convection. Therefore, 5 % of the diffusion limited current was induced by the heat conducted by SAW radiation into the chamber. However, the heat does not cause an adverse effect on quantitative data measurement as long as the temperature is kept at the same level. This can be done by keeping the SAW parameters, frequency and power, at same values.

The energy absorption and the heat generation problems of the PDMS chamber can be solved by various ways. For example, using SAW tunnels at the bottom of the PDMS layer can increase the SAW radiation into the chamber. SAW tunnels are the structures opened on the walls of the sample chambers. End of the tunnel is closed in order to prevent the liquid leakage. The structures are made to decrease the thickness of the chamber walls at specific locations. This enables to decrease the acoustic energy absorption on the walls. Another solution can be performing further research on the chamber material and its bonding process. Thus, a new sample chamber, with better acoustic wave transmission characteristics, can be developed.

The evaluations of experimental results showed that the SAW on an electroanalytical sensing platform may have a very minor and negligible direct interference during the measurements. Therefore, the receiver like working problem of the electrodes was not an issue for the system.

4.5.   Conclusion

SAW induced electrochemical measurements offered improvements in the magnitude of diffusion limited current. This new technique is capable of being replaced with conventional hydrodynamic analysis methods. Additionally, it can be applied to chemical and biochemical sensor applications. Since the streaming rate directly increases the current, it is advantageous to use the highest possible SAW power to enhance the sensitivity of the system depending upon the sensitivity requirement. Another advantage of this method is small (μ) scale sample requirement.

Piezoelectric devices are commonly used for various purposes in harsh environment conditions. Thus, the SAW induced electro- analysis device has potential to be modified for severe circumstances. In comparison with conventional techniques, this new hydrodynamic electro-analysis method has no moving components which improves its solidity and significantly reduces the breaking/failing probability. The mono-block design also prevents the tendency of deterioration with use. So the system can keep working for a longer time without any performance loss due to the friction affect in between moving parts.

Streaming effect provided by SAW has the advantage of being very manoeuvrable, thanks to the unique transducer designs. Therefore, precise arrangements for the streaming direction and velocity can be done easily according to the requirement of the analysis or sensing application.

For sensitive measurements, direct SAW interference on sensing electrode system can be completely removed with some minor design improvements such as moving the sensing electrodes out of the SAW beam path. So the acoustic waves will only interact with the sample solution but not with the sensing electrodes.

The design is well-suited to cost effective lab-on-a-chip applications since the electrochemical sensing unit can be fabricated on a separate disposable substrate (superstrate) and coupled on the primary substrate. However, this requires further research about the coupling process and the materials used.

Overall, we envision that this moving part free and reliable microfluidic technique can not only be utilized to study electro-analysis but also as a means to perform more sensitive and automated assays.

5. Label-free haemoglobin detection and system instrumentation

5.1. Introduction

This chapter explains the experimental work conducted on a label-free haemoglobin (Hb) sensing system and the instrumentation prepared for the future system designs. Usually, less than 50 mg Hb in a mg of stool is not visible [124]. However, more than 2 mg/gr Hb in an adult stool can be caused by gastrointestinal carcinoid tumours [124]. Bowel cancer is one of the four most common causes of cancer deaths in the world [125][126]. Periodic faecal occult blood test (FOBT) checks can enable the early detection of blood in the stool. This can lead to early and successful treatments and save lives.
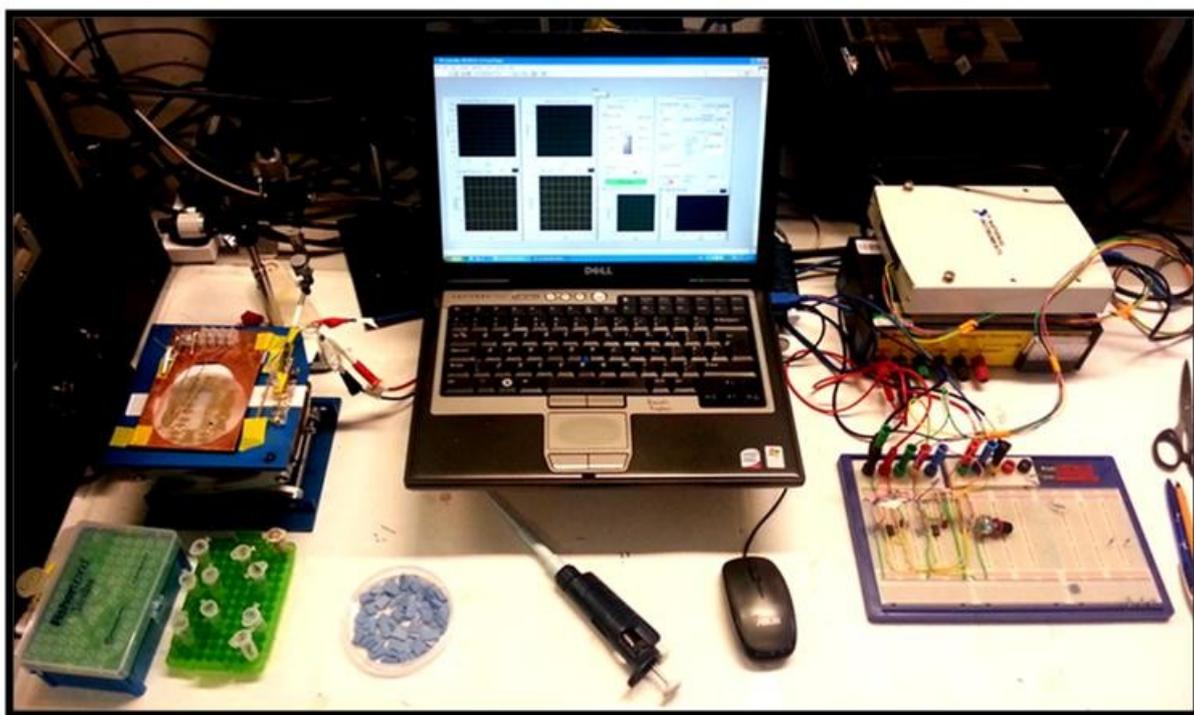
Figure 5. 1 Final electroanalytical system setup. A signal (triangle or a constant signal) is produced by the LabVIEW interface and a data acquisition device (NI DAQpad-6015), and sent to the sensing chamber via the potentiostat circuit. Signal output is obtained back from the sensor by the potentiostat and sent to the PC through the DAQpad. Finally, the results are observed on the LabVIEW interface screen.

The label-free method investigated in this work has the potential to give reliable measurements by avoiding the use of a secondary antibody. This approach requires a simpler protocol, which has fewer processing steps than traditional immunoassays. Therefore, these assays are suitable candidates for miniaturisation onto microfluidic Lab-on-a-Chip devices.

Moreover, the sensitivity of the system can be enhanced by the acoustically enhanced mass transfer rates in electroanalytical tests. This provision was supported by the results obtained in a model bio-analytical system. SAW enhanced biosensing applications have several advantages. Acoustic wave induced streaming phenomenon reduces cost and waste during ELISA tests. This benefit can be helpful on various biosensing techniques such as electrochemical impedance measurement, cyclic voltammetry (CV), amperometry, fluorescent method, surface plasmon resonance (SPR). SAW induced streaming also has a positive effect on the avoidance of non-specific binding issues.

The electroanalytical systems require potentiostat devices to operate. As a part of this work, a potentiostat circuit and its controlling interface are designed to control the system without using bulky commercial devices. The LabVIEW based flexible software design can also be modified to be used for rapid analytical processes and the synchronised control of the acoustic mixing platform. Therefore, the final complex design will have the ability to control the acoustically enhanced electroanalytical system fully and provide rapid analytical results.

5.2. Biosensing- label free Hb detection

Various studies have been carried out to obtain highly sensitive and fast responsive H_2O_2 sensors [127][128][129][130][131]. Moreover, highly sensitive and quick H_2O_2 sensors based on the direct electron transfer Hb, due to its peroxidase activity, are reported [132][133]. The direct electron transfer happens between Hb and the electrode due to the intrinsic peroxidase like the activity of Hb. Thereby the Hb to catalyse the reduction of H_2O_2 [132] [134]. Furthermore, the reaction system can be used in an opposite way for Hb detection by the addition of a mediator in the Hb - H_2O_2 reaction mechanism. The technique is a "label free" assay since it does not require any secondary antibody or enzyme labels. It is based on simple protocols due to its few processing steps. This also makes it very suitable for miniaturised Lab-on-a-Chip applications. The method developed here can detect Hb in turbid solutions such as bowel fluid, thanks to the electrochemical sensing platform. The results obtained from the investigation of this label-free detection technique is explained in this section.

The electroanalytical assays need to be conducted by an electron passing mediator. Benzidine is widely used for direct Hb detection in plasma and urine since 1923 [135][136][137]. But, it was defined as a carcinogenic material. However, TMB (3,3',5,5'-Tetramethylbenzidine) has is found as a safe derivative of benzidine [137]. TMB, which is the most commonly used chromogen for HRP detection, does not get into direct reaction with H_2O_2. Therefore, TMB

was used as a mediator in Hb detection experiments. The samples also included KCl (100 mM) as a supporting electrolyte for electroanalytical tests.

5.2.1. Electroanalytical tests in batch conditions

The feasibility of electroanalytical Hb recognition by using TMB as a mediator is investigated. The technique does not require any secondary Ab or an antigen with a recognition label attached on them. As a first stage, the label-free immunoassay was examined by CV without any Ab immobilisation on the surfaces. 20 µl sample solutions, included TMB - H_2O_2 system (T 8665, Sigma- Aldrich) and varying Hb concentrations (5, 0.5, 0.05 and 0 mg/ml), were tested in a PDMS reaction chamber after 1 hour incubation. The samples also included 10 mM KCl as supporting electrolyte. The working mechanism of the label-free method is shown below.

$$Hb_{(Red)} + H_2O_2 \rightarrow Hb_{(Ox)} + H_2O$$

$$Hb_{(Ox)} + TMB_{(Red)} \rightarrow Hb_{(Red)} + TMB_{(Ox)}$$

$$TMB_{(Ox)} + e^- \rightarrow TMB_{(Red)}$$
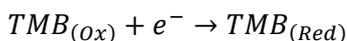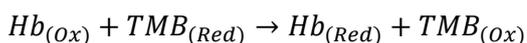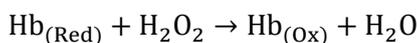
A three-electrode (10 nm Ti and 100 nm Gold) sensing system was microfabricated on a 1mm thick glass slide. The voltage applied (scan rate: 0.05 V/s) during CV test was between - 0.2 V and 0.5 V vs. a pseudo gold reference electrode. Top of the chamber was covered with a thin glass in order to block the evaporation. Excess protein builds up on the electrodes that could decrease the sensitivity were cleaned with bleach after each experiment. The sample in the chamber remained from the last experiments was removed. Then the sensing chamber was kept as filled with 30 µl of bleach for one minute and it was diluted with water for five times. Following test was started after the chamber was emptied and dried with N_2 blow. The filling and washing process was performed with pipettes.
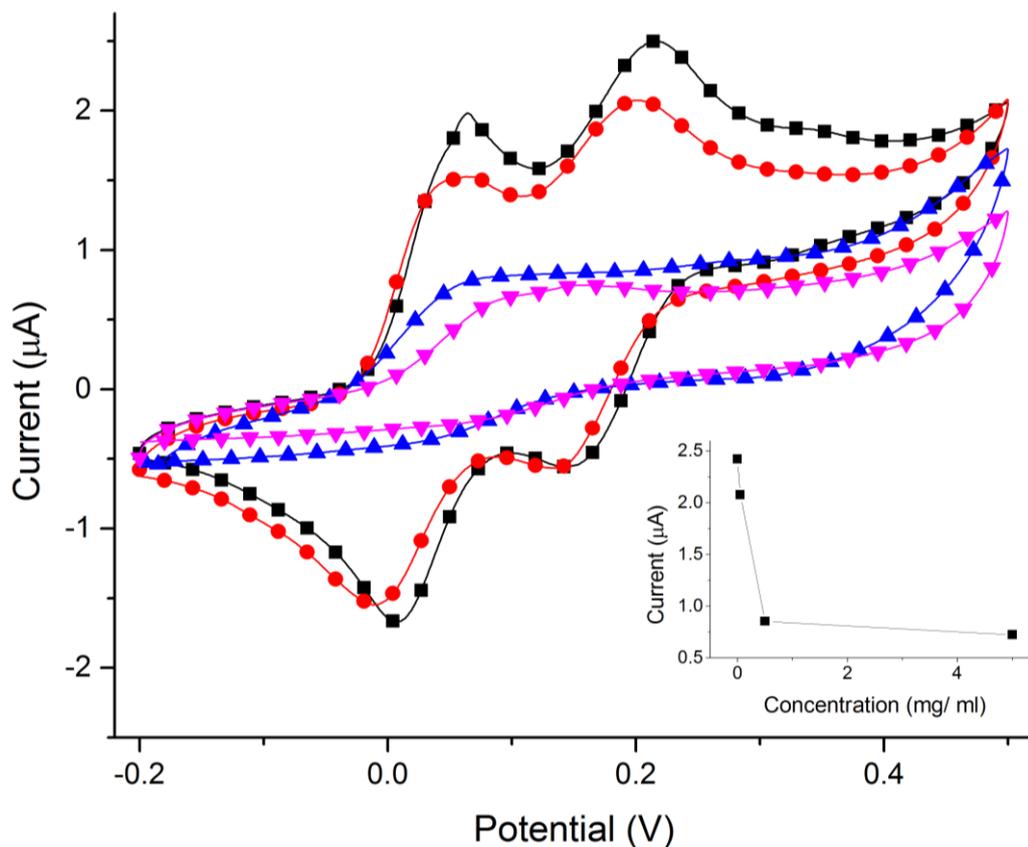
Figure 5. 2   Voltammograms (scan rate: 50mV/s) obtained from the batch condition Hb electroanalytical tests. The inset presents the oxidative currents obtained at 0.2 V. Measurements were performed on different Hb concentrations; 5 mg/ml (down triangle), 0.5 mg/ml (up triangle), 0.05mg/ml (circle) and 0 mg /ml (square) mixed with the TMB system (including 10mM KCl as the supporting electrolyte)

Voltammograms presented in Figure 5. 2 shows that TMB can give relevant data about the amount of Hb existing in the chamber. The label-free technique has fewer steps than a sandwich type electrochemical immunoassay [138] and has only one antibody (this particular test series did not include any antibody). Therefore, the technique is rapid and more reliable since the cross-reactivity of the second antibody is eliminated from the system.

5.2.2.   Antibody effect on Hb - TMB interaction

The oxidation of TMB changes its transparent colour to blue [139]. This enables TMB to be used in optical measurements via colorimetric observations. Hb and anti-haemoglobin (anti-Hb) binding can block the reactive sides of Hb molecules and decrease the reaction rate or stop the reaction completely. Therefore, the colour change characteristics can be changed. In this section, the effect of Ab on TMB-Hb reaction was tested via optical monitoring method. Experiments were performed in batch conditions without any antibody immobilisation process.
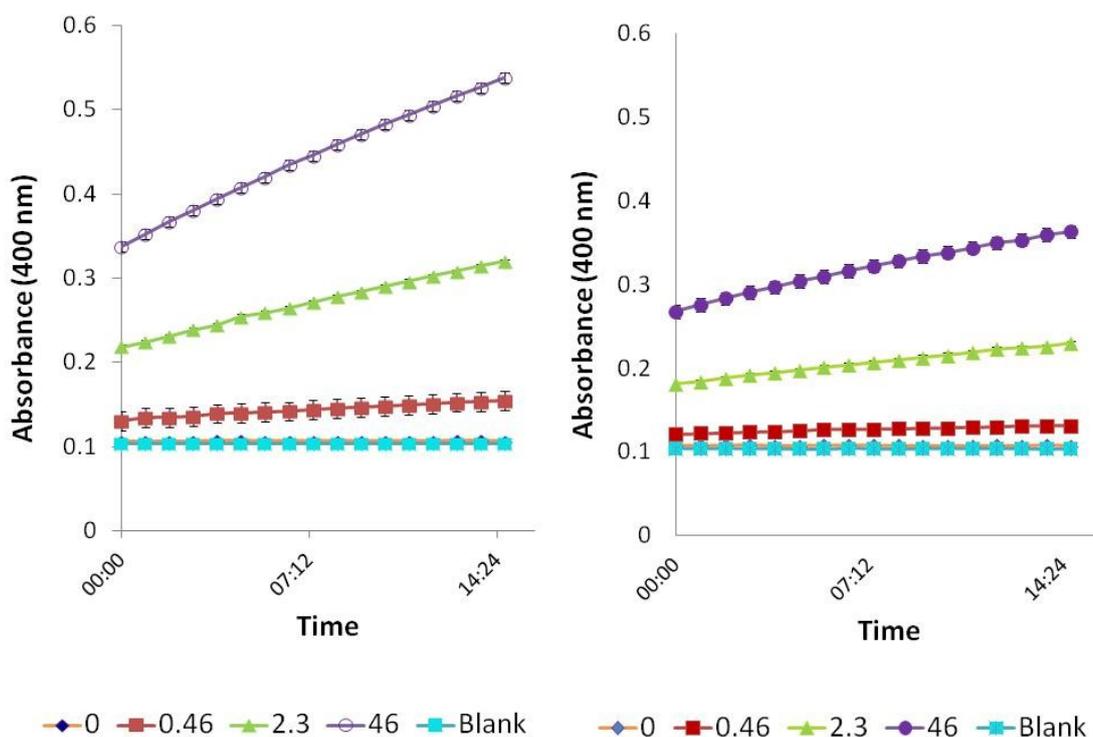
Figure 5. 3 Absorbance measurement (400 nm) conducted on TMB - Hb interaction in the absence (Left) and the existence (Right) of antibody (15 mM). The batch condition tests were performed by mixing different Hb molarities (1, 0.46, 2.3, 46 μM) with the same amount (volume) of the TMB-H_2O_2 substrate system.

Figure 5. 3 show that the existence of Ab decreases the efficiency of Hb to oxidise TMB. This can decrease the sensitivity level during the measurements, but it does not completely block the reaction between Hb and TMB as shown in Figure 5. 3- Right graph.

5.2.3.   Bio-receptor entrapment methods

Polymerisation

There are various methods to form a sensitive layer (proteins) on the electrodes or in the polystyrene wells such as using artificial entrapment (polymer or gel) membranes [140][141] and self-assembled layers [142]. A part of this chapter covers the application of polypyrrole (PPy) chains on the electrode surfaces. During the polymerization process, NaCl was used as the supporting analyte in the solution (50mM NaCl, 150mM Pyrrole). As shown in Figure 5. 4, the voltage range of the CV was between 0 V and 0.8 V. This was defined by the characteristics of pyrrole monomer in a separate test. Voltammetry was performed 12 times (scans) at 0.05 V scan rate. Two-dimensional surface profile measurements (measured with Veeco Dektak 6M height profiler) and atomic force microscope (AFM) based surface

topography scans (NanoWizard II atomic force microscope - JPK Instruments AG, Germany) enabled the investigation of the polymerised surface and the electropolymerization ratio. Figure 5. 5 shows that the thickness of the electrode was increased from 80 nm to 198 nm after 12 times CV scan in pyrrole solution. Each CV scan produced 9.8 nm thick PPy film on the surface of the gold electrodes (3.14 mm²).
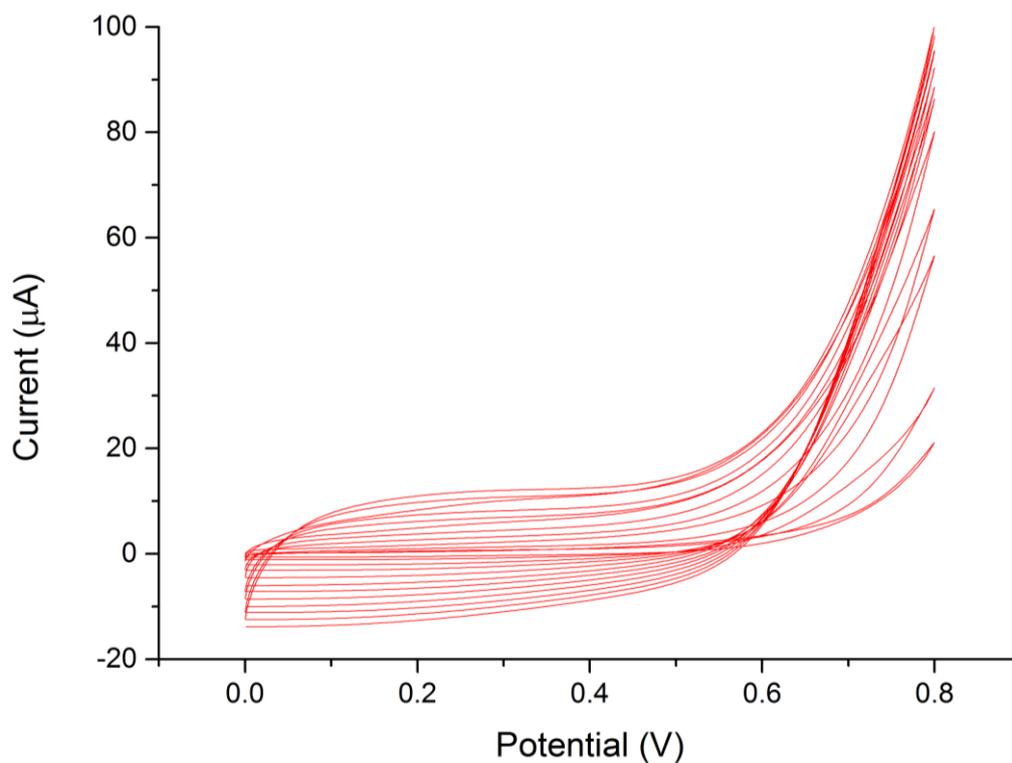
Figure 5. 4 Voltammogram obtained during PPy growth on the gold electrode surface. Twelve scan CV performed with 0.05 V/s scan rate between 0 V and 0.8 V (vs. Ag/AgCl reference electrode). The chemical solution was comprised of 50mM NaCl and 150mM Pyrrole.
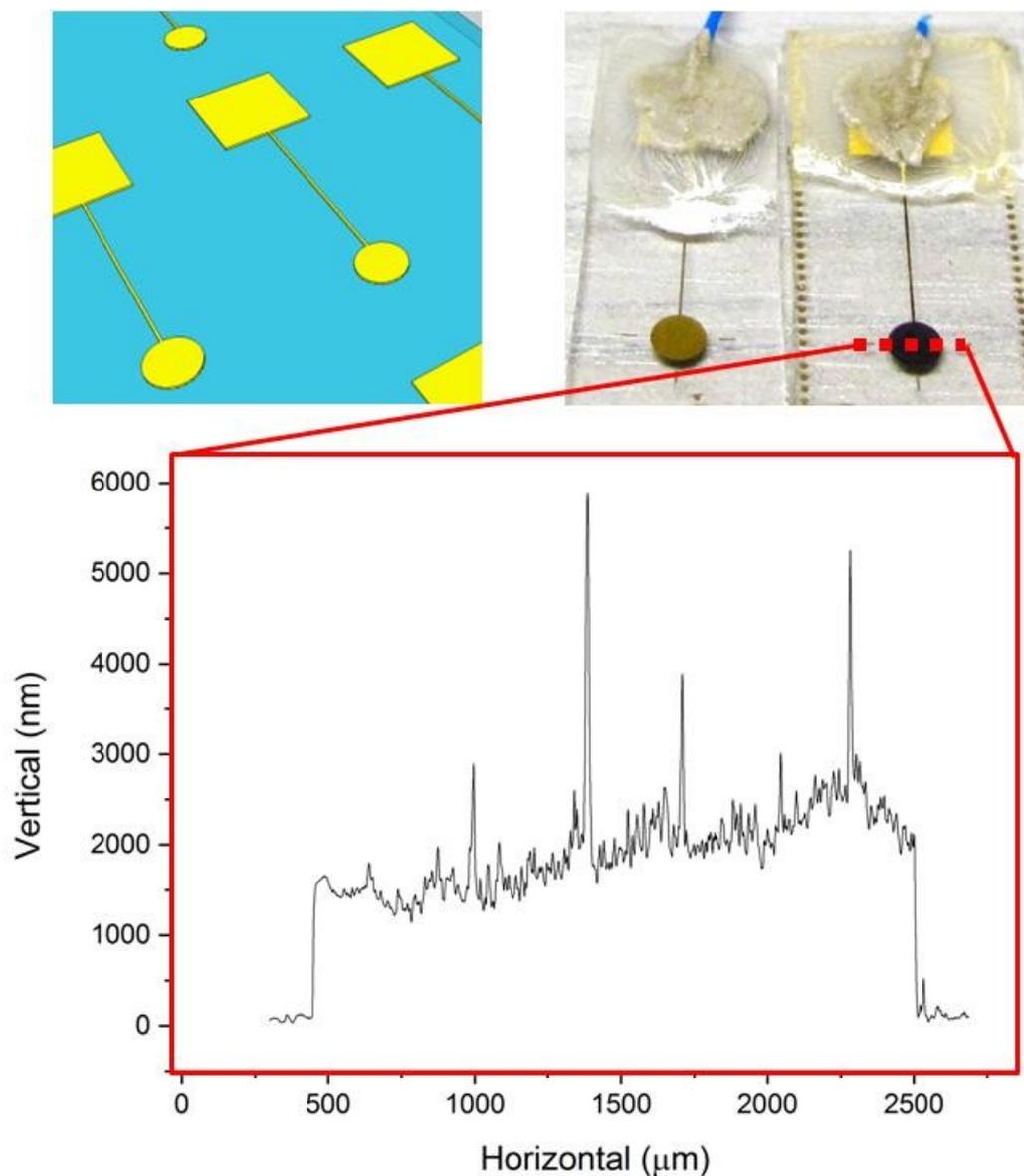
Figure 5. 5 Top Left: Depiction of lollypop shaped electrodes (10nm Ti, 10nm Pt, 60nm Au) fabricated on a 1 mm thick glass slide by photolithography. Top-middle & Top-right: Images of electrodes before and after the polymerisation process. Bottom: shows the surface structure (2D), on the polymerised electrode, obtained by profilometry measurements (DEKTAK, Veto Instruments Ltd).
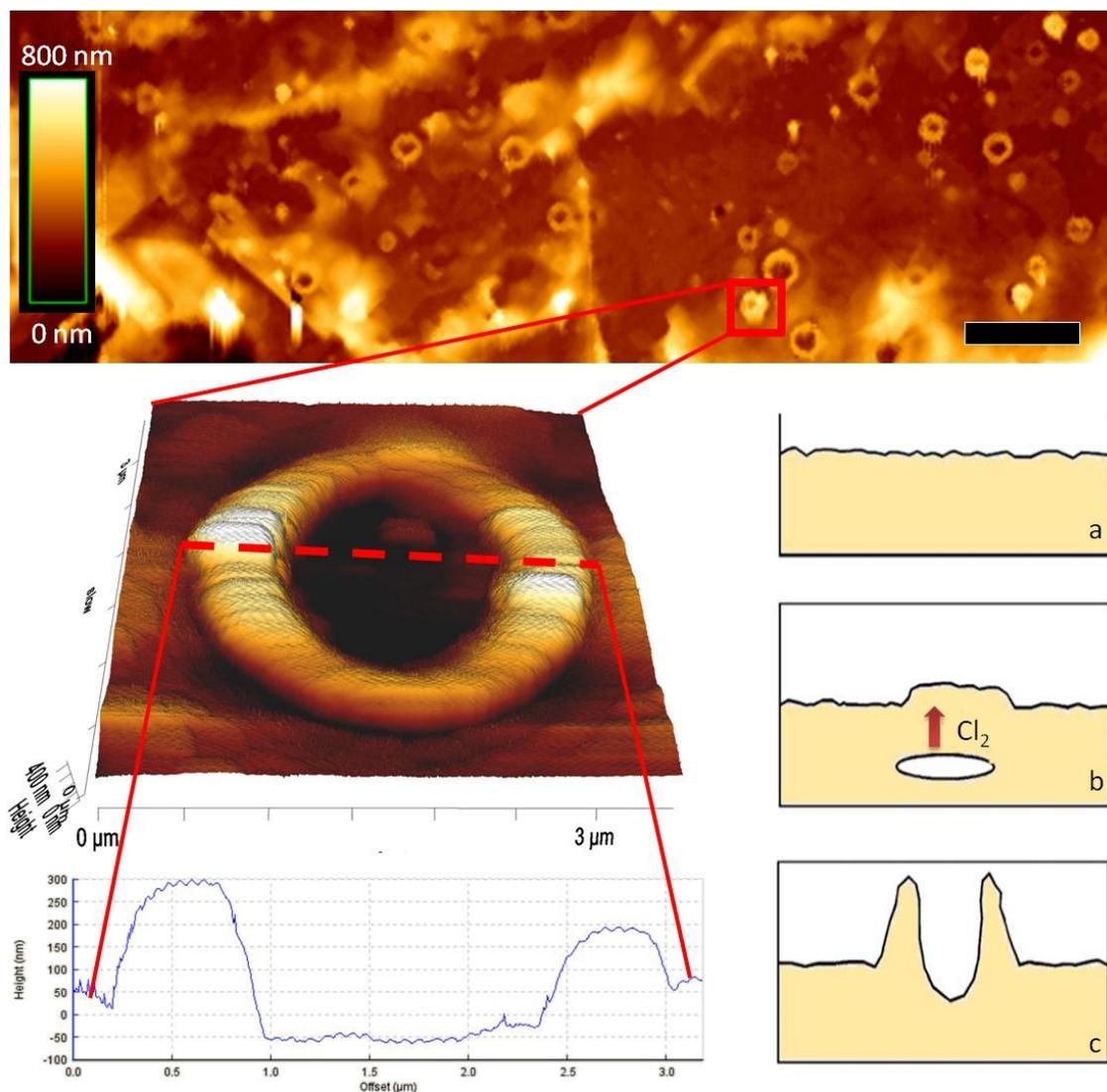
Figure 5. 6   Atomic force microscopy scan obtained from the polymerised electrode surface. The depiction (right side) presents the production mechanism of the circular (donut shaped) PPy structures [143]. (Scale bar in image at top is 10 μm)

Figure 5. 6 presents AFM measurements obtained from the polymer surface. The image was obtained after the 12th cycle of polymerisation. Circular (donut shaped) structures appeared randomly on the PPy film. These features may be structured by the release of gas bubbles (Cl_2) trapped in the region between the substrate and the film [143].
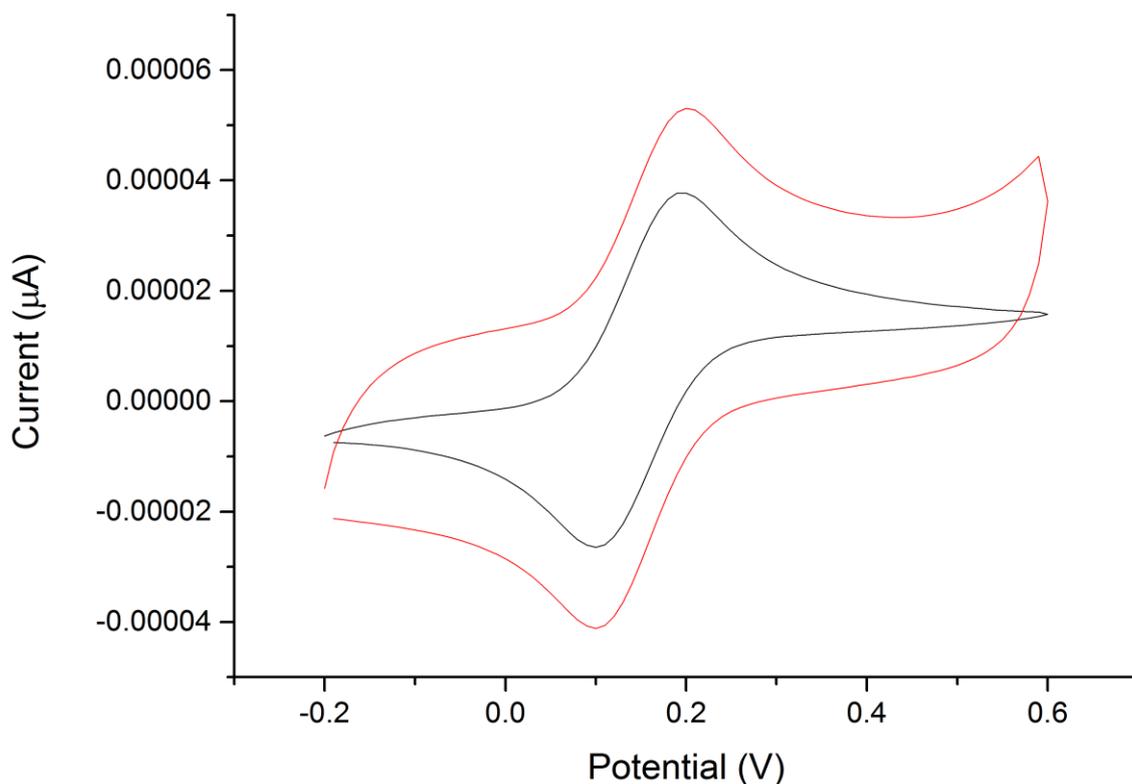
Figure 5. 7 CV graphs performed by two different working electrodes; a bare gold electrode and a polymerised electrode. CV performed with 0.05 V/s scan rate between -0.2 V and 0.8 V (vs. Ag/AgCl reference electrode). The chemical solution was comprised 10 mM potassium ferrocyanide and 10 mM KCl.

Electroanalytical characteristics of the electrodes before and after the PPy film coating were investigated (Figure 5. 7). The PPy modification led to more background current flow due to the increased surface area of the electrode. Therefore, it can be possible to obtain more sensitive systems by obtaining rough surfaces made of conductive polymer layers.

SAM binding test with fluorescent beads

In this section the binding efficiency of two different methods, for antibody entrapment, were experimentally compared. First, biotin labelled bead (1.0 μm, yellow-green fluorescent, Life Technologies) binding on streptavidin attached SAM layer and second, the binding of amine-modified beads (1.0 μm, yellow-green fluorescent, Life Technologies) on SAM layer were tested. The SAM used in both systems was 11-mercaptoundecanoic acid (11-MUA). Binding rates were tested by observing the entrapped fluorescent beads via a microscope (Carl Zeiss Axio Observer Z1).
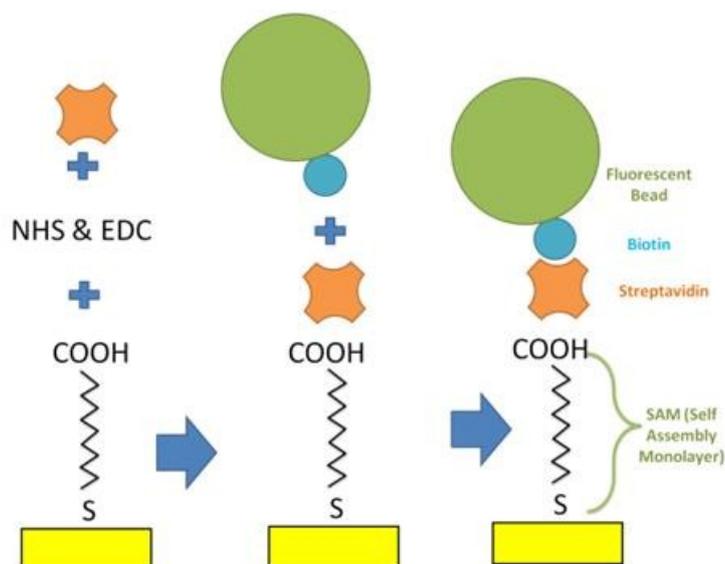
Figure 5. 8 The schematic of streptavidin - biotin based binding. The gold surfaces functionalized with 11-MUA solution (under nitrogen atmosphere) were exposed to streptavidin solution. Finally, biotin labelled latex beads were applied to the functionalised surfaces.
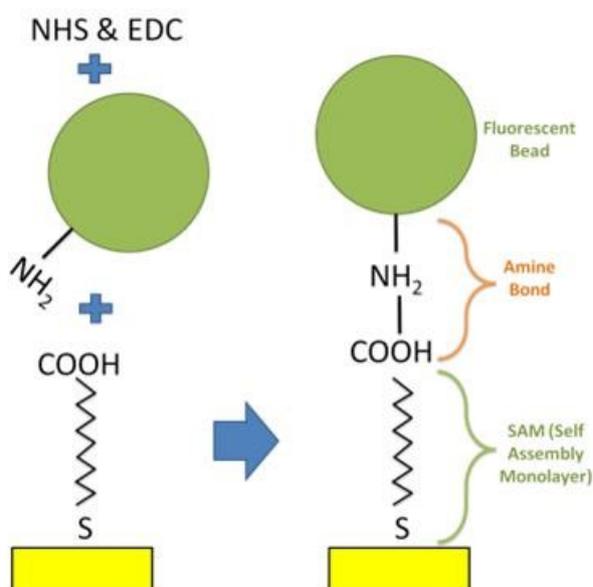
Figure 5. 9   Schematic of amine-based binding. The electrode surfaces functionalised with 11-mercaptoundecanoic acid (11-MUA) solution (under nitrogen atmosphere) were exposed to amine modified latex beads (1 µm in diameter) solution (with EDC and NHS in it) for 2 hours.

Firstly, both samples were cleaned by acetone sonication (5 m), water rinse (2min) and nitrogen drying. The surfaces were activated by oxygen plasma (60 W, 90 seconds) and, functionalised with ethanolic 11-MUA (20mM) solution, under a nitrogen atmosphere (2 hours). The substrates were washed with ethanol then water and dried under a nitrogen stream. After this point the first sample with the SAM layer was modified by applying the streptavidin solution (10 µl Streptavidin, 10 mg EDC and 5 mg NHS in 1 ml MES buffer) at 38 ˚C for 2 hours. Its surface washed by 5-minute sonication in 10 % Tween 20 (Polyethylene glycol sorbitan monolaurate- Aldrich) PBS solution and dried with nitrogen. Biotin labelled

latex beads (100 μl in 1 ml PBS) were applied on the surface for 2 hours. Finally, the sample was sonicated in 10 % Tween 20-PBS solution (5min), sonicated in PBS (5 minutes) and dried with nitrogen. The second sample, with 11-MUA on its surface, was treated with an MES (1 ml) solution containing EDC (10 mg), NHS (5 mg) and amine-modified latex beads for 2 hours. Lastly, the sample was washed in the same way as the first sample. Then both samples were ready for investigation.
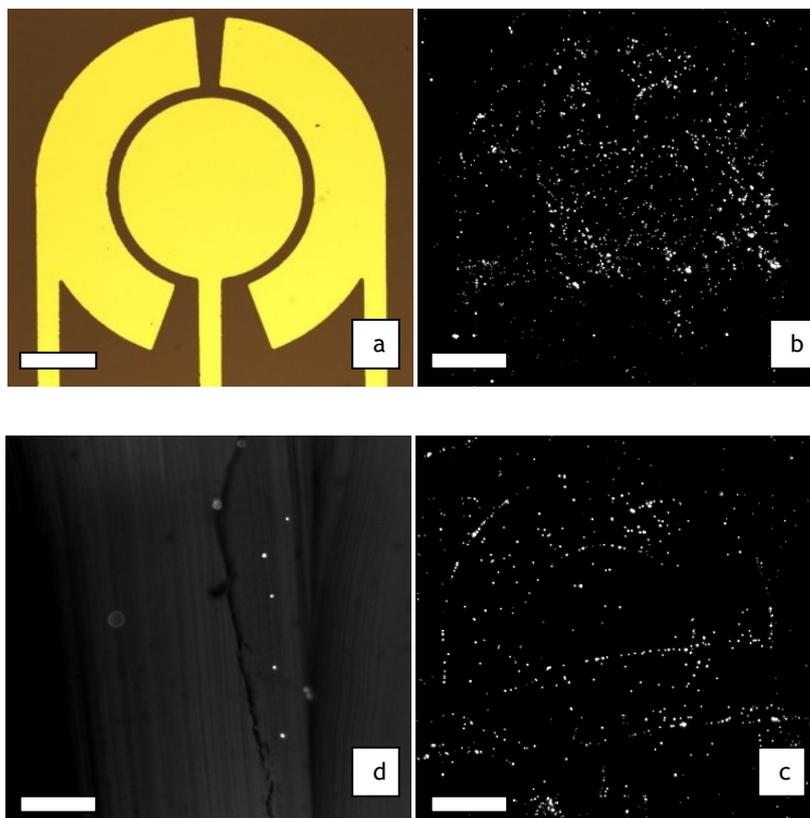
Figure 5. 10 Binding tests via laser microscopy. Microscope image (5x) of the bare gold electrode (a). Biotin modified fluorescent latex beads immobilised on the electrode surface (b). Amine modified fluorescent latex immobilised on gold electrode (c). Biotin beads were bonded via the interaction between streptavidin-biotin which was immobilised on 11-mercaptoundecanoic acid (11-MUA) modified the gold surface. A microscope image obtained from PDMS wall showing that some beads stacked on the scratches appeared due to drilling process (d). (Scale bars 0.3mm)

Images of fluorescent beads (Figure 5. 10), immobilised on electrodes, were obtained with a ZEISS microscope (Observer Z1). Results showed that streptavidin - biotin based binding, which is also defined as the strongest covalent bond [144], resulted in an improved binding ratio than amine binding. Images are also showing some non-specifically bonded latex beads on the glass surface. This can be cancelled by adding PEGylation process, as the first step, for the passivation of the glass surfaces around the gold electrodes.

5.2.4. CV tests on functionalised electrodes

The antibody immobilisation process on the electrodes was conducted by a streptavidin - biotin binding method due to the results obtained in the comparison process explained above. The sensing electrode (Figure 5. 10-a) was surrounded by a PDMS chamber. Therefore, the electrode area to be used during the immunoassay process was fixed. Moreover, handling the sample in a closed chamber gives better performances in SAW induced hydrodynamic systems because the noise and the evaporation issues are avoided (see details in "SAW induced electroanalysis" chapter). Therefore, the PDMS chamber attached design can also operate in a SAW enhanced hydrodynamic setup (However, no SAW applied in this particular test series). The depiction of the antibody immobilisation process is shown in Figure 5. 11.

Oxygen plasma (100W for 50 seconds) treated PDMS and glass surfaces were modified with a silane monolayer containing poly(ethylene glycol) (PEG) groups (Aldrich) [145]. PEG (2-[methoxy(polyethyleneoxy)propyl]trichlorosilane) is used to decrease the nonspecific binding and adsorption of proteins by glass surfaces and PDMS walls [146][147]. This process is essential especially for the batch condition tests, to obtain clean surfaces for new experiments. Toluene, which is the universal solvent for PEG-silanisation, was replaced by ethanol since the PDMS chamber was already coupled on the surface via plasma technique [67]. This revision was done to avoid the swelling effect of PDMS by toluene [148]. After the passivation of the glass surface, the samples were immersed in a mixture of COOH-terminated self-assembled monolayers (SAMs), 11-mercaptoundecanoic acid and 3-mercaptopropionic acid ((MUA/MPA) 1/10 (v/v)) in 20 mM ethanolic solution, for 6 hours. The SAM layer was further modified by immersing the samples into streptavidin solution for 2 hours (at 37 °C). The solution was comprised of streptavidin (10 μl), NHS (5 mg) and EDAC (10 mg). After sterilisation with 70 % ethanol for 15 minutes they were exposed to biotinylated antibody solution (Biotin-conjugated chicken anti-human haemoglobin, Gallus Immunotech Inc.) in PBS buffer, with the ratio of 1/10 (v/v), for one hour at room temperature. The chambers were washed with PBS by five times dilution. These chambers were then blocked by non-specific protein - protein interaction by adding blocking solution, casein in PBS (0.5% - w/v), for 45 minutes.

Bio-functionalised sensing electrodes were exposed to different antibody concentrations (0, 0.25, 1, 4 mg/ml in PBS) for 2 hours. The chambers were washed with 0.1 % tween20 (in PBS), rinsed three times with PBS and dried with N_2. Chambers were filled with 20 μl substrate system solution (TMB-H_2O_2 system, 100mM KCl, 9:1 v/v) for 1 hour. The reaction

was stopped by the adding 5 µl stop solution (1 M H_2SO_4). Voltammetric measurements were performed between -0.4 V and 0.4 V (scan rate: 0.03 V/s).
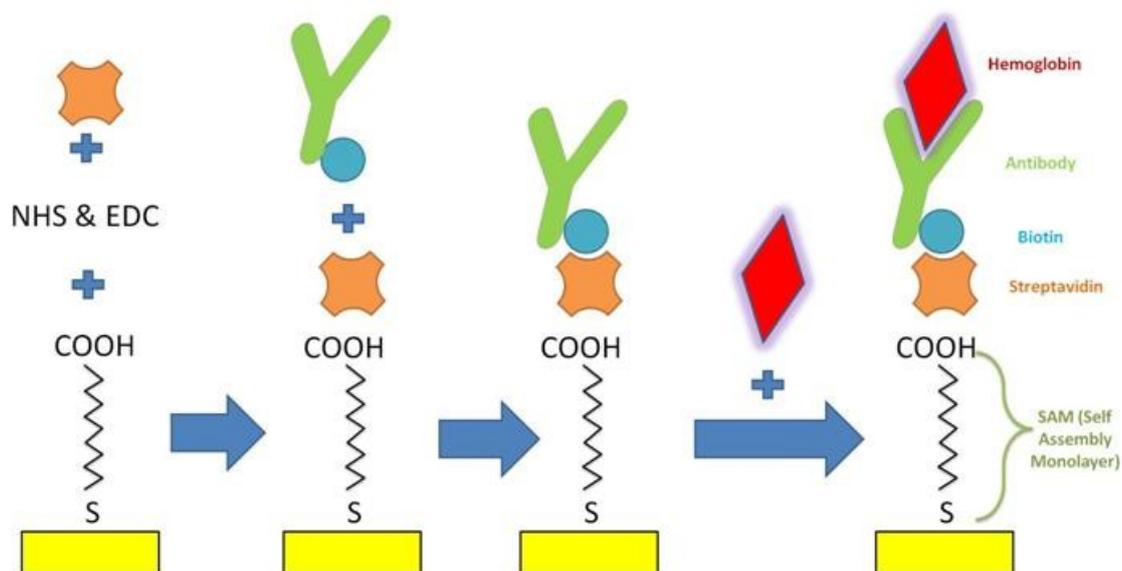
Figure 5. 11   The schematic of the anti-human Hb immobilisation on gold electrodes, and Hb entrapment. Firstly two types of the self-assembled monolayer, MUA and MPA, is formed on the gold surfaces. Biotinylated antibodies are immobilised on the streptavidin attached SAM layer. The Hb included in the sample is captured by the bio-functionalised electrode surface.

Result voltammograms (Figure 5. 12) show that the label free Hb detection technique, based on the TMB-Hb interaction, can give quantitative results. The anti-Hb layer, used for the detection of Hb, did not block the reactivity of Hb, and the technique worked. Moreover, the application of stopping solution increases the reliability of the measurements since the reactions in each chamber are terminated at the same time.
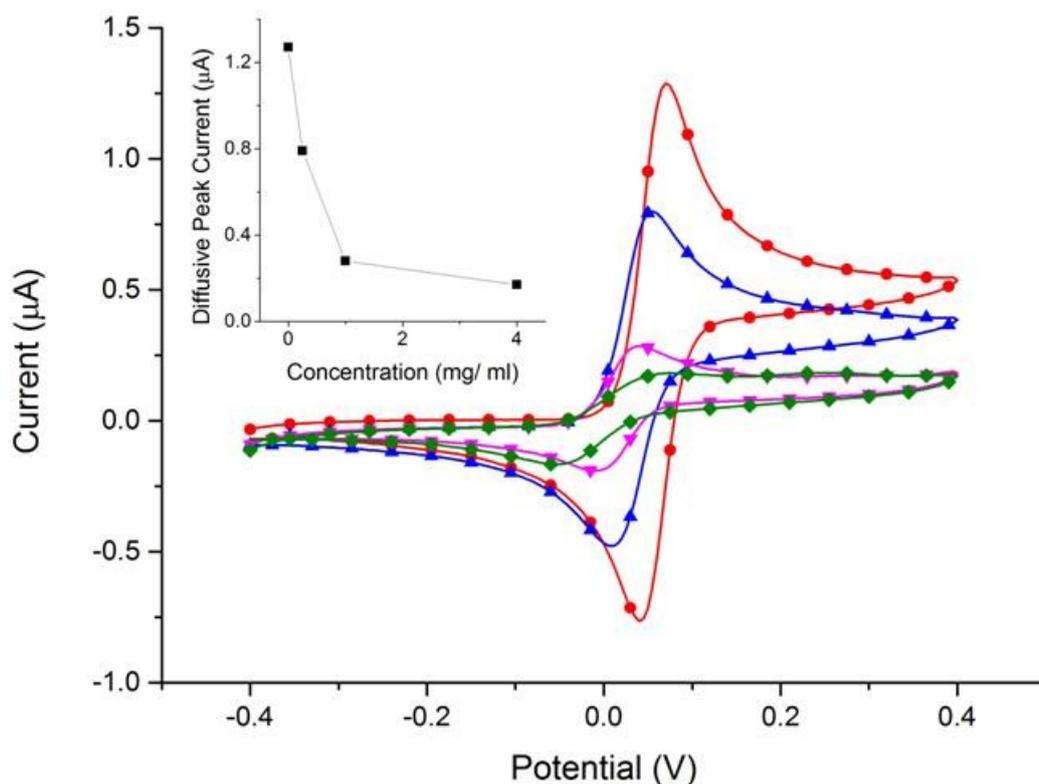
Figure 5. 12 CV results obtained at different Hb concentrations. The reaction was stopped by the adding 5 µl stop solution (1 M H_2SO_4). Applied voltage range was from -0.4V to 0.4 V vs. pseudo gold electrode (scan rate: 0.03 V/s). The inset shows the diffusive peak variation according to the Hb concentration variation.

5.2.5. Colorimetric tests on polystyrene wells

This section explains the optical results obtained after a modification made on the sensing method. This revision made the system relatively less complicated, and more reliable comparing to the previous one that was based on the functionalisation of the electrode surface. In the new method, the sensitive layer is formed on the polystyrene wells which has no other material pattern (i.e., metal) on it. No passivation process was required on the surface of wells. The final product (yellow coloured TMB) is easier to analyse optically easier than the previous method since the chamber is completely transparent, and there is no light absorbing pattern on it. Then the amperometric and/or voltammetric tests can still be performed, by removing a portion of the product solution, in a separate electroanalytical sensing chamber.
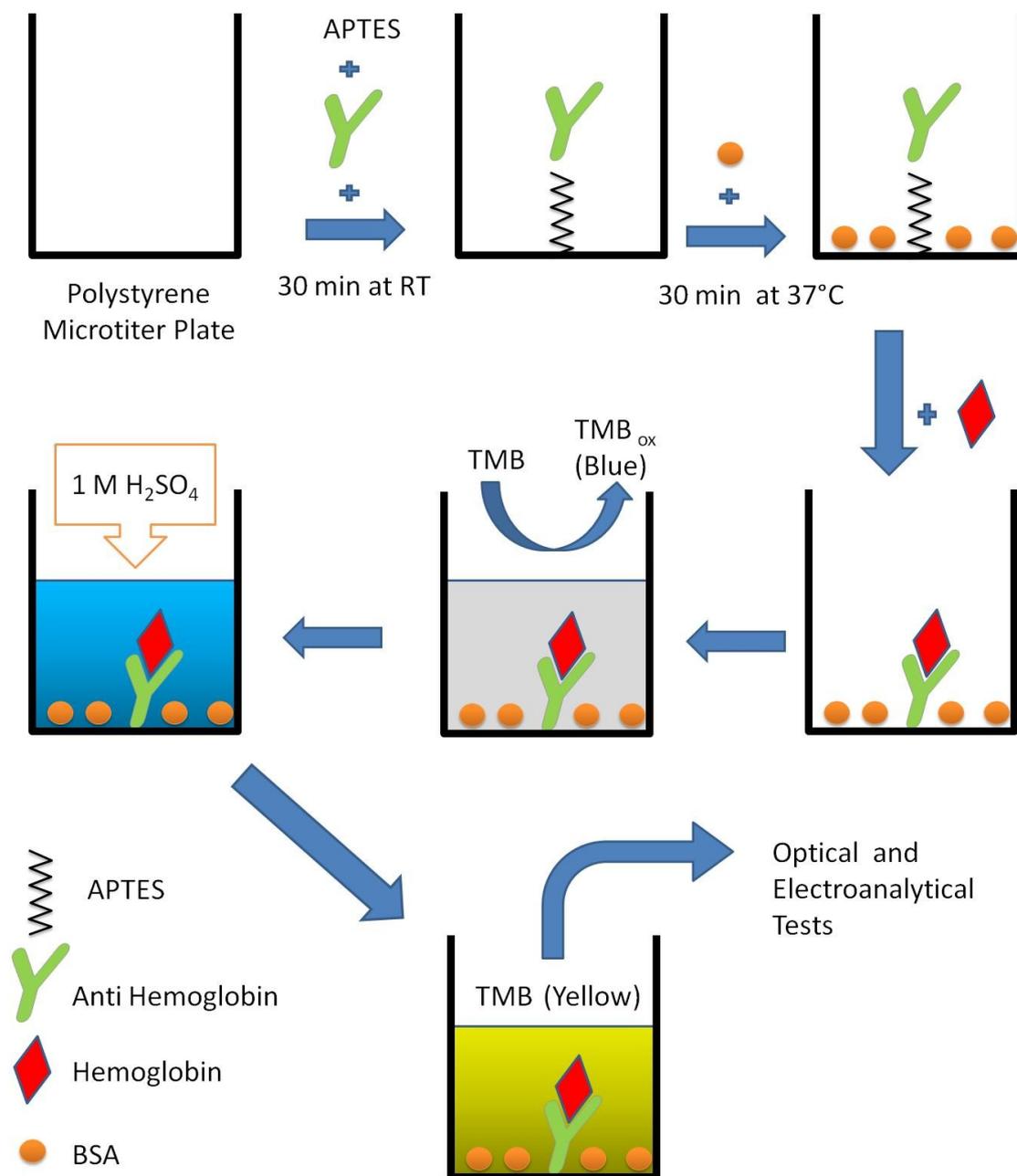
Figure 5. 13 Schematic of the antibody immobilisation on polystyrene wells, and label-free Hb measurement processes. Both optical and chemical measurements can be performed with the final product obtained from the substrate (TMB).

A rapid technique was applied for the antibody immobilisation in polystyrene microtiter plates [149]. The polystyrene wells were exposed to the mixture (1:1 - v/v) of antibody (Anti-human haemoglobin, 8μg/ml in PBS) and 3-aminopropyltriethoxysilane (APTES) solutions (10 μl/ml in water) for 30 minutes at room temperature. Unbound parts were blocked by 300 μl of 1% (w/v) BSA in PBS for 30 min at 37°C. The wells were exposed to 300 μl of Hb solutions (4, 2, 1, 0.5, 0.25, 0 mg/ml) for 1 hour and washed five times with 300 μl PBS. Then 300 μl mediator, TMB- H_2O_2 system (3,3',5,5'-Tetramethylbenzidine- Sigma-Aldrich), was applied to the wells for 20 minutes. Half the sample (150 μl) was placed in another chamber, and its reaction was stopped by 50 μl of stop solution (1 M H_2SO_4).

Figure 5. 14 presents the spectrum analysis obtained from the label free Hb detection method at different steps. Measurements were performed on Hb solution (4 mg/ml) before the washing step, substrate system (after 20 minutes incubation in the antibody immobilised chamber) before the stop solution, substrate system after the addition of stop solution and a blank well. Spectrum results show that the optical density measurements can be performed at 450 nm [149] for stopped solutions and 380 or 650 nm for substrate without stop solution. Absorption values obtained from different Hb concentrations are presented in Figure 5. 15.
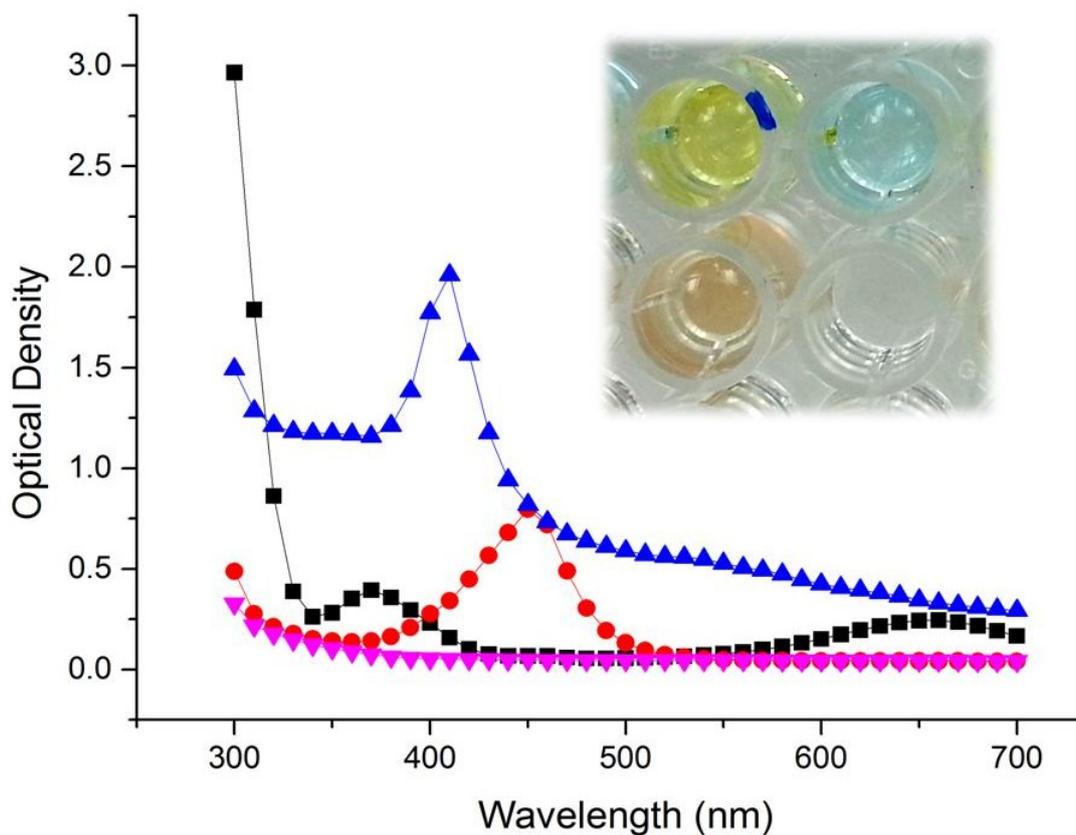
Figure 5. 14 Optical density measurements, between 300 nm and 700nm wavelength. Spectrum results obtained from the Hb solution (blue- up triangle), Hb+TMB (black- square), Hb+TMB+Stop solution (red- circle) and blank samples (pink-down triangle).
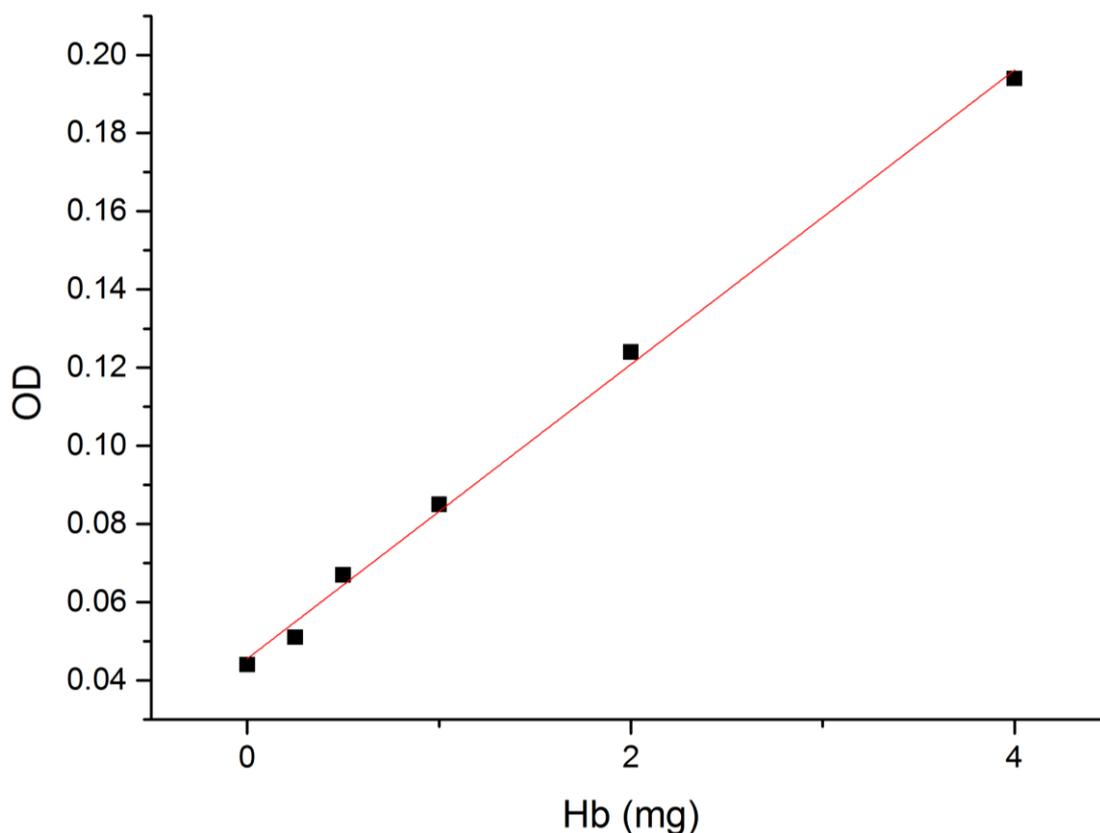
Figure 5. 15 Optical density measurements (630 nm) of substrate (TMB) samples incubated in wells exposed to different Hb concentrations (4, 2, 1, 0.5, 0.25 mg/ml).

Consequently, the results showed that the rapid immobilisation method works for antibody entrapment on polystyrene surfaces. This technique requires fewer steps in comparison to the previously performed antibody immobilisation on gold electrodes. The biosensitive area is larger than the previous method since it is not limited only to the electrode area. No surface passivation is required prior the immobilisation process. Moreover, the same electrode can be used more than once. Therefore running the assay in polystyrene chambers and conducting electroanalytical tests in a separate chamber is a faster, more sensitive and repeatable technique in comparison to previous one.

5.3.   SAW enhanced assay

Enzymes are powerful tools to obtain bio-analytical sensors due to their ability to recognise specifically their own substrate [150]. Oxidoreductase enzymes that perform oxidation-reduction reactions are commonly used in biochemical sensing applications [19]. The most widely used oxidoreductase enzyme is horseradish peroxidase (HRP), and TMB is the most popular substrate for HRP based immunosensors. The working mechanism of the HRP - TMB system is shown below.

$$HRP_{(Red)} + H_2O_2 \rightarrow HRP_{(Ox)} + H_2O$$

$$HRP_{(Ox)} + TMB_{(Red)} \rightarrow HRP_{(Red)} + TMB_{(Ox)}$$

$$TMB_{(Ox)} + e^- \rightarrow TMB_{(Red)}$$
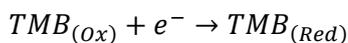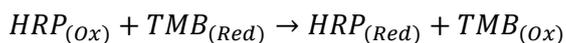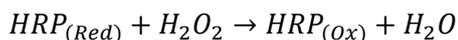
This part of the research presents the sensitivity enhancements in an electrochemical immunoassay led by the surface acoustic wave (SAW) induced streaming. Experiments were performed in batch conditions without any sensitive layer immobilisation process. SAW is a mechanical oscillation, travelling on a surface of a solid material [107] (see the details in introduction chapter). As shown in Figure 5. 16, the acoustic waves are generated in the SAW platform (Gold IDTs on LiNbO$_3$ substrate) and transmitted to the glass (0.2 mm) based disposable sensing platform, through a water-based coupling gel (KY). Radiation of the acoustic wave creates a fluid streaming inside the droplet.
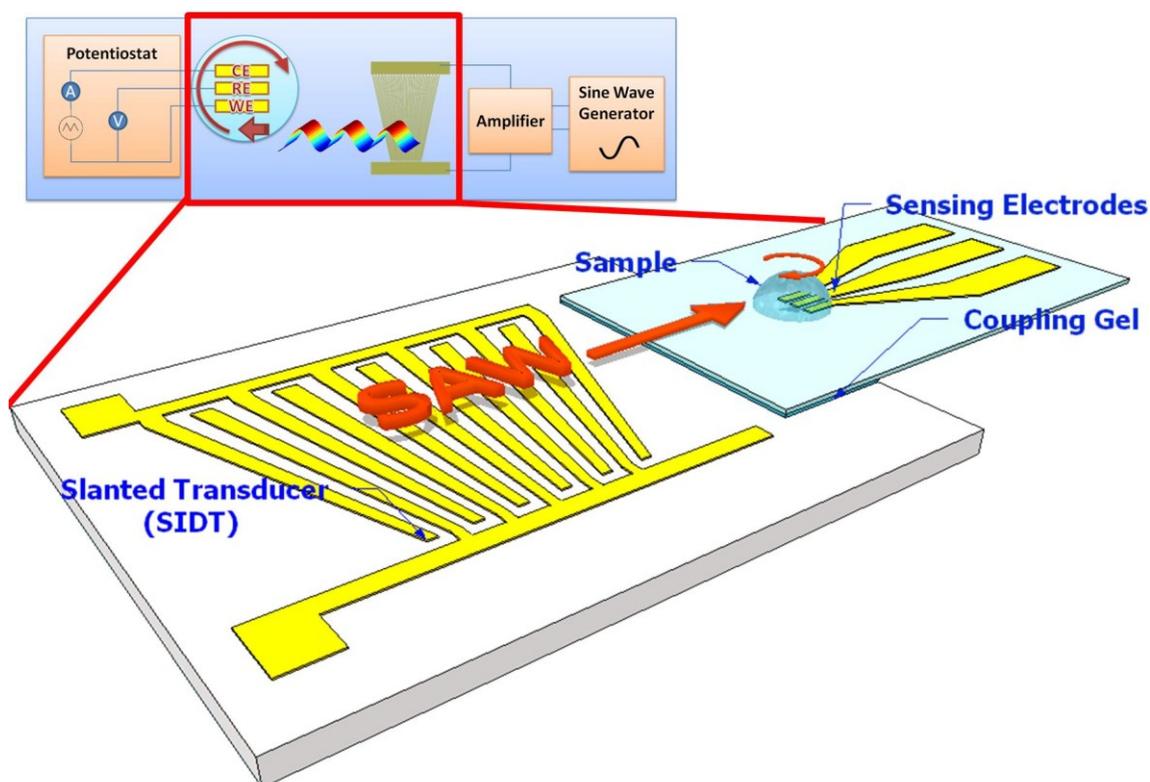
Figure 5. 16 Top: Schematic of the complete system setup which composes a potentiostat (CHI760C), a three-electrode sensing system (with a 3μl sample pipetted onto it), a slanted SAW IDT (10nm Ti, 100nm Gold), an amplifier (Mini-Circuits ZHL-5W-1, 5-500 MHz with a 3 A, 24 V DC power supply) and a function generator (Agilent Technologies MXG Signal Generator N5181A). Bottom: Schematic of the diagnostic device design. It includes an electrochemical sensing device coupled on a SAW platform on LiNbO$_3$ piezoelectric material.

The 43 finger SFIDT's working range was between 7.6 MHz and 16.6 MHz. The SAW induced streaming effect in the sample was obtained at 10.5 MHz frequency. The aperture of the

travelling acoustic beam was obtained as 1.1 mm by an ultra-high-frequency vibrometer (Polytec UHF-120).

The three-electrode sensing platform (10nm Ti, 100nm Gold) was fabricated on a 0.2 mm thick coverslip. The area of the straight electrodes used in the system was 0.19 mm^2. Droplet shape was kept as circular with PVC tape (0.1 mm thick) surrounding a circular region (1.5 mm radius) around the electrodes. SAW actuated hydrodynamic electrochemistry results were obtained with a CHI760C electrochemical analyzer.
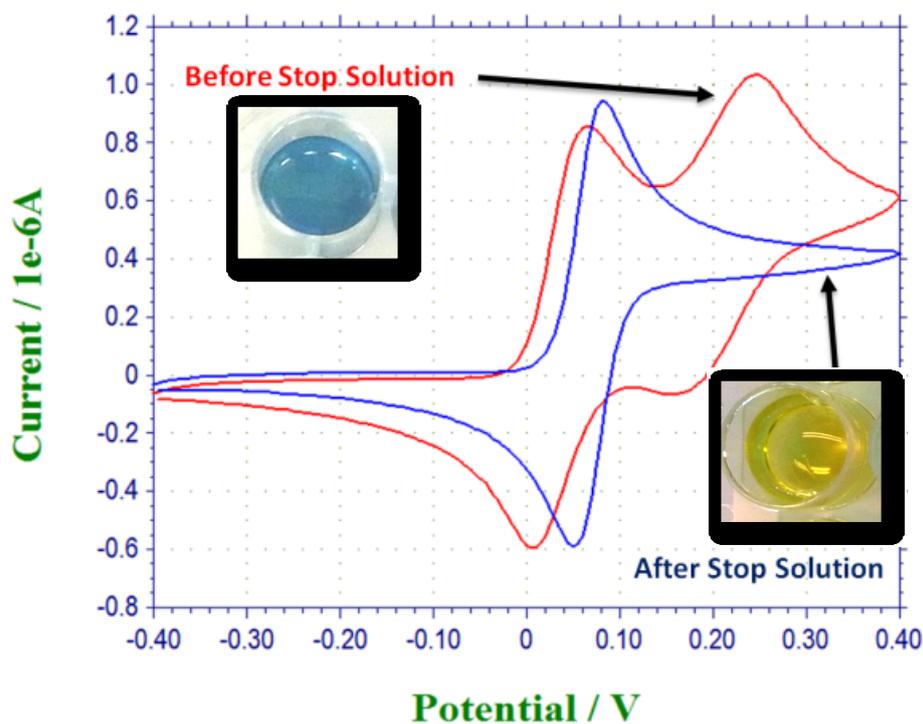
Figure 5. 17 CV results obtained from the substrate system (TMB- T8665 substrate system - Sigma). The red graph is the voltammogram of the solution (TMB Substrate including 100 mM KCl and 0.25fM HRP), and the blue graph is the voltammogram after the addition of the stop solution (1M H$_2$SO$_4$).

Electroanalytical (CV) measurements performed on 3 µl sample droplets pipetted onto the sensing electrodes (Figure 5. 16). The sample solutions included 1 µl TMB-H$_2$O$_2$ substrate system (with 100 mM KCl), 1 µl HRP solution (5 fm, 0.2 fm and 0.008 fm in PBS) and 1 µl stopping solution (1 M H$_2$SO$_4$). The enzymatic reaction, between HRP and TMB, was stopped by the addition of H$_2$SO$_4$ solution after 15 minutes incubation. Figure 5. 17 presents the two peaks (before the stopping solution) and the one peak (after the stopping solution) voltammograms. The reaction of TMB-HRP system is known as a two-step oxidation process. First oxidation of the transparent TMB is made by HRP, which creates blue colour, and the last oxidation that is carried by a stopping solution converts the TMB colour to yellow [151].
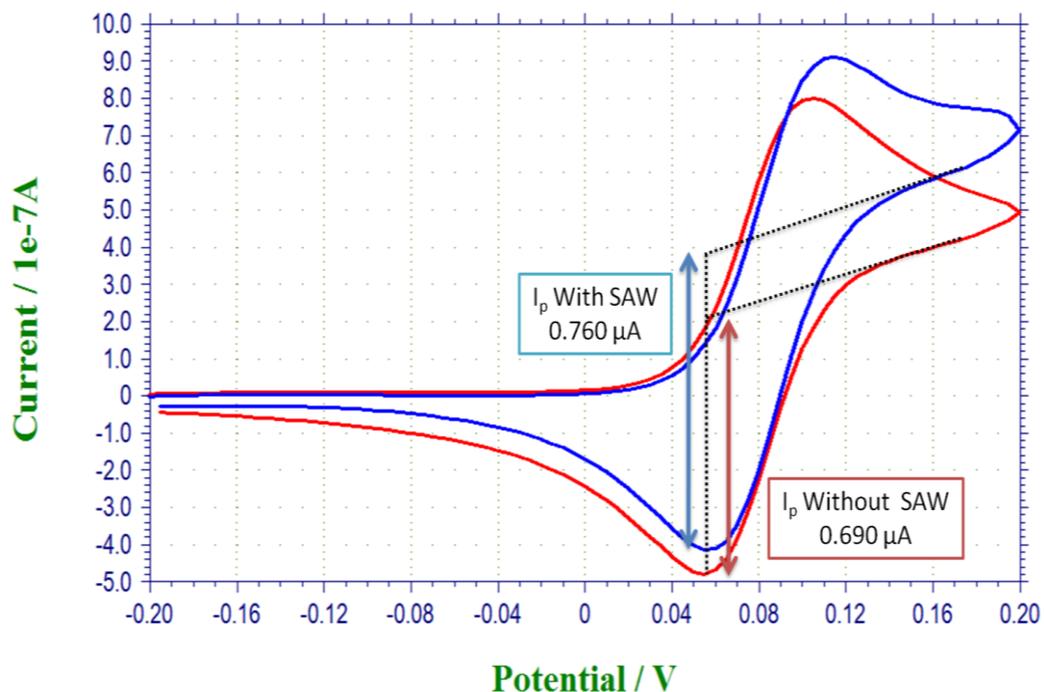
Figure 5. 18 The voltammograms obtained in the absence and the presence of SAW (10.5MHz, 1W) streaming. The sample solutions were comprised of 1 μl TMB-H$_2$O$_2$ substrate system (with 100 mM KCl), 1 μl HRP solution (0.008 fm in PBS) and 1 μl stopping solution (1 M H$_2$SO$_4$).

Figure 5. 19 shows the diffusive peak currents obtained from the voltammograms measured on various HRP concentrations in the absence and presence of SAW streaming. Results show that the acoustic streaming creates 16.8 % (+/- 0.3) average signal enhancement on both oxidation and reduction peak currents. Application of higher SAW powers can increase the diffusion limited peak currents further, by dragging more fresh material towards the electrode surface. However, increased SAW power generates more heat and leads to the evaporation of the sample. Therefore, the system requires a closed chamber in order to avoid the evaporation problem.
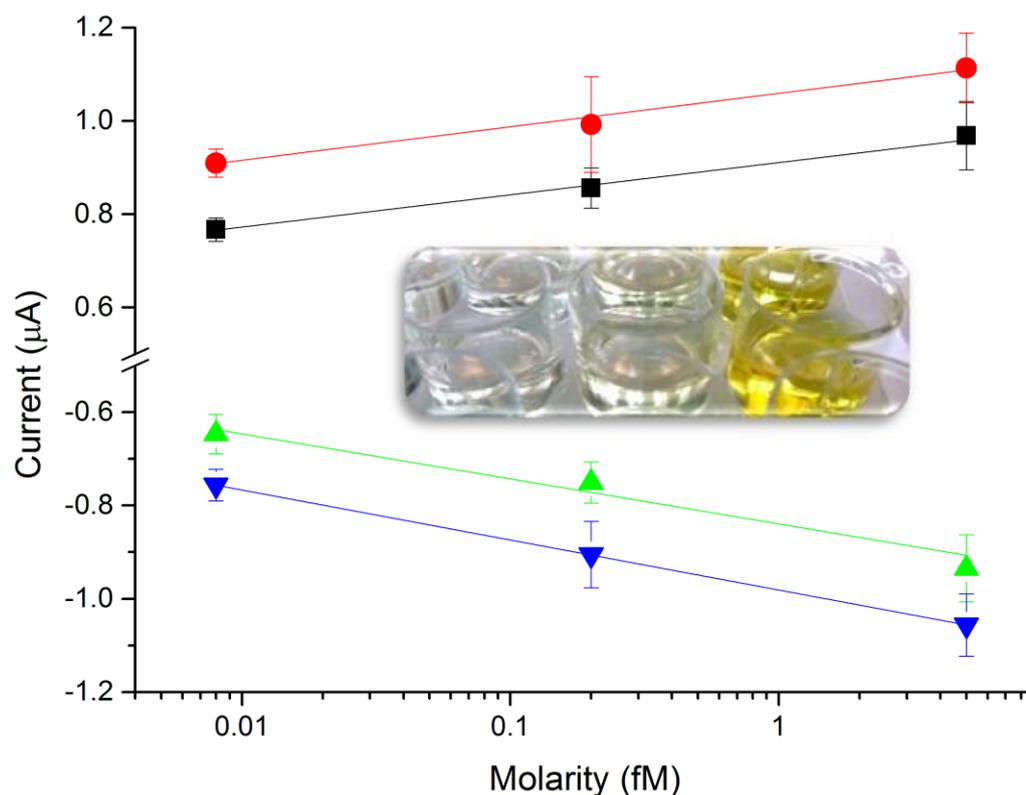
Figure 5. 19 SAW enhanced diffusive peak currents obtained from CV measurements on different reporting enzyme concentrations (5 fM, 0.2 fM and 0.008 fM HRP). Reduction (green up triangle) and oxidation (black square) peak currents are increased to higher values (blue down triangle and red circle) thanks to the SAW (10.5MHz, 1W) induced streaming in the samples.

5.4.   Instrumentation

All the electroanalytical measurements in the experimental research period were performed by a commercial electrochemical analyzer (CHI 760C). However, two extra custom made potentiostat circuits were tested separately on a potassium ferrocyanide redox model. As shown in Figure 5. 20, they were a standard scale circuit and an application-specific integrated circuit (ASIC) (designed by Dr. Sandeep Manjunath). The target was to decrease the amount of equipment and their size. Additionally the new designs would be suitable to be programmed for specific measurements, to obtain rapid analytical results from multiple measurements.
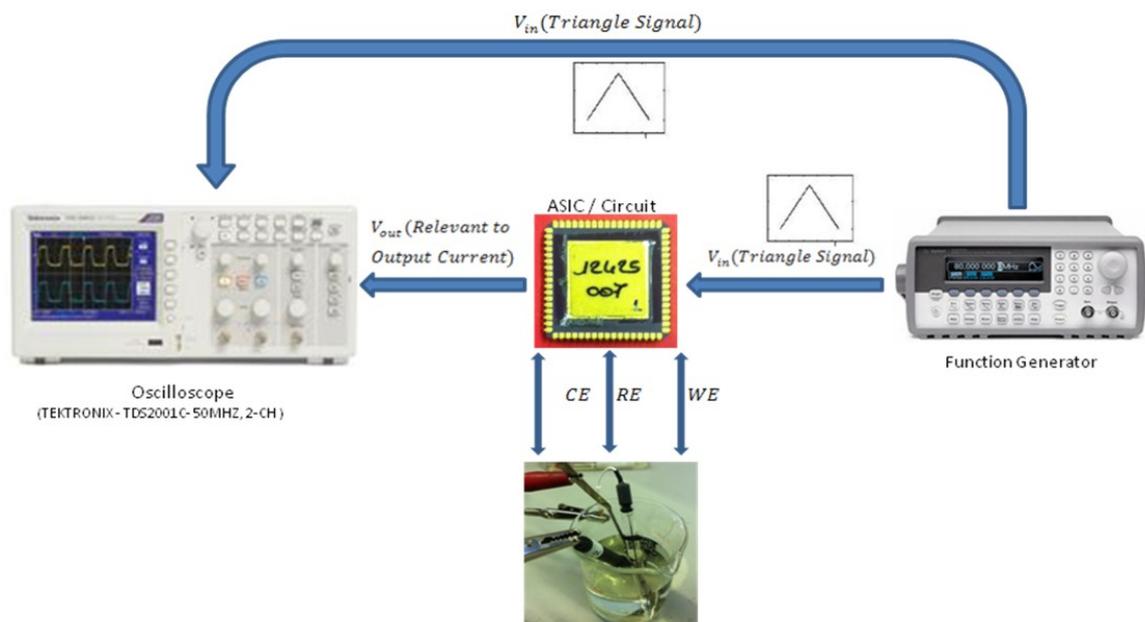
Figure 5. 20 Instrumental system setup includes a potentiostat circuit (ASIC or the average scale circuit design), a function generator, an oscilloscope and an electrochemical cell. The electrochemical cell consists of a sample chamber and a three electrode sensing system connected to the potentiostat. The function generator provides an electrical signal required for the electroanalytical test (CV or amperometry). Potentiostat follows the voltage applied to the sample and corrects it. Final results observed via an oscilloscope connected to the potentiostat and the function generator. The ASIC was previously developed at the Glasgow University, is connected on to test board.
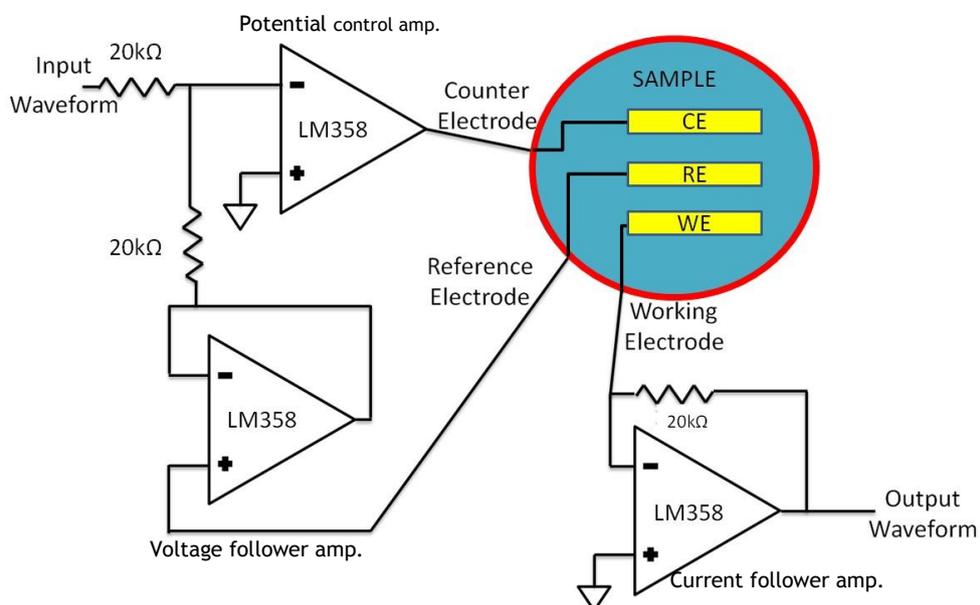
Figure 5. 21   Three operational amplifier potentiostatic circuit. This control circuitry is used to monitor the current flow through the working electrode. The circuit includes single voltage supply and op-amps (LM358). Electrode connections are made as presented in the depiction.

The custom design circuits were tested via CV technique. According to the requirements of CV, the square root of the peak currents, of a reversible redox system, changes as proportional to the square root of the sweep rate. Figure 5. 22, presents the peak currents of

the voltammograms obtained from the following three setups; a commercial device, custom made potentiostat and the potentiostat designed in ASIC format. The results show that the peak current values change as proportional to the square root of the scan rate. Therefore, both setups with custom made circuits can be used for the electroanalytical measurements.
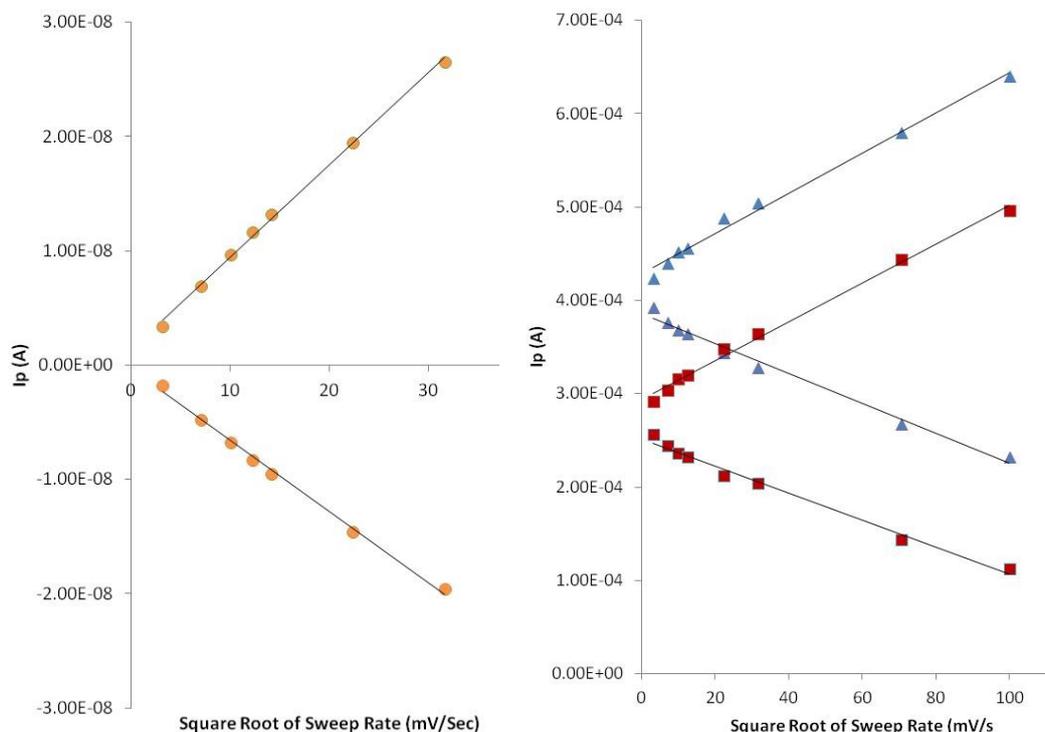
Figure 5. 22   Peak currents of voltammograms obtained via three different instrumental setups; a commercial electrochemical analyzer/ workstation (orange- circle), an average scale circuit design (blue- triangle) and an ASIC circuit design (red- square). Cyclic voltammograms were obtained from a 10mM ferrocyanide redox system at various scan rates. The solution was also included 0.1 M Potassium Chloride (KCl) as a supporting electrolyte. The size of the sensing electrodes used with the electrochemical workstation were different from the other tests.

5.4.1.   LabVIEW based system control

In the following stage, a potentiostat controller interface was designed on the LabVIEW platform. This graphic based program enables the design of user-friendly interfaces to control the hardware through a data acquisition device. After the interface had been involved in the system, the entire setup was changed to the case shown in Figure 5. 23.
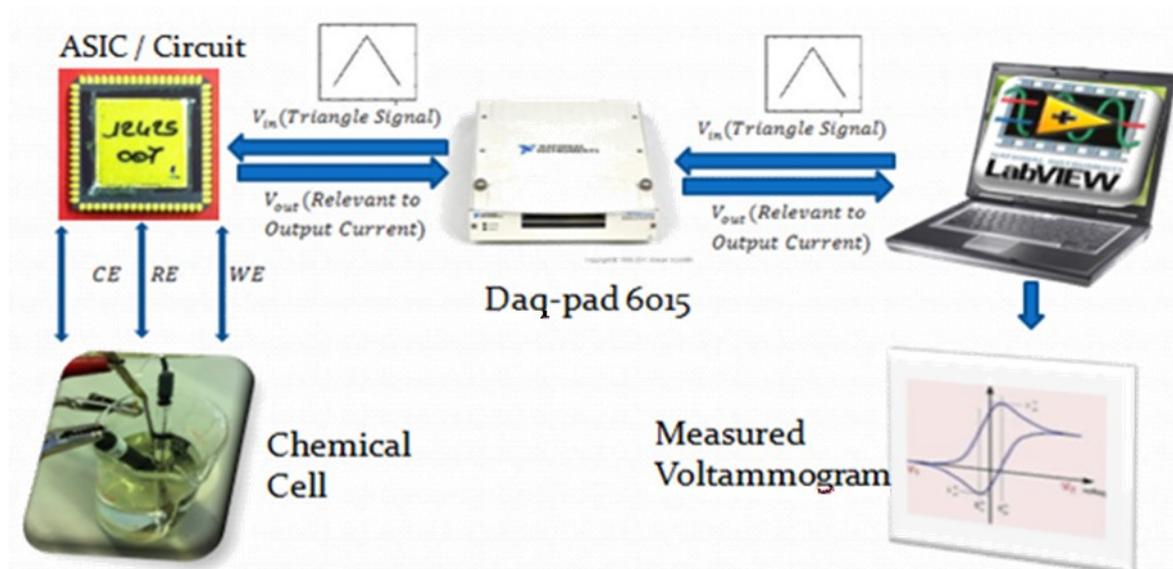
Figure 5. 23 Schematic of the LabVIEW controlled electroanalytical system setup. A function signal (triangle or a constant signal) is produced by the LabVIEW interface and a data acquisition device (NI DAQpad-6015), and sent to the sensing chamber via the potentiostat. Signal output is obtained back from the sensor (chemical cell) by the potentiostat and sent to the PC through the DAQpad. Finally, the results are observed on the LabVIEW interface screen.
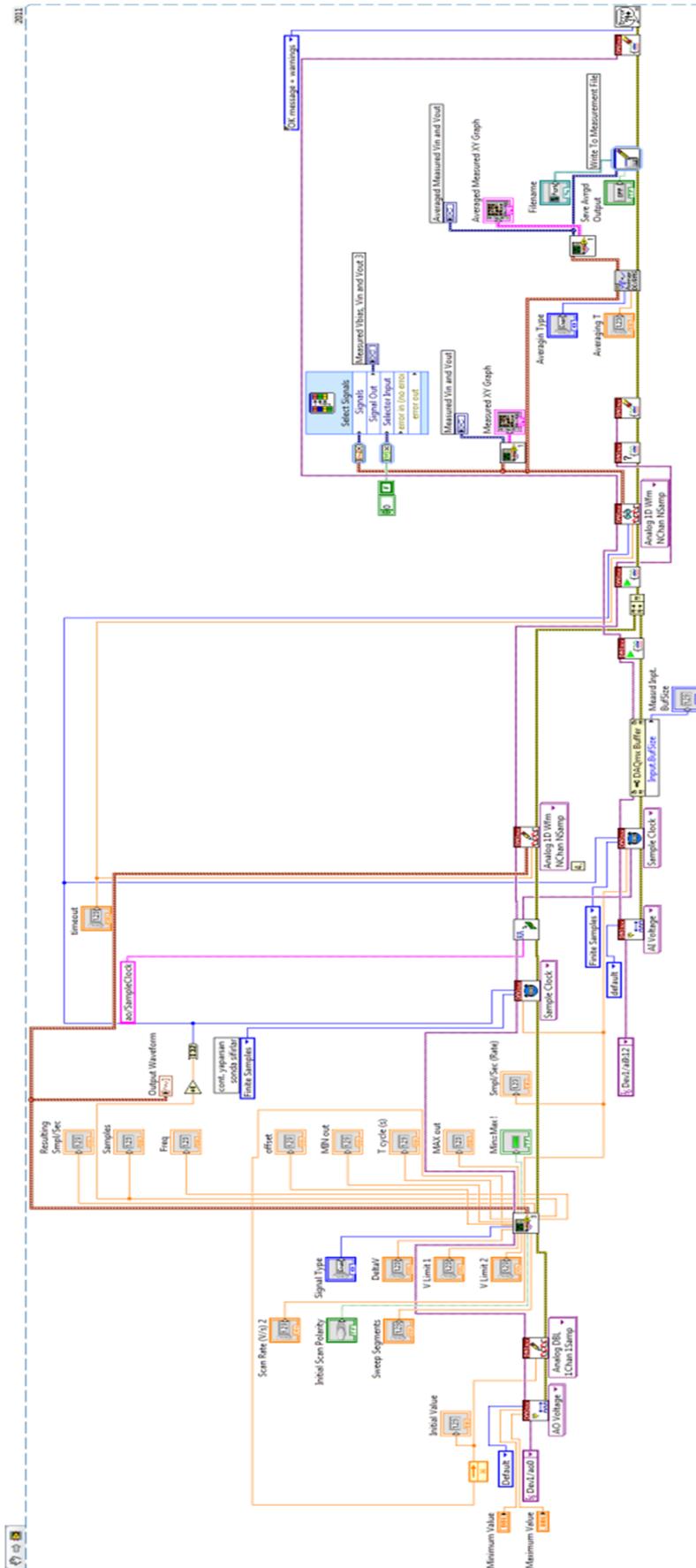
Figure 5. 24 The block diagram of the LabVIEW based program. The main parts of the design are a signal generator, analogue signal output blocks, analogue signal input blocks, signal averaging block, graphical screens and data storage parts.
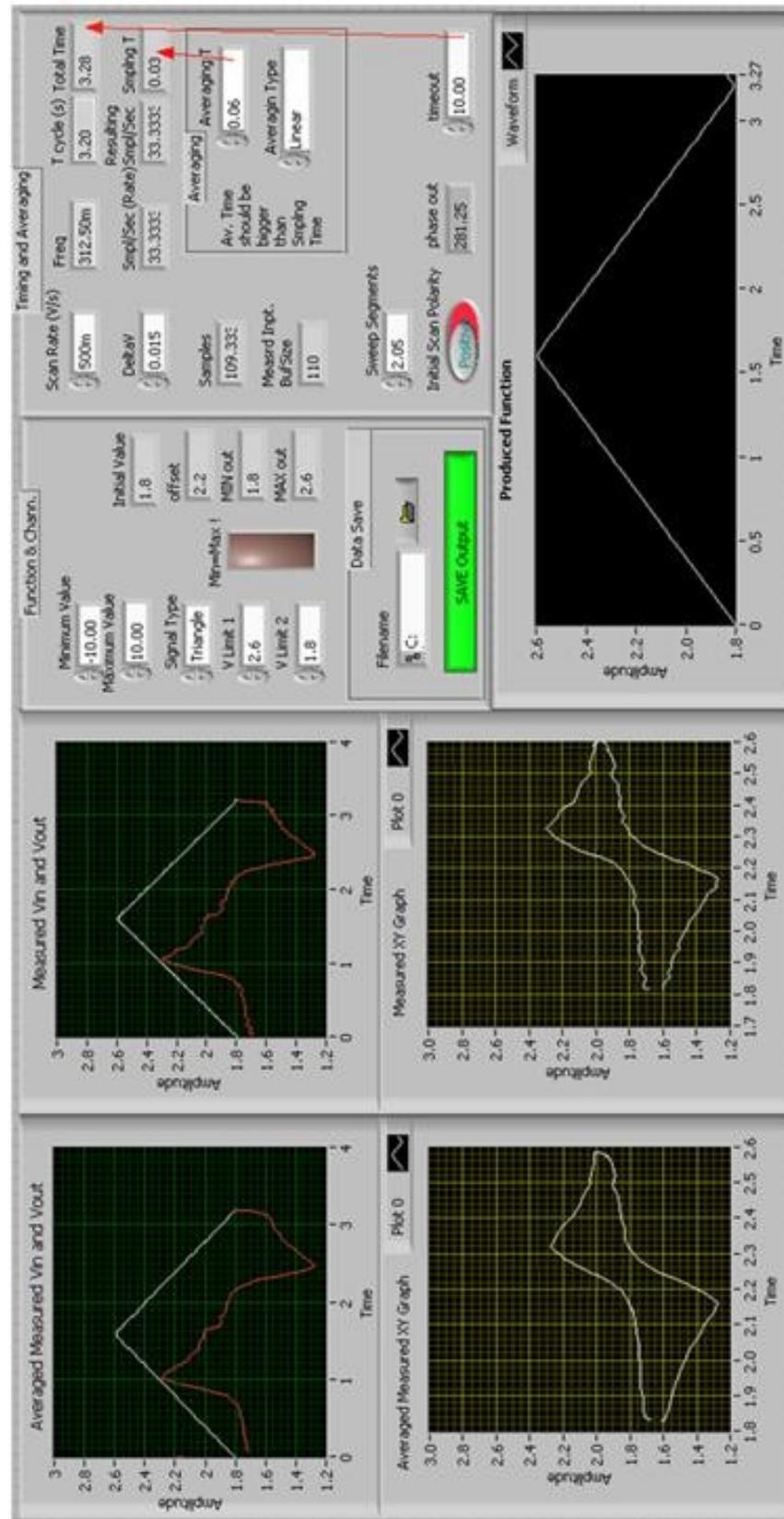
Figure 5. 25 Front panel of potentiostat controller. Changeable variables at front panel are minimum, maximum values, signal type, signal limits, scan rate, delta V which is the resolution of function, sweep segments, timeout which limits the running time of the block design, averaging time and data saving parts.

The LabVIEW based controller is capable of producing a functional signal according to the variables defined by the user, apply it to physical circuits and get the resulting signal back from the system. Those significant variables that can be adjusted from the front panel are; minimum value, maximum value, signal type, signal voltage limits (min and max), scan rate, delta V (resolution of function signal), sweep segment number, timeout (limits the running time of the block design), averaging time and data saving section. In order to prevent errors caused by wrongly entered voltage parameters, the signal generation part is capable of differentiating the randomly introduced limits as minimum and maximum. In addition, the user can view other relevant values from the front panel such as the frequency, cycle time of the signal, sample rate, measured input buffer size and proposed signal from the produced function graph. Direct and averaged versions of measured signals according to the time and XY graph, which gives the cyclic voltammograms, are presented in the front panel of the LabVIEW program. The additional graph screen, under the parameter block, shows the measured input signal and the bias voltage of the circuit.

5.5.   Conclusion

This chapter covers the experimental work conducted to develop an acoustically enhanced Hb sensing system. A novel, substrate (TMB) based label-free Hb sensing method is tested. The technique proved to be giving relevant data, according to the Hb concentration. The label-free method has fewer steps than ELISA and has only one antibody. Therefore, it is quick and the cross-reactivity of the second antibody is eliminated from the system. Moreover, the technique was further developed by changing the sensation process. Instead of the forming the sensitive layer on the electrodes it was localised on polystyrene wells by a one-step rapid process. This modification of the technique decreased the time to prepare the sensing platform because the passivation steps (i.e., pegylation), prior to structuring a sensitive layer were ignored. This avoidance also increased the reliability and repeatability of the measurements. Optical measurements performed on the samples proved that the modified method also can give quantitative results. The method also enables us to run experiments on the same system including the same electrodes. This reduces the cost of the device and most importantly improves the repeatability of the measurements.

SAW application can decrease the incubation time. Therefore, it would be possible to obtain more current flow relevant to the Hb concentration in the sample. Additionally, the sensitivity of the system is expected to be enhanced by the acoustic streaming. SAW enhanced biosensing measurements on a model bio-recognition system, based on the oxidation of TMB by HRP reporting enzymes, delivered promising signal enhancements. This

increment allows more sensitivity enhancements to be obtained due to the decreased thickness of diffusion layer on the sensing electrodes.

A software program and a custom potentiostat circuit were developed to obtain a fully controllable (via a PC) electroanalytical system. The LabVIEW based system could conduct amperometric and voltammetric measurement. The advantage of the design was its flexibility to be modified according to requirements of a particular analytical sensing platform.

6. Conclusion and future work

6.1.   General conclusion

The work conducted in this Ph.D. research is primarily based on three stages. Development of a SAW actuated micro-mixing platform and its adaptation on a three electrode sensing system. The developed system was tested through electroanalytical experiments. At the final stage, the device was used in assays, and a label-free Hb detection mechanism was tested in stagnant case. Consequently, a new microfluidic platform for enhanced sensitivity on electroanalytical methods was developed using the SAW technology. The platform provides simplicity for use and enables the samples to be analysed on low-cost LOC devices.

6.1.1.   SAW device

The SAW actuator was one of the main focus points of the thesis. Various SAW devices were designed and tested. Adaptation of a slanted SAW device presented highly controllable and efficient mixing characteristics in sample chambers. This design enabled the system to give similar characteristic with the rotating disc electrode application which is a standard technique in the hydrodynamic electrochemistry analysis.

Further investigations were conducted for the enhancement of SAW transducers efficiency. The use of wide fingers showed that the increased M/S ratio enhances the performance of the transducers without requiring any additional equipment or increasing the applied power on the system. More importantly, the enhancement was obtained without requiring any extra cost for the system setup or the fabrication process.

6.1.2.   SAW enhanced electroanalysis

The hydrodynamic effect obtained by the SAW generator platform led to increments on diffusion-limited currents measured via CV and amperometry analysis. The enhancement on the sensitivity level was reached up to 600 %. The moving part free system does not need bulky equipment to get a fluid motion on the surface of the electrode. The design is well-suited for cost-effective lab-on-a-chip applications since the electrochemical sensing unit can be fabricated on a separate disposable substrate (superstrate) and coupled on the primary substrate. However, this needs further research to obtain a coupling method which can give consistent characteristics on SAW transition.

6.1.3.   SAW enhanced Assay

A novel, a substrate (TMB) based label-free Hb sensing method is developed. The technique gave relevant data, according to the Hb concentration. The elimination of the secondary antibody from the system removed the possible cross-reactivity effects from the sensing mechanism. Moreover, the label-free technique was further developed by modifying the device preparation protocol. Therefore, the time to prepare the sensing platform was decreased. Simplification of the device also increased the reliability and repeatability of the measurements. Additionally, the modified method enabled the sensing device to be used for more than one sample tests. This reduced the cost of the device and most importantly improved the repeatability of the measurements.

SAW enhanced biosensing measurements on a model bio-recognition system, based on the oxidation of TMB by HRP reporting enzymes, delivered promising signal enhancements. This showed that the technique can be applied to a broad range of electroanalytical ASSAYs for further sensitivity achievements.

6.2.   Future plan

SAW is a technology being used for various purposes in LOC designs. Application of mechanical waves in electroanalytical sensors may be a separate research area in electrochemistry based LOC researchers and attract the attention of researchers.

6.2.1.   SAW transducer

Various SAW devices have been developed and tested for filtering applications in electronic systems. However, still different types of researches can be performed on the SAW device design for more active microfluidic manipulations. The result showed that wider electrodes are capable o generating more powerful mechanical waves without requiring any impedance matching circuit. Even the amount of gold sputtered on the piezoelectric wafer during the fabrication process does not need to change to obtain this enhancement. This method will be applied in future works such as micromixer and droplet manipulation development researches.

6.2.2.　　SAW actuated sensing device
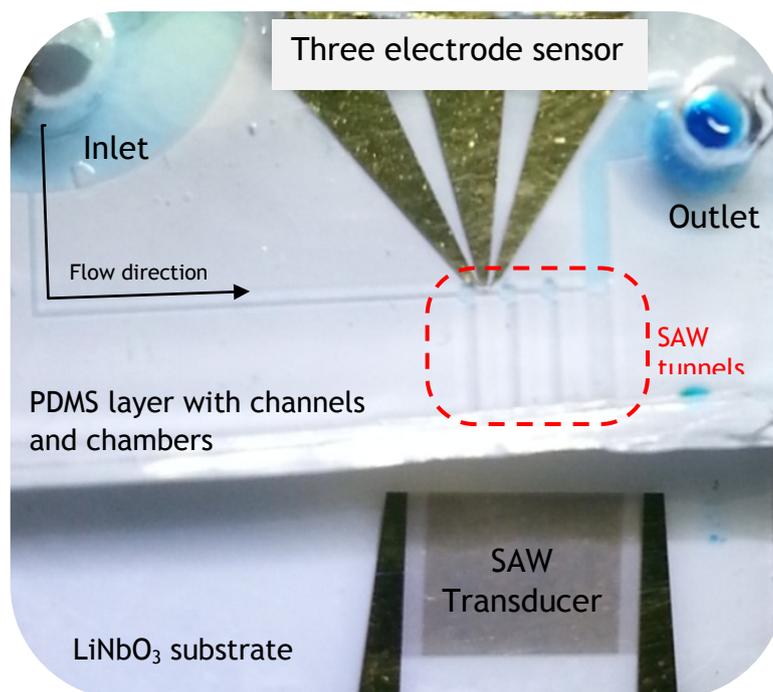
Figure 6. 1　A very first attempt to obtain a SAW enhanced electroanalytical LOC system with micro-scale sensing electrodes. The working frequency of the SAW IDT of the design was 115 MHz. The system had a three electrode sensing system on it. All metal patterns (20 nm Ti and 100 nm Au) were fabricated on a LiNbO3 substrate (128° Y-cut X-propagating c=3996ms−1). The channels and the chambers of the LOC were fabricated on a PDMS layer. The sample was flowing between the substrate and the PDMS layer.

The next generation SAW actuator design is planned to have a further improved streaming efficiency with a micro-scale sensing platform. This will create more sensitivity enhancement and decrease both the size of the device and the fabrication costs. The result of a first attempt to obtain such a device is presented in Figure 6. 1. The system was covered with a PDMS layer including micro-channels and SAW tunnels. These tunnels enable SAW to induce inside the micro-scale chambers through the PDM layer.

The micro-scale sensing chamber will be able to have a streaming effect with a tiny SAW power. However, the miniaturisation has also adverse effects on the streaming efficiency due to the increased surface tension in microscale channels and chambers. The mixing platform is proposed to be further developed in order to compensate such issues and make the device more efficient. The acoustic actuator platform will be designed as unidirectional focused IDT. Therefore, the SAW propagation will be only in a single direction. A targeted finger design will induce a concentrated dragging effect into the chamber. However, the PDMS bonding on the surface is needed to be very strong since the SAW power can be very dense and high at particular points of the device.

The SAW enhanced electroanalysis method could be used for different sensing applications in different areas such as chemistry and agriculture. Therefore, the next stage will be testing the final device concept with particular sensing experiments.

6.2.3.   Label-free Hb detection

The Hb recognition experiments performed in the research were the preliminary work. Further experimental investigations will be performed on the well plate based label-free Hb sensing method. Electroanalytical measurements (voltammetric and amperometric) will be conducted, after the optical measurements are completed, on various Hb concentration levels (down to 1 ng/ml). The acoustic mixing will be applied to the electroanalytical sensing chamber to enhance the sensitivity by increasing the mass transfer in the media. SAW and the sensing platforms will be fabricated on the same substrate in order to maximise the efficiency of acoustic streaming. Additionally, an extra sensitivity enhancement is expected on the Hb sensitivity by inducing another SAW mixing in the first chamber where the sensitive layer is formed. This will increase the binding efficiency (Hb - Anti Hb) and decrease the nonspecific binding effects on the sensitive layer. Therefore, the false positive result ratio of the sensor is also expected to decrease.

6.2.4.   Controller interface

As the next step, the software will be developed to gather different data series, comprised of voltammetric or amperometric graphs, and analyse explicitly defined parts of the result graphs. The software will be able to detect the background currents in order to obtain diffusive peak currents from voltammograms. These features will enable the system to perform rapid electroanalytical analysis on different chemical or biochemical systems.

The LabVIEW based controller block of the system will be modified to control the SAW platform. The SAW signal, usually generated by a separate signal generator, will be provided by the control unit that comprises a PC and a data acquisition device. Therefore the settings of the signal will be controlled via the LabVIEW interface, and this will synchronise the acoustic mixing platform directly with the sensing platform.

References

[1]   "World cancer toll is on the rise, says research | Society | The Guardian." [Online]. Available: http://www.guardian.co.uk/world/2011/sep/19/world-cancer-toll-research. [Accessed: 23-Jan-2015].

[2]   Cancer Research UK, "The bowel." [Online]. Available: http://www.cancerresearchuk.org/about-cancer/type/bowel-cancer/about/the-bowel#liver. [Accessed: 25-Mar-2015].

[3]   Institute National Cancer and at the N. I. of Health, "Gastrointestinal Carcinoid Tumors Treatment - National Cancer Institute." [Online]. Available: http://www.cancer.gov/cancertopics/pdq/treatment/gastrointestinalcarcinoid/Patient/page1. [Accessed: 29-Mar-2015].

[4]   "WHO | Cancer." [Online]. Available: http://www.who.int/mediacentre/factsheets/fs297/en/. [Accessed: 25-Mar-2015].

[5]   "Colorectal Cancer Facts & Figures 2011-2013." [Online]. Available: http://www.cancer.org/acs/groups/content/@epidemiologysurveilance/documents/document/acspc-028312.pdf. [Accessed: 25-Apr-2015].

[6]   D. R. Thevenot, C. Toth, R. A. Durst, and G. S. Wilson, "Electrochemical biosensors: recommended definitions and classification," *Biosens. Bioelectron.*, vol. 16, pp. 121–131, 2001.

[7]   M. P. Byfield and R. A. Abuknesha, "Biochemical aspects of biosensors," *Biosens. Bioelectron.*, vol. 9, pp. 373–400, 1994.

[8]   L. C. Clark and C. Lyons, "Electrode systems for continuous monitoring in cardiovascular surgery," *Ann. N. Y. Acad. Sci.*, vol. 102, no. 1, pp. 29–32, Dec. 1962.

[9]   J. Wang, "Electrochemical glucose biosensors.," *Chem. Rev.*, vol. 108, no. 2, pp. 814–25, Feb. 2008.

[10]   S. J. Updike and G. P. Hicks, "Enzyme electrode," *Nature*, vol. 214, pp. 986–991, 1967.

[11]   J. Wang, *Analytical Electrochemistry, Secon Edit.* 2000.

[12]   A. R. Rezk, A. Qi, J. R. Friend, W. H. Li, and L. Y. Yeo, "Uniform mixing in paper-based microfluidic systems using surface acoustic waves," *Lab Chip*, vol. 12, no. 4, p. 773, Feb. 2012.

[13]   Q. Wei, H. Qi, W. Luo, D. Tseng, S. J. Ki, Z. Wan, Z. Göröcs, L. A. Bentolila, T. Wu, R. Sun, A. Ozcan, G. Q. Wei, H. Qi, W. Luo, D. Tseng, S. J. Ki, Z. Wan, L. A. Bentolila, T. Wu, R. Sun, A. Ozcan, M. Pharmacology, L. Angeles, and U. States, "Fluorescent imaging of single nanoparticles and viruses on a smart phone.," *ACS Nano*, vol. 7, no. 10, pp. 9147–55, Oct. 2013.

[14] F. Sassa, K. Morimoto, W. Satoh, and H. Suzuki, "Electrochemical techniques for microfluidic," *Electrophoresis*, vol. 29, pp. 1787–1800, 2008.

[15] R. Paper, "Electrochemical Biosensors - Sensor Principles and Architectures," no. January, pp. 1400–1458, 2008.

[16] F. Ricci, G. Adornetto, and G. Palleschi, "Electrochimica Acta Review article A review of experimental aspects of electrochemical immunosensors," *Electrochim. Acta*, vol. 84, pp. 74–83, 2012.

[17] A. C. Fisher, *Electrode Dynamics*. New York, USA: Oxford University Press, 1996.

[18] R. Holze, *Experimental Electrochemistry*. Germany: Wiley-VCH, 2009.

[19] D. Leca-bouvier, *Enzyme for Biosensing Applications*. 2010.

[20] S. Shrikrishnan and V. Lakshminarayanan, "Electron transfer studies of redox probes in bovine milk.," *J. Colloid Interface Sci.*, vol. 370, no. 1, pp. 124–31, Mar. 2012.

[21] E. Smela, "Microfabrication of PPy microactuators and other conjugated polymer devices," *J. Micromechanics Microengineering*, vol. 9, no. 1, pp. 1–18, Mar. 1999.

[22] A. J. Bard and Faulkner, *Electrochemical methods : fundamentals and applications*, vol. 6. New York ; Chichester ET - 2nd: John Wiley, 2001.

[23] I. Svancara, K. Kalcher, A. Walcarius, and K. Vytras, *Electroanalysis with Carbon Paste Electrodes*. CRC Press, 2012.

[24] M. Ciobanu, J. P. Wilburn, M. L. Krim, and D. E. Cliffel, "Fundamentals," in *Handbook of Electrochemistry*, Elsevier, 2007, pp. 1–28.

[25] V. Levich, *Physicochemical hydrodynamics*. Englewood Cliffs N.J.: Prentice-Hall, 1962.

[26] A. Alexiadis, A. Cornell, and M. P. P. Dudukovic, "Comparison between CFD calculations of the flow in a rotating disk cell and the Cochran/Levich equations," *J. Electroanal. Chem.*, vol. 669, pp. 55–66, Mar. 2012.

[27] K. Tokuda, K. Aoki, and H. Matsuda, "Hydrodynamic voltammetry at channel electrodes: Part III. Theory of kinetic currents," *J. Electroanal. Chem. Interfacial Electrochem.*, vol. 80, no. 2, pp. 211–222, 1977.

[28] N. Moriguchi, "The effect of supersonic waves on chemical phenomena,(III). The effect on the concentration polarization," *J. Chem. Soc. Jpn*, 1934.

[29] K. S. Suslick, "Sonochemistry.," *Science*, vol. 247, no. 4949, pp. 1439–45, Mar. 1990.

[30] G.-U. Flechsig and A. Walter, "Electrically Heated Electrodes: Practical Aspects and New Developments," *Electroanalysis*, vol. 24, no. 1, pp. 23–31, Jan. 2012.

[31] J. P. Lorimer, B. Pollet, S. S. Phull, T. J. J. Mason, D. J. J. Walton, and U. Geissler, "The effect of ultrasonic frequency and intensity upon limiting currents at rotating disc and stationary electrodes," *Electrochim. Acta*, vol. 41, no. 17, pp. 2737–2741, Aug. 1996.

[32] T. a. Franke and A. Wixforth, "Microfluidics for miniaturized laboratories on a chip.," *Chemphyschem*, vol. 9, no. 15, pp. 2140–56, Oct. 2008.

[33] J. K. Luo, Y. Q. Fu, and W. I. Milne, "Acoustic Wave Based Microfluidics and Lab-on-a-Chip," in *Modeling and Measurement Methods for Acoustic Waves and for Acoustic Microdevices*, M. G. Beghi, Ed. 2013, pp. 516–556.

[34] D. Fernandez Rivas, P. Cintas, and H. J. G. E. Gardeniers, "Merging microfluidics and sonochemistry: towards greener and more efficient micro-sono-reactors.," *Chem. Commun. (Camb).*, vol. 48, no. 89, pp. 10935–47, Nov. 2012.

[35] W. Ehrfeld, V. Hessel, and H. Löwe, *Microreactors: New Technology for Modern Chemistry*. Wiley, 2000.

[36] C.-C. Chang and R.-J. Yang, "Electrokinetic mixing in microfluidic systems," *Microfluid. Nanofluidics*, vol. 3, no. 5, pp. 501–525, Jun. 2007.

[37] R. Shilton, M. K. Tan, L. Y. Yeo, J. R. Friend, L. Y. Yeo, M. K. Tan, R. Shilton, M. K. Tan, L. Y. Yeo, and J. R. Friend, "Particle concentration and mixing in microdrops driven by focused surface acoustic waves," *J. Appl. Phys.*, vol. 104, no. 1, p. 014910, 2008.

[38] "On Waves Propagated along the Plane Surface of an Elastic Solid," vol. iv, no. 42, 1886.

[39] M. F. Hribšek, D. V Tošiü, M. Tasiü, Z. Filipoviü, and Z. Živkoviü, "Design and Realization of Transversal Surface Acoustic Wave RF filters," pp. 82–85, 2010.

[40] Y. Bourquin, J. Reboud, R. Wilson, and J. M. Cooper, "Tuneable surface acoustic waves for fluid and particle manipulations on disposable chips.," *Lab Chip*, vol. 10, no. 15, pp. 1898–1901, Aug. 2010.

[41] H. Fatemi, M. J. Modarres-zadeh, R. Abdolvand, and C. Florida, "Passive wireless temperature sensing with piezoelectric mems resonators," in *MEMS 2015*, 2015, pp. 909–912.

[42] C. Ruppel and T. Fjeldly, *Advances in surface acoustic wave technology, systems and applications*. World Scientific, 2001.

[43] R. W. Brocato, T. A. Brocato, J. R. Wendt, C. A. Sanchez, L. G. Stotts, S. N. Laboratories, and P. O. B. Albuquerque, "Optimized SAW Chemical Sensor with Microfluidic Packaging," pp. 936–941.

[44] K. Chang, Y. Pi, W. Lu, F. Wang, F. Pan, F. Li, S. Jia, J. Shi, S. Deng, and M. Chen, "Label-free and high-sensitive detection of human breast cancer cells by aptamer-based leaky surface acoustic wave biosensor array.," *Biosens. Bioelectron.*, vol. 60, pp. 318–24, Oct. 2014.

[45] J. Reboud, Y. Bourquin, R. Wilson, G. S. G. S. Pall, M. Jiwaji, a. R. A. R. Pitt, A. Graham, A. P. a. P. Waters, and J. M. J. M. Cooper, "Shaping acoustic fields as a toolset for microfluidic manipulations in diagnostic technologies," *PNAS,* vol. 109, no. 38, pp. 15162–1567, Sep. 2012.

[46] T. Dung Luong and N. Trung Nguyen, "Surface Acoustic Wave Driven Microfluidics – A Review," *Micro Nanosyst.*, vol. 2, no. 3, pp. 217–225, Sep. 2010.

[47] L. Schmid, A. Wixforth, D. a. Weitz, and T. Franke, "Novel surface acoustic wave (SAW)-driven closed PDMS flow chamber," *Microfluid. Nanofluidics*, vol. 12, no. 1–4, pp. 229–235, Aug. 2011.

[48] R. Wilson, J. Reboud, Y. Bourquin, S. L. Neale, Y. Zhang, and J. M. Cooper, "Phononic crystal structures for acoustically driven microfluidic manipulations.," *Lab Chip*, vol. 11, no. 2, pp. 323–8, Jan. 2011.

[49] R. V. R. Raghavan, J. J. R. Friend, L. Y. L. Yeo, R. V. R. Raghavan, J. J. R. Friend, and L. Y. L. Yeo, "Particle concentration via acoustically driven microcentrifugation: microPIV flow visualization and numerical modelling studies," *Microfluid. Nanofluidics*, vol. 8, no. 1, pp. 73–84, May 2009.

[50] A. Qi, L. Yeo, J. Friend, and J. Ho, "The extraction of liquid, protein molecules and yeast cells from paper through surface acoustic wave atomization.," *Lab Chip*, vol. 10, no. 4, pp. 470–6, Feb. 2010.

[51] D. Vatansever, E. Siores, and T. Shah, "Alternative Resources for Renewable Energy : Piezoelectric and Photovoltaic Smart Structures," 2012.

[52] P. Mason and G. Ses-, "Piezoelectricity , its history and applications," vol. 70, no. 6, pp. 1561–1566, 2015.

[53] A. Safari and E. K. Akdoğan, *Piezoelectric and Acoustic Materials for Transducer Applications*. Boston, MA: Springer US, 2008.

[54] R. M. White and F. W. Voltmer, "Direct Piezoelectric Coupling To Surface Elastic Waves," *Appl. Phys. Lett.*, vol. 7, no. 12, p. 314, Dec. 1965.

[55] T. Frommelt, M. Kostur, M. Wenzel-Schäfer, P. Talkner, P. Hänggi, A. Wixforth, P. Ha, and A. Wixforth, "Microfluidic Mixing via Acoustically Driven Chaotic Advection," *Phys. Rev. Lett.*, vol. 100, no. 3, p. 034502, Jan. 2008.

[56] A. Arnau, *Piezoelectric transducers and applications (Google eBook)*. 2008.

[57] S. Datta, *Surface acoustic wave devices*. Prentice-Hall, 1986.

[58] "Shaping surface waves for diagnostics Yannyk Parulian Julian Bourquin," 2012.

[59] X. Ding, P. Li, S.-C. S. Lin, Z. S. Stratton, N. Nama, F. Guo, D. Slotcavage, X. Mao, J. Shi, F. Costanzo, and T. J. Huang, "Surface acoustic wave microfluidics.," *Lab Chip*, vol. 13, no. 18, pp. 3626–49, Sep. 2013.

[60] J. Reboud, R. Wilson, Y. Zhang, M. H. Ismail, Y. Bourquin, and J. M. J. M. Cooper, "Nebulisation on a disposable array structured with phononic lattices," *Lab Chip*, vol. 12, no. 7, pp. 1268–1273, Apr. 2012.

[61] T. Kundu, "A new technique for measuring Rayleigh and Lamb wave speeds," *J. Acoust. Soc. Am.*, vol. 93, p. 95 103, 1993.

[62] R. M. Arzt and K. Dransfeld, "Excitation of rayleigh waves at high frequencies and at low temperatures," *Appl. Phys. Lett.*, vol. 7, no. 6, p. 156, Nov. 1965.

[63] W. R. Jones, "Propagation of Surface Waves at the Boundary Between a Piezoelectric Crystal and a Fluid Medium," *Sonics Ultrason. IEEE Trans.*, vol. 17, no. 2, pp. 71–76, Apr. 1970.

[64] M. Alghane, B. X. Chen, Y. Q. Fu, Y. Li, J. K. Luo, and a J. Walton, "Experimental and numerical investigation of acoustic streaming excited by using a surface acoustic wave device on a 128° YX-LiNbO 3 substrate," *J. Micromechanics Microengineering*, vol. 21, no. 1, p. 015005, Jan. 2011.

[65] L. Y. Yeo and J. R. Friend, "Surface Acoustic Wave Microfluidics," *Annu. Rev. Fluid Mech.*, vol. 46, pp. 379–406, 2014.

[66] E. Sayar, "Acoustically and electrokinetically driven transport in microfluidic devices," Drexel University, 2012.

[67] Q. Zeng, F. Guo, L. Yao, H. W. W. Zhu, L. Zheng, Z. X. X. Guo, W. Liu, Y. Chen, S. S. S. Guo, and X. Z. Z. Zhao, "Milliseconds mixing in microfluidic channel using focused surface acoustic wave," *Sensors Actuators B Chem.*, vol. 160, no. 1, pp. 1552–1556, Dec. 2011.

[68] J. Deval and P. Tabeling, "A dielectrophoretic chaotic mixer," in *Technical Digest. MEMS 2002 IEEE International Conference. Fifteenth IEEE International Conference on Micro Electro Mechanical Systems (Cat. No.02CH37266)*, pp. 36–39.

[69] D. W. Branch, G. D. Meyer, C. J. Bourdon, and H. G. Craighead, "Active Mixing in Microchannels using Surface Acoustic Wave Streaming on Lithium Niobate," 2005.

[70] A. Renaudin, V. Chabot, E. Grondin, V. Aimez, and P. G. Charette, "Integrated active mixing and biosensing using surface acoustic waves (SAW) and surface plasmon resonance (SPR) on a common substrate," pp. 111–115, 2010.

[71] S. Collignon, J. R. Friend, and L. Yeo, "Planar Microfluidic Drop Splitting and Merging," *Lab Chip*, vol. 15, pp. 1942–1951, 2015.

[72] A. Renaudin, J.-P. Sozanski, B. Verbeke, V. Zhang, P. Tabourier, and C. Druon, "Monitoring SAW-actuated microdroplets in view of biological applications," *Sensors Actuators B Chem.*, vol. 138, no. 1, pp. 374–382, Apr. 2009.

[73] G. Yu, X. Chen, and J. Xu, "Acoustophoresis in variously shaped liquid droplets," *Soft Matter*, vol. 7, no. 21, p. 10063, Oct. 2011.

[74] a. Renaudin, P. Tabourier, V. Zhang, J. C. C. Camart, and C. Druon, "SAW nanopump for handling droplets in view of biological applications," *Sensors Actuators B Chem.*, vol. 113, no. 1, pp. 389–397, Jan. 2006.

[75] S. A. Makohliso, H. J. Mathieu, M. Ilegems, L. Giovangrandi, D. Le, and P. Aebischer, "Application of Teflon-AF ® thin films for bio-patterning of neural," vol. 13, pp. 1227–1235, 1998.

[76] I. Czolkos, B. Hakonen, O. Orwar, and A. Jesorka, "High-resolution micropatterned Teflon AF substrates for biocompatible nanofluidic devices.," *Langmuir*, vol. 28, no. 6, pp. 3200–5, Feb. 2012.

[77] I. a Eydelnant, U. Uddayasankar, B. Li, M. W. Liao, and A. R. Wheeler, "Virtual microwells for digital microfluidic reagent dispensing and cell culture.," *Lab Chip*, vol. 12, no. 4, pp. 750–7, Feb. 2012.

[78] R. J. Shilton, N. R. Glass, P. Chan, L. Y. Yeo, and J. R. Friend, "Rotational microfluidic motor for on-chip microcentrifugation," *Appl. Phys. Lett.*, vol. 98, no. 25, p. 254103, 2011.

[79] DuPont, *Amorphous Fluoropolymer*, vol. 1. 2010, pp. 1–4.

[80] G. Destgeer, B. H. Ha, J. H. Jung, and H. J. Sung, "Submicron separation of microspheres via travelling surface acoustic waves," *Lab Chip*, Sep. 2014.

[81] D. Beyssen, T. R. I. Perry, F. Sarry, U. De Lorraine, and I. J. Lamour, "Correlation of rayleigh-saw streaming and thermal effect for prediction of heat transfer mechanism (s) within microdroplet," *17th Int. Conf. Miniaturized Syst. Chem. Life Sci. Freiburg, Ger.*, no. October, pp. 2–4, 2013.

[82] Y. Kazoe, K. Yamamoto, K. Mawatari, and T. Kitamori, "Functionalized particle image velocimetry for simultaneous measurements in micro / nanochannel flows," in *17th International Conference on Miniaturized Systems for Chemistry and Life Sciences*, 2013, no. October, pp. 1547–1549.

[83] W. P. Mason, *Physical Acoustics V15: Principles and Methods ebook*. Academic Press, 2012.

[84] E. Kaplan, J. Reboud, A. Glidle, and J. M. Cooper, "Ultra Sensitive Hydrodynamic Electrochemicstry Using Sound Wave Driven Microstreaming," in *17th International Conference on Miniaturized Systems for Chemistry and Life Sciences, Freiburg, Germany*, 2013, no. October, pp. 251–253.

[85] D. J. Collins, T. Alan, K. Helmerson, and A. Neild, "Surface acoustic waves for on-demand production of picoliter droplets and particle encapsulation.," *Lab Chip*, vol. 13, no. 16, pp. 3225–31, Aug. 2013.

[86] Y. Bourquin and J. M. Cooper, "Swimming using surface acoustic waves.," *PLoS One*, vol. 8, no. 2, p. e42686, Jan. 2013.

[87] X. Ding, J. Shi, S.-C. S. Lin, S. Yazdi, B. Kiraly, and T. J. Huang, "Tunable patterning of microparticles and cells using standing surface acoustic waves.," *Lab Chip*, vol. 12, no. 14, pp. 2491–7, Jul. 2012.

[88] D. J. Collins, T. Alan, K. Helmerson, and A. Neild, "On-demand picoliter-scale droplet generation using surface acoustic waves," in *17th International Conference on Miniaturized*, 2013, no. October, pp. 1604–1606.

[89] M. K. Tan, J. R. Friend, and L. Y. Yeo, "Interfacial Jetting Phenomena Induced by Focused Surface Vibrations," *J. Aerosol Sci.*, vol. 024501, no. 7, pp. 1–4, 2009.

[90] G. Destgeer, K. H. Lee, J. H. Jung, A. Alazzam, and H. J. Sung, "Continuous separation of particles in a PDMS microfluidic channel via travelling surface acoustic waves (TSAW).," *Lab Chip*, vol. 13, no. 21, pp. 4210–6, Nov. 2013.

[91] C. K. Campbell, "Obtaining the fundamental and harmonic radiation conductances of a reflective SAW interdigital transducer," in *1998 IEEE Ultrasonics Symposium. Proceedings (Cat. No. 98CH36102)*, 1998, vol. 1, pp. 169–174.

[92] Z. Guttenberg, a. Rathgeber, S. Keller, J. Rädler, a. Wixforth, M. Kostur, M. Schindler, and P. Talkner, "Flow profiling of a surface-acoustic-wave nanopump," *Phys. Rev. E*, vol. 70, no. 5, p. 056311, Nov. 2004.

[93] S. Ruttinger, V. Buschmann, and B. Kramer, "Comparison and accuracy of methods to determine the confocal volume for quantitative fluorescence correlation spectroscopy," *Society*, vol. 232, no. May, pp. 343–352, Oct. 2008.

[94] J. Friend and L. Yeo, "Microscale acoustofluidics: Microfluidics driven via acoustics and ultrasonics," *Rev. Mod. Phys.*, vol. 83, no. 2, pp. 647–704, Jun. 2011.

[95] M. Alghane, Y. Q. Fu, B. X. Chen, Y. Li, M. P. Y. Desmulliez, and a. J. Walton, "Scaling effects on flow hydrodynamics of confined microdroplets induced by Rayleigh surface acoustic wave," *Microfluid. Nanofluidics*, vol. 13, no. 6, pp. 919–927, Jul. 2012.

[96] P. Brunet, M. Baudoin, O. B. Matar, and F. Zoueshtiagh, "Droplets displacement and oscillations induced by ultrasonic surface acoustic waves: a quantitative study," *Phys. Rev. E*, vol. 81, no. 3, p. 9, Mar. 2010.

[97] K. Miyamoto, S. Nagatomo, Y. Matsui, and S. Shiokawa, "Nonlinear Vibration of Liquid Droplet by Surface Acoustic Wave Excitation," *Jpn. J. Appl. Phys.*, vol. 41, no. Part 1, No. 5B, pp. 3465–3468, May 2002.

[98] Y. Cui, Q. Wei, H. Park, and C. M. Lieber, "Nanowire nanosensors for highly sensitive and selective detection of biological and chemical species.," *Science*, vol. 293, no. 5533, pp. 1289–92, Aug. 2001.

[99] I. Bakas, Z. Salmi, M. Jouini, F. Geneste, I. Mazerie, D. Floner, B. Carbonnier, Y. Yagci, and M. M. Chehimi, "Picomolar Detection of Melamine Using Molecularly Imprinted Polymer-Based Electrochemical Sensors Prepared by UV-Graft Photopolymerization," *Electroanalysis*, vol. 27, pp. 429–439, 2015.

[100] P. Jothimuthu, R. a. Wilson, J. Herren, E. N. Haynes, W. R. Heineman, and I. Papautsky, "Lab-on-a-chip sensor for detection of highly electronegative heavy metals by anodic stripping voltammetry," *Biomed. Microdevices*, vol. 13, pp. 695–703, 2011.

[101] S. M. Usman Ali, O. Nur, M. Willander, and B. Danielsson, "A fast and sensitive potentiometric glucose microsensor based on glucose oxidase coated ZnO nanowires grown on a thin silver wire," *Sensors Actuators, B Chem.*, vol. 145, no. 2, pp. 869–874, 2010.

[102] B. Levich, "The theory of concentration polarisation," *Discuss. Faraday Soc.*, vol. 1, p. 37, 1947.

[103] K. J and B. Levich, "The use of a rotating disc electrode for studying kinetic and catalytic processes in electrochemistry," *Donkland*, vol. 117, no. 3, pp. 441–444, 1957.

[104] J. Heyrovský, "[Reproduction of: J. Heyrovský, Chemické Listy 1922, 16, 256-264].," *Chem. Rec.*, vol. 12, no. 1, pp. 17–25, Feb. 2012.

[105] C. E. Banks, A. O. Simm, R. Bowler, K. Dawes, and R. G. Compton, "Hydrodynamic electrochemistry: design for a high-speed rotating disk electrode.," *Anal. Chem.*, vol. 77, no. 6, pp. 1928–30, Mar. 2005.

[106] J. K. Luo, Y. Q. Fu, Y. Li, X. Y. Du, a J. Flewitt, a J. Walton, and W. I. Milne, "Moving-part-free microfluidic systems for lab-on-a-chip," *J. Micromechanics Microengineering*, vol. 19, no. 5, p. 054001, May 2009.

[107] Y. Bourquin, J. Reboud, R. Wilson, Y. Zhang, and J. M. Cooper, "Integrated immunoassay using tuneable surface acoustic waves and lensfree detection," *Lab Chip*, vol. 11, no. 16, pp. 2725–2730, 2011.

[108] R. J. Shilton, L. Y. Yeo, and J. R. Friend, "Quantification of surface acoustic wave induced chaotic mixing-flows in microfluidic wells," *Sensors Actuators B Chem.*, vol. 160, no. 1, pp. 1565–1572, Dec. 2011.

[109] M. C. Jo and R. Guldiken, "Effects of polydimethylsiloxane (PDMS) microchannels on surface acoustic wave-based microfluidic devices," *Microelectron. Eng.*, vol. 113, pp. 98–104, Jan. 2014.

[110] A. Renaudin, V. Chabot, E. Grondin, V. Aimez, and P. G. Charette, "Integrated active mixing and biosensing using surface acoustic waves (SAW) and surface plasmon resonance (SPR) on a common substrate.," *Lab Chip*, vol. 10, no. 1, pp. 111–5, Jan. 2010.

[111] A. Renaudin, V. Chabot, E. Grondin, V. Aimez, and P. G. Charette, "Accelerated binding kinetics by surface acoustic waves (SAW) micromixing in surface plasmon resonance (SPR) system for biodetection.," vol. 7929, p. 79290M–79290M–9, Feb. 2011.

[112] S. Cular, D. W. Branch, V. R. Bhethanabotla, G. D. Meyer, and H. G. Craighead, "Removal of Nonspecifically Bound Proteins on Microarrays Using Surface Acoustic Waves," *IEEE Sens. J.*, vol. 8, no. 3, pp. 314–320, Mar. 2008.

[113] U. Rde, Z. Jia, G. Yin, J. Zhang, W. Xing, M. Yin, Q. Lv, Y. Hu, C. Liu, J. Zhang, A. Chemistry, C. Academy, C. Du, Y. Sun, T. Shen, G. Yin, J. Zhang, F. Si, Y. Zhang, L. Yan, J. Zhu, M. Xiao, C. Liu, W. Xing, and J. Zhang, *Rotating Electrode Methods and Oxygen Reduction Electrocatalysts*. Elsevier, 2014.

[114] E. Galopin, M. Beaugeois, B. Pinchemel, J. C. Camart, M. Bouazaoui, and V. Thomy, "SPR biosensing coupled to a digital microfluidic microstreaming system," *Biosens. Bioelectron.*, vol. 23, no. 5, pp. 746–750, Dec. 2007.

[115] A. J. Bard, G. Inzelt, and F. Scholz, *Electrochemical Dictionary*. Berlin, Heidelberg: Springer Berlin Heidelberg, 2012.

[116] T. R. Tsao, R. M. Moroney, B. a. Martin, and R. M. White, "Electrochemical detection of localized mixing produced by ultrasonic flexural waves," *IEEE 1991 Ultrason. Symp.*, pp. 937–940, 1991.

[117] K. Kulkarni, J. Friend, L. Yeo, and P. Perlmutter, "Surface acoustic waves as an energy source for drop scale synthetic chemistry.," *Lab Chip*, vol. 9, no. 6, pp. 754–5, Mar. 2009.

[118] G. D. Christian, *Flow injection analysis*, vol. 16, no. 3. 1997.

[119] J. Wang, L. Chen, and H. Wu, "AlvAuTIcA Gradient flow-injection amperometry based on induced retention by the detector coating," vol. 300, pp. 127–132, 1995.

[120] V. S. Bagotsky, *Fundamentals of electrochemistry*, vol. 298. Wiley, 2005.

[121] H. R. De Oliveira and A. D. O. D. A. Alchorne, *Modern Electrochemistry*, vol. 86, no. 5. 2011.

[122] H. A. O. Hill, Y. Nakagawa, S. P. Road, F. Marken, and R. G. Compton, "Voltammetry in the Presence of Ultrasound : Sonovoltammetric Detection of Cytochrome c under Very Fast Mass Transport Conditions," vol. 2, no. 96, pp. 17395–17399, 1996.

[123] Y. Matsui and S. Shiokawa, "Liquid Heating Effects by SAW Streaming on the," vol. 52, no. 10, pp. 1881–1883, 2005.

[124] J. D. Ostrow, "Tests for Fecal Occult Blood." Butterworths, 1990.

[125] "Cancer Research UK- Cancer Insight." [Online]. Available: http://publications.cancerresearchuk.org/downloads/Product/CR_PNnews7_for_web .pdf. [Accessed: 17-Apr-2015].

[126] Cancer Research UK, "Worldwide cancer statistics," 2012. [Online]. Available: http://www.cancerresearchuk.org/cancer-info/cancerstats/world/cancer-worldwide-the-global-picture. [Accessed: 16-Apr-2015].

[127] M. Zhang and J. Hu, "Indium tin oxide electrode modified by a SH+ ion implantation technique for direct electrocatalytic sensing of hydrogen peroxide," *Anal. Methods*, vol. 5, no. 5, p. 1273, 2013.

[128] C. Wang, X. Zou, Q. Wang, K. Shi, J. Tan, X. Zhao, Y. Chai, and R. Yuan, "A nitrite and hydrogen peroxide sensor based on Hb adsorbed on Au nanorods and graphene oxide coated by polydopamine," *Anal. Methods*, vol. 6, no. 3, p. 758, 2014.

[129] X.-C. Tan, J.-L. Zhang, S.-W. Tan, D.-D. Zhao, Z.-W. Huang, Y. Mi, and Z.-Y. Huang, "Amperometric hydrogen peroxide biosensor based on immobilization of hemoglobin on a glassy carbon electrode modified with fe(3)o(4)/chitosan core-shell microspheres.," *Sensors (Basel).*, vol. 9, no. 8, pp. 6185–99, Jan. 2009.

[130] Q. Wang, G. Lu, and B. Yang, "Hydrogen peroxide biosensor based on direct electrochemistry of hemoglobin immobilized on carbon paste electrode by a silica sol–gel film," *Sensors Actuators B Chem.*, vol. 99, no. 1, pp. 50–57, Apr. 2004.

[131] J. Zhang and M. Oyama, "A hydrogen peroxide sensor based on the peroxidase activity of hemoglobin immobilized on gold nanoparticles-modified ITO electrode," *Electrochim. Acta*, vol. 50, no. 1, pp. 85–90, Nov. 2004.

[132] S. Palanisamy, S. Cheemalapati, and S.-M. Chen, "Highly sensitive and selective hydrogen peroxide biosensor based on hemoglobin immobilized at multiwalled carbon nanotubes-zinc oxide composite electrode.," *Anal. Biochem.*, vol. 429, no. 2, pp. 108–15, Oct. 2012.

[133] S. George and H. K. Lee, "Direct electrochemistry and electrocatalysis of hemoglobin in nafion/carbon nanochip film on glassy carbon electrode.," *J. Phys. Chem. B*, vol. 113, no. 47, pp. 15445–54, Nov. 2009.

[134] X. Han, W. Huang, J. Jia, S. Dong, and E. Wang, "Direct electrochemistry of hemoglobin in egg Á phosphatidylcholine films and its catalysis to H 2 O 2," vol. 17, pp. 741–746, 2002.

[135] H. Wu, "STUDIES ON HEMOGLOBIN. III. An Ultra-Micro-method for the Determination of Hemoglobin as a Peroxidase," *J. Biochem.*, vol. 2, no. 2, pp. 189–194, 1923.

[136] W. H. Crosby, F. W. Furth, C. E. Thibeault, L. St, and W. Dc, "A Modification of the Benzidine Method for Measurement of Hemoglobin in Plasma and Urine Information about reproducing this article in parts or in its entirety may be found online at :," pp. 380–383, 2014.

[137] P. Using, "Quantitative Determination of Hemoglobin and Cytochemical A Safe Substitute for Benzidine," pp. 388–393, 1979.

[138] M. Rochelet, S. Solanas, C. Grossiord, P. Maréchal, C. Résa, F. Vienney, C. Barranger, and M. Joannes, "A thin layer-based amperometric enzyme immunoassay for the rapid and sensitive diagnosis of respiratory syncytial virus infections.," *Talanta*, vol. 100, pp. 139–44, Oct. 2012.

[139] M.-A. A. Woo, M. Il Kim, J. H. Jung, K. S. Park, T. S. Seo, and H. G. Park, "A novel colorimetric immunoassay utilizing the peroxidase mimicking activity of magnetic nanoparticles," *Int. J. Mol. Sci.*, vol. 14, no. 5, pp. 9999–10014, Jan. 2013.

[140] A. Ahmad and E. Moore, "Electrochemical immunosensor modified with self-assembled monolayer of 11-mercaptoundecanoic acid on gold electrodes for detection of benzo[a]pyrene in water.," *Analyst*, vol. 137, no. 24, pp. 5839–44, Dec. 2012.

[141] P. B. Lillehoj, M.-C. Huang, N. Truong, and C.-M. Ho, "Rapid electrochemical detection on a mobile phone.," *Lab Chip*, vol. 13, no. 15, pp. 2950–5, May 2013.

[142] S. Y. Ng, J. Reboud, K. Y. P. P. Wang, K. C. Tang, L. Zhang, P. Wong, K. T. Moe, W. Shim, and Y. Chen, "Label-free impedance detection of low levels of circulating endothelial progenitor cells for point-of-care diagnosis.," *Biosens. Bioelectron.*, vol. 25, no. 5, pp. 1095–1101, Jan. 2010.

[143] J. G. Ibanez, A. Alatorre-Ordaz, S. Gutierrez-Granados, and N. Batina, "Nanoscale degradation of polypyrrole films under oxidative stress: An atomic force microscopy study and review," *Polym. Degrad. Stab.*, vol. 93, no. 4, pp. 827–837, Apr. 2008.

[144] W. Kusnezow and J. D. Hoheisel, "Solid supports for microarray immunoassays," *J. Mol. Recognit.*, vol. 16, no. 4, pp. 165–176 ST – Solid supports for microarray immuno, 2003.

[145] A. Papra, D. Juncker, N. B. Larsen, B. Michel, and E. Delamarche, "Microfluidic Networks Made of Poly (dimethylsiloxane), Si , and Au Coated with Polyethylene Glycol for Patterning Proteins onto Surfaces," no. 12, pp. 4090–4095, 2001.

[146] M. Hervás, M. a. López, and A. Escarpa, "Electrochemical immunosensing on board microfluidic chip platforms," *TrAC Trends Anal. Chem.*, vol. 31, pp. 109–128, Jan. 2012.

[147] K. Siderakis, *Concise Encyclopedia of High Performance Silicones*. Wiley, 2014.

[148] S. Demming, C. Lesche, H. Schmolke, C.-P. Klages, and S. Büttgenbach, "Characterization of long-term stability of hydrophilized PEG-grafted PDMS within different media for biotechnological and pharmaceutical applications," *Phys. Status Solidi*, vol. 208, no. 6, pp. 1301–1307, Jun. 2011.

[149] S. K. Vashist, E. M. Schneider, E. Lam, S. Hrapovic, and J. H. T. Luong, "One-step antibody immobilization-based rapid and highly-sensitive sandwich ELISA procedure for potential in vitro diagnostics," pp. 1–7, 2014.

[150] D. Leca-bouvier, M. Zourob, K. Kahn, K. W. Plaxco, M. Zourob, K. Kahn, K. W. Plaxco, N. A. E. Hopkins, and M. Zourob, *Recognition Receptors in Biosensors*. New York, NY: Springer New York, 2010.

[151] J.-K. Lee, M. Park, J. Jose, M.-J. Kang, and J. Pyun, "Electrochemical ELISA based on Escherichia coli with autodisplayed Z-domains," *Sensors Actuators B Chem.*, vol. 175, pp. 46–52, Dec. 2012.